

## Cross-correlations in NMR

Anil Kumar<sup>a,b,\*</sup>, R. Christy Rani Grace<sup>a</sup>, P.K. Madhu<sup>a,1</sup>

<sup>a</sup>Department of Physics, Indian Institute of Science, Bangalore 560012, India

<sup>b</sup>Sophisticated Instruments Facility, Indian Institute of Science, Bangalore 560012, India

Received 10 April 2000

### Contents

1. Introduction	193
2. Theory	195
2.1. Equation of motion	195
2.1.1. Redfield kite	197
2.2. Relaxation Hamiltonians	198
2.2.1. Intramolecular direct dipole–dipole interaction	198
2.2.2. Chemical shift anisotropy	199
2.2.3. Quadrupolar interaction	199
2.2.4. Scalar spin–spin coupling	199
2.2.5. Expressions for the spectral densities	200
3. Cross-correlations in longitudinal relaxation	201
3.1. Magnetization modes	202
3.1.1. Representation of modes	205
3.1.2. Initial rate approximation	206
3.1.3. Magnitude of the cross terms	207
3.1.4. Cross-correlations contribute only to $W_1$	207
3.2. Multiplet and net effect of cross-correlations	208
3.2.1. Multiplet effect in three spin system $AMX$	209
3.2.2. The net effect	210
3.2.3. Spin diffusion	213
3.3. Effect of cross-correlations in equivalent and strongly coupled spins	216
3.3.1. $A_2$ spin system	216
3.3.2. $A_3$ spin system	216
3.3.3. $AX_2$ spin system	219
3.3.4. $AX_3$ spin system	219

\* Corresponding author. Department of Physics and Sophisticated Instruments Facility, Indian Institute of Science, Bangalore 560012, India. Tel.: +91-80-3092724; fax: +91-80-3601550.

E-mail addresses: anilnmr@physics.iisc.ernet.in (A. Kumar), grace@sif.iisc.ernet.in (R. Christy Rani Grace), kovilakathu.madhu@jk.uni-linz.ac.at (P.K. Madhu).

<sup>1</sup> Present address: Institute Fur Chemie, Department of Organische Chemie, Johannes Kepler Universitat, Altenbergerstrasse 69, A-4040 Linz, Austria.

3.3.5.	<i>AB</i> spin system	219
3.3.6.	<i>ABX</i> spin system	220
3.4.	Experimental observation of longitudinal cross-correlations	222
3.4.1.	Non-exponential recovery in longitudinal relaxation	222
3.4.2.	Non-exponential <sup>13</sup> C relaxation	223
3.4.3.	Multiplet effect in inversion recovery and NOE experiments	223
3.4.4.	Multiplet effect in NOESY experiments	226
3.4.5.	Observation of antiphase magnetization	228
3.5.	Isolation of longitudinal relaxation pathways using RF pulses	229
3.5.1.	The Homogeneous-Master-Equation (HME) approach	231
3.5.2.	Isolation of coupling networks by application of RF pulses	234
4.	Cross-correlations in transverse relaxation	236
4.1.	Time evolution of transverse coherence in the absence of simple-line approximation	239
4.2.	Time evolution of transverse coherence under the simple-line approximation	240
4.2.1.	Cross-correlations in the heteronuclear <i>AX</i> spin system	240
4.2.2.	Cross-correlations in strongly coupled two-spin system <i>AB</i>	242
4.2.3.	Cross-correlations in heteronuclear three-spin system <i>AMX</i>	244
4.2.4.	Dipole–dipole cross-correlations in a strongly coupled homonuclear three-spin system <i>ABX</i>	248
4.2.5.	<i>AX</i> <sub>2</sub> spin system	255
4.2.6.	<i>AX</i> <sub>3</sub> spin system	256
4.2.7.	Spin-(1/2) coupled to spin > (1/2) system	257
4.3.	Experimental observation of transverse cross-correlations	257
4.3.1.	Direct observations of differential line broadening	257
4.3.2.	Motional information from non-axial CSA and dipole cross-correlations	259
4.3.3.	Break down of coherence transfer rules in equivalent spin systems	259
4.3.4.	Relaxation-allowed coherence transfer	259
4.4.	Remote cross-correlations	260
4.4.1.	Remote CSA–CSA cross-correlations	261
4.4.2.	Remote CSA–dipole cross-correlations	263
4.4.3.	Remote dipole–dipole cross-correlations	267
4.5.	Cross-correlations involving quadrupolar nuclei	270
5.	Cross-correlations in the presence of a radio frequency field	272
5.1.	Theory	273
5.2.	Effect of CSA–dipole cross-correlations for an <i>AX</i> spin system	273
5.2.1.	No spin locking	275
5.2.2.	Selective spin locking	275
5.2.3.	Spin locking both spins <i>A</i> and <i>X</i>	275
5.3.	Effect of cross-correlations for an <i>AMX</i> spin system	276
5.3.1.	Case (i): when $\theta_A = \theta_M = \theta_X = 0$	278
5.3.2.	Case (ii): when $\theta_A = 90^\circ$ , $\theta_M = \theta_X = 0$	278
5.3.3.	Case (iii): when $\theta_A = \theta_M = 90^\circ$ and $\theta_X = 0$	278
5.3.4.	Case (iv): when $\theta_A = \theta_M = \theta_X = 90^\circ$	279
5.4.	Experimental observations	279
6.	Dynamic frequency shift	281
6.1.	Functional form of the dynamic frequency shift	284
6.2.	Dynamic frequency shift for various spin systems	284
6.2.1.	Two unlike spin-1/2 system ( <i>AX</i> )	284
6.2.2.	Three spin-1/2 system ( <i>AMX</i> )	285
6.2.3.	Three identical spin-(1/2) system ( <i>A</i> <sub>3</sub> )	286
6.3.	Dynamic frequency shifts for quadrupolar nuclei	286
6.3.1.	Spin-1 system	286

6.3.2. General case of spin $I > 1$ . . . . .	287
6.4. Dynamic frequency shifts of $I = 1/2$ spins scalar coupled to efficiently relaxed quadrupolar spins ( $S$ ) . . . . .	287
6.5. Experimental observations of the dynamic frequency shifts . . . . .	290
7. Other recent developments . . . . .	293
7.1. Cross-correlations in paramagnetic molecules . . . . .	293
7.2. Determination of chemical shift anisotropy . . . . .	296
7.2.1. $^{15}\text{N}$ CSA measurements . . . . .	296
7.2.2. $^1\text{H}$ CSA measurements . . . . .	297
7.2.3. $^{13}\text{C}_\alpha$ CSA measurements . . . . .	299
7.3. Isolation of relaxation pathways by linear combination of various modes . . . . .	301
7.3.1. Longitudinal modes . . . . .	301
7.3.2. Transverse modes . . . . .	301
7.3.3. Combination of longitudinal and transverse modes . . . . .	301
7.4. Dipole–dipole cross-correlations in $\text{CH}_2$ and $\text{CH}_3$ spin systems . . . . .	302
7.5. Combined use of transverse and longitudinal cross-correlations . . . . .	303
7.6. TROSY: transverse relaxation optimized spectroscopy . . . . .	306
7.7. Cross-correlation under magic angle spinning . . . . .	310
8. Experiments that avoid cross-correlations . . . . .	310
9. Conclusions . . . . .	311
Appendix A. Operator formalism for relaxation . . . . .	311
Acknowledgements . . . . .	311
References . . . . .	314

## 1. Introduction

The phenomenon of nuclear magnetic resonance (NMR) involves placing magnetically active nuclear spins embedded in a gas, liquid or solid phase in a constant, large and uniform magnetic field, causing a splitting of magnetic energy levels. Energy can be absorbed by these spins from a resonant radio-frequency (RF) field causing transitions between these levels. Immediately following this absorption, the spins start to exchange this energy among themselves and also pass it on to other degrees of freedom, that is, the spins start to relax. Relaxation is central to the NMR phenomenon as a necessary prerequisite for its detection. It is also used as a probe for obtaining information on the local environment of the spins and about the dynamics of the molecules in which the spins are embedded.

One of the most important interactions that couples nuclear spins to each other and to the environment is the dipole–dipole interaction between the spins. In static solids, the dipolar interaction provides only a static coupling between the spins and causes mutual exchange of energy within the spin system, but does

not provide any coupling to the outside environment. In other words, it provides no contact with the lattice and causes no relaxation. However, if the internal motions in solids are at rates comparable to the Larmor frequency, the dipolar interaction becomes time dependent and couples the spins to the rotational motion and acts as a mechanism for transferring the energy from the spin system to the rotational degrees of freedom and causes spin–lattice relaxation. In liquids, the intramolecular dipolar interaction, between the spins of the same rigid molecule, becomes time dependent due to rapid molecular reorientations. Intermolecular dipolar interaction (between the spins of two different molecules) becomes time dependent additionally due to translational motion. There are dipolar interactions between several spins at the same time, many of which have identical time dependences arising from the same reorientational or translational motion.

Additionally, there are other sources of relaxation for the nuclear spins. The electrons surrounding the nuclei contribute to the magnetic interactions in several ways. In paramagnetic systems, the electron spin has a strong coupling with nuclear spins and can

cause rapid relaxation of nuclear spins, resulting in very short lifetimes of the excited nuclear magnetic states giving rise to broad NMR lines. In diamagnetic systems, this strong interaction is absent as the electron spins are paired. However, the applied magnetic field  $B_0$  causes an induced precession of the electrons, which produces a magnetic field at the site of the nucleus. This induced field which is small compared to  $B_0$  (only parts per million, ppm) and proportional to the applied field, causes a shift in the resonance frequency of the nuclear spins known as the chemical shift. This field, hence the shift, is dependent on the orientation of the molecule with respect to the applied magnetic field. In single crystals, the shift has a definite value for each orientation, giving sharp shifted resonances; in powders, there are a large number of orientations, yielding broad powder patterns; in liquids, it becomes time dependent and for isotropically reorienting molecules, only the trace of the shift tensor survives, yielding a chemical shift for a functional group and different chemical shifts for different functional groups. However, the time-dependent part of the chemical shift tensor (if anisotropic) causes relaxation of the nuclear spins. The chemical shift anisotropy (CSA) relaxation has been a well-known source of relaxation of nuclei with large CSA tensors such as  $^{13}\text{C}$ ,  $^{15}\text{N}$ ,  $^{19}\text{F}$  and  $^{31}\text{P}$ . However, with the use of high magnetic fields for NMR studies, this mechanism is becoming important even for smaller CSA tensors of nuclei such as protons. There are yet other mechanisms of relaxation of spins such as the spin rotation interaction and scalar relaxation of first and second kinds [1]. In addition, nuclei having spin angular momenta greater than  $(1/2)$  have a quadrupole moment. This quadrupolar interaction becomes time dependent due to rapid fluctuations in electric field gradients at the site of the nucleus and causes rapid relaxation of such nuclei. Quadrupolar relaxation of nuclei with spins greater than  $(1/2)$  usually dominates all the other relaxation processes in diamagnetic systems.

Thus there are several mechanisms acting simultaneously by which nuclear spins can relax. The simultaneous presence of various mechanisms gives rise to cross terms between these mechanisms. These cross terms, known as cross-correlations, are the interference effects in relaxation between distinct interactions with the same tensorial character, have been known

from the early days of NMR [2,3] and repeatedly rediscovered. In the 1950s, it was observed that the ESR spectra of various paramagnetic centres in solution (copper complexes, vanadyl ions, etc.) split into several lines by hyperfine interactions with nuclear spins, had different widths for the various lines, a description of these experiments, along with the references to the original articles can be found in Ayscough [4] and Artherton [5]. The origin of this effect was traced to an interference between the anisotropic electronic  $g$  factor and the electron–nuclear couplings by McConnell [6], who also gave an approximate solution of the relaxation equations. An extensive theory of electron resonance linewidths, including the effect of quadrupolar interactions and chemical exchange, was given by Freed and Fraenkel [7]. In high-resolution liquid state NMR, the effects of cross-correlations were observed in double resonance experiments used for studying the relaxation of coupled spins [8–12].

The mathematical aspects of the theory of cross-correlations were put into a sound footing by the works of Schneider [13–16], Blicharski [17–20], Hubbard [21], Pyper [22,23] and others. Later, the field of NMR saw the extraction of useful physiochemical information from these, which was illustrated by the work from the groups of Vold [24–29], and Grant [30–33]. In these early works, it was shown that while cross-correlations lead to differential line broadening of resolved multiplets, they also lead to non-exponential spin–lattice relaxation. Many early observations concentrated on the latter feature, even though it was well known that there can be several sources for non-exponential recovery [34,35]. For example, while non-exponential  $T_1$  behavior of methyl groups in solids due to cross-correlations was predicted by Hilt and Hubbard [36], it was pointed out that in powder samples and in single crystals, the multiple orientations of methyl groups in a unit cell can also lead to multi-exponential behavior of spin–lattice relaxation [37]. Careful experiments on single crystals with a single orientation of methyl groups established the presence of cross-correlations in methyl groups. However, unequivocal evidence for the presence of cross-correlations in spin–lattice relaxation were obtained by the observation that different lines of a multiplet are found to relax at different rates giving rise to a “multiplet effect”

[38–46]. Currently, the manipulation of multi-spin order by multi-pulse NMR methodologies leads to the measurement of cross-correlations systematically, opening up new areas of interest. Interest in these cross terms has been further rejuvenated in recent years due to a rapid development of NMR methodology for structure determination of biomolecules using saturation transfer experiments also known as nuclear Overhauser effect (NOE).

The development of 2D and multi-dimensional NMR spectroscopy made it possible to obtain resonance assignments of large number of biomolecules and to obtain large numbers of internuclear distances using NOE, resulting in the calculation of 3D structure of the molecules in solution [47–49]. The information on internuclear distances is usually obtained using qualitative estimates of NOE intensities. However, attempts are often made to obtain accurate quantitative distances from the NOE intensities [50]. In all such cases, it becomes necessary to probe the saturation transfer process in detail. A semi-quantitative estimate is often made by including the simultaneous presence of several relaxation mechanisms and spins but by neglecting the cross terms between the various relaxation mechanisms. In recent years, attention has been focused on the contributions of these cross terms. Several justifications have been given for their neglect in NOE measurements. One of the main justifications is that the multiplets of a spin are often not resolved, canceling out the first-order differential effect of cross-correlations, or that a 90° measuring pulse can suppress the multiplet effect. Since the dimension of the relaxation matrix to be handled for inclusion of cross-correlations increases rapidly with the number of interacting spins, their inclusion requires a very convincing justification. Several authors, on the other hand, have pointed out that these cross terms can be put to good use by obtaining additional and often crucial information on the structures of molecules, molecular reorientations and internal motions [51–57]. Furthermore, in recent years, with the availability of higher magnetic fields which enhance the contribution of CSA to relaxation and in particular its cross terms with other dominant mechanisms, the study of cross-correlations has become attractive. Significant effects of CSA–dipole, dipole–dipole and quadrupole–dipole cross-correlation have been observed in recent

years, especially in transverse relaxation of coupled spins.

This review is devoted to describing the work that has been carried out in this field in recent years. There are already several outstanding reviews on relaxation, which treat cross-correlations in some detail by, Werbelow and Grant [58], Vold and Vold [59], Canet [60] and the recent ones by Bull [61] and Werbelow [62]. The present review is organized in the following manner. Section 2 covers the basic Redfield theory of relaxation, points out the contribution of cross terms to the relaxation elements and separates out the longitudinal and transverse relaxation. Sections 3 and 4, respectively, cover the contribution of cross-correlations to longitudinal and transverse relaxation and their experimental observation. Section 5 deals with cross-correlations in the rotating frame and Section 6 with the dynamic frequency shift (DFS). Section 7 deals with other recent experimental observation of cross-correlations and Section 8 deals with experiments that avoid cross-correlations.

## 2. Theory

### 2.1. Equation of motion

The von Neumann–Liouville equation, which describes the time evolution of the magnetic resonance phenomenon using spin density matrix  $\sigma(t)$  can be written as [1]:

$$\frac{d\sigma(t)}{dt} = -i[\mathcal{H}_0 + \mathcal{H}^l(t), \sigma(t)] \quad (1)$$

where  $\mathcal{H}_0$  is the time-independent part of the Hamiltonian which contains the spin Hamiltonian and  $\mathcal{H}^l(t)$  describes the time-dependent part, which contains the relaxation Hamiltonians. This equation is solved using second-order time-dependent perturbation theory, by first removing the major time dependence via transformation to the interaction representation using the transformation operator:

$$T = \exp(i\mathcal{H}_0 t), \quad (2)$$

yielding,

$$\frac{d\sigma^*(t)}{dt} = -i[\mathcal{H}^{l*}(t), \sigma^*(t)], \quad (3)$$

where

$$\sigma^*(t) = T\sigma(t)T^{-1} \quad (4)$$

and

$$\mathcal{H}^{I*}(t) = T\mathcal{H}^I(t)T^{-1}. \quad (5)$$

Eq. (3) can be solved by successive approximations as [1]:

$$\begin{aligned} \sigma^*(t) = & \sigma^*(0) - i \int_0^t [\mathcal{H}^{I*}(t'), \sigma^*(0)] dt' \\ & - \int_0^t dt' \int_0^{t'} dt'' [\mathcal{H}^{I*}(t'), [\mathcal{H}^{I*}(t''), \sigma^*(0)]]. \end{aligned} \quad (6)$$

Taking the time derivative of this equation, one gets

$$\begin{aligned} \frac{d\sigma^*(t)}{dt} = & -i[\mathcal{H}^{I*}(t), \sigma^*(0)] \\ & - \int_0^t dt' [\mathcal{H}^{I*}(t), [\mathcal{H}^{I*}(t'), \sigma^*(0)]]. \end{aligned} \quad (7)$$

Since  $\mathcal{H}^I(t)$  is a stationary random function, so is  $\mathcal{H}^{I*}(t)$ . On substituting  $\tau = t - t'$ , after taking the ensemble average and making several approximations [1] namely; (i)  $\mathcal{H}^{I*}(t)$  and  $\sigma^*(0)$  are not correlated and can be separately averaged; (ii) assuming  $\overline{\mathcal{H}^{I*}(t)} = 0$  where the bar indicates an ensemble average, the first term on the right-hand side (RHS) is zero; (iii) in the second term on the RHS,  $\sigma^*(0)$  can be replaced by  $\sigma^*(t)$  and all higher order terms are neglected; (iv)  $\sigma^*(t)$  is replaced by  $\sigma^*(t) - \sigma(\infty) = \sigma^*(t) - \sigma_0$ , where the system relaxes towards  $\sigma_0$ ; (v) the integral on the RHS can be extended to  $\infty$  since the memory between  $\mathcal{H}(t)$  and  $\mathcal{H}(t - \tau)$  only lasts for a short time, one obtains:

$$\frac{d\sigma^*(t)}{dt} = - \int_0^\infty \overline{[\mathcal{H}^{I*}(t), [\mathcal{H}^{I*}(t - \tau), \sigma^*(t) - \sigma_0]]} d\tau. \quad (8)$$

Taking matrix elements of the above equation in the eigenstates  $|\alpha\rangle, |\beta\rangle$  of the unperturbed Hamiltonian  $\mathcal{H}_0$  with eigenvalues  $\omega_\alpha, \omega_\beta$ , one obtains [1]:

$$\frac{d\sigma_{\alpha\alpha'}^*(t)}{dt} = \sum_{\beta\beta'} \exp[i(\omega_{\alpha\alpha'} - \omega_{\beta\beta'})t] \Gamma_{\alpha\alpha'\beta\beta'} [\sigma^*(t) - \sigma_0]_{\beta\beta'} \quad (9)$$

where  $\omega_{\alpha\alpha'} = \omega_\alpha - \omega_{\alpha'}$  is the frequency of the transition  $\alpha \rightarrow \alpha'$  and  $\Gamma$  the relaxation superoperator such that its elements  $\Gamma_{\alpha\alpha'\beta\beta'}$  connect the time evolution of  $\sigma_{\beta\beta'}$  to that of  $\sigma_{\alpha\alpha'}$ . Here due to the stationary nature of  $\mathcal{H}^I(t)$ , elements of  $\mathbf{R}$  matrix (coefficients  $\Gamma_{\alpha\alpha'\beta\beta'}$ ) become independent of time and due to the Hermitian nature of  $\mathcal{H}^I(t)$ , one obtains the following symmetry relations:

$$\Gamma_{\alpha\alpha'\beta\beta'} = \Gamma_{\beta\beta'\alpha\alpha'}^* = \Gamma_{\alpha'\alpha\beta'\beta}^* = \Gamma_{\beta'\beta\alpha'\alpha}. \quad (10)$$

Elements of  $\Gamma$  are linear combinations of spectral densities given by:

$$\begin{aligned} \Gamma_{\alpha\alpha'\beta\beta'} = & j_{\alpha\beta\alpha'\beta'}(\omega_{\alpha\beta}) + j_{\alpha\beta\alpha'\beta'}(\omega_{\beta'\alpha'}) \\ & - \delta_{\alpha\beta} \sum_{\gamma} j_{\beta'\gamma\alpha'\gamma}(\omega_{\beta'\gamma}) - \delta_{\alpha'\beta'} \sum_{\gamma} j_{\alpha\gamma\beta\gamma}(\omega_{\gamma\beta}) \end{aligned} \quad (11)$$

where the spectral densities are the Fourier transforms [63] of the correlation function and are defined as:

$$\begin{aligned} j_{\alpha\beta\alpha'\beta'}(\omega) = & \int_0^\infty G_{\alpha\beta\alpha'\beta'}(\tau) e^{-i\omega\tau} d\tau \\ = & \frac{1}{2} \int_{-\infty}^\infty G_{\alpha\beta\alpha'\beta'}(\tau) \cos(\omega\tau) d\tau \\ & - i \int_0^\infty G_{\alpha\beta\alpha'\beta'}(\tau) \sin(\omega\tau) d\tau \\ = & J_{\alpha\beta\alpha'\beta'}(\omega) - iK_{\alpha\beta\alpha'\beta'}(\omega). \end{aligned} \quad (12)$$

Here  $G_{\alpha\beta\alpha'\beta'}(\tau)$  is the correlation function,  $J_{\alpha\beta\alpha'\beta'}(\omega)$  and  $K_{\alpha\beta\alpha'\beta'}(\omega)$ , respectively, are the real and imaginary parts of the spectral densities. Substituting Eq. (12) in Eq. (11) one can write:

$$\Gamma_{\alpha\alpha'\beta\beta'} = R_{\alpha\alpha'\beta\beta'} - iL_{\alpha\alpha'\beta\beta'} \quad (13)$$

where

$$\begin{aligned} R_{\alpha\alpha'\beta\beta'} = & J_{\alpha\beta\alpha'\beta'}(\omega_{\alpha\beta}) + J_{\alpha\beta\alpha'\beta'}(\omega_{\beta'\alpha'}) \\ & - \delta_{\alpha\beta} \sum_{\gamma} J_{\beta'\gamma\alpha'\gamma}(\omega_{\beta'\gamma}) - \delta_{\alpha'\beta'} \sum_{\gamma} J_{\alpha\gamma\beta\gamma}(\omega_{\gamma\beta}) \end{aligned} \quad (14)$$

and

$$L_{\alpha\alpha'\beta\beta'} = K_{\alpha\beta\alpha'\beta'}(\omega_{\alpha\beta}) + K_{\alpha\beta\alpha'\beta'}(\omega_{\beta'\alpha'}) - \delta_{\alpha\beta} \sum_{\gamma} K_{\beta'\gamma\alpha'\gamma}(\omega_{\beta'\gamma}) - \delta_{\alpha'\beta'} \sum_{\gamma} K_{\alpha\gamma\beta\gamma}(\omega_{\gamma\beta}) \quad (15)$$

The relaxation matrix ( $\Gamma$ ) therefore, contains a real part ( $R$ ) and an imaginary part ( $L$ ). The real part  $R$ , which contains  $J(\omega)$  contributes to the relaxation. The imaginary part  $L$ , which contains  $K(\omega)$  can be identified with a frequency shift, known as the “dynamic frequency shift” (DFS) [64,65]. The DFS has been observed in several cases, which will be discussed separately in Section 6 of this article. The major emphasis in this article will be on relaxation, described by the real part of the relaxation matrix. It may also be noted that while

$$R(\omega) = R(-\omega); \quad L(\omega) = -L(-\omega). \quad (16)$$

The second equation of Eq. (16) states that  $L(0) = 0$ , since  $L$  is odd and continuous, that there is no contribution to the DFS from zero-frequency spectral densities, or in other words, there are no adiabatic contributions to the DFS. This also means that the time evolution of populations are unaffected by the imaginary part of spectral densities. The correlation function  $G_{\alpha\beta\alpha'\beta'}(\tau)$  is given by,

$$G_{\alpha\beta\alpha'\beta'}(\tau) = \overline{\langle \alpha | \mathcal{H}^l(t) | \beta \rangle \langle \alpha' | \mathcal{H}^l(t - \tau) | \beta' \rangle^*} \quad (17)$$

where the bar represents an ensemble average. The relaxation Hamiltonian may contain several terms and can be written as:

$$\mathcal{H}^l(t) = \sum_n \mathcal{H}_n^l(t) \quad (18)$$

each representing a particular interaction which, for example, can be dipolar interactions between pairs of spins or CSA relaxation of a spin. The correlation function will then contain several auto and cross-correlation terms given by:

$$G_{\alpha\beta\alpha'\beta'}(\tau) = \sum_n \overline{\langle \alpha | \mathcal{H}_n^l(t) | \beta \rangle \langle \alpha' | \mathcal{H}_n^l(t - \tau) | \beta' \rangle^*} + \sum_{n < n', n \neq n'} \overline{\langle \alpha | \mathcal{H}_n^l(t) | \beta \rangle \langle \alpha' | \mathcal{H}_{n'}^l(t - \tau) | \beta' \rangle^*}. \quad (19)$$

The first term on the RHS is the auto-correlation term and the second term is the cross-correlation term. This

article is specifically devoted to the study of the effect of the cross-correlations on the longitudinal and the transverse relaxation of coupled spins.

### 2.1.1. Redfield kite

From Eq. (9), it is seen that the time dependence of  $\sigma_{\alpha\alpha'}^*$  is described by the various elements of the  $\Gamma$  matrix and the oscillating factor,  $\exp[i(\omega_{\alpha\alpha'} - \omega_{\beta\beta'})t]$ . The contribution of the elements of  $\Gamma$  to the time development of  $\sigma^*$  for rapidly oscillating terms, for which  $(\omega_{\alpha\alpha'} - \omega_{\beta\beta'}) \neq 0$ , are small and their contributions are therefore neglected. This is known as the secular approximation [65]. Under this approximation Eq. (9) reduces to:

$$\frac{d\sigma_{\alpha\alpha'}^*(t)}{dt} = \sum_{\beta\beta'}' \Gamma_{\alpha\alpha'\beta\beta'} [\sigma_{\beta\beta'}^*(t) - \sigma_{\beta\beta'}], \quad (20)$$

where the prime on the summation indicates that only terms for which  $\omega_{\alpha\alpha'} = \omega_{\beta\beta'}$  are retained. This approximation decouples the time evolution of the diagonal elements of  $\sigma^*$  from the off-diagonal elements. However, since for the diagonal elements there is no oscillatory part, the time evolution of all the diagonal elements is mutually coupled. The time evolution of the off-diagonal elements is further decoupled into various multiple quantum orders ( $\omega_{\alpha\alpha'} = \omega_{\beta\beta'} = n\omega_0$ ). Eq. (20) then breaks up into a block structure as indicated by the dashed lines in Fig. 1. If in addition, all the transitions in each single and multiple quantum manifold are non-degenerate and well separated, such that  $|\omega_{\alpha\alpha'} - \omega_{\beta\beta'}| \gg \Gamma_{\alpha\alpha'\beta\beta'}$ , then each coherence  $\sigma_{\alpha\alpha'}^*$  evolves independent of all others and decays exponentially with a time constant,  $R_{\alpha\alpha'\alpha\alpha'}$ , the real part of  $\Gamma$ . The effective Redfield matrix then looks like a “kite” (Fig. 1) [49].

Eq. (20) is transformed into the laboratory frame as:

$$\frac{d\sigma_{\alpha\alpha'}(t)}{dt} = -i\omega_{\alpha\alpha'}\sigma_{\alpha\alpha'}(t) + \sum_{\beta\beta'} \Gamma_{\alpha\alpha'\beta\beta'} (\sigma_{\beta\beta'}(t) - \sigma_{\beta\beta'}). \quad (21)$$

The first term on the RHS of Eq. (21) gives the frequencies of various coherences (for  $\alpha \neq \alpha'$ ) and the second term gives their relaxation including the DFS, if any. For diagonal elements ( $\alpha = \alpha'$ ), the first term is zero and the time evolution of all diagonal elements is coupled. All the above discussion is valid only in the absence of a RF field. In the presence

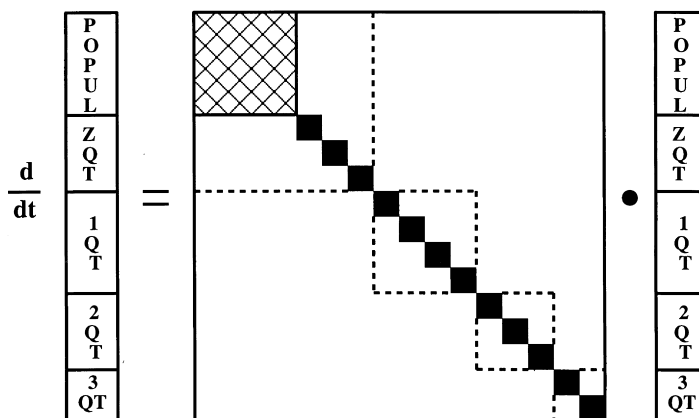


Fig. 1. A pictorial representation of the Redfield relaxation equation. The relaxation matrix is block structured under the secular approximation shown by dashed lines. If, in addition all the transitions are nondegenerate, the off-diagonal elements between various coherences of same order can be neglected, or in other words, there is no transverse cross-relaxation process and the Redfield matrix takes the form of a kite known as the “Redfield kite” [49].

of RF fields, the evolution of various elements of  $\sigma$  become coupled and the above kite structure is modified. The dynamics of  $\sigma$  in the presence of the RF field will be treated in Section 5.

## 2.2. Relaxation Hamiltonians

As mentioned in Section 1, there are several mechanisms for the relaxation of a spin. The main ones are (i) dipolar, (ii) CSA, (iii) quadrupolar, (iv) spin-rotation and (v) scalar relaxation of kind I and II. Yet another often used mechanism, called “random field mechanism”, is a model for relaxation in which it is assumed that a randomly varying time dependent isotropic field is produced at the site of the spin by outside sources (the details of which are unspecified), which causes relaxation of the spin. This field can be either uncorrelated, partially or fully correlated at two or more spins. The random field mechanism has been a convenient tool for describing the relaxation of spins in magnetic resonance. Conditions under which the spectral densities of several of the above mechanisms reduce to those of the random field mechanism have also been given [66,67].

The various relaxation Hamiltonians can in general be expressed as products of irreducible tensors of the type [1,12,66]:

$$\mathcal{H}^l(t) = \sum_q (-)^q A^{(q)} F^{(-q)}(t) \quad (22)$$

where  $A^{(q)}$  are spin operators and  $F^{(q)}(t)$  are random functions of lattice variables and  $q$  is the rank of the tensors. The reason for expressing the relaxation Hamiltonians in this form is that, the time dependence in these interactions arises due to molecular motions a description of which requires a series of transformations which in turn can then be conveniently described in terms of transformation properties of spherical harmonics. The Hermiticity of  $\mathcal{H}^l(t)$  requires that

$$A^{(q)\dagger} = (-)^q A^{(-q)} \quad \text{and} \quad F^{(q)\dagger}(t) = (-)^q F^{(-q)}(t), \quad (23)$$

and the secular approximation mentioned earlier leads to

$$\langle F^{(q)}(t) F^{l(q)*}(t') \rangle_{av} = \delta_{qq'} \langle F^{(q)}(t) F^{(q)*}(t') \rangle_{av}. \quad (24)$$

The form of various relaxation Hamiltonians, discussed extensively in the literature [1,65–70] is briefly outlined below.

### 2.2.1. Intramolecular direct dipole–dipole interaction

This is the most significant interaction with which the nuclear spins exchange their energy with each other and with other degrees of freedom. This is also the interaction responsible for transfer of magnetization from a spin to its neighbors known as NOE, which has become a major source of structural information for molecules, especially biomolecules. The

direct dipolar interaction between two spins can be written as [68,69]:

$$\mathcal{H}_D = \vec{I}(i) \cdot \mathbf{D}_{ij} \cdot \vec{I}(j). \quad (25)$$

The coupling tensor  $\mathbf{D}$  of rank 2 is traceless and axially symmetric, which in a molecular fixed principal axis coordinate system, is given by:

$$\mathbf{D}_{ij} = \left( \frac{\mu_0}{4\pi} \right) \left( \frac{\gamma_i \gamma_j \hbar}{r_{ij}^3} \right) \begin{pmatrix} -1 & 0 & 0 \\ 0 & -1 & 0 \\ 0 & 0 & 2 \end{pmatrix} \quad (26)$$

with the principal  $z$ -axis being given by the internuclear vector. The significance of  $\mathbf{D}$  being traceless is that for an ensemble of rapidly and isotropically tumbling molecules in space, there is no net change of energy and the dipolar interaction does not contribute to the time averaged Hamiltonian of a high-resolution NMR spectrum. However, it does contribute to the relaxation of various transitions of the spectrum. Upon transforming to the laboratory fixed frame with  $B_0$  field along the  $z$ -axis, the spin operators of the dipolar interaction are given by [70]:

$$\begin{aligned} A^{\pm 2} &= I_i^{\pm} I_j^{\pm} \\ A^{\pm 1} &= \mp (I_i^{\pm} I_j^z + I_i^z I_j^{\pm}) \end{aligned} \quad (27)$$

$$A^0 = [4I_i^z I_j^z - (I_i^+ I_j^- + I_i^- I_j^+)] / \sqrt{6}$$

while the space part is given by

$$F^q = - \left( \frac{6\pi}{5} \right)^{1/2} \hbar \gamma_i \gamma_j r_{ij}^{-3} Y_2^q(\theta, \phi). \quad (28)$$

Here  $Y_2^q(\theta, \phi)$  are the spherical harmonics of second rank with  $\theta$  and  $\phi$  being the polar and azimuthal angles, between the two frames respectively,  $r_{ij}$  is the internuclear distance between spins  $i$  and  $j$  and  $\gamma_i, \gamma_j$  are the gyromagnetic ratios of the concerned nuclei.

### 2.2.2. Chemical shift anisotropy

This interaction can be written in the form:

$$\mathcal{H}_{\text{CSA}} = \vec{I} \cdot \boldsymbol{\sigma} \cdot \vec{H}, \quad (29)$$

where  $\vec{H}$  is the external magnetic field, and  $\boldsymbol{\sigma}$  the chemical shift tensor. In general,  $\boldsymbol{\sigma}$  is neither axially symmetric nor traceless. The isotropic part of  $\boldsymbol{\sigma}$  gives

rise to chemical shift in reorientating molecules and does not cause relaxation. The anisotropic part causes relaxation. The spin operators of the CSA interaction in the molecule fixed (prime) frame are given by [12]:

$$\begin{aligned} A^0 &= [3H'_z I'_z - I' \cdot H'] \\ A^{\pm 1} &= \mp \frac{\sqrt{6}}{2} (H'_z I'_{\pm} + I'_z H'_{\pm}) \\ A^{\pm 2} &= \frac{\sqrt{6}}{2} (I'_{\pm} H'_{\pm}), \end{aligned} \quad (30)$$

and the space part is given by:

$$F^0 = \frac{1}{2} \gamma \sigma'_z, \quad F^{\pm 1} = 0, \quad F^{\pm 2} = \frac{\gamma \sigma'_z}{2\sqrt{6}}. \quad (31)$$

### 2.2.3. Quadrupolar interaction

The form of the quadrupolar interaction between the nuclear spin  $I$  and the electric field gradient at the site of the nuclear spin is given by [70]:

$$\mathcal{H}_Q = \vec{I} \cdot \mathbf{Q} \cdot \vec{I}. \quad (32)$$

where  $\mathbf{Q}$  is the quadrupole coupling tensor given by:

$$\mathbf{Q} = \frac{eQ}{2I(2I-1)\hbar} \mathbf{V} \quad (33)$$

with  $\mathbf{V}$  being the electric field gradient tensor. The quadrupolar interaction comes into play only for nuclei with spin  $I > (1/2)$  where it proves to be a major relaxation mechanism.

The spin operators of the quadrupolar interaction in the laboratory frame are given by:

$$\begin{aligned} A^0 &= 3I_z^2 - I(I+1) \\ A^{\pm 1} &= \frac{1}{2} \sqrt{6} (I_z I_{\pm} + I_{\pm} I_z) \\ A^{\pm 2} &= \frac{1}{2} \sqrt{6} I_{\pm}^2. \end{aligned} \quad (34)$$

and the space part  $F^{(m)}(\Omega)$  is proportional to the spherical harmonics  $Y_2^{(m)}(\alpha, \beta, \gamma)$  of order two. Cross-correlation between quadrupolar relaxation of spin  $I$  with its dipolar relaxation to spin  $S(1/2)$  is an important source of relaxation of spin  $S$ , and is discussed in Section 4.5.

### 2.2.4. Scalar spin–spin coupling

The Hamiltonian for scalar spin–spin coupling can

be written as:

$$\mathcal{H}_J = I \cdot \mathbf{J} \cdot S \quad (35)$$

where  $I$  and  $S$  correspond to the two nuclear spins.  $\mathbf{J}$  has two parts, a traceless tensor  $\mathbf{J}'$  and a diagonal tensor  $\mathbf{J}^0$ . For isotropic molecular reorientations,  $\mathbf{J}'$  does not contribute to coherent splitting, but contributes to relaxation, exactly like dipolar relaxation. Indeed, for all practical purposes, this part can be combined with dipolar relaxation (some times called pseudo dipolar) and needs no further elaboration [1]. The diagonal part gives rise to the well-known coherent J-coupling. This part can also become time dependent in two different ways, which are known as scalar relaxation of the first and second kinds [1]. In the first kind, the J-coupling becomes time dependent due to rapid chemical exchange between coupled and uncoupled sites. If the exchange rate ( $1/\tau_c$ )  $\gg$  J, then the splitting collapses and the coupling becomes a source of relaxation. In the second kind, one of the coupled spins has a rapid self relaxation of its own, either because it is a quadrupolar nucleus having rapid self-relaxation or due to its coupling with a strong paramagnetic or quadrupolar center. In such cases, its spin state becomes time dependent which can then be lumped with the lattice. The spin operators for this interaction are given by [1]:

$$A^0 = I_z, \quad A^{\pm 1} = I_{\pm} \quad (36)$$

and the space part is given by

$$F^0 = JS_z, \quad F^1 = \frac{1}{2}JS_-, \quad F^{-1} = \frac{1}{2}JS_+. \quad (37)$$

### 2.2.5. Expressions for the spectral densities

The correlation function  $G_{\alpha\beta\alpha'\beta'}$  (Eq. (17)), for isotropic reorientation of rigid molecules is obtained as:

$$G_{\alpha\beta\alpha'\beta'}(\tau) = \overline{\langle \alpha | \mathcal{H}^1(t) | \beta \rangle \langle \alpha' | \mathcal{H}^1(t) | \beta' \rangle} \exp(-\tau/\tau_c) \quad (38)$$

where  $\tau_c$  is the correlation time for the isotropic motion. On Fourier transforming the correlation function, one obtains the various spectral densities. The expressions for the real parts of the various spectral densities are given below.

(i) For auto correlated dipolar( $ij$ ) relaxation,

$$J_{ijij}(\omega) = \frac{3}{10} \left( \frac{\mu_0}{4\pi} \right)^2 \frac{\gamma_i^2 \gamma_j^2 \hbar^2}{r_{ij}^6} \left[ \frac{\tau_c}{1 + \omega^2 \tau_c^2} \right], \quad (39)$$

where  $r_{ij}$  is the distance between the spins  $i$  and  $j$ .

(ii) For auto correlated CSA( $i$ ) relaxation,

$$J_{ii}(\omega) = \frac{1}{30} \gamma_i^2 B_0^2 (\Delta\sigma_i)^2 \left[ \frac{\tau_c}{1 + \omega^2 \tau_c^2} \right], \quad (40)$$

where  $\Delta\sigma_i = (\sigma_{\parallel}^i - \sigma_{\perp}^i)$  is a measure of the CSA.

(iii) For auto correlated quadrupolar ( $Q_S$ ) relaxation,

$$J^{Q_S}(\omega) = \frac{3}{160} \left( \frac{e^2 q Q_S}{\hbar} \right)^2 \left[ \frac{\tau_c}{1 + \omega^2 \tau_c^2} \right], \quad (41)$$

where  $Q_S$  is the quadrupolar coupling constant of the nucleus  $S$ .

(iv) For CSA( $i$ )–dipole( $ij$ ) cross-correlation,

$$J_{i,ij}(\omega) = \frac{1}{10} \left( \frac{\mu_0}{4\pi} \right) \frac{\gamma_i^2 \gamma_j \hbar}{r_{ij}^3} B_0 (\Delta\sigma_i) \times \frac{1}{2} (3 \cos^2 \theta_{i,ij} - 1) \left[ \frac{\tau_c}{1 + \omega^2 \tau_c^2} \right], \quad (42)$$

where  $\theta_{i,ij}$  is the angle between the principal axis of the CSA tensor, assumed to be axially symmetric and the internuclear vector  $r_{ij}$ .

(v) For CSA( $i$ )–CSA( $j$ ) cross-correlation,

$$J_{ij}(\omega) = \frac{1}{30} \gamma_i \gamma_j B_0^2 (\Delta\sigma_i) (\Delta\sigma_j) \times \frac{1}{2} (3 \cos^2 \theta_{i,j} - 1) \left[ \frac{\tau_c}{1 + \omega^2 \tau_c^2} \right], \quad (43)$$

where  $\theta_{i,j}$  is the angle between the principal axis of the two CSA tensors, both of which are assumed to be axially symmetric.

(vi) For dipole( $ij$ )–dipole( $kl$ ) cross-correlation,

$$J_{ijkl}(\omega) = \frac{3}{10} \left( \frac{\mu_0}{4\pi} \right)^2 \frac{\gamma_i \gamma_j \gamma_k \gamma_l \hbar^2}{r_{ij}^3 r_{kl}^3} \times \frac{1}{2} (3 \cos^2 \theta_{ij,kl} - 1) \left[ \frac{\tau_c}{1 + \omega^2 \tau_c^2} \right], \quad (44)$$

where  $\theta_{ij,kl}$  is the angle between the two dipolar vectors  $r_{ij}$  and  $r_{kl}$ .

(vii) For quadrupole( $Q_s$ )–CSA( $i$ ) cross-correlation,

$$J^{Q_s, CSA_i}(\omega) = \frac{1}{80} (e^2 q Q_s) (\omega_i \Delta \sigma_i) \times (3 \cos^2 \theta_{Q_s, CSA_i} - 1) \times \left[ \frac{\tau_c}{1 + \omega^2 \tau_c^2} \right], \quad (45)$$

where  $\theta_{Q_s, CSA_i}$  is the angle between the quadrupolar and CSA tensors, both of which are assumed to be axially symmetric.

(viii) For quadrupole( $Q_s$ )–dipole( $ij$ ) cross-correlation,

$$J^{Q_s, D_{ij}}(\omega) = \frac{3}{80} \left( \frac{\mu_0}{4\pi} \right) (e^2 q Q_s) \left( \frac{\gamma_i \gamma_j \hbar}{r_{ij}^3} \right) \times (3 \cos^2 \theta_{Q_s, D_{ij}} - 1) \left[ \frac{\tau_c}{1 + \omega^2 \tau_c^2} \right], \quad (46)$$

where  $\theta_{Q_s, D_{ij}}$  is the angle between the dipolar vector  $ij$  and the axis of the quadrupolar tensor, which is assumed to be axially symmetric.

The expressions for the DFS ( $K$ ) can be obtained from the above Eqs. (39)–(46) by converting the absorptive Lorentzians into dispersive Lorentzians, by multiplying the numerators on the RHS with  $\omega \tau_c$ .

Cross-correlations which do not contain the distance between the relevant interactions explicitly, namely, CSA–CSA cross-correlations  $J_{i,j}(\omega)$ ,  $K_{i,j}(\omega)$ ; CSA–dipole cross-correlations  $J_{i,jl}(\omega)$ ,  $K_{i,jl}(\omega)$ ; dipole–dipole cross-correlations  $J_{ij,kl}(\omega)$ ,  $K_{ij,kl}(\omega)$ ; and those involving quadrupole interaction  $J^{Q_s, CSA_i}(\omega)$ ,  $K^{Q_s, CSA_i}(\omega)$  and  $J^{Q_s, D_{ij}}(\omega)$ ,  $K^{Q_s, D_{ij}}(\omega)$  are termed as “remote” in this article.

### 3. Cross-correlations in longitudinal relaxation

According to the phenomenological Bloch equations [71–73], the longitudinal magnetization recovers exponentially to its equilibrium value via the spin–lattice relaxation time constant  $T_1$ . This

time constant describes the rate at which the spins exchange their energy with the lattice. A single time constant is obtained only for a two-level system. When there are more than two levels, the relaxation recovery is complex, described by the relaxation matrix given in Eq. (9). The longitudinal relaxation refers to the recovery of the diagonal elements of the density matrix to their equilibrium value governed by the first block of the kite in Fig. 1. In the absence of RF irradiation and under the “secular approximation”, the time evolution of the diagonal elements is separated from that of the off-diagonal elements. It is thus possible to discuss the time evolution of longitudinal and transverse magnetization independently. In this section, the relaxation behavior of the longitudinal magnetization is discussed. The time evolution of all the diagonal elements is in general coupled and following Eq. (20), is given (since there is no contribution from the imaginary part of  $\Gamma$ ) by [65]:

$$\frac{d\sigma_{\alpha\alpha}}{dt} = \sum_{\beta} R_{\alpha\alpha\beta\beta} (\sigma(t) - \sigma_0)_{\beta\beta}. \quad (47)$$

where

$$R_{\alpha\alpha\beta\beta} = 2J_{\alpha\beta\alpha\beta}(\omega_{\alpha\beta}) - 2\delta_{\alpha\beta} \sum_{\gamma} J_{\gamma\alpha\gamma\alpha}(\omega_{\gamma\alpha}). \quad (48)$$

For  $\alpha = \beta$ ,

$$R_{\alpha\alpha\alpha\alpha} = -2 \sum_{\gamma \neq \alpha} J_{\gamma\alpha\gamma\alpha}(\omega_{\gamma\alpha}) \quad (49)$$

and for  $\alpha \neq \beta$ ,

$$R_{\alpha\alpha\beta\beta} = 2J_{\alpha\beta\alpha\beta}(\omega_{\alpha\beta}) \quad (50)$$

This means that there is no adiabatic contribution to longitudinal relaxation. However, the flip–flop term of dipolar interaction between homonuclear spins, which does contribute to longitudinal relaxation has a very low or zero frequency and looks “adiabatic”.

Eq. (47) is identical to the rate equation describing the recovery of the populations of various energy levels ( $P_{\alpha} = \sigma_{\alpha\alpha}$ ) to their equilibrium values ( $P_{\alpha}^0$ ) through the transition probability approach, written as [1,74]:

$$\frac{dP_{\alpha}}{dt} = \sum_{\beta} W_{\alpha\beta} (P_{\beta} - P_{\beta}^0) \quad (51)$$

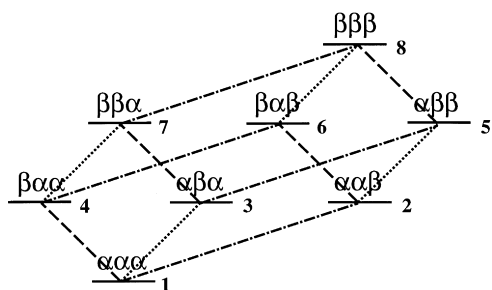


Fig. 2. Energy level diagram of a weakly coupled three-spin system, *AMX*. Here  $\alpha$  and  $\beta$  correspond to the eigenstates of  $I_z$  for each spin [ $\alpha \equiv m_z = (1/2)$ ,  $\beta \equiv m_z = -(1/2)$ ] and their product represents the various eigenstates of the three-spin system. The dashed lines represent the four single quantum transitions of the *A*-spin, the dotted those of spin *M* and the dash–dot lines those of spin *X*.

where  $W_{\alpha\beta} = R_{\alpha\alpha\beta\beta}$  are the transition probabilities, and  $W_{\alpha\alpha} = -\sum_{\beta \neq \alpha} W_{\alpha\beta}$ . For a two-spin-(1/2) system (*AX*), Eq. (51), when expanded is obtained as:

$$\frac{d}{dt} \begin{pmatrix} P_1 \\ P_2 \\ P_3 \\ P_4 \end{pmatrix} = - \begin{pmatrix} -(W_{12} + W_{13} + W_2) & W_{12} & W_{13} & W_2 \\ W_{12} & -(W_{12} + W_0 + W_{24}) & W_0 & W_{24} \\ W_{13} & W_0 & -(W_{13} + W_0 + W_{34}) & W_{34} \\ W_2 & W_{24} & W_{34} & -(W_2 + W_{24} + W_{34}) \end{pmatrix} \begin{pmatrix} P_1 - P_1^0 \\ P_2 - P_2^0 \\ P_3 - P_3^0 \\ P_4 - P_4^0 \end{pmatrix}, \quad (52)$$

where the various transition probabilities assuming CSA and mutual dipolar relaxations, are given by [45]:

$$\begin{pmatrix} W_{12} \\ W_{34} \end{pmatrix} = \frac{1}{2} \begin{pmatrix} 1 & 4 & 4 \\ 1 & 4 & -4 \end{pmatrix} \begin{pmatrix} J_{AXAX}(\omega) \\ J_{AA}(\omega) \\ J_{A,AX}(\omega) \end{pmatrix} \quad (53)$$

and

$$W_2 = W_{14} = 2J_{AXAX}(2\omega) \quad W_0 = W_{23} = \frac{1}{3}J_{AXAX}(0). \quad (54)$$

The single quantum transition probabilities of the other spin can be obtained by interchanging the labels. The two single quantum transition probabilities of spin *A* ( $W_{12}$  and  $W_{34}$ ) differ only due to CSA–dipole

cross-correlation,  $J_{A,AX}(\omega)$ , which gives an equal and opposite contribution to  $W_{12}$  and  $W_{34}$ . At this point, it may be worth pointing out that while the relaxation of the various populations is described by the above rate equations, the result of a measurement is dependent upon whether all the transitions of a spin are resolved or not. In the presence of J-coupling, one can monitor differences between the intensities of various transitions yielding a “multiplet” and a “net” effect, while in its absence, it is not possible to detect the “multiplet” effect and only the “net” effect is observable. In the presence of strong coupling, a clean separation of the multiplet and the net effect is not possible and one has to calculate the total effect on each transition. The discussion on longitudinal relaxation is continued in the next sections along the following lines. First, the magnetization modes are introduced, and their utility in cross-correlation studies is pointed out. The multiplet and the net effects of cross-correlations are discussed for various spin systems, followed by a

review of experimental observations. Isolation of relaxation pathways by pulses is discussed in the last section.

### 3.1. Magnetization modes

While Eqs. (47) and (51) are the natural descriptions of longitudinal relaxation, an elegant and much more informative description, in weakly coupled spin systems, is through the “magnetization modes”. One defines single-spin magnetization modes, such as  $A_z$ ,  $M_z$ ,  $X_z, \dots$ , two-spin magnetization modes,  $2A_zM_z$ ,  $2A_zX_z$ ,  $2M_zX_z, \dots$ , and multi-spin modes up to *N* spins. Each mode represents the expectation value of the products of the corresponding spin operators. For example  $A_z(t) = \langle I_{zA} \rangle(t) = \text{Tr}\{\sigma(t)I_{zA}\}$  and  $2A_zM_z(t) = \langle 2I_{zA}I_{zM} \rangle(t) = \text{Tr}\{\sigma(t)2I_{zA}I_{zM}\}$ . It is possible to express the magnetization modes as a

linear combination of populations of various levels. As an example, we will discuss a three spin-(1/2) system *AMX*, which can easily be reduced to the two-spin system *AM* or generalized to higher spin systems without symmetry. Fig. 2 defines the labels of various states in the three-spin system *AMX*. The relation between populations  $P_i$  and magnetization modes is given by [75–77]:

$$\begin{pmatrix} E \\ A_z \\ M_z \\ X_z \\ 2A_zM_z \\ 2A_zX_z \\ 2M_zX_z \\ 4A_zM_zX_z \end{pmatrix} = \frac{1}{8} \begin{pmatrix} 1 & 1 & 1 & 1 & 1 & 1 & 1 & 1 \\ 1 & 1 & 1 & -1 & 1 & -1 & -1 & -1 \\ 1 & 1 & -1 & 1 & -1 & 1 & -1 & -1 \\ 1 & -1 & 1 & 1 & -1 & -1 & 1 & -1 \\ 1 & -1 & 1 & -1 & -1 & 1 & -1 & 1 \\ 1 & 1 & -1 & -1 & -1 & -1 & 1 & 1 \\ 1 & -1 & -1 & 1 & 1 & -1 & -1 & 1 \\ 1 & -1 & -1 & -1 & 1 & 1 & 1 & -1 \end{pmatrix} \begin{pmatrix} P_{\alpha\alpha\alpha} \\ P_{\alpha\alpha\beta} \\ P_{\alpha\beta\alpha} \\ P_{\beta\alpha\alpha} \\ P_{\alpha\beta\beta} \\ P_{\beta\alpha\beta} \\ P_{\beta\beta\alpha} \\ P_{\beta\beta\beta} \end{pmatrix} \quad (55)$$

There are  $2^N$  populations and as many magnetization modes. Eq. (55) can also be written as:

$$\vec{M} = \mathbf{V}\vec{P} \quad (56)$$

where  $\mathbf{V}$  is the transformation matrix connecting populations to modes. Similarly inverse transformation connects modes to populations and is given by:

$$\vec{P} = \mathbf{V}^{-1}\vec{M}. \quad (57)$$

The equation of motion of the modes from Eqs. (47) or (51) is obtained as:

$$\frac{d\vec{M}}{dt} = \hat{\Gamma}(\vec{M}(t) - \vec{M}^0) \quad (58)$$

where

$$\hat{\Gamma} = \mathbf{V}\mathbf{W}\mathbf{V}^{-1} \quad (59)$$

and  $\vec{M}^0$  represents the equilibrium value of each mode. For the three-spin system *AMX*, the various transition probabilities of the *A* spin, for CSA and

dipolar relaxation mechanisms are given by [78]:

$$\begin{pmatrix} W_{14} \\ W_{37} \\ W_{26} \\ W_{58} \end{pmatrix} = \begin{pmatrix} W_{1A}^{\alpha\alpha} \\ W_{1A}^{\beta\alpha} \\ W_{1A}^{\alpha\beta} \\ W_{1A}^{\beta\beta} \end{pmatrix} = \frac{1}{2} \begin{pmatrix} 1 & 1 & 4 \\ 1 & 1 & 4 \\ 1 & 1 & 4 \\ 1 & 1 & 4 \end{pmatrix} \begin{pmatrix} J_{AMAM}(\omega_A) \\ J_{AXAX}(\omega_A) \\ J_{AA}(\omega_A) \end{pmatrix} + \begin{pmatrix} 1 & -2 & -2 \\ -1 & 2 & -2 \\ -1 & -2 & 2 \\ 1 & 2 & 2 \end{pmatrix} \begin{pmatrix} J_{AMAX}(\omega_A) \\ J_{A,AM}(\omega_A) \\ J_{A,AX}(\omega_A) \end{pmatrix}$$

$$W_{2AM} = 2J_{AMAM}(\omega_A + \omega_M)$$

$$W_{0AM} = (\frac{1}{3})J_{AMAM}(\omega_A - \omega_M) \quad (60)$$

with similar expressions for the *M* and *X* spins with appropriate change of indices. It may be noted that while auto-correlations give equal contributions to all the  $W_1$ , cross-correlations contribute differentially to various  $W_1$  and make them unequal. Furthermore, cross-correlations contribute only to  $W_1$  and not to  $W_2$  or  $W_0$  terms (see Section 3.1.4). The equation of motion for the magnetization modes (Eq. (58)) in the

expanded form is obtained as:

$$\begin{aligned}
 & -\frac{d}{dt} \begin{pmatrix} E \\ A_z(t) \\ M_z(t) \\ X_z(t) \\ 2A_z M_z(t) \\ 2A_z X_z(t) \\ 2M_z X_z(t) \\ 4A_z M_z X_z(t) \end{pmatrix} \\
 & = \begin{pmatrix} 0 & 0 & 0 & 0 & 0 & 0 & 0 & 0 \\ 0 & \rho_A & \sigma_{AM} & \sigma_{AX} & \delta_{A,AM} & \delta_{A,AX} & 0 & \delta_A \\ 0 & \sigma_{AM} & \rho_M & \sigma_{MX} & \delta_{M,AM} & 0 & \delta_{M,MX} & \delta_M \\ 0 & \sigma_{AX} & \sigma_{MX} & \rho_X & 0 & \delta_{X,AX} & \delta_{X,MX} & \delta_X \\ 0 & \delta_{A,AM} & \delta_{M,AM} & 0 & \rho_{AM} & \delta_A + \sigma_{MX} & \delta_M + \sigma_{AX} & \delta_{A,AX} + \delta_{M,MX} \\ 0 & \delta_{A,AX} & 0 & \delta_{X,AX} & \delta_A + \sigma_{MX} & \rho_{AX} & \delta_X + \sigma_{AM} & \delta_{A,AM} + \delta_{X,MX} \\ 0 & 0 & \delta_{M,MX} & \delta_{X,MX} & \delta_M + \sigma_{AX} & \delta_X + \sigma_{AM} & \rho_{MX} & \delta_{M,AM} + \delta_{X,AX} \\ 0 & \delta_A & \delta_M & \delta_X & \delta_{A,AX} + \delta_{M,MX} & \delta_{A,AM} + \delta_{X,MX} & \delta_{M,AM} + \delta_{X,AX} & \rho_{AMX} \end{pmatrix} \\
 & \times \begin{pmatrix} E \\ A_z(t) - A_z^0 \\ M_z(t) - M_z^0 \\ X_z(t) - X_z^0 \\ 2A_z M_z(t) \\ 2A_z X_z(t) \\ 2M_z X_z(t) \\ 4A_z M_z X_z(t) \end{pmatrix} \tag{61}
 \end{aligned}$$

Here the various  $\rho$  terms describe the self-relaxation of each mode,  $\sigma$ , the cross relaxation between modes of the same order, and  $\delta$  the cross relaxation between modes of different orders. The expressions for these elements, for the three spin system, are obtained as:

$$\begin{aligned}
 \rho_A & = (W_{2AM} + W_{0AM}) + (W_{2AX} + W_{0AX}) \\
 & + \frac{1}{2}(W_{1A}^{\alpha\alpha} + W_{1A}^{\beta\alpha} + W_{1A}^{\alpha\beta} + W_{1A}^{\beta\beta})
 \end{aligned}$$

$$\begin{aligned}
 \rho_{AM} & = (W_{2AX} + W_{0AX}) + (W_{2MX} + W_{0MX}) \\
 & + \frac{1}{2}[(W_{1A}^{\alpha\alpha} + W_{1A}^{\beta\alpha} + W_{1A}^{\alpha\beta} + W_{1A}^{\beta\beta}) \\
 & + (W_{1M}^{\alpha\alpha} + W_{1M}^{\beta\alpha} + W_{1M}^{\alpha\beta} + W_{1M}^{\beta\beta})] \\
 \rho_{AMX} & = \frac{1}{2}[(W_{1A}^{\alpha\alpha} + W_{1A}^{\beta\alpha} + W_{1A}^{\alpha\beta} + W_{1A}^{\beta\beta}) \\
 & + (W_{1M}^{\alpha\alpha} + W_{1M}^{\beta\alpha} + W_{1M}^{\alpha\beta} + W_{1M}^{\beta\beta}) \\
 & + (W_{1X}^{\alpha\alpha} + W_{1X}^{\beta\alpha} + W_{1X}^{\alpha\beta} + W_{1X}^{\beta\beta})] \tag{62}
 \end{aligned}$$

or in terms of the spectral densities as:

$$\begin{pmatrix} \rho_A \\ \rho_{AM} \\ \rho_{AMX} \end{pmatrix} = \frac{1}{3} \begin{pmatrix} 1 & 1 & 0 \\ 0 & 1 & 1 \\ 0 & 0 & 0 \end{pmatrix} \begin{pmatrix} J_{AMAM}(\omega_A - \omega_M) \\ J_{AXAX}(\omega_A - \omega_X) \\ J_{MXMX}(\omega_M - \omega_X) \end{pmatrix} \\
 + \begin{pmatrix} 1 & 0 & 1 & 0 & 0 & 0 \\ 1 & 1 & 1 & 0 & 1 & 0 \\ 1 & 1 & 1 & 1 & 1 & 1 \end{pmatrix} \begin{pmatrix} J_{AMAM}(\omega_A) \\ J_{AMAM}(\omega_M) \\ J_{AXAX}(\omega_A) \\ J_{AXAX}(\omega_X) \\ J_{MXMX}(\omega_M) \\ J_{MXMX}(\omega_X) \end{pmatrix} \\
 + 2 \begin{pmatrix} 1 & 1 & 0 \\ 0 & 1 & 1 \\ 0 & 0 & 0 \end{pmatrix} \begin{pmatrix} J_{AMAM}(\omega_A + \omega_M) \\ J_{AXAX}(\omega_A + \omega_X) \\ J_{MXMX}(\omega_M + \omega_X) \end{pmatrix} \\
 + 4 \begin{pmatrix} 1 & 0 & 0 \\ 1 & 1 & 0 \\ 1 & 1 & 1 \end{pmatrix} \begin{pmatrix} J_{AA}(\omega_A) \\ J_{MM}(\omega_M) \\ J_{XX}(\omega_X) \end{pmatrix} \quad (63)$$

and

$$\begin{aligned} \sigma_{AM} &= W_{2AM} - W_{0AM} \\ &= 2J_{AMAM}(\omega_A + \omega_M) - \frac{1}{3}J_{AMAM}(\omega_A - \omega_M) \\ \delta_{A,AM} &= \frac{1}{2}(-W_{1A}^{\alpha\alpha} + W_{1A}^{\beta\alpha} - W_{1A}^{\alpha\beta} + W_{1A}^{\beta\beta}) \\ &= 4J_{A,AM}(\omega_A) \\ \delta_{A,AX} &= \frac{1}{2}(-W_{1A}^{\alpha\alpha} - W_{1A}^{\beta\alpha} + W_{1A}^{\alpha\beta} + W_{1A}^{\beta\beta}) \\ &= 4J_{A,AX}(\omega_A) \\ \delta_A &= \delta_{AMAX} = \frac{1}{2}(W_{1A}^{\alpha\alpha} - W_{1A}^{\beta\alpha} - W_{1A}^{\alpha\beta} + W_{1A}^{\beta\beta}) \\ &= 2J_{AMAX}(\omega_A). \end{aligned} \quad (64)$$

It may be noted that  $\rho$  and  $\sigma$  contain exclusively only auto-correlation spectral densities. Modes of different orders are coupled exclusively by cross-correlations ( $\delta_{i,ij}$  and  $\delta_i$ ). The even order modes are connected to odd order modes by cross-correlation between CSA and dipolar relaxation ( $\delta_{i,ij}$

terms); the odd order modes are connected to odd order modes and even order modes to even order modes by cross-correlation between different dipolar interactions of the spin ( $\delta_i = \delta_{ij,ik}$  terms). In the absence of cross-correlations,  $\hat{T}$  would be block-diagonal with off-diagonal elements only within the modes of the same order. The block connecting the single-spin modes yields an equation of motion for the single-spin modes given by:

$$\frac{dI_{zi}(t)}{dt} = \mathcal{R}[I_{zi}(t) - I_{zi}(\infty)], \quad (65)$$

where  $I_{zi}(t)$  is the longitudinal magnetization of spin  $i$  at time  $t$ ,  $I_{zi}(\infty)$  its equilibrium value and  $\mathcal{R}$  connects various  $I_{zi}(t)$ .  $\mathcal{R}$  is a subset of the  $\hat{T}$  matrix given for the three spin system by:

$$\mathcal{R} = \begin{pmatrix} \rho_A & \sigma_{AM} & \sigma_{AX} \\ \sigma_{AM} & \rho_M & \sigma_{MX} \\ \sigma_{AX} & \sigma_{MX} & \rho_X \end{pmatrix}. \quad (66)$$

Eq. (65) is Solomon's equation [79]. This equation describes the self-relaxation ( $\rho_i$ ) of each spin and cross relaxation ( $\sigma_{ij}$ ) of the spins with each other (NOE) in the absence of cross-correlations. This equation is widely used for the interpretation of NOE in many systems including biomolecular structural studies. In such cases, coupled relaxation of a large number of spins is analyzed by fitting the calculated NOE to the experimental NOE assuming a certain geometry for the molecule. When cross-correlations are present, the higher spin modes come into play and the longitudinal relaxation as well as NOE predicted by Eq. (65) are incorrect. It is therefore necessary to take the higher spin modes into account, even when J-couplings are absent.

### 3.1.1. Representation of modes

The advantage of the modes description is that they represent various observable quantities in a convenient form. The single-spin modes ( $A_z, M_z, \dots$ ) represent the total magnetization of a spin and the higher modes represent the differences in the intensities of various transitions of a spin. The intensities of various transitions of a spin are given by:

$$I_{\alpha\beta} = |(I_x)_{\alpha\beta}|^2 (P_\alpha - P_\beta). \quad (67)$$

For weakly coupled spins (each of spin 1/2) all

$|(I_x)_{\alpha\beta}|^2$  are equal. Therefore the relative intensities of the various transitions are given by:

$$I_{\alpha\beta} = P_{\alpha} - P_{\beta}. \quad (68)$$

For a weakly coupled three-spin system of the type *AMX*, the intensities of the various transitions of the spin *A* are then obtained (from Eq. (55)) as:

$$\begin{aligned} A_1 &= P_{\alpha\alpha\alpha} - P_{\beta\alpha\alpha} \\ &= \frac{1}{4}(A_z - 2A_zM_z - 2A_zX_z + 4A_zM_zX_z) \\ A_2 &= P_{\alpha\alpha\beta} - P_{\beta\alpha\beta} \\ &= \frac{1}{4}(A_z - 2A_zM_z + 2A_zX_z - 4A_zM_zX_z) \\ A_3 &= P_{\alpha\beta\alpha} - P_{\beta\beta\alpha} \\ &= \frac{1}{4}(A_z + 2A_zM_z - 2A_zX_z - 4A_zM_zX_z) \\ A_4 &= P_{\alpha\beta\beta} - P_{\beta\beta\beta} \\ &= \frac{1}{4}(A_z + 2A_zM_z + 2A_zX_z + 4A_zM_zX_z). \end{aligned} \quad (69)$$

The total intensity of all the four transitions is given by  $A_z$ . Any difference in the intensities of these transitions indicates the presence of modes of higher order. For example, if  $A_1 = A_4 \neq A_2 = A_3$  and  $A_z \neq 0$ , single- and three-spin modes are present and two-spin modes are absent (Fig. 3(a)). On the other hand, if  $A_1 = A_2 \neq A_3 = A_4$  or  $A_1 = A_3 \neq A_2 = A_4$  with  $A_z = 0$  indicates the presence of only two-spin modes and absence of one and three spin modes (Fig. 3(c)). However, if  $A_1 \neq A_2 \neq A_3 \neq A_4$  with  $A_z = 0$  indicates the presence of both two- and three-spin modes. The differences in the intensities of these transitions can be created either by selective perturbation of one or more transitions of the spin system or by cross correlated relaxation of a non-equilibrium state.

Before proceeding further, it may be pointed out that the inclusion of cross-correlations increases exponentially the dimension of the relaxation matrix to be handled. For example, Solomon's equations (Eq. (65)) in which cross-correlations are neglected, consist of  $N$  simultaneous equations with the dimensions of the relaxation matrix being  $N \times N$ , where  $N$  is the number of relaxation-coupled spins. Inclusion of cross-correlation requires the use of either Eqs. (47), (51) or (58), with the relaxation matrix of dimension  $2^N \times 2^N$ , if all

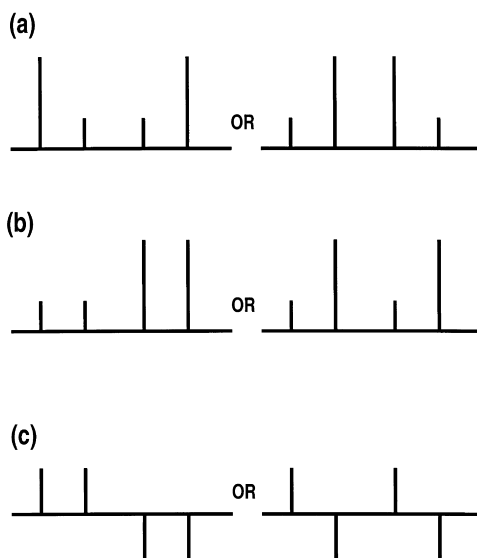


Fig. 3. Schematic representation of the intensities of the four SQCs of a spin of an *AMX* spin system, in the presence of (a) single- and three-spin modes, (b) single- and two-spin modes and (c) only two-spin modes.

the  $N$  spins are spin  $1/2$ , or of dimension  $(2I + 1)^N \times (2I + 1)^N$  if all the spins are of spin  $I$ . Thus for 10 relaxation-coupled spins of spin  $1/2$ , Solomon's equations (Eq. (65)), require only a  $10 \times 10$  relaxation matrix, while inclusion of cross-correlations requires a  $1024 \times 1024$  matrix. In biomolecular NMR studies a  $100 \times 100$  relaxation matrix for 100 relaxation-coupled spins is often solved, neglecting cross-correlations, but it will be impossible to include cross-correlations for all the 100 relaxation-coupled spins. It is therefore important to study the effect of cross-correlations in NOE and relaxation measurements. If it turns out that cross-correlations contribute significantly, then one either takes into account the main cross-correlations or designs experiments inhibiting the effect of cross-correlations.

### 3.1.2. Initial rate approximation

The formal solution of Eq. (58) is given by:

$$\vec{M}(\tau) = \exp(-\hat{\Gamma}\tau)[\vec{M}(\tau) - \vec{M}^0]. \quad (70)$$

The time evolution of various modes is coupled and a general solution of Eq. (70) requires diagonalization of the relaxation matrix,  $\hat{\Gamma}$ . On the other hand, a

simple solution of Eq. (70) is obtained, in the initial rate approximation for small values of  $\tau$  as:

$$\vec{M}(\tau)|_{\tau \rightarrow 0} = (1 - \hat{F}\tau)[\vec{M}(\tau) - \vec{M}^0]. \quad (71)$$

Further, if at  $\tau = 0$  one creates an initial state in which only one of the modes is selectively disturbed from equilibrium, then from Eq. (71) it is seen that in the initial rate approximation, the rate of conversion of this mode into other modes is directly proportional to various elements of  $\hat{F}$ . For example, in the three-spin system described by Eq. (61), if at  $\tau = 0$  one inverts the magnetization of spin A [ $A_z(0) = -A_z^0$ ] and leaves all the other modes undisturbed [ $M_z(0) - M_z^0 = X_z(0) - X_z^0 = 0$  and all the multi-spin modes are zero] then, in the initial rate approximation the growth of all the other modes are given by:

$$\begin{aligned} M_z(\tau) &= 2\sigma_{AM}\tau A_z^0, & X_z(\tau) &= 2\sigma_{AX}\tau A_z^0, \\ 2A_z M_z(\tau) &= 2\delta_{AAM}\tau A_z^0, & 2A_z X_z(\tau) &= 2\delta_{AAX}\tau A_z^0, \\ 4A_z M_z X_z(\tau) &= 2\delta_A\tau A_z^0, & 2M_z X_z(\tau) &= 0, \end{aligned} \quad (72)$$

and the decay of the  $A_z$  mode is given by:

$$A_z(\tau) = -2(1 - \rho_A\tau)A_z^0. \quad (73)$$

The initial rate approximation thus provides a direct measure of the various elements of  $\hat{F}$ .

### 3.1.3. Magnitude of the cross terms

In this section, the magnitude of cross terms is compared with the auto terms. For dipole–dipole interactions, cross-correlation terms depend both on the distances between the interacting spins and their geometric disposition, while the auto-correlation terms depend only on the distances between the spins. The ratio of the geometric factors of cross versus auto terms in the three-spin system (AMX), for dipole–dipole cross-correlation is given (using Eqs. (39) and (44)) by:

$$\frac{\delta_{AMMX}}{\sigma_{AM}} = \frac{1}{2} \left( \frac{r_{AM}}{r_{MX}} \right)^3 (3\cos^2\theta_{AMMX} - 1) \quad (74)$$

where  $\theta_{AMMX}$  is the angle between the AM and MX dipolar vectors and  $r_{AM}$  and  $r_{MX}$ , respectively, their lengths. For  $r_{AM} = r_{MX}$ , this ratio is  $-(1/8)$ ,  $-(1/2)$ ,  $(1/2)$  and 1, respectively, for  $\theta = 60, 90, 145$  and

$180^\circ$ . Dipole–dipole cross-correlations are thus most significant for linear geometry and are zero for magic angles  $54^\circ 44'$  and  $125^\circ 16'$  [75,76]. The cross terms between CSA and dipolar interaction depend both on the values of these interactions as well as their geometric disposition. The magnitude of CSA for several nuclei such as  $^{13}\text{C}$ ,  $^{15}\text{N}$  and  $^{19}\text{F}$  is large and at high fields the CSA contribution becomes a major source of relaxation for these spins [80–86]. On the other hand, the CSA for protons is small and hence usually the relaxation resulting from auto-correlation terms is negligible. While the CSA auto-correlation terms may be negligible, the cross terms with dipolar interaction can be quite significant. For example, if the dipolar interaction is 10 times the CSA, then the contribution to relaxation of the spin by CSA auto-correlation terms is 1/100th of its relaxation by dipolar auto-correlation terms, whereas that of the cross terms will be 1/10th of dipolar auto-correlation terms. Thus, although the auto-correlation contribution of CSA may be negligible, its cross term with large dipolar interaction will not be. The magnitude of the cross terms additionally depends on the angle  $\theta$  between the dipolar vector and the principal axis of an axially symmetric CSA tensor via a multiplicative factor  $(1/2)(3\cos^2\theta - 1)$  for isotropically reorienting molecules (see Eq. (42)).

### 3.1.4. Cross-correlations contribute only to $W_1$

It was pointed out in Section 3.1 that in weakly coupled spins, in the absence of RF fields, cross-correlations contribute to longitudinal relaxation only through spectral densities at the Larmor frequency, that is only to  $W_1$  and not to  $W_0$  and  $W_2$  (Eq. (60)). This can also be explained via the following argument. Longitudinal relaxation is governed by the first block of the Redfield matrix (Fig. 1), which connects the various diagonal elements of  $\sigma$  through elements such as:

$$R_{\alpha\alpha\beta\beta} = J_{\alpha\beta\alpha\beta} \propto \overline{\langle \alpha | \mathcal{H}'(t) | \beta \rangle \langle \alpha | \mathcal{H}'(t + \tau) | \beta \rangle} \quad (75)$$

with

$$R_{\alpha\alpha\alpha\alpha} = - \sum_{\beta \neq \alpha} R_{\alpha\alpha\beta\beta}. \quad (76)$$

Longitudinal relaxation thus requires spectral density elements  $J_{\alpha\beta\alpha\beta}$  for which  $\alpha \neq \beta$ . Diagonal operators

$I_{iz}$  and  $I_{iz}I_{jz}$  of  $\mathcal{H}^1$  therefore do not contribute to longitudinal relaxation of weakly coupled spins while the operator  $I_{i\pm}I_{j\mp}$  contributes to  $W_0$ , operators  $I_{i\pm}$  and  $I_{iz}I_{j\pm}$  to  $W_1$  and  $I_{i\pm}I_{j\pm}$  to  $W_2$ . Cross-correlations require that two different interactions connect the same pair of states. This is possible only by spin operators in which the flipping (active) spin is common and non-flipping (passive) spin is different. Two different operators such as  $I_{i\pm}I_{jz}$  and  $I_{i\pm}I_{kz}$  can connect the same pair of spin states. For example, in the three-spin system, states  $\alpha\alpha\alpha$  and  $\beta\alpha\alpha$  can be connected by dipolar interaction between spins 1 and 2 as well as between 1 and 3, respectively, by terms,  $I_{1\pm}I_{2z}$  and  $I_{1\pm}I_{3z}$  where the active spin is 1 and the passive spins are 2 and 3. Thus, in weakly coupled spins cross-correlations can only contribute to values of  $W_1$ , while auto-correlations contribute to the spectral densities at all the three frequencies. The auto-correlation terms contribute equal rates to various  $W_1$  terms of a spin and cross-correlations make the various  $W_1$  terms of a spin unequal. For example, in the weakly coupled three spin system the presence of dipole–dipole cross-correlation makes the  $W_1^A$  of outer and inner transitions unequal such that  $W_1^{A1} = W_1^{A4} \neq W_1^{A2} = W_1^{A3}$ , while the cross-correlations between CSA and dipolar interaction makes  $W_1^{A1} = W_1^{A2} \neq W_1^{A3} = W_1^{A4}$ . The dipole–dipole cross-correlation between the spin pairs 1, 2 and 1, 3 yields:

$$\begin{aligned} W_1^{A1} &\propto \langle \alpha\alpha\alpha | I_{1+}I_{2z} | \beta\alpha\alpha \rangle \langle \alpha\alpha\alpha | I_{1+}I_{3z} | \beta\alpha\alpha \rangle \\ W_1^{A2} &\propto \langle \alpha\alpha\beta | I_{1+}I_{2z} | \beta\alpha\beta \rangle \langle \alpha\alpha\beta | I_{1+}I_{3z} | \beta\alpha\beta \rangle = -W_1^{A1} \\ W_1^{A3} &\propto \langle \alpha\beta\alpha | I_{1+}I_{2z} | \beta\beta\alpha \rangle \langle \alpha\beta\alpha | I_{1+}I_{3z} | \beta\beta\alpha \rangle = -W_1^{A1} \\ W_1^{A4} &\propto \langle \alpha\alpha\beta | I_{1+}I_{2z} | \beta\beta\beta \rangle \langle \alpha\beta\beta | I_{1+}I_{3z} | \beta\beta\beta \rangle = W_1^{A1}, \end{aligned} \quad (77)$$

and the CSA–dipole cross-correlation on the other hand yields:

$$\begin{aligned} W_1^{A1} &\propto \langle \alpha\alpha\alpha | I_{1+}^{\text{CSA}} | \beta\alpha\alpha \rangle \langle \alpha\alpha\alpha | I_{1+}I_{2z} | \beta\alpha\alpha \rangle \\ W_1^{A2} &\propto \langle \alpha\alpha\beta | I_{1+}^{\text{CSA}} | \beta\alpha\beta \rangle \langle \alpha\alpha\beta | I_{1+}I_{2z} | \beta\alpha\beta \rangle = W_1^{A1} \\ W_1^{A3} &\propto \langle \alpha\beta\alpha | I_{1+}^{\text{CSA}} | \beta\beta\alpha \rangle \langle \alpha\beta\alpha | I_{1+}I_{2z} | \beta\beta\alpha \rangle = -W_1^{A1} \\ W_1^{A4} &\propto \langle \alpha\beta\beta | I_{1+}^{\text{CSA}} | \beta\beta\beta \rangle \langle \alpha\beta\beta | I_{1+}I_{2z} | \beta\beta\beta \rangle = -W_1^{A1}. \end{aligned} \quad (78)$$

Cross-correlations thus contribute a purely differential effect to the transition probabilities.

The contribution of cross-correlations is also sensitive to the parameter  $\omega\tau_c$ . As  $\omega\tau_c$  increases beyond 1, the contributions of  $W_1$  and  $W_2$  decrease compared to  $W_0$ . This has several consequences. The magnitude of the NOE increases and tends towards its maximum value of  $-1$ , while the effect of cross-correlations on NOE decreases. While  $W_0$  distributes magnetization between the spins, the energy from the spin system to the lattice can only be carried away through  $W_1$  and  $W_2$ . Thus longitudinal relaxation via intramolecular dipolar interaction becomes weaker. The spins in the rigid part of the molecule in such a case have weaker longitudinal relaxation which is either dominated by processes other than the dipolar interactions or by migration of magnetization (through strong  $W_0$ ) to other parts of the molecule, where they encounter spins undergoing internal motion through which the energy is finally exchanged with the lattice. Thus in the rigid part of the molecule for  $\omega\tau_c > 1$ , the influence of  $W_1$  and  $W_2$  and hence the longitudinal relaxation and the effect of cross-correlations become weaker. Strong coupling mixes eigenstates, which makes all  $W_0$ ,  $W_1$  and  $W_2$  depend on cross-correlations. Furthermore, in the presence of RF field (in the so called “rotating frame experiments”) cross-correlations come into play in  $W_0$  and  $W_2$  as well. This is again due to the mixing of states by the RF field. While strong coupling mixes states within the same  $F_z (= \sum_i I_{zi})$  manifold of states, the RF field mixes states which differ in their  $F_z$  values by  $\pm 1$ . The following section discusses the multiplet and net effect of cross-correlation in relaxation of weakly coupled spins, in the absence of RF fields.

### 3.2. Multiplet and net effect of cross-correlations

The effects of cross-correlation can be classified into two types. A multiplet effect is a case in which various transitions of a spin have different intensities. This is obtained by the creation of multi-spin orders from single-spin orders by cross-correlations and is a first-order process in time. A second-order effect, the net effect, which is a two-step process, involves creation of multi-spin order from single-spin order and reconversion of multi-spin order into single-spin order, both by cross-correlations. Observation of the

multiplet effect requires that the various transitions of the spin are resolved via the J-couplings. If the J-couplings are either not resolved or absent, the created multi-spin orders are not observable. Even when the J-couplings are resolved, observation of the multi-spin order (or multiplet effect) requires the use of either a selective measuring pulse on one of the spins or a small angle non-selective pulse on more than one spin. A non-selective  $90^\circ$  measuring pulse converts the multi-spin longitudinal order into undetectable multiple quantum coherences and thus suppresses the multiplet effect. However, the net effect is always present and not easily suppressed. There are several experiments, which are used for the detection of the multiplet and net effect of cross-correlations. Single-spin order can be created by selective inversion of a spin, or non-selective inversion of all coupled spins. The inverted spins exchange magnetization via the  $\sigma$  terms (NOE) and recover non-exponentially due to the presence of several cross-relaxation terms containing auto and cross-correlations, giving rise to multiplet and net effects. The selective inversion experiments are equivalent to various cross-sections of a 2D NOESY experiment. Each cross-section of the 2D NOESY experiment using an  $\alpha^\circ$  measuring pulse ( $90^\circ-t_1-90^\circ-\tau_m-\alpha^\circ-t_2$  experiment) is equivalent [except for a factor of  $(1/2)$ ] [72,73] to a 1D transient NOE experiment in which the whole multiplet of a spin is selectively inverted at  $\tau_m = 0$  and the state of the spin system after  $\tau_m$  is detected by an  $\alpha^\circ$  pulse [87,88]. The multiplet [87–91] and the net effects [92–95] due to dipole–dipole cross-correlations have been studied in detail by several investigators and are described in detail in the following sections. The main emphasis in these studies is to describe the effect of dipole–dipole cross-correlations on NOE. A particularly illustrative example is the weakly coupled three-spin system, which will be described here in some detail. Dipole–dipole cross-correlations, which couple only odd orders (single and triple) and even orders (zero and double) among themselves will be considered. It will be further assumed that the initial perturbation creates only single-spin order.

### 3.2.1. Multiplet effect in three spin system AMX

The multiplet effect of dipole–dipole cross-correlation, in a weakly coupled three-spin system has been described in the literature in detail [87–91]. Fig. 4

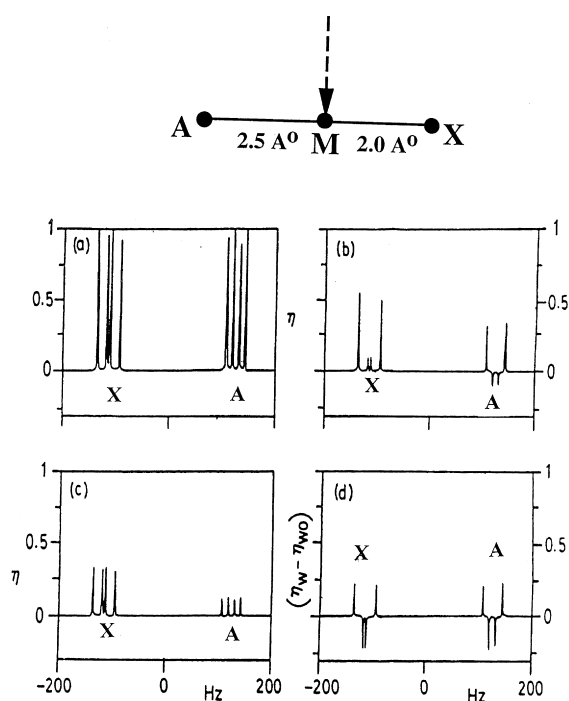


Fig. 4. Calculated transient NOE spectra of the A and X parts of the linear AMX spin system, for selective inversion of the M spin at  $\tau_m = 0$ . (a) Normal spectrum; (b) and (c) are the transient difference NOE spectra calculated with and without cross-correlations; (d) is the difference between (b) and (c). The parameters used to calculate the spectra are  $J_{AM}/\delta_{AM} = 0.05$ ,  $J_{AM} = 12$  Hz,  $J_{AX} = 9$  Hz and  $J_{MX} = 6$  Hz,  $r_{AM} = 2.5$  Å and  $r_{MX} = 2.0$  Å,  $\tau_m = 2$  s,  $\omega\tau_c = 0.1$  and  $\omega/(2\pi) = 270$  MHz. [Reproduced with permission from V.V. Krishnan, Anil Kumar, J. Magn. Reson. 92 (1991) 293.]

shows an example of the calculated NOE on spins A and X, with and without cross-correlation for selective inversion of spin M at  $\tau_m = 0$  in an AMX spin system. The NOE is larger at spin X than spin A, but the effect of cross-correlations in the form of the multiplet effect is identical. This is due to the creation of a single three-spin-order term by cross-correlations. Since CSA–dipole cross-correlations have not been considered in this study, the two-spin orders are not created. The effect of variation of the angle,  $\beta = \angle MAX$ , keeping the distances,  $r_{AX} = 4.5$  Å and  $r_{AM} = 2.5$  Å, constant is shown in Fig. 5. The total NOE on spin A remains practically unaffected but on spin X decreases monotonically, since as  $\beta$  increases  $r_{MX}$  increases. The multiplet effect is however sensitive to  $\beta$  and is maximum for  $\beta = 0^\circ$ .

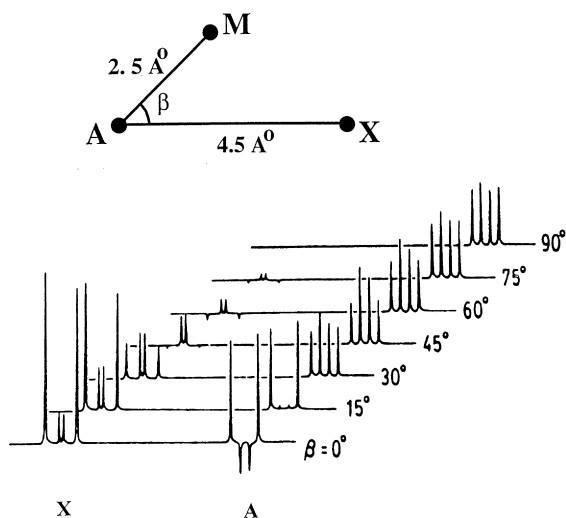


Fig. 5. Calculated transient NOE spectra of the A and X parts of the AMX spin system with dipole–dipole cross-correlations for various geometric disposition of the three spins, obtained by changing  $\angle MAX = \beta$  from 0 to 90°. The remaining parameters and conditions used for this simulation are the same as Fig. 4. [Reproduced with permission from V.V. Krishnan, Anil Kumar, J. Magn. Reson. 92 (1991) 293.]

The time evolution of cross-correlations as a function of mixing time is given in Fig. 6 for the  $\beta = 0^\circ$  case. The dashed curves show the NOE on each transition in the absence of cross-correlations, for three motional regimes namely,  $\omega\tau_c = 0.1$ , 1.118 and 10 corresponding to short, critical and long correlation times, respectively. In the absence of cross-correlations, the NOE on all transitions of a spin is equal. The difference between the NOE calculated with and without cross-correlations is shown with solid curves. In the case of weakly coupled spins, considering only dipole–dipole cross-correlations, the intensities of inner as well as the two outer transitions of each spin are equal, that is,  $A_1 = A_4 \neq A_2 = A_3$  and  $X_1 = X_4 \neq X_2 = X_3$ . Therefore only two transitions of each spin are shown. Furthermore, since in a three-spin system, there is only one three-spin order term namely  $4A_z M_z X_z$ , its contribution to all the three spins is identical, yielding  $A_1 - A_2 = M_1 - M_2 = X_1 - X_2 = 4A_z M_z X_z$ . These curves show that there is a very large multiplet effect of cross-correlations in all motional regimes, which starts from zero, builds up to a maximum value and decreases to zero, in a manner similar to the transient NOE (single-spin order). The multiplet

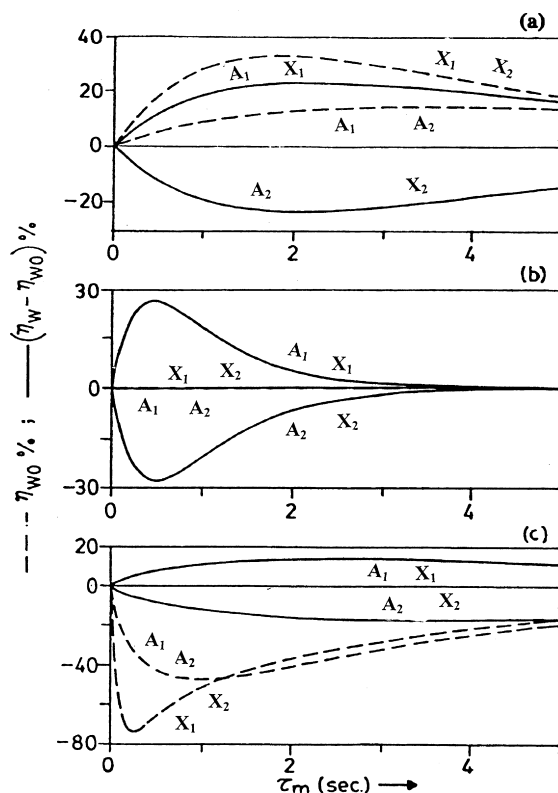


Fig. 6. Difference between the calculated transient NOE for an AMX spin system with and without cross-correlations ( $\eta_W - \eta_{W_0}$ ) in percentage (continuous curves) and the NOE without cross-correlations,  $\eta_{W_0}$  in percentage (dashed curves), for the A and X multiplets, when the M spin transitions are nonselectively inverted at  $\tau_m = 0$ , plotted as a function of the mixing time  $\tau_m$  for (a)  $\omega\tau_c = 0.1$ , (b)  $\omega\tau_c = 1.118$  and (c)  $\omega\tau_c = 10$ . The remaining parameters and conditions used for this simulation are the same as in Fig. 4. [Reproduced with permission from V.V. Krishnan, Anil Kumar, J. Magn. Reson. 92 (1991) 293.]

effect at  $\omega\tau_c = 1.118$  is particularly interesting since at this correlation time, the NOE without cross-correlations is zero. For  $\omega\tau_c = 10$ , the magnitude of cross-correlation rate is small. But for this  $\omega\tau_c$  value, the leakage term in the self-relaxation rates is also small, the magnetization remains within the spin system for long times, building-up the NOE and the three-spin order term, yielding significant effect of cross-correlation.

### 3.2.2. The net effect

The net effect of cross-correlations is the difference in single-spin orders in the presence and absence of

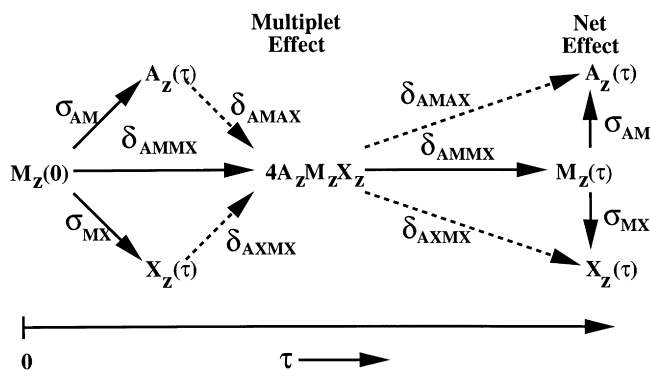


Fig. 7. Pictorial representation of the magnetization evolution, in a linear three-spin AMX system, after selective inversion of  $M$  spin at  $\tau_m = 0$  for the long correlation time limit ( $\omega\tau_c \gg 1$ ). In this situation, the NOE on spin  $A$  and  $X$  builds up quickly via the  $\sigma$  terms. At the same time, the three-spin order term  $4A_z M_z X_z$  is created via the cross-correlation  $\delta_{AMMX}$ . As a second-order process in time, the three-spin order term is reconverted to  $M_z$  via  $\delta_{AMMX}$ , which on further evolution is converted back to  $A_z$  and  $M_z$ . A three-spin-order term is also created from  $A_z$ ,  $M_z$  and converted back to  $A_z$ ,  $M_z$  via the smaller cross-correlations (in the linear spin system) namely,  $\delta_{AMAX}$  and  $\delta_{AXMX}$ . These pathways are shown by the dashed lines.

cross-correlations. This effect has been discussed in detail by several workers [92–95]. The presence of the net effect on NOE is also noticeable in the curves of Fig. 6, a careful examination of which shows that the multiplet effect on various transitions, though opposite in sign, is not completely identical in magnitude. This net effect arises from second-order processes in time. If at  $\tau_m = 0$ , one creates a single-spin mode (say  $M_z$ ), then as a function of  $\tau_m$ , it is converted into the three-spin mode  $4A_z M_z X_z$  and back to single-spin mode  $M_z$  by the cross-correlation rate  $\delta_{AMMX}$ . The single-spin mode  $M_z$  thus created is converted by cross-relaxation rates  $\sigma_{AM}$  and  $\sigma_{AX}$  into  $A_z$  and  $X_z$ , respectively, changing the net NOE on spins  $A$  and  $X$  and self relaxation of spin  $M$  (Fig. 7). The magnitude of the calculated net effect in the three spin system, AMX, after selective inversion of spin  $M$  for linear, right isosceles and equilateral triangle geometries, for  $\omega\tau_c = 0.1$ , 1.118 and 10, are shown in Fig. 8(a)–(c) [93]. In these diagrams, the NOE on spins  $A$  and  $X$  are identical due to symmetry. For these geometries, for isotropic reorientations, the ratio of  $\delta_{AMMX}/\sigma_{AM} = 1$ , 0.5 and 0.125, respectively. It is clearly seen that the effect of cross-correlations is large for the linear case, and small for the remaining geometries for all correlation times. Furthermore, for  $\omega\tau_c = 1.118$ , the total NOE on spins  $A$  and  $X$  builds up via cross-correlations, since all terms are zero for this correlation time. A common feature of net NOE for all

correlation times is that for short mixing times, the net effect is small and builds-up slowly to its maximum value at fairly large mixing times, indicative of the second-order process in time as well as magnitude. For  $\omega\tau_c = 10$ , there is little leakage and the magnetization remains within the spin system for a very long time, building up the net effect of cross-correlations similar to the multiplet effect. From the above curves, it seems that the net effect on NOE builds up to a significant value for large mixing times. However, these curves do not represent all correlation times properly. In order to investigate the net effect on NOE due to cross-correlations for different correlation times, the net effect is plotted in Fig. 9 for the linear case, at fixed mixing times of 100, 200 and 400 ms as a function of  $\omega\tau_c$  [93]. This figure shows that even at  $\tau_m = 400$  ms, there is a significant net effect at  $\omega\tau_c \sim 1.6$ , and that there is significant effect for  $\omega\tau_c = 2$ –5. This shows that the error arising from the neglect of cross-correlations for a given mixing time, although small, is not negligible. The error reaches its maximum value of approximately 1, 2 and 7% of the total magnetization for mixing times of 100, 200 and 400 ms, respectively, for  $\omega\tau_c$  between 1.2 and 1.6. It may be noted that the net NOE at  $\omega\tau_c = 1.6$  with cross-correlations, for the above mixing times, is 6, 11 and 16% of the total magnetization, respectively. Thus the error is about 16, 18 and 44% of the net NOE at these mixing times.

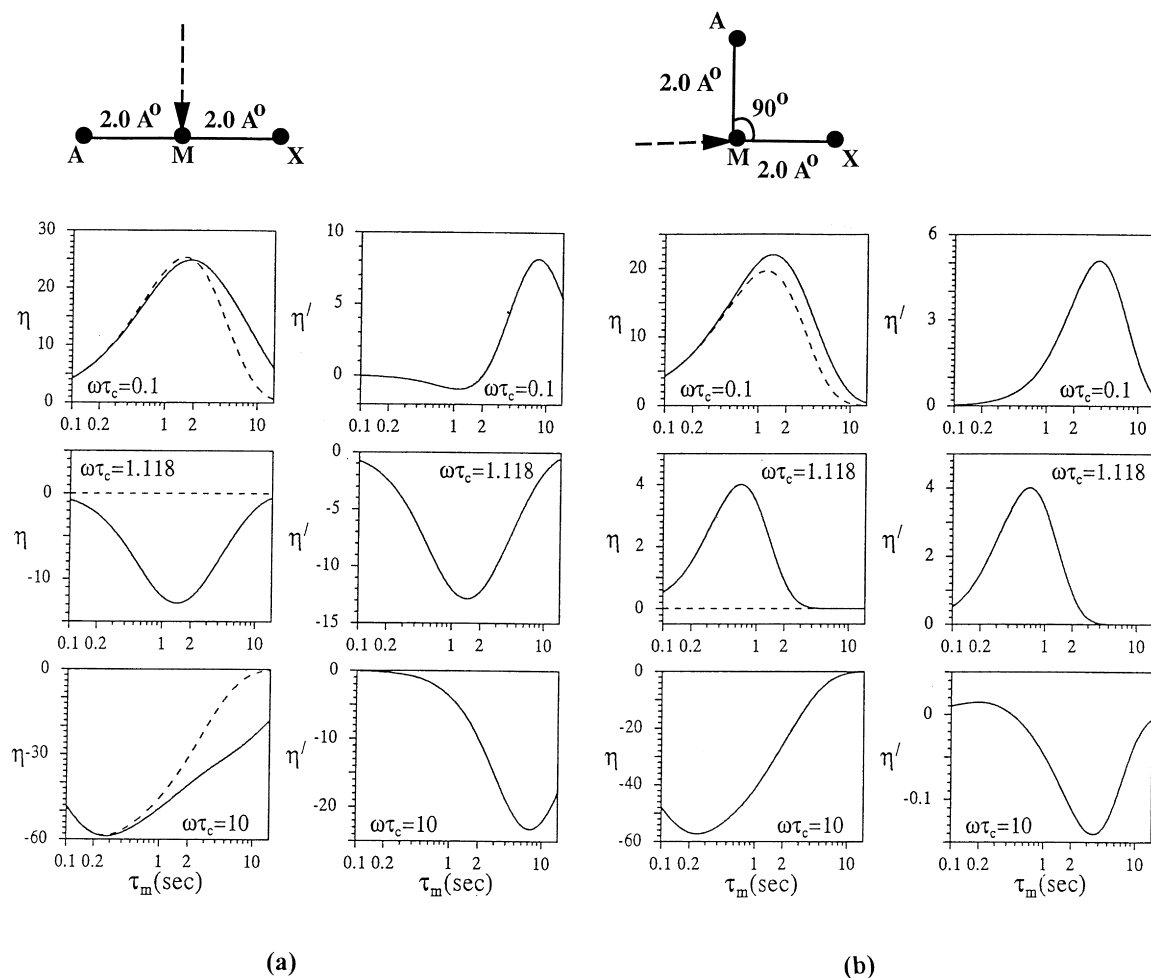
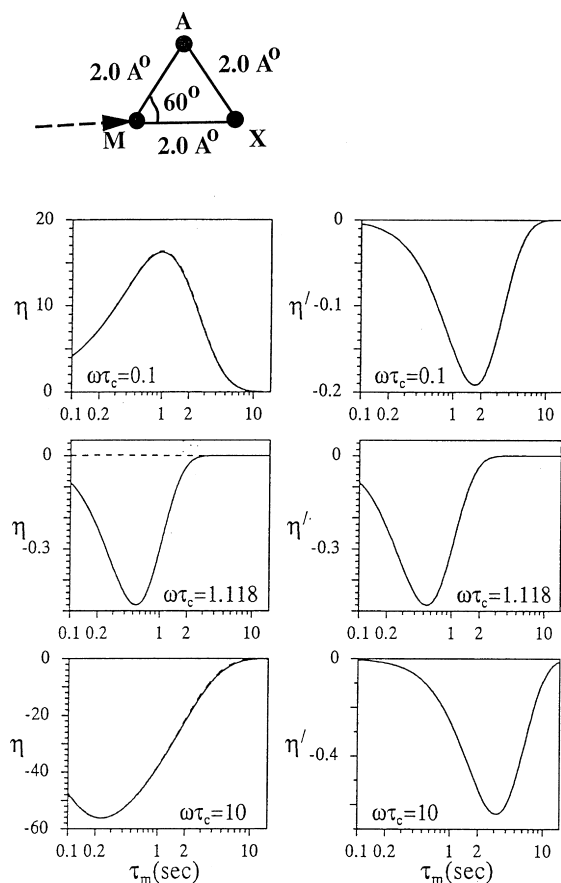


Fig. 8. (a) Calculated net NOE for the AMX spin system in percentage ( $\eta$ ) on the spin A and X (equal because of symmetry), after selective inversion of the spin M, at  $\tau_m = 0$ , is shown as a function of  $\tau_m$  on a logarithmic scale for a linear configuration of the three spins A, M and X, with inter-spin distance of 2 Å. In the left-hand diagrams, the dashed curves represent the calculated net NOE without cross-correlations and the solid curves with cross-correlations. In the right-hand diagrams, the difference ( $\eta'$ ) between these two calculated NOEs are shown by solid curves. The top, middle and bottom traces correspond to  $\omega\tau_c = 0.1$ , 1.118 and 10, respectively, for  $\omega/2\pi = 300$  MHz. The three-spin system is shown at the top, with the arrow representing the selective inversion of spin M, at  $\tau_m = 0$ . (b) Same as (a), except that a right isosceles configuration is assumed for the three spins A, M and X. (c) Same as (a), except that an equilateral configuration is assumed for the three spins A, M and X. [Reproduced with permission from P.K. Madhu, Anil Kumar, Conc. Magn. Reson. 8 (1996) 139.]

Since there are many biomolecules which fall in the region  $\omega\tau_c = 2$ –5 for which Fig. 9 predicts a significant effect of cross-correlations, the net effect of cross-correlations is analyzed in the three-spin system assuming a linear configuration for  $\omega\tau_c = 2$ –5, given in Fig. 10. It is seen that the net effect of NOE is quite large especially if it is monitored as a percentage of the total NOE. The curves show that at intermediate

mixing times such as 400 ms, the NOE with cross-correlations is 24, 35 and 48% of the total magnetization and the error is 7, 5 and 3% of the total magnetization, at  $\omega\tau_c = 2$ , 3 and 5, respectively [93]. Hence the error is a significant fraction of the net NOE given by 28, 15 and 6%, respectively, for the three correlation times. At these correlation times, cross-correlations thus have significant influence on net



(c)

Fig. 8. (continued)

NOE. The maximum error on net NOE, however, is much larger and appears at very long mixing times, reaching a value of 22, 23 and 24% of the total magnetization at mixing times of 1.8, 2.6 and 3.9 s, respectively, for the three correlation times [93].

### 3.2.3. Spin diffusion

The above analysis of three-spin system highlights the effect of cross-correlations in a closed system. As mentioned earlier, for  $\omega\tau_c \gg 1$ , there is little leakage of magnetization from the spin system and the magnetization remains within the spin system for a long time, building up the net effect of cross-correlations. However, unless special experiments involving spin-locking a selected number of spins are performed,

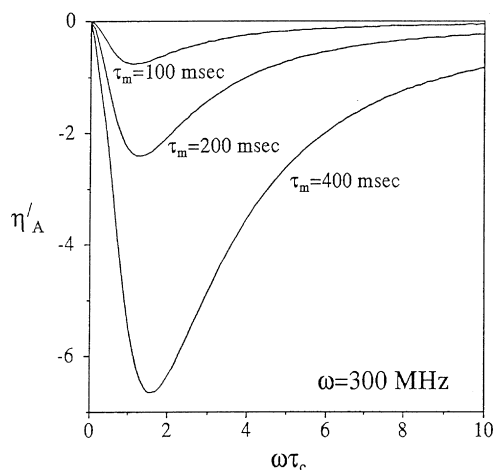


Fig. 9. The difference in net NOE on spin A for an AMX spin system (after selective inversion of spin M at  $\tau_m = 0$  for a linear arrangement of the spins A, M and X having inter-spin distance of 2 Å), calculated with and without cross-correlations in percentage and is plotted as a function of  $\tau_c$  for mixing times shown on the curves for  $\omega/2\pi = 300$  MHz.  $\eta'_A$  is defined as  $\eta'_A = (A_z(\tau_m)/A_0)\%$  while  $\eta'_A = (\eta_A)_w - (\eta_A)_{w_0}$  where  $(\eta_A)_w$  is the NOE calculated with cross-correlations and  $(\eta_A)_{w_0}$  is the NOE calculated without cross-correlations. Identical curves are obtained for the spin X in this case. [Reproduced with permission from P.K. Madhu, Anil Kumar, Conc. Magn. Reson. 8 (1996) 139.]

there are always additional relaxation-coupled spins present. These additional spins while on the one hand carry away the magnetization from the spins of interest reducing the NOE and the effect of cross-correlations, on the other hand, act as sources for additional cross-correlations. In order to investigate the effect of spin diffusion on the net effect of cross-correlations, the addition of fourth and fifth spins in a linear configuration has been carried out for  $\omega\tau_c = 3$ . Figs. 11 and 12 represent the effect of spin-diffusion and cross-correlation on four- (AMKP) and five- (AMKPx) spin systems in a linear configuration [95].

#### 3.2.3.1. Four-spin system.

For the linear configuration of spins, it is found that the addition of the fourth spin, while inverting the second spin, reduces the net NOE, with and without cross-correlations, on the third spin, while the net NOE without cross-correlations on the first spin (A) remains relatively unaffected. For example, on selective inversion of spin M, the NOE at  $\tau_m = 400$  ms, on the spin K is reduced to 18, 26 and 33% of the total magnetization, while the errors due to

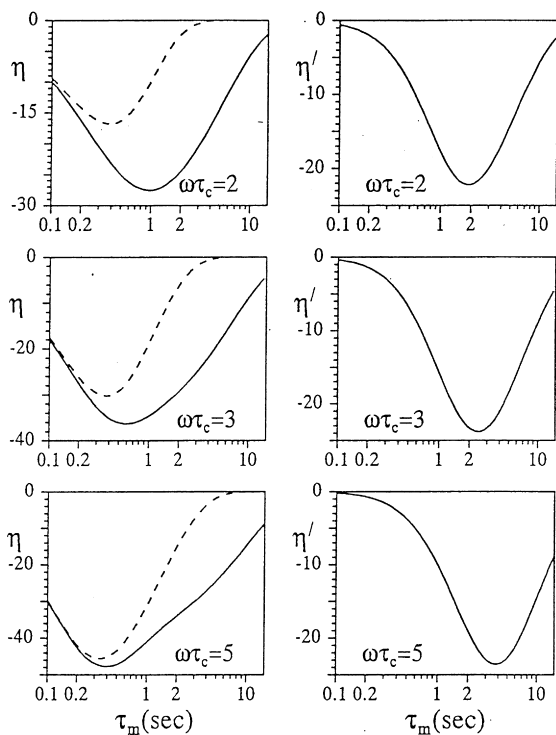


Fig. 10. Calculated net NOE for an AMX spin system in percentage ( $\eta$ ) on the spins A and X after selective inversion of spin M at  $\tau_m = 0$ , is shown as a function of  $\tau_m$  for a linear arrangement of the spins A, M and X having inter-spin distance of 2 Å. In the left-hand diagrams, the dashed curves represent the calculated net NOE without cross-correlations and the solid-curves with cross-correlations. In the right-hand diagrams, the difference ( $\eta'$ ) between these two calculated NOEs are shown by solid curves. The top, middle and bottom traces correspond to  $\omega\tau_c = 2, 3$  and 5, respectively, for  $\omega/2\pi = 300$  MHz. Identical curves are obtained for the spin X in this case as well. [Reproduced with permission from P.K. Madhu, Anil Kumar, Conc. Magn. Reson. 8 (1996) 139.]

neglect of cross-correlation as a percentage of the total magnetization, remain unchanged given by 6, 5 and 3% for  $\omega\tau_c = 2, 3$  and 5, respectively. It may be noted that the error as a fraction of the total NOE has actually increased in this case. On the other hand, at longer mixing times, the net NOE on the spin K as well as the maximum error on both spins K and A is significantly reduced for all  $\omega\tau_c$ . The maximum error for  $\omega\tau_c = 5$  decreases more dramatically than that for  $\omega\tau_c = 2$ , since in the case of  $\omega\tau_c = 2$  and for the short correlation limit, there is already significant leakage in the relaxation process of the three-spin system, and the addition of the fourth spin adds only an additional

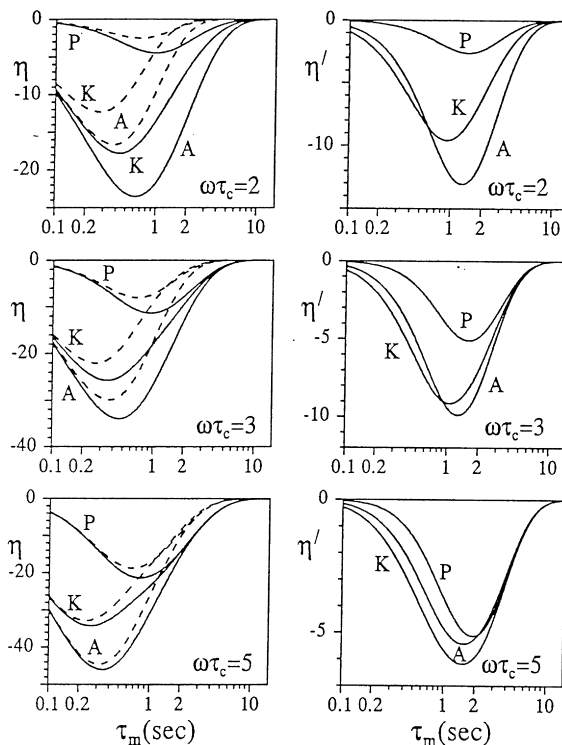


Fig. 11. Calculated net NOE in percentage ( $\eta$ ) on the spins A, K and P in a linear four-spin system (AMKP) after selective inversion of the spin M at  $\tau_m = 0$ , for  $\omega\tau_c = 2, 3$  and 5 for  $\omega/2\pi = 300$  MHz. In the left-hand diagrams, the dashed curves represent the calculated net NOE without cross-correlations and the solid-curves with cross-correlations. In the right-hand diagrams, the difference ( $\eta'$ ) between the NOEs calculated with and without cross-correlations is shown for each spin. The interproton distance in the linear configuration is taken as 2.0 Å. [Reproduced with permission from P.K. Madhu, Anil Kumar, J. Magn. Reson. A 127 (1997) 168.]

leakage pathway for the magnetization. On the other hand, for  $\omega\tau_c \geq 5$ , there is little leakage in the three-spin system, resulting in a significant effect of cross-correlation as seen from Fig. 10, which is attenuated when the fourth spin is added (Fig. 11). It may also be noted that though both the net NOE and the maximum errors are reduced, the errors as a percentage of net NOE are still quite significant [95].

**3.2.3.2. Five-spin system.** The effect of cross-correlations on the net NOE on various spins has been analyzed for a linear configuration of an equidistant five-spin system, when the second spin is inverted at  $\tau_m = 0$  (Fig. 12). It can be seen that the

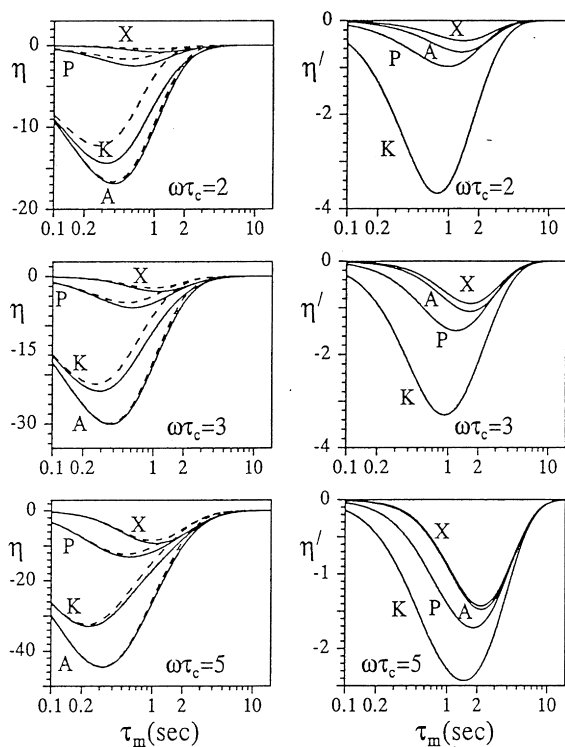


Fig. 12. Same as Fig. 11 except that a linear arrangement of five spins  $A$ ,  $M$ ,  $K$ ,  $P$  and  $X$  is considered, with the  $X$  spin being added at  $2.0 \text{ \AA}$  from spin  $P$ . [Reproduced with permission from P.K. Madhu, Anil Kumar, J. Magn. Reson. A 127 (1997) 168.]

maximum errors are small in all cases and are less than those in the four-spin case and that the errors are significantly reduced even at intermediate mixing times such as  $\tau_m = 400 \text{ ms}$ . It can be seen from these curves that while the calculated net NOE without cross-correlations on spins  $A$  and  $K$  changes little when the fifth spin is added, the effect of cross-correlations decreases significantly. On the other hand, with the addition of the fifth spin, the net NOE calculated with and without cross-correlations on the fourth spin ( $P$ ) decreases significantly. These calculations indicate that as magnetization migrates along the chain, the NOE and the effect of cross-correlations decrease. However, the effect of cross-correlations as a percentage of NOE still continues to be significant [95].

In order to verify whether spin diffusion and cross-correlation can be mimicked by a leakage process, the four- and five-spin calculations with cross-

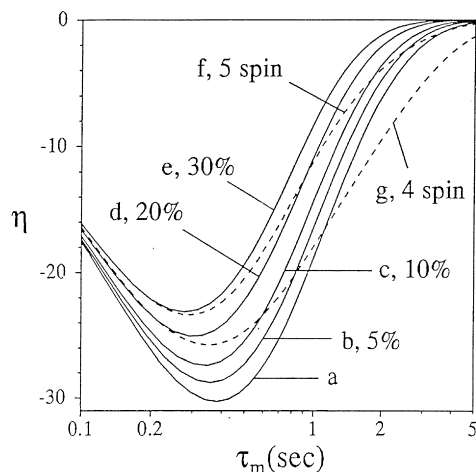


Fig. 13. Net NOE (curve  $a$ ) in percentage on the spin  $K$  in a linear  $AMK$  spin system calculated without cross-correlations after selective inversion of the spin  $M$  at  $\tau_m = 0$ . Curves  $b$ – $e$  correspond to the above situation, with the addition of non-selective leakage terms corresponding to 5, 10, 20 and 30% of the average relaxation rates of single-spin-orders,  $(1/3)(\rho_A + \rho_M + \rho_K)$ , respectively, to each of the diagonal elements of the rate matrix. Dashed curves  $f$  and  $g$  correspond to the net NOE calculated on the spin  $K$  in a linear arrangement of four ( $AMKP$ ) and five ( $AMKPX$ ) spins, respectively, without any leakage but with cross-correlations, after selective inversion of the spin  $M$  at  $\tau_m = 0$ . In all the above calculations, the inter-spin distance is taken as  $2 \text{ \AA}$ ,  $\omega\tau_c = 3$  and  $\omega/2\pi = 300 \text{ MHz}$ . [Reproduced with permission from P.K. Madhu, Anil Kumar, J. Magn. Reson. A 127 (1997) 168.]

correlations have been compared with the three-spin calculation excluding cross-correlation, but with leakage terms added to the diagonal elements of the relaxation matrix. If this leads to an acceptable result, it will establish whether one can use Solomon's equations, (Eq. (65) contains evolution of only single-spin modes) and neglect all cross-correlations, with leakage terms added to the diagonal elements. Fig. 13 shows the calculated transient NOE as a function of mixing time, on the spin  $K$  in the linear  $AMK$  spin system, on inversion of the spin  $M$  at  $\tau_m = 0$ , calculated without cross-correlations but with different amounts of leakage added to all the diagonal elements of Solomon's equations, for  $\omega\tau_c = 3$  [95]. Curve  $a$  is without any leakage and curves  $b$ – $f$  are with leakage amounting to 5, 10, 20 and 30%. The same figure also shows the calculated transient NOE on spin  $K$  in the linear  $AMKP$  and  $AMKPX$  spin systems with spin  $M$  being inverted at  $\tau_m = 0$ , calculated with

cross-correlations (dashed curves) for  $\omega\tau_c = 3$ . It is seen from these curves that for short mixing times the four-spin net NOE including cross-correlations matches the three-spin net NOE calculation without cross-correlations but with 20% leakage. For longer mixing times, the amount of leakage must be reduced, and at very long mixing times beyond 1 s, the three-spin NOE without cross-correlations becomes smaller than the four-spin NOE with cross-correlations. Leakage then cannot account for the spin diffusion. The five-spin NOE matches the three-spin NOE with 30% leakage for short mixing times and the reduced leakage for long mixing times with the three spin NOE without leakage becoming smaller than the five-spin case after  $\tau_m = 3$  s. These results indicate that in the presence of significant spin diffusion, the effect of cross-correlations on the net NOE becomes small and leakage can account for cross-correlations only for short mixing times [95].

The conclusion of this section is that there is a significant effect of cross-correlations on net NOE especially in the region  $\omega\tau_c = 1-3$  and unless cross-correlations are explicitly taken into account, the distances obtained from NOE should be treated as estimates rather than accurate measurements, especially for analyses, which go beyond initial rate approximations.

### 3.3. Effect of cross-correlations in equivalent and strongly coupled spins

In the three-spin analysis given above, the recovery of the second inverted spin has also been calculated with and without dipolar cross-correlations. It is found that there is a significant effect of cross-correlations in the recovery of the inverted spin and that it is highly non-exponential (Fig. 14) [93]. The origin of this non-exponentiality is well understood in the context of the above discussion. The recovery is non-exponential in the presence of cross-correlations (a sum of seven exponentials for a three-spin system, Eq. (61)), as well as in the absence of cross-correlation (a sum of three exponentials for three relaxation-coupled spins, Eq. (65)). This behavior is independent of J-coupling, when the recovery of net magnetization of a spin is monitored. However, the situation requires that all the relaxation-coupled spins have resolved chemical shifts. In case of over-

lapping chemical shifts, only the sum mode of the degenerate spins can be monitored and the modes defined above have to be transformed into a symmetrized basis [58,96–101]. The cases involving  $A_2$ ,  $A_3$ ,  $AX_2$  and  $AX_3$  as well as strongly coupled  $AB$  and  $ABX$  spins are discussed in the following sections.

#### 3.3.1. $A_2$ spin system

For equivalent spins, the rate equation (Eq. (58)) should be transformed into a basis set, which corresponds to the irreducible representation of the symmetry point group of the spin system. The simplest spin system of this kind consisting of two relaxation-coupled spin-(1/2) nuclei, which are magnetically and chemically equivalent, have been studied by several workers [17,58,101]. Here it is assumed that the dipolar relaxation between the two spins is the major source of relaxation. One must define three normal modes to describe the longitudinal spin evolution. These modes are defined in the following way [58]:

$$\begin{aligned} {}^a\nu_1^{A_2} &= \text{Tr}\{(I_z^A + I_z^{A'})\sigma\} \\ {}^s_u\nu_2^{A_2} &= \frac{1}{\sqrt{3}} \text{Tr}\{[3I_z^A I_z^{A'} - I^A \cdot I^{A'}]\sigma\} \\ {}^s_u\nu_3^{A_2} &= \frac{2}{\sqrt{6}} \text{Tr}\{[I^A \cdot I^{A'}]\sigma\} \end{aligned} \quad (79)$$

where the antisymmetric mode  ${}^a\nu_1^{A_2}$  is the only observable mode. In the absence of CSA–dipole cross-correlations, only the observable mode  ${}^a\nu_1^{A_2}$  is created and it relaxes monoexponentially through the auto-correlated dipolar relaxation. In the presence of a random field mechanism, the modes have coupled evolution [58].

#### 3.3.2. $A_3$ spin system

The effect of multi-spin dipole–dipole cross-correlations in systems with three identical spin-(1/2) nuclei ( $A_3$ ) is discussed here. Only three irreducible modes are coupled by dipole–dipole cross-correlations. Their definitions and the rate equations are

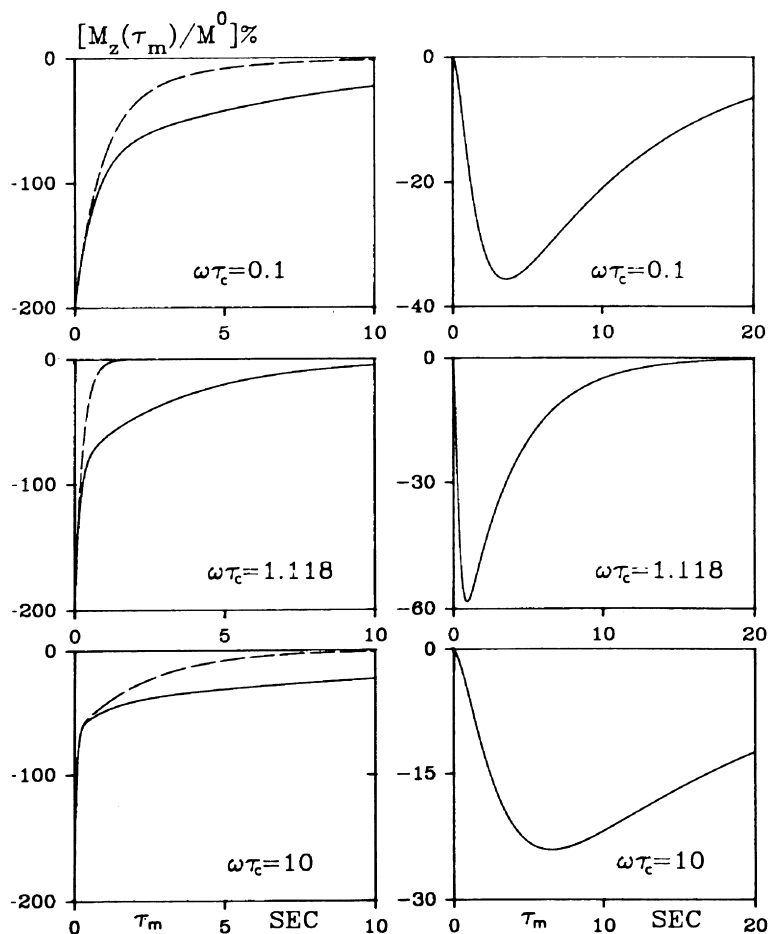


Fig. 14. Calculated net magnetization in percentage of spin  $M$  as a function of  $\tau_m$ , after selective inversion of spin  $M$ , at  $\tau_m = 0$ , for the linear geometry of three spins  $AMX$  for three different values of  $\omega\tau_c$ . In the left-hand diagrams, the dashed curves represent the calculated magnetization without cross-correlations and the solid curves with cross-correlations. In the right-hand diagrams, the differences between these two calculated magnetizations are shown by solid curves. [Reproduced with permission from P.K. Madhu, R.C.R. Grace, Anil Kumar, Bull. Magn. Reson. 16 (1994) 115.]

given by [58]:

$$\begin{aligned}
 {}^a\nu_1^{A_3} &= \text{Tr}\{(I_z^A + I_z^{A'} + I_z^{A''})\sigma\} \\
 {}^a\nu_2^{A_3} &= \frac{4}{\sqrt{5}}\text{Tr}\{[I_z^A(I^{A'}\cdot I^{A''}) + I_z^{A'}(I^A\cdot I^{A''}) + I_z^{A''}(I^A\cdot I^{A'})]\sigma\} \\
 {}^a\nu_3^{A_3} &= \frac{\sqrt{8}}{\sqrt{15}}\text{Tr}\{[15I_z^A I^{A'} I^{A''} - [I_z^A(I^{A'}\cdot I^{A''}) \\
 &\quad + I_z^{A'}(I^A\cdot I^{A''}) + I_z^{A''}(I^A\cdot I^{A'})]\sigma\}
 \end{aligned} \tag{80}$$

$$-\frac{d}{dt} \begin{pmatrix} {}^a\nu_1^{A_3}(t) \\ {}^a\nu_2^{A_3}(t) \\ {}^a\nu_3^{A_3}(t) \end{pmatrix} = \begin{pmatrix} {}^a\hat{\Gamma}_{11}^{A_3} & {}^a\hat{\Gamma}_{12}^{A_3} & {}^a\hat{\Gamma}_{13}^{A_3} \\ {}^a\hat{\Gamma}_{21}^{A_3} & {}^a\hat{\Gamma}_{22}^{A_3} & {}^a\hat{\Gamma}_{23}^{A_3} \\ {}^a\hat{\Gamma}_{31}^{A_3} & {}^a\hat{\Gamma}_{32}^{A_3} & {}^a\hat{\Gamma}_{33}^{A_3} \end{pmatrix} \times \begin{pmatrix} {}^a\nu_1^{A_3}(t) \\ {}^a\nu_2^{A_3}(t) \\ {}^a\nu_3^{A_3}(t) \end{pmatrix}. \tag{81}$$

The various elements of the relaxation matrix in Eq.

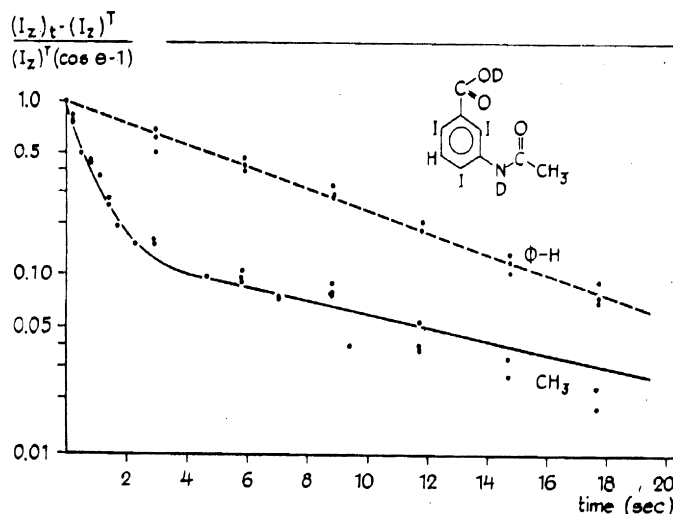


Fig. 15. Intensity profile for the ring proton ( $\phi\text{H}$ ) and the methyl proton in an inversion recovery experiment, carried out on 0.1 M acerizonate dissolved in  $\text{D}_2\text{O}$ , phosphate–KCl buffer, ionic strength  $\mu = 0.2$ ,  $\text{pH} = 7.0$  at  $32^\circ\text{C}$ . The points represent the experimental data and the lines show the theoretical fit to the experimental data. The relaxation of the methyl protons is non-exponential. [Reproduced with permission from J.F.R. Miranda, C.W. Hilbers, J. Magn. Reson. 19 (1975) 11.]

(81) are given by [58]:

$${}^a\hat{T}_{11}^{A_3} = 2[J_a(\omega) + 4J_a(2\omega)]$$

$${}^a\hat{T}_{12}^{A_3} = \frac{2}{\sqrt{5}}[J_c(\omega) + 4J_c(2\omega)]$$

$${}^a\hat{T}_{13}^{A_3} = \frac{4\sqrt{6}}{\sqrt{5}}[J_c(\omega) - 4J_c(2\omega)]$$

$${}^a\hat{T}_{22}^{A_3} = \frac{1}{5}\{[6J_a(0) - J_c(0)] + 4[J_a(2\omega) + J_c(2\omega)] + 10J_a(\omega) - 8J_c(\omega)\}$$

$${}^a\hat{T}_{23}^{A_3} = \frac{\sqrt{6}}{5}\{-3[J_a(0) - J_c(0)] - 2[J_a(2\omega) + J_c(2\omega)] + 5J_a(\omega) - J_c(\omega)\}$$

$${}^a\hat{T}_{33}^{A_3} = \frac{1}{5}\{9[J_a(0) - J_c(0)] + 6[J_a(2\omega) + J_c(2\omega)] + 30J_a(\omega) + 18J_c(\omega)\} \quad (82)$$

Here  $J_a(\omega) = J_{ijj}(\omega)$  and  $J_c(\omega) = J_{ijk}(\omega)$ . The indices  $i$ ,  $j$  and  $k$  are dropped since we are dealing with

equivalent spins. It is interesting to note that  $J_c(0)$  and  $J_c(2\omega)$  contribute in the case of equivalent spins, unlike the weakly coupled case. It turns out, as will be discussed in a later section, that cross-correlations from spectral densities at zero and  $2\omega$  contribute to relaxation in the strong coupling situations [75,102] as well; equivalent spins being extreme examples of strongly coupled spins.

Out of the three modes in Eq. (80), only the mode  ${}^a\nu_1^{A_3}$  is observable and is coupled to the unobservable modes  ${}^s\nu_2^{A_3}$  and  ${}^s\nu_3^{A_3}$  via the cross-correlation terms. On the other hand, the unobservable modes are coupled to each other by auto- and cross-correlation terms. In an experiment, it is possible to excite and observe only the  ${}^a\nu_1^{A_3}$  mode, which in the absence of cross-correlation relaxes with a single exponential. In the presence of cross-correlations, this mode  ${}^a\nu_1^{A_3}$  converts to the unobservable modes  ${}^s\nu_2^{A_3}$  and  ${}^s\nu_3^{A_3}$  and back to the mode  ${}^a\nu_1^{A_3}$ , giving rise to multi-exponential relaxation (Fig. 15) [103–108]. This is the source of non-exponential methyl relaxation mentioned in many earlier analyses of cross-correlations, along with solid-state NMR studies of methyl and ammonium group reorientations [36,109–118].

### 3.3.3. $AX_2$ spin system

Several workers have studied the  $AX_2$  spin system, theoretically as well as experimentally [58,119–140]. For such a system, in the presence of only dipole–dipole cross-correlations, three antisymmetric physically observable normal modes namely,  $I_Z^A$ ,  $(I_Z^X + I_Z^{X'})/\sqrt{2}$  and  $4I_Z^A I_Z^X I_Z^{X'}$  are needed. One also needs a fourth non-measurable mode,  $\sqrt{2}[(I_+^X I_-^{X'} + I_-^X I_+^{X'})I_Z^A]$ , which is coupled to the first two modes via dipole–dipole cross-correlations and to the third mode via both auto and cross-correlations. The relaxation matrix elements for such a system are given by [58]:

$$\begin{aligned}
 {}^a\hat{T}_{11} &= 2[(1/3)J_{AXAX}(\omega_A - \omega_X) + J_{AXAX}(\omega_A) \\
 &\quad + 2J_{AXAX}(\omega_A + \omega_X)] \\
 {}^a\hat{T}_{12} &= \sqrt{2}[-(1/3)J_{AXAX}(\omega_A - \omega_X) \\
 &\quad + 2J_{AXAX}(\omega_A + \omega_X)] \\
 {}^a\hat{T}_{13} &= 2J_{AXAX'}(\omega_A) \\
 {}^a\hat{T}_{14} &= \sqrt{2}[(1/3)J_{AXAX'}(\omega_A - \omega_X) \\
 &\quad + 2J_{AXAX'}(\omega_A + \omega_X)] \\
 {}^a\hat{T}_{22} &= (1/3)J_{AXAX}(\omega_A - \omega_X) + J_{AXAX}(\omega_X) \\
 &\quad + 2J_{AXAX}(\omega_A + \omega_X) + J_{XX'XX'}(\omega_X) \\
 &\quad + 4J_{XX'XX'}(2\omega_X) \\
 {}^a\hat{T}_{23} &= \sqrt{8}J_{AXX'}(\omega_X) \\
 {}^a\hat{T}_{24} &= 2J_{AXAX'}(\omega_A - \omega_X) - (1/3)J_{AXAX'}(\omega_A - \omega_X) \\
 &\quad - 2J_{AXX'}(\omega_X) \\
 {}^a\hat{T}_{33} &= 2J_{AXAX}(\omega_A) - 2J_{AXAX}(\omega_X) + 2J_{XX}(\omega_X) \\
 {}^a\hat{T}_{34} &= \frac{4}{3}[J_{AXAX}(0) - J_{AXAX'}(0)] + \frac{1}{3}J_{AXAX}(\omega_A - \omega_X) \\
 &\quad + J_{AXAX}(\omega_X) + 2J_{AXAX}(\omega_A + \omega_X) + J_{XX}(\omega_X)
 \end{aligned} \tag{83}$$

While the relaxation matrix elements  ${}^a\hat{T}_{11}$ ,  ${}^a\hat{T}_{12}$ ,  ${}^a\hat{T}_{22}$ ,  ${}^a\hat{T}_{33}$  depend only on auto-correlations,  ${}^a\hat{T}_{13}$ ,  ${}^a\hat{T}_{14}$ ,  ${}^a\hat{T}_{23}$  and  ${}^a\hat{T}_{24}$  only on cross-correlations.  ${}^a\hat{T}_{34}$  depends on both auto and cross-correlations.

Thus in the presence of dipole–dipole cross-correlations, there is differential relaxation between the outer and the inner transitions of the  $A$  spin multiplet, but the transitions of the  $X$ -spin doublet relax identically. However, if one considers the CSA of spins  $A$  and  $X$ , several two-spin modes coupled by CSA–dipole cross-correlations have to be considered, the expressions of Eq. (83) become fairly complicated and lead to differential relaxation of the  $X$ -spin doublet as well [134].

### 3.3.4. $AX_3$ spin system

The methyl group  $^{13}\text{CH}_3$  belongs to this type of four-spin case and is encountered in several systems. The dipolar interactions among the various protons and carbon-protons have been considered by several authors [135–175]. The antisymmetric modes for the  $AX_3$  system consist of three measurable modes namely:  $\nu_1$ , the total  $A$ -spin magnetization ( $I_Z^A$ ),  $\nu_2$ , the total  $X$ -spin magnetization ( $I_Z^X + I_Z^{X'} + I_Z^{X''}$ ) and  $\nu_3$ , the weighted sum of the outer components minus the central components of the  $A$ -spin quartet [ $I_Z^A(I_Z^X I_Z^{X'} + I_Z^X I_Z^{X''} + I_Z^{X'} I_Z^{X''})$ ]. Coupled to these three measurable modes are three non-measurable modes:  $\nu_4$ , the quartet minus the doublet contributions to the central lines in the  $A$ -spin quartet ( $I_Z^X I_Z^{X'} I_Z^{X''}$ ) and  $\nu_5$  and  $\nu_6$ , two combinations of forbidden transitions in the  $X$ -spin manifold [ $I_Z^X(I_+^{X'} I_-^{X''} + I_-^{X'} I_+^{X''}) + I_Z^{X'}(I_+^X I_-^{X''} + I_-^X I_+^{X''}) + I_Z^{X''}(I_+^X I_-^{X'} + I_-^X I_+^{X'})$  and  $I_Z^A(I_+^X I_-^{X'} + I_-^X I_+^{X'} + I_+^X I_-^{X''} + I_-^X I_+^{X''} + I_+^{X'} I_-^{X''} + I_-^{X'} I_+^{X''})$ ]. The relaxation matrix elements for this system in the presence of dipole–dipole cross-correlations are given in Ref. [58] and for CSA–dipole cross-correlations are given in Refs. [134,176,177]. In the absence of cross-correlations, modes  $\nu_1$  to  $\nu_4$  have the same relaxation rates. In the presence of dipole–dipole cross-correlations, the outer lines relax at a different rate compared to the inner lines which has been observed experimentally [89,150,157].

### 3.3.5. $AB$ spin system

The simplest case of a strongly coupled spin system is the two-spin system ( $AB$ ). The rate equation for such a system is given by Eq. (52). If one considers the CSA of both spins as well as the dipolar interaction between the two spins, the single quantum

transition probabilities (numbering the states as,  $|1\rangle = |\alpha\alpha\rangle$ ,  $|2\rangle = \cos\theta|\alpha\beta\rangle + \sin\theta|\beta\alpha\rangle$ ,  $|3\rangle = -\sin\theta|\alpha\beta\rangle + \cos\theta|\beta\alpha\rangle$  and  $|4\rangle = |\beta\beta\rangle$ ) are given by [178,179]:

$$\begin{aligned}
 -\begin{pmatrix} W_{13} \\ W_{24} \\ W_{12} \\ W_{34} \end{pmatrix} &= \begin{pmatrix} 1 + \cos 2\theta & 2 \sin^2 \theta & \frac{1}{2} - \sin 2\theta \\ 1 + \cos 2\theta & 2 \sin^2 \theta & \frac{1}{2} + \sin 2\theta \\ 2 \sin^2 \theta & 1 + \cos 2\theta & \frac{1}{2} + \sin 2\theta \\ 2 \sin^2 \theta & 1 + \cos 2\theta & \frac{1}{2} - \sin 2\theta \end{pmatrix} \begin{pmatrix} J_{AA}(\omega) \\ J_{BB}(\omega) \\ J_{ABAB}(\omega) \end{pmatrix} \\
 &+ \begin{pmatrix} -\sin 2\theta + \cos 2\theta + 1 & -\sin 2\theta + 2 \sin^2 \theta & 2 \sin 2\theta \\ -\sin 2\theta + \cos 2\theta + 1 & -\sin 2\theta - 2 \sin^2 \theta & -2 \sin 2\theta \\ \sin 2\theta + 2 \sin^2 \theta & \sin 2\theta + \cos 2\theta + 1 & -2 \sin 2\theta \\ \sin 2\theta - 2 \sin^2 \theta & \sin 2\theta - \cos 2\theta - 1 & 2 \sin 2\theta \end{pmatrix} \begin{pmatrix} J_{A,AB}(\omega) \\ J_{B,AB}(\omega) \\ J_{A,B}(\omega) \end{pmatrix} \quad (84)
 \end{aligned}$$

In the presence of cross-correlations and strong coupling, all the four  $W_1$  terms are unequal. The contribution of CSA–CSA cross-correlation [ $J_{A,B}(\omega)$ ] becomes observable as a differential effect between the inner and the outer transitions of the  $AB$  multiplet.

For equivalent spin systems, where the sum mode is the only physical observable, the contribution of this remote term to longitudinal relaxation cancels out.

The double and zero quantum transition probabilities are given by [178,179]:

$$\begin{aligned}
 -\begin{pmatrix} W_{14} \\ W_{23} \end{pmatrix} &= \frac{1}{3} \begin{pmatrix} 0 & 0 & 0 \\ 4 \sin^2 2\theta & 4 \sin^2 2\theta & 1 - \sin^2 2\theta \end{pmatrix} \begin{pmatrix} J_{AA}(0) \\ J_{BB}(0) \\ J_{ABAB}(0) \end{pmatrix} \\
 &+ \frac{4}{3} \begin{pmatrix} 0 & 0 & 0 \\ -\sin 2\theta \cos 2\theta & \sin 2\theta \cos 2\theta & -2 \sin^2 2\theta \end{pmatrix} \begin{pmatrix} J_{A,AB}(0) \\ J_{B,AB}(0) \\ J_{A,B}(0) \end{pmatrix} + \begin{pmatrix} 0 & 0 & 2 \\ 0 & 0 & 0 \end{pmatrix} \begin{pmatrix} J_{AA}(2\omega) \\ J_{BB}(2\omega) \\ J_{ABAB}(2\omega) \end{pmatrix} \quad (85)
 \end{aligned}$$

As can be seen from this equation, the double quantum transition probability is independent of strong coupling as well as cross-correlations. On the other hand, the zero quantum transition probability has contributions from all auto and

cross-correlation spectral densities, including the remote term  $J_{A,B}(0)$ .

### 3.3.6. $ABX$ spin system

The effect of strong coupling and cross-correlations on longitudinal relaxation has been investigated theoretically, for  $ABX$  spin systems [74,76,178–180]. It is found that while the effects of cross-correlation in weakly coupled spins are limited to spectral densities at the Larmor frequency ( $W_1$  terms), which decrease in magnitude as  $\omega\tau_c$  increases beyond 1, strong coupling mixes states and therefore cross-correlations affect spectral densities at zero and  $2\omega$ .

Table 1 contains the contribution of dipole–dipole

cross-correlations to various transition probabilities in the presence and absence of strong coupling. It is seen that under strong coupling dipolar cross-correlations contribute to transition probabilities at zero, and twice the Larmor frequency as well.

Table 1

Difference between the transition probabilities with and without dipole-dipole cross-correlations

$W_{\alpha\beta}$	Strong coupling <sup>a</sup>	Weak coupling
<i>Zero quantum transition probabilities (<math>W_0</math>)</i>		
$W_{23}$	$2[J_{AXBX}(0)c_{+s_+}]/3$	0
$W_{24}$	$-2[J_{AXBX}(0)c_{+s_+}]/3$	0
$W_{34}$	$4[(J_{ABAX}(0) - J_{ABBX}(0))(c_+^3s_+ - c_+s_+^3) - 2J_{AXBX}(0)c_+^2s_+^2]/3$	0
$W_{56}$	$-4[(J_{ABAX}(0) - J_{ABBX}(0))(c_-^3s_- - c_-s_-^3) + 2J_{AXBX}(0)c_-^2s_-^2]/3$	0
$W_{57}$	$2[J_{AXBX}(0)c_{-s_-}]/3$	0
$W_{67}$	$-2[J_{AXBX}(0)c_{-s_-}]/3$	0
<i>Double quantum transition probabilities (<math>W_2</math>)</i>		
$W_{15}$	$4[J_{AXBX}(2\omega)c_{-s_-}]$	0
$W_{16}$	$-4[J_{AXBX}(2\omega)c_{-s_-}]$	0
$W_{17}$	0	0
$W_{28}$	0	0
$W_{38}$	$4[J_{AXBX}(2\omega)c_{+s_+}]$	0
$W_{48}$	$-4[J_{AXBX}(2\omega)c_{+s_+}]$	0
<i>Single quantum transition probabilities (<math>W_1</math>)</i>		
$W_{12}$	$J_{AXBX}(\omega)$	$J_{AXBX}(\omega)$
$W_{13}$	$[J_{ABBX}(\omega)(c_+^2 + c_+s_+) + J_{ABAX}(\omega)(s_+^2 + c_+s_+) + J_{AXBX}(\omega)c_+s_+]$	$J_{ABBX}(\omega)$
$W_{14}$	$[J_{ABBX}(\omega)(s_+^2 - c_+s_+) + J_{ABAX}(\omega)(c_+^2 - c_+s_+) - J_{AXBX}(\omega)c_+s_+]$	$J_{ABAX}(\omega)$
$W_{25}$	$-[J_{ABBX}(\omega)(c_-^2 + c_-s_-) + J_{ABAX}(\omega)(s_-^2 - c_-s_-) - J_{AXBX}(\omega)c_-s_-]$	$-J_{ABBX}(\omega)$
$W_{26}$	$-[J_{ABBX}(\omega)(s_-^2 - c_-s_-) + J_{ABAX}(\omega)(c_-^2 - c_-s_-) + J_{AXBX}(\omega)c_-s_-]$	$-J_{ABAX}(\omega)$
$W_{35}$	$-[J_{AXBX}(\omega)(c_+c_- - s_+s_-)^2]$	$J_{AXBX}(\omega)$
$W_{36}$	$-[J_{AXBX}(\omega)(c_+s_- + s_+c_-)^2]$	0
$W_{37}$	$-[J_{ABBX}(\omega)(s_+^2 + c_+s_+) + J_{ABAX}(\omega)(c_+^2 + c_+s_+) - J_{AXBX}(\omega)c_+s_+]$	$-J_{ABAX}(\omega)$
$W_{45}$	$= W_{36}$	0
$W_{46}$	$= W_{35}$	$J_{AXBX}(\omega)$
$W_{47}$	$-[J_{ABBX}(\omega)(c_+^2 - c_+s_+) + J_{ABAX}(\omega)(s_+^2 - c_+s_+) + J_{AXBX}(\omega)c_+s_+]$	$-J_{ABBX}(\omega)$
$W_{58}$	$[J_{ABBX}(\omega)(s_+^2 + c_-s_-) + J_{ABAX}(\omega)(c_-^2 + c_-s_-) + J_{AXBX}(\omega)c_-s_-]$	$J_{ABAX}(\omega)$
$W_{68}$	$[J_{ABBX}(\omega)(c_-^2 - c_-s_-) + J_{ABAX}(\omega)(s_-^2 - c_-s_-) - J_{AXBX}(\omega)c_-s_-]$	$J_{ABBX}(\omega)$
$W_{78}$	$J_{AXBX}(\omega)$	$J_{AXBX}(\omega)$

<sup>a</sup>  $c_+ = \cos(\theta_+)$ ;  $s_+ = \sin(\theta_+)$ ;  $c_- = \cos(\theta_-)$ ;  $s_- = \sin(\theta_-)$ .

NOEs on A and B spins have been calculated for non-selective irradiation/inversion of all transitions of X spin. While in a transient experiment, the effect of cross-correlations is significant in both weak and strong coupling situations, it is found that for a steady-state experiment, the effect of cross-correlation is absent for the weakly coupled case and small for the strongly coupled case [75,76]. The absence of the effect of cross-correlations for a steady state experiment in the weakly coupled case is because, irradiation of a spin saturates the single-spin mode (magnetization of the spin) as well as all modes containing that spin. If the X spin is saturated, then

modes,  $X_z$ ,  $2A_zX_z$ ,  $2B_zX_z$  and  $4A_zB_zX_z$  become zero. The three-spin calculation then reduces to a pseudo-two-spin system [75,178]. Since in a weakly coupled case, the dipole-dipole cross-correlations connect single-spin orders only to three-spin order, the effect of dipolar cross-correlation becomes analytically zero. If CSA-dipole cross-correlations were included, they would affect the steady-state NOE. In a weakly coupled four-spin system, saturation of the fourth spin, reduces the relaxation dynamics to a pseudo-three-spin system and the dipole-dipole cross-correlation also affects the NOE to the remaining three spins.

Recently, the effect of CSA along with dipolar contribution has been calculated for an *ABX* spin system [178,179]. While the dipolar contribution to relaxation is given in Table 1, the remote CSA–dipole and CSA–CSA cross-correlation contributions are given here. For the single quantum transition probabilities of the *AB* spins, the remote cross-correlations contribute in the following manner [178]:

$$\begin{pmatrix} W_{13} \\ W_{14} \\ W_{25} \\ W_{26} \\ W_{37} \\ W_{47} \\ W_{58} \\ W_{68} \end{pmatrix} = \begin{pmatrix} \sin 2\theta_+ & \sin 2\theta_+ & -2 \sin 2\theta_+ \\ \sin 2\theta_+ & \sin 2\theta_+ & -2 \sin 2\theta_+ \\ \sin 2\theta_- & \sin 2\theta_- & 2 \sin 2\theta_- \\ -\sin 2\theta_- & -\sin 2\theta_- & -2 \sin 2\theta_- \\ \sin 2\theta_+ & \sin 2\theta_+ & -2 \sin 2\theta_+ \\ \sin 2\theta_+ & \sin 2\theta_+ & -2 \sin 2\theta_+ \\ \sin 2\theta_- & \sin 2\theta_- & 2 \sin 2\theta_- \\ -\sin 2\theta_- & -\sin 2\theta_- & -2 \sin 2\theta_- \end{pmatrix} \times \begin{pmatrix} J_{A,BX}(\omega) \\ J_{B,AX}(\omega) \\ J_{A,B}(\omega) \end{pmatrix}. \quad (86)$$

It may be noted that the remote CSA–dipole cross-correlation terms  $J_{A,BX}$  and  $J_{B,AX}$  and CSA–CSA term  $J_{A,B}$  also contribute to the various  $W_1$ 's. These contributions vanish in the weak coupling approximation. The single quantum transition probabilities of the *X* spin are unaffected by these remote cross-correlations. These remote terms however, affect the zero quantum transition probabilities between the mixed states  $3 \rightarrow 4$  and  $5 \rightarrow 6$  in the following manner [178,179]:

$$\begin{pmatrix} W_{34} \\ W_{56} \end{pmatrix} = \frac{2}{3} \begin{pmatrix} (1 - \cos 4\theta_+) & (1 - \cos 4\theta_+) & -2(1 - \cos 4\theta_+) \\ -(1 - \cos 4\theta_-) & -(1 - \cos 4\theta_-) & -2(1 - \cos 4\theta_-) \end{pmatrix} \begin{pmatrix} J_{A,BX}(0) \\ J_{B,AX}(0) \\ J_{A,B}(0) \end{pmatrix}. \quad (87)$$

These terms which have contribution at zero frequency drop out in the weak coupling approximation. All the other zero- and double-quantum transition probabilities are unaffected by these remote cross-correlation terms.

### 3.4. Experimental observation of longitudinal cross-correlations

There are many experiments in which the presence and the utility of cross terms have been demonstrated. We classify them into the following types: (i) non-exponential recovery in longitudinal relaxation; (ii) direct detection of multi-spin order as a multiplet effect in inversion recovery and NOE experiments with or without multiple-quantum filters; (iii) multiplet effect in 2D NMR experiments (mainly NOESY); (iv) creation of multi-spin order and its recovery and conversion to single-spin order.

#### 3.4.1. Non-exponential recovery in longitudinal relaxation

One of the early observations of cross-correlations originating from cross terms between proton–proton dipolar interactions is the non-exponential recovery of methyl magnetization in solids as predicted by Hubbard [105,106] and observed by Hilt and Hubbard [36], Anil Kumar and Johnson [118], van Putte and others [157,158] and Buchner et al. [159–164]. There have been several observations of non-exponential relaxation during the early 1960s and 1970s, which have been attributed to cross-correlations. As briefly indicated in Section 3.3.1, non-exponential proton spin–lattice relaxation, which is a signature of cross-correlations, was observed in powder samples containing  $\text{CH}_3$  groups [109–118]. It has been pointed out that, in powder samples, the methyl relaxation can be non-exponential due to several reasons, namely cross-correlations, anisotropic reorientations and overlap of multiple sites [37]. One of the unequivocal experiment, for the observation of non-exponential relaxation due to cross-correlations was performed

by Mehring and Raber by studying the relaxation behavior of  $^{19}\text{F}$  in a  $\text{CF}_3\text{COOAg}$  single crystal, where the three-fold axes of all the molecules in the unit cell are collinear [37]. The experimental results agree well with the prediction of the Hubbard–Hilt

theory and is a definitive experimental confirmation of the same. In a series of articles published between 1967 and 1972, Blicharski and coworkers made an extensive theoretical analysis of interference between dipolar, quadrupolar and CSA interactions in systems of 2–4, like or unlike spins along with an experimental study of the non-exponential longitudinal relaxation of  $^{19}\text{F}$  in  $\text{C}_2\text{F}_2\text{Cl}_2$  and  $\text{BF}_3$  [17–20].

From a spectroscopist's viewpoint, the utility of cross-correlations in yielding finer details of molecular structure and dynamics than conventional relaxation parameters was noted in the early years itself and the inclusion of cross-correlation spectral densities was attempted to exploit nuclear spin relaxation to its maximum. For example, in a series of papers, Vold et al. clearly demonstrate the usefulness of cross-correlations in the study of planar molecules [24–29]. Alternatively, the exploitation of non-axially symmetric interactions proved useful as elegantly illustrated by the pioneering work of Huntress [181], and Dolle and Bluhm [182]. While auto-correlation is responsible in thermalization and/or dissipative processes, and can be associated with the measurements of  $T_1$ ,  $T_2$ ,  $T_1$ , or cross relaxation, cross-correlation initiates polarization and coherence transfer and is manifested in higher forms of transient spin orders [183,184].

### 3.4.2. Non-exponential $^{13}\text{C}$ relaxation

There have been several studies involving non-exponential recovery of  $^{13}\text{C}$  magnetization due to cross-correlations in the presence of proton decoupling. Notable among these studies are those by Buchner et al. [159–164], Werbelow and Marshall [165], and Brown et al. [166]. Buchner and Emmerich in 1971 observed a multiplet effect in the dynamic nuclear polarization of  $^{13}\text{C}$  nuclei in the methyl groups of toluene and similar compounds. A difference in relaxation times of  $^{13}\text{C}$  depending on whether the protons are in a quartet or in a doublet state has been found to be the reason for the observed multiplet effect [159]. This difference in  $^{13}\text{C}$  relaxation times is shown to give rise to non-exponential longitudinal relaxation of the methyl group  $^{13}\text{C}$  line in proton-decoupled spectra [160]. Further, it has been theoretically shown that cross-correlations between spin rotation interactions in methyl groups can give rise to non-exponential  $^{13}\text{C}$  relaxation [160]. Proton

decoupled  $^{13}\text{C}$  relaxation was investigated in detail in  $^{13}\text{CH}_2$  and  $^{13}\text{CH}_3$  systems by Werbelow and coworkers [138,165]. They obtained in these systems a biexponential recovery of magnetization, the reason for which was attributed to cross-correlations. It may be noted that cross-correlation effects play a minimal role in  $\text{CH}_3$  where the effects are masked by motional criteria that are rather unlikely to be satisfied except in unusual cases [153]. However, variability in the motional geometries, disappearances of proton-proton influence, and the possibility of zero eigenvalues in the relaxation equations are realistic problems in the  $\text{CH}_2$  case where cross-correlations are more significant [167–171]. An observation of non-exponentiality in  $^1\text{H}$ -coupled  $^{13}\text{C}$ -methyl relaxation was reported by Brown et al. in enriched  $^{13}\text{CH}_3\text{HgO}_2\text{CH}_3$  in  $\text{D}_2\text{O}$  [166]. Contribution of CSA to  $^{13}\text{C}$  relaxation in this system was ruled out by lack of asymmetry in the relaxation of the fully coupled quartet and by observing the same NOE values in two different magnetic fields.

### 3.4.3. Multiplet effect in inversion recovery and NOE experiments

There have been many investigations involving recovery of  $^{13}\text{C}$  magnetization in the presence of proton couplings. In this case, the cross-correlations show up as differential relaxation of the lines of the multiplets, yielding direct evidence of the presence of cross-correlations. Notable among the early studies are by Daragan et al. [39–41], Vold et al. [24–29], Fuson and Prestegard [124–127], Nery et al. [185,186] and Grant et al. [187,188]. One of the earliest observations of multiplet effect was reported in 1966 by Mackor and Maclean, where they have observed differential relaxation of  $^{19}\text{F}$  and its dipolar relaxation with the attached proton [189]. Another clear experimental evidence of cross-correlations is the observation of differential NOE on the  $^{13}\text{C}$  triplet of  $^{13}\text{CH}_2\text{I}_2$  in benzene- $d_6$ , on inversion of protons by Mayne et al. [190] (Fig. 16). The intensities of the carbon-13 triplet deviates from 1:2:1 ratio as a function of the recovery time, except at very short and very long times, clearly establishing the creation of multi-spin order in this  $\text{AX}_2$  spin system.

Fuson and Prestegard observed differential relaxation in polyethylene glycol by using the pulse sequence  $180(^{13}\text{C}, ^1\text{H})-\tau-90(^{13}\text{C})$ -Acquisition [125]

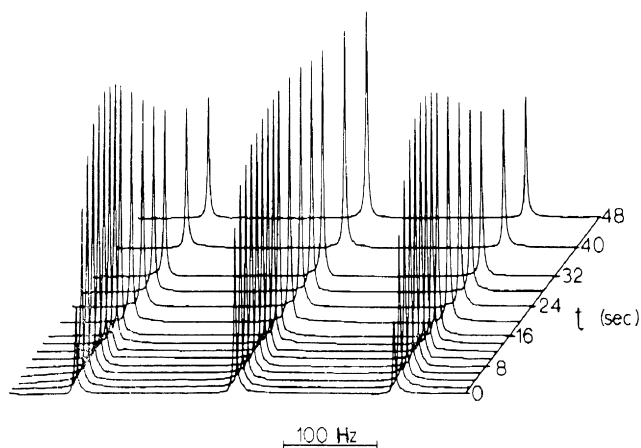


Fig. 16.  $^{13}\text{C}$  NMR time resolved spectra of  $^{13}\text{C}$ -enriched methylene iodide obtained at various times  $t$ , shown in the figure, subsequent to the complete inversion of the proton doublet. [Reproduced with permission from C.L. Mayne, D.M. Grant, D.W. Alderman, J. Chem. Phys. 65 (1976) 1684.]

(Fig. 17). With the help of this sequence, the magnetization mode, which is the difference in the intensities of the outer and inner lines of the triplet of  $\text{CH}_2$  carbons, could be observed. The differences in intensities arise due to  $\text{CH}-\text{CH}'$  and  $\text{CH}-\text{HH}'$  dipole-dipole cross-correlations. An interesting study is the unequal recovery of the proton doublet in an  $^{15}\text{N}$ -enriched sample of a substituted uridine (Fig. 18) by Guéron et al. [191]. They observed that the proton doublet exhibited differential relaxation behavior after selective inversion. This was explained as due to cross-correlation between the CSA of H and H-N dipolar relaxation. This study marks the beginning of several observations of CSA and dipolar cross-correlations through unequal multiplet relaxation as direct evidence of cross-correlations.

Another important development in the observation of CSA-dipole cross-correlations in coupled protons was published by Dalvit and Bodenhausen [45] in a system having two ortho aromatic protons mutually J- and relaxation-coupled. Selective inversion of each doublet followed by a small angle ( $20^\circ$ ) measuring pulse, showed differential recovery of the two lines of the doublet, indicating the creation of two-spin-order terms during the recovery period (Fig. 19). An interesting remark by the authors of this paper is, "the use of  $90^\circ$  measuring pulse is the reason for the non-detection of cross-correlations in 20 years of inversion recovery  $T_1$  measurements in homonuclear coupled

spin systems". Following this work, Dalvit [192] did selective inversion-recovery experiments [using a small-angle ( $30^\circ$ ) observation pulse] on amide protons of the undecapeptide cyclosporine-A, that are J coupled to their respective  $\alpha$ -protons (Fig. 20). The observed differential relaxation of each amide doublet was attributed to the cross-correlation term between the CSA of the amide proton and the  $\text{H}_\text{N}-\text{H}_\alpha$  dipole-dipole interaction [192].

Similar experiments have been performed in heteronuclear spin systems of  $^{13}\text{C}$ ,  $^{19}\text{F}$  and  $^{31}\text{P}$  [193–202]. Unlike the homonuclear spin systems, there is no need for a small angle measuring pulse in the heteronuclear case. Heteronuclear dipolar cross-correlation was observed by Daragan and Mayo in  $^{13}\text{C}$  relaxation measurements in the form of unequal relaxation of individual multiplet lines [51,203]. Typical examples for  $^{13}\text{C}$  are given in Fig. 21 [89],  $^{19}\text{F}$  in Fig. 22 [197] and  $^{31}\text{P}$  in Fig. 23 [198]. Several groups have conclusively shown that the analysis of cross-correlation spectral density terms obtained from the relaxation of  $^{13}\text{C}$  multiplet of  $\text{CH}_2$  and  $\text{CH}_3$  groups can give additional information for molecular rotational motions. Fuson and Prestegard have used this methodology to analyze motions executed by a fatty acyl chain in phospholipid vesicles [127]. This was followed by Daragan and Mayo where they showed that the differential relaxation of  $^{13}\text{C}$  multiplet in a peptide [51,203] can be correlated to the order

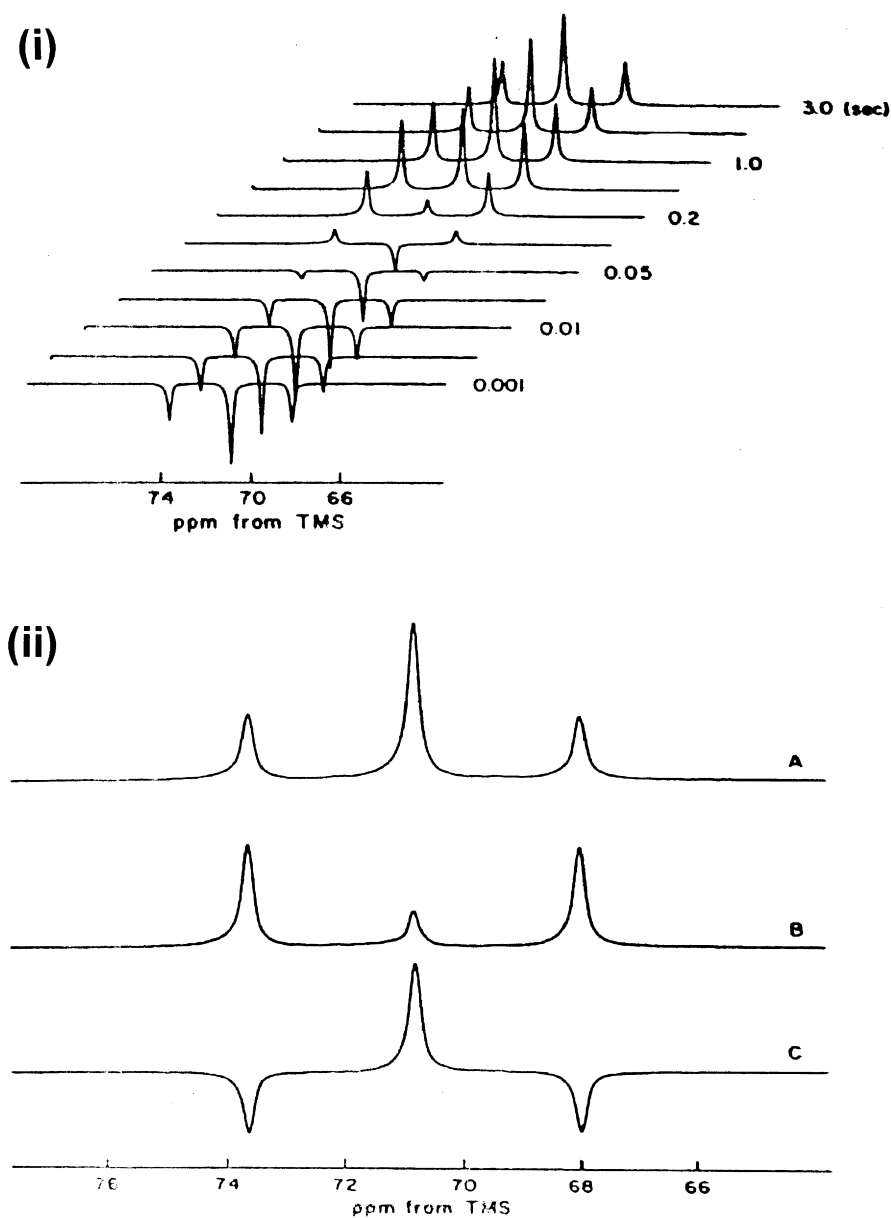


Fig. 17. (i) Inversion recovery spectra for a 20% polyethylene glycol sample at 25°C. Spectra were recorded on a Bruker CXP200 spectrometer using a phase-alternating pulse sequence with a repetition rate of 3 s. Each spectrum is the average of 120 scans. Pulse sequence used was  $180(^{13}\text{C}, ^1\text{H})-\tau-90(^{13}\text{C})-\text{acq}$ . (ii) The 0.2 s spectrum of (i) is reproduced in B. A is the 0.2 s delay spectrum obtained with the addition of a  $90^\circ$  proton pulse along with the  $^{13}\text{C}-90^\circ$  observation pulse. The two  $90^\circ$  pulses suppress the two-spin order term giving rise to spectrum A containing only single-spin  $^{13}\text{C}$  order. C is the difference between A and B, containing exclusively the two-spin order terms. [Reproduced with permission from M.M. Fuson, J.H. Prestegard, *J. Magn. Reson.* 41 (1980) 179.]

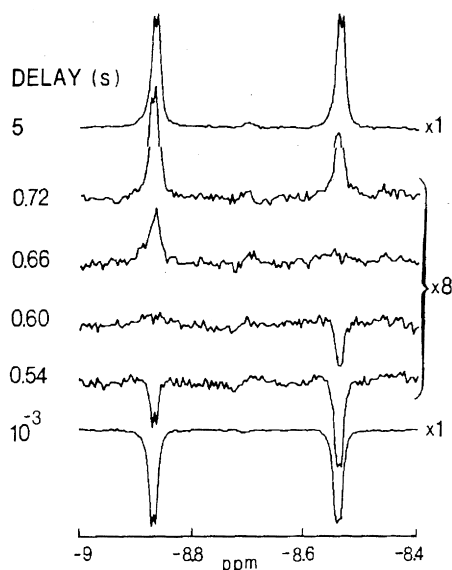


Fig. 18. Inversion-recovery proton NMR spectra for the two components of the imino doublet of 3-<sup>15</sup>N-substituted 2', 3', 5'-tri-*O*-benzoyluridine. The difference in the relaxation rates is ascribed to CSA–dipole cross-correlations. The relative differential in the relaxation rate is  $(11 \pm 2)\%$ . A value of 5.7 ppm is derived for the proton chemical shift anisotropy. [Reproduced with permission from M. Guéron, J.L. Leroy, R.H. Griffey, *J. Am. Chem. Soc.* 105 (1983) 7262.]

parameter or local correlation time along a hydrocarbon chain.

Keeler and Ferrando have shown that the presence of CSA–dipole cross-correlations can give rise to different NOE enhancements for the different lines of a weakly coupled multiplet [42]. In some special cases, the effect is sufficiently large that some lines of the multiplet can show positive enhancements and some negative. Similar effects can also occur due to cross-correlations between separate dipolar relaxation pathways [42]. An earlier study by Nery et al. also considered the effect of CSA–dipole cross-correlations on the NOE [102,185,186].

Cross-correlation effects have also been observed in nucleotides. It has been observed that cross-correlation between <sup>31</sup>P CSA and <sup>31</sup>P–<sup>31</sup>P dipolar relaxation gives rise to differential longitudinal relaxation in adenosine triphosphate (ATP) and diphosphate (ADP) [204]. Batta et al. [205] have recently measured <sup>13</sup>C–<sup>1</sup>H dipolar and <sup>13</sup>C CSA cross-correlation contributions to longitudinal relaxation in <sup>13</sup>CHCl<sub>3</sub>,

triphenylsilane and trehalose using initial rate 1D and 2D experiments, in which the two-spin full relaxation matrix ( $3 \times 3$ ) has been analyzed. Attention was paid to careful experimentation, in terms of normalization of 2D experiments to zero mixing time and to the influence of insufficient relaxation delay in such studies. The various rates have been measured to a high accuracy.

#### 3.4.4. Multiplet effect in NOESY experiments

A widely used method for the observation of cross-correlations is the conversion of multi-spin longitudinal order created by cross-correlations into multiple quantum coherences, which in turn, are detected via multiple quantum-filtered NOESY. Dalvit and Bodenhausen have combined the principle of double quantum filtration with 2D spectroscopy for the study of homonuclear spin systems [45]. This experiment is referred to as DQF NOESY, which is employed to measure the build up of longitudinal two-spin order [45]. This also provides unequivocal evidence for the presence of the cross terms between CSA of proton and the proton–proton dipolar interactions particularly for the aromatic protons. In this experiment, the initial longitudinal single-spin order at  $\tau_m = 0$  is converted during  $\tau_m$  into two-spin longitudinal order by CSA–dipole cross-correlations, which in turn gets converted into two-spin transverse coherence containing both double- and zero-quantum coherences of which only double-quantum coherence is detected by the double-quantum filter. The diagonal and the cross peaks in this experiment imply the presence of CSA–dipole cross-correlation terms (Fig. 24). This experiment is similar to the triple-quantum filtered NOESY [206,207], which monitors the build-up of the longitudinal three-spin order created from the longitudinal single-spin order by dipolar cross-correlations in three-spin systems (Fig. 25).

Oschkinat et al. have used a small angle NOESY experiment ( $90^\circ\text{--}\alpha\text{--}\beta$  with  $\alpha = \beta = 20^\circ$ ), which allows observation of the multi-spin order created from single-spin order via cross-correlations during the mixing time of NOESY [87]. A modification of this experiment has been suggested by Grace and Kumar in which the second pulse is  $90^\circ$  and the third is a small angle pulse or vice versa [208]. This suppresses the direct pumping effects and renders the differences in the intensities of various lines of a

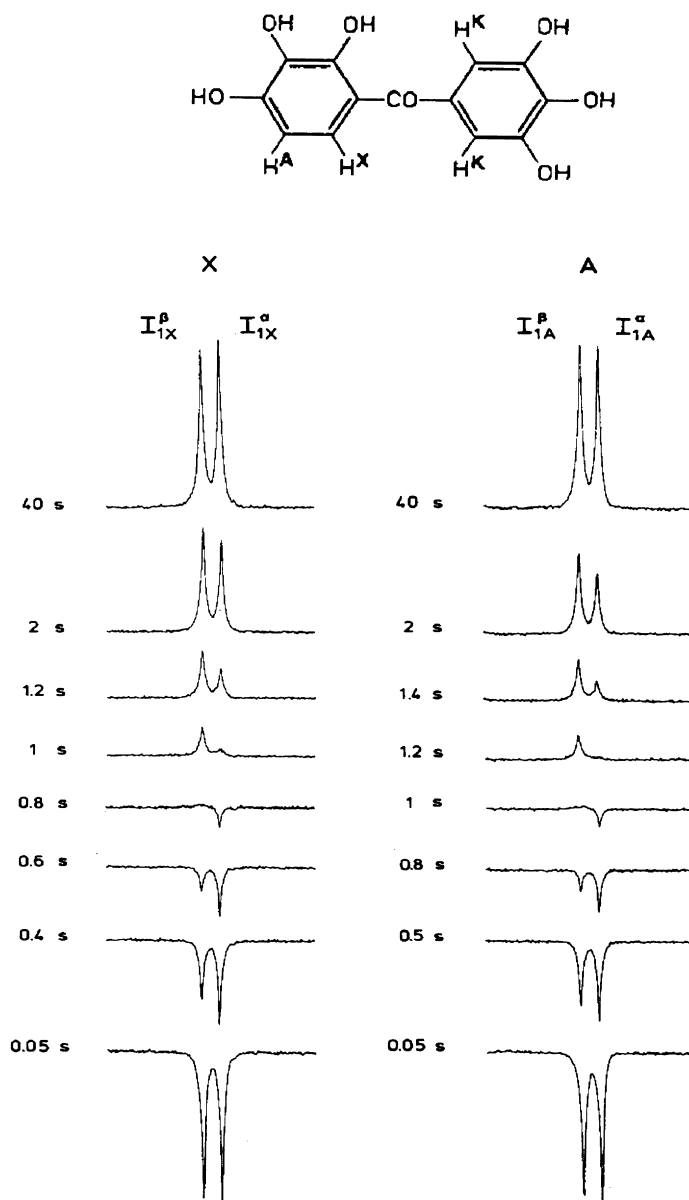


Fig. 19. Selective inversion-recovery spectra, at 500 MHz corresponding to each doublet of the two-spin system of ring protons of Adlone recorded with a 20° measuring pulse. The differential relaxation of the doublets of each proton arises from creation of the two-spin-order term during the recovery period by the cross terms between CSA of the aromatic proton and its dipolar coupling with the other aromatic proton. [Reproduced with permission from C. Dalvit, G. Bodenhausen, Chem. Phys. Lett. 161 (1989) 554.]

multiplet as entirely due to cross-correlations. Since resolution along  $\omega_2$  is usually better than that along  $\omega_1$ , the NOESY 90°–90°– $\alpha$  experiment is preferred. Hence, these flip-angle-dependent NOESY experi-

ments, where the various multiplets of a spin are well resolved yield direct evidence for cross-correlations.

Several sensitive pulse sequences have been

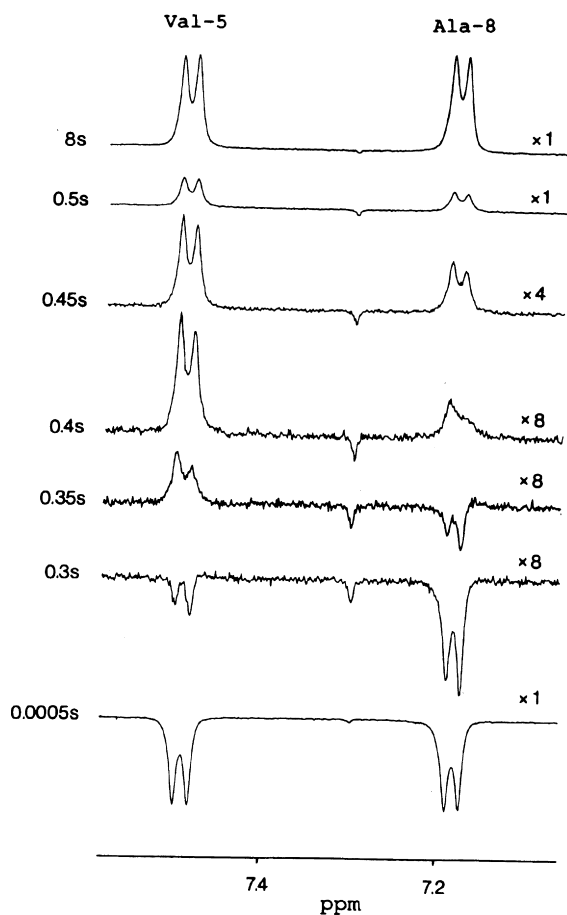


Fig. 20. Selective inversion-recovery spectra of the amide proton region of cyclosporine A (30 mg in 0.6 ml  $\text{CDCl}_3$ ) recorded at 300 K with a  $30^\circ$  detection pulse. The spectra were recorded on a Bruker AM-500 spectrometer. The two doublets correspond to the NH proton resonances for the residues Val-5 (left) and Ala-8 (right). The time indicated on the left of each spectrum is the interval between the  $180^\circ$  pulse and the detection pulse. [Reproduced with permission from C. Dalvit, *J. Magn. Reson.* 95 (1991) 410.]

developed to monitor the CSA–dipole cross-correlations such as polarization transfer [183,184], 2D Soft NOESY [209], Ortho ROESY [210], SLOESY [211] and Overbodenhausen [212] experiments.

### 3.4.5. Observation of antiphase magnetization

Jaccard et al. have shown that in heteronuclear spin systems one can selectively observe the conversion of

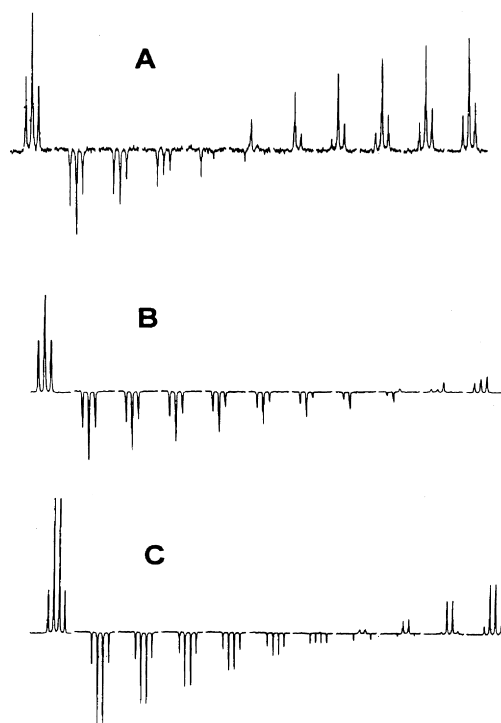


Fig. 21. Proton-coupled  $^{13}\text{C}$  inversion-recovery spectra showing relaxation in the multiplets of  $^{13}\text{C}$  spins in a peptide and in a small molecule. (A) Measurements of selectively enriched  $\text{C}^\alpha$  of Gly-10 in the hexadecapeptide GVKGDKNPGWPGAPY recorded at 283 K at the carbon resonance frequency of 150 MHz. Time intervals are 2, 0.025, 0.05, 0.075, 0.1, 0.15, 0.2, 0.25, 0.3, 0.35 and 0.4 s. (B) and (C) give comparative data, respectively, for methylene and methyl carbons of ethanol, recorded at 299 K. Time intervals are 20, 0.5, 1, 1.5, 2, 2.5, 3, 3.5, 4, 5 and 6 s. For the glycine, the inner line relaxes faster than the outer lines (A); for the  $\text{CH}_2$  group of ethanol, the outer lines relax faster than the inner line (B). For the ethanolic methyl carbon, the inner lines relax faster than the outer lines (C). All these differential relaxations demonstrate the presence of cross-correlation between the CSA of carbon and its dipolar relaxation with the attached protons. [Reproduced with permission from V.A. Daragan, K.H. Mayo, *Chem. Phys. Lett.* 206 (1993) 393.]

single-spin order to two-spin longitudinal order term via the cross-correlation between CSA and dipolar interactions by converting it into antiphase magnetization by a small angle pulse acting on both spins or by a selective  $90^\circ$  acting on one of them [213]. The antiphase term could also be detected by suppressing the single-spin order term. The growth and decay of antiphase  $^{13}\text{C}$  magnetization was observed as a

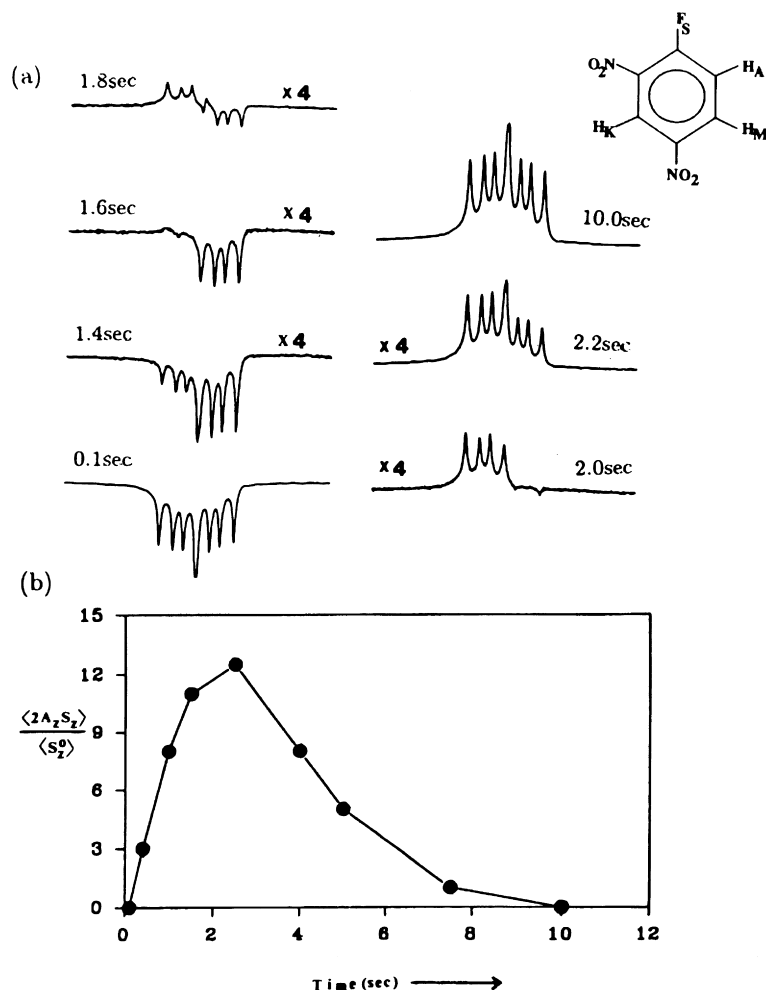


Fig. 22. (a)  $^{19}\text{F}$  inversion-recovery spectra of 1-fluoro-2,4-dinitrobenzene using Bruker AMX-400 spectrometer and the pulse sequence  $180^\circ-\tau-90^\circ$ -Acquire, recorded for recovery times indicated in the spectra. The differential relaxation of the  $^{19}\text{F}$  multiplet reveals the creation of a two-spin order term,  $\langle 2A_z S_z \rangle$ , which reaches a maximum value of about 12% of the single-spin  $^{19}\text{F}$  order and is created by the cross-correlation between the CSA of  $^{19}\text{F}$  and its dipolar relaxation with the proton ortho to it. (b) Normalized build-up of the two-spin order  $\langle 2A_z S_z \rangle / \langle S_z^0 \rangle$  derived from experiment (a). [Reproduced with permission from R.C.R. Grace, Anil Kumar, J. Magn. Reson. A 115 (1995) 87.]

function of recovery time (Fig. 26) [213] in a sample of methyl formate, where there is cross-correlation between the carboxylic  $^{13}\text{C}$  CSA and the  $^{13}\text{C}$ - $^1\text{H}$  dipolar interaction. The experiment used the pulse sequence  $180^S-\tau-90_y^S(90_x^I 90_{\pm x}^I)$ , and the difference of the spectra gives the magnitude of the two-spin order  $2I_z S_z$ . By this difference method, it is possible to detect very small two spin orders of the order of 0.1%.

### 3.5. Isolation of longitudinal relaxation pathways using RF pulses

Levitt and Di Bari [214,215] recently demonstrated a remarkable experiment in which multi-spin longitudinal orders, created by cross-correlations, are “spin-locked” for very long times (steady state). This is obtained by isolating the relaxation pathways by the use of a series of selective and

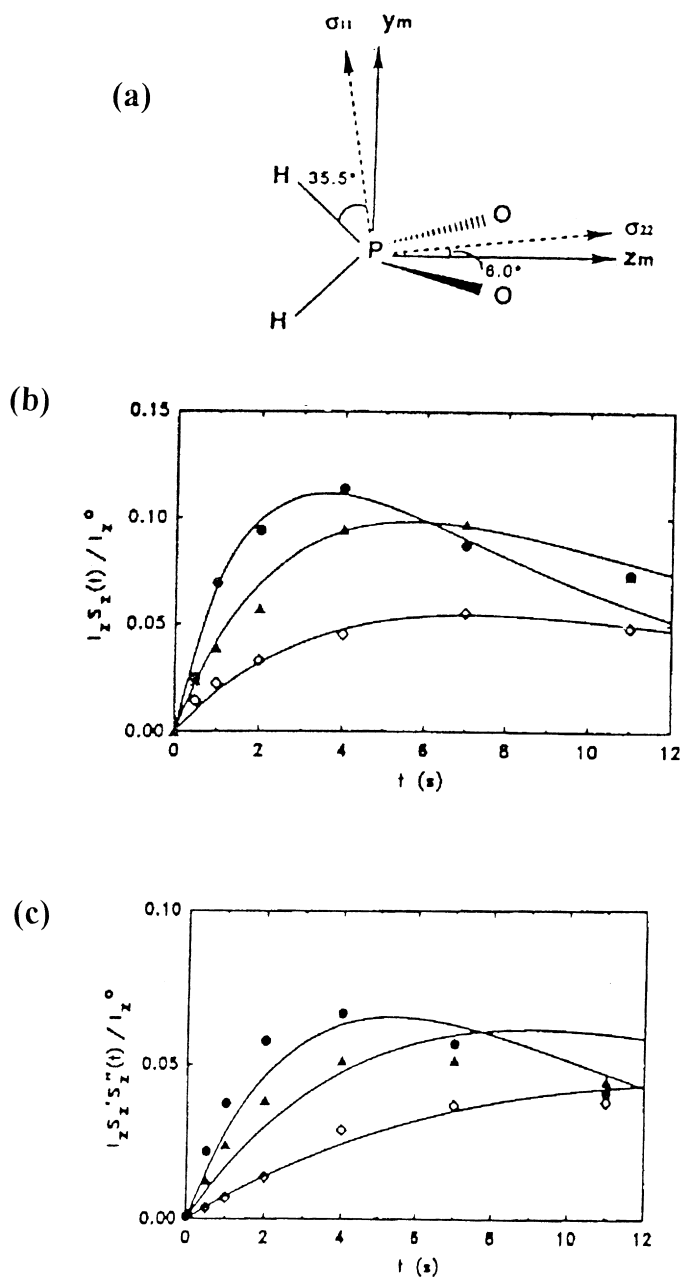


Fig. 23. (a) Schematic diagram of the hypophosphite (HP) ion showing the relative orientation of the chemical shielding tensor with respect to the molecular frame. The subscript *m*, denotes the molecular frame. (b) Normalized  $\langle I_Z S_Z \rangle(t) / I_Z^0$ , two-spin order relaxation profiles of HP, at various temperatures (filled circles—276 K, filled triangles—294 K and open diamonds—329 K), obtained by inversion recovery of the  $^{31}\text{P}$  nuclei. The solid curves were calculated at the respective temperatures with  $\tau_c = 13.9$ , 7.6 and 3.1 ps. The two-spin order is created by the cross-correlation between the CSA of  $^{31}\text{P}$  and its dipolar interaction with the protons coupled to it. (c) Normalized  $\langle I_Z S'_Z S''_Z \rangle(t) / I_Z^0$ , three-spin orders, for various temperatures (same as (b)), obtained with the inversion of both  $^{31}\text{P}$  and  $^1\text{H}$  nuclei. The three-spin order is created due to the dipole–dipole cross-correlations. Theoretical calculations used the same parameters as that of (b). [Reproduced with permission from C.L. Tsai, W.S. Price, Y.C. Chang, B.C. Perng, L.P. Hwang, *J. Phys. Chem.* 95 (1991) 7546.]

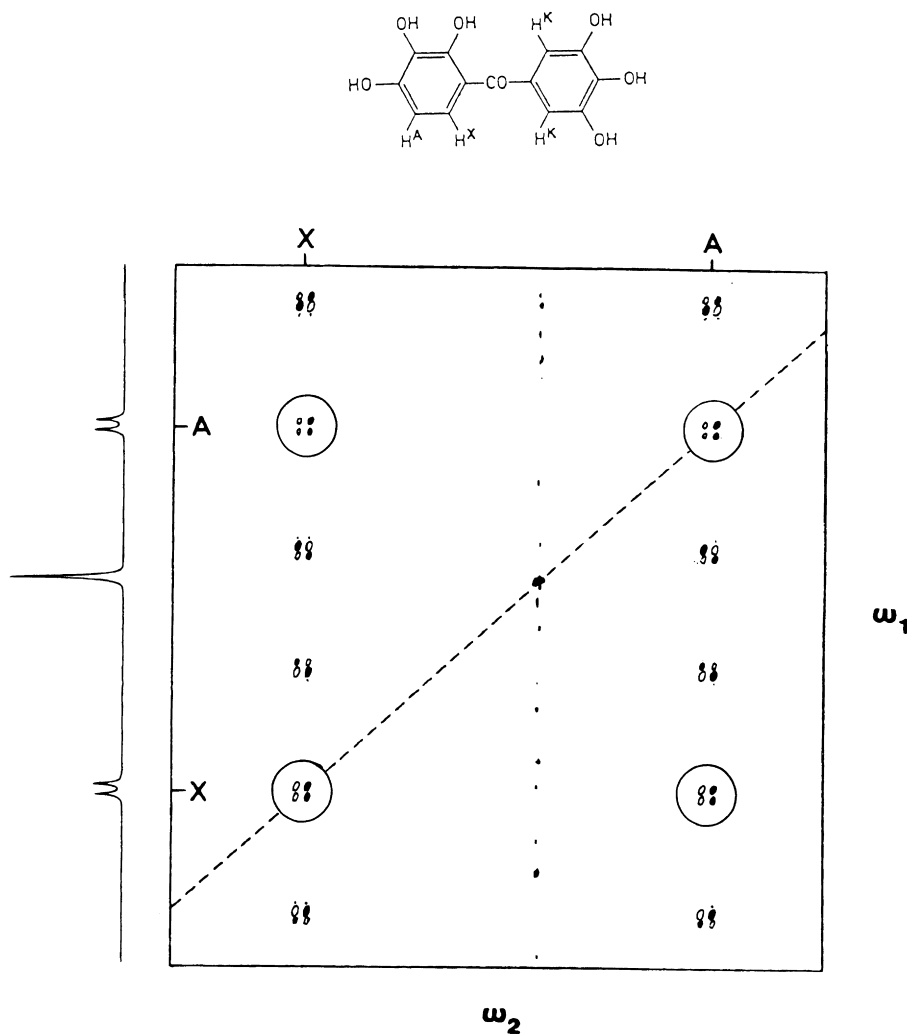


Fig. 24. Double-quantum filtered NOESY proton spectrum at 500 MHz of Adlone recorded with the pulse sequence  $90_{\phi 1}^0-t_1-90_{\phi 2}^0-(\tau_m + \mu t_1)-90_{\phi 3}^0-\Delta-90_{\phi 4}^0-t_2$  with a mixing time of 2.6 s and  $\mu = (1/3)$ . The spectrum contains four multiplets (peaks inside the circles) at  $(\omega_A, \omega_A)$ ,  $(\omega_A, \omega_X)$ ,  $(\omega_X, \omega_A)$  and  $(\omega_X, \omega_X)$  because of longitudinal two-spin order. These multiplets have pure absorptive phase in both dimensions and are in-phase in  $\omega_1$  and antiphase in  $\omega_2$ , with respect to  $J_{AX}$ . The remaining eight multiplets arise from zero-quantum terms and can be identified because of their displacement in  $\omega_1$ . The zero-quantum multiplets are antiphase in both dimensions; they have pure absorptive phase in  $\omega_2$ , but they feature a mixture of absorptive and dispersive phase in  $\omega_1$  which depends on the duration of the mixing time. [Reproduced with permission from C. Dalvit, G. Bodenhausen, Chem. Phys. Lett. 161 (1989) 554.]

non-selective  $180^\circ$  pulses. They also demonstrated that this method can be used for the detection of very small cross-correlations. The explanation of the experiment is through the Homogeneous-Master-Equation (HME) approach which is outlined in the following.

### 3.5.1. The Homogeneous-Master-Equation (HME) approach

The equation of motion of the density matrix (Eq. (21)):

$$\frac{d\sigma}{dt} = -i[\mathcal{H}_{\text{coh}}, \sigma] + \Gamma(\sigma - \sigma_{\text{eq}}), \quad (88)$$

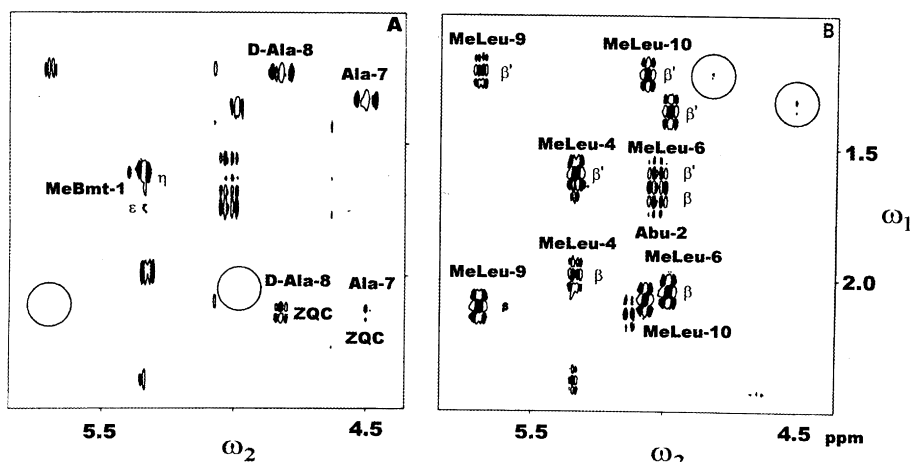


Fig. 25. Parts of triple-quantum filtered (A) NOESY and (B) COSY proton spectra of the  $\alpha$ - $\beta$  region of the cyclic undecapeptide cyclosporin-A in  $\text{CDCl}_3$ , recorded at 400 MHz. The zero-quantum peaks in (A) have been shifted using the mixing time as  $\tau_m + kt_1$  with  $k = (1/3)$  and have been identified. In COSY, peaks are doubly antiphase in both  $\omega_1$  and  $\omega_2$  dimensions. In NOESY, the peaks arise due to cross-correlations and are antiphase in  $\omega_2$ , but in-phase in  $\omega_1$ . A large number of such peaks are present indicating the presence of significant dipole-dipole cross-correlations in several residues. Circled peaks are strong in one spectrum and weak in the other. The peaks missing in NOESY and present in COSY are due to spins which have resolved J-couplings but weak cross-correlations. On the other hand, peaks present in NOESY and absent in COSY are due to spin systems which have no resolved J-couplings, but show cross-correlations. Weak alanine peaks (circled) in COSY are due to violation of coherence transfer selection rules. Negative contours have been filled in for clarity. [Reproduced with permission from C. Dalvit, G. Bodenhausen, J. Am. Chem. Soc. 110 (1988) 7924.]

is an inhomogeneous differential equation, in which the inhomogeneous term  $\sigma_{\text{eq}}$  has been added in an adhoc manner to conform to the equilibrium magnetization ( $M_0$ ) in the presence of  $B_0\vec{k}$  field. Here  $\mathcal{H}_{\text{coh}}$  represents the coherent part and  $\Gamma$  the relaxation part of the Hamiltonian. The equilibrium density matrix is given by:

$$\sigma_{\text{eq}} = Z^{-1} \exp(-\mathcal{H}_{\text{coh}}\tau_\theta) \quad (89)$$

where  $Z$  is the partition function. The temperature ( $T$ ) of the lattice is introduced through a time constant:

$$\tau_\theta = \frac{\hbar}{kT} \quad (90)$$

Using the high temperature approximation  $|\mathcal{H}_{\text{coh}}\tau_\theta| \ll 1$ ,  $\sigma_{\text{eq}}$  reduces to:

$$\sigma_{\text{eq}} \cong \frac{1}{n} (1 - \mathcal{H}_{\text{coh}}\tau_\theta) \quad (91)$$

where  $n$  is the number of states of each individual spin system. Since  $\mathcal{H}_{\text{coh}}$  commutes with  $\sigma_{\text{eq}}$ , the master equation leads to the correct convergence of  $\sigma$  to  $\sigma_{\text{eq}}$  at long times.

The master equation (88) has a peculiar asymmetric form in which the coherence part applies to the full density matrix and the relaxation part only to the deviation from equilibrium. It is possible to isolate the various relaxation pathways of a spin system by applying radio frequency pulses, but theoretically one runs into difficulty, because of the inhomogeneous nature of Eq. (88). Levitt and Di Bari have solved this problem by homogenizing the master equation [214,215]. Following Jeener [216], they showed that instead of adding a  $\sigma_{\text{eq}}$  term, the relaxation super-operator  $\Gamma$  can be “improved” such that, in Liouville space the new master-equation has the form:

$$\frac{d\sigma}{dt} = (-i\hat{\mathcal{H}} + \hat{Y})\sigma = -i[\mathcal{H}_{\text{coh}}, \sigma] + \hat{Y}\sigma \quad (92)$$

where

$$\hat{Y} = \hat{\Gamma} + \hat{\Theta}. \quad (93)$$

An expression for  $\hat{\Theta}$  can be derived by the following argument. The matrix elements of  $\hat{\Gamma}(\langle P_r | \hat{\Gamma} | P_s \rangle)$  are the transition probabilities,  $W_{rs}$ . For a lattice at temperature  $T$ ,  $W_{rs}$  differs from  $W_{sr}$  by a small factor

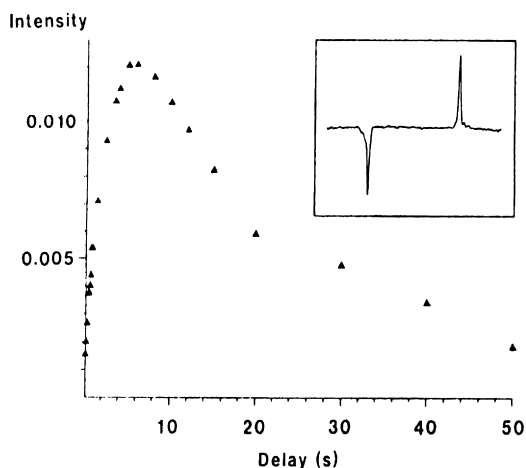


Fig. 26. Intensity of the longitudinal, two-spin order  $(-2I_z S_z)/\Delta S_z$  as a function of the recovery delay  $\tau$  for an experiment on the  $^{13}\text{C}$ -enriched carboxylic carbon of methyl formate, where two spectra with  $\phi = \pm x$  were recorded and stored separately for each value of the delay  $\tau$  in the sequence  $180^{0S}-\tau-90^{0S}(90^{0I}90^{0I})$ -Acquire. The difference of the spectra gives the two-spin-order term,  $2I_z S_z$ . This difference method allowed detection of very small two-spin orders (0.1%). The insert shows the difference spectrum observed after a relaxation delay of 6 s. The spectra were recorded at 100 MHz carbon frequency. [Reproduced with permission from G. Jaccard, S. Wimperis, G. Bodenhausen, Chem. Phys. Lett. 138 (1987) 601.]

given by  $\exp[(\omega_r - \omega_s)\tau_\theta]$  where  $\tau_\theta = \hbar/kT$ . This suggests the following form for the adjusted relaxation superoperator

$$\hat{Y} = \hat{\Gamma} \exp\{\hat{\omega}\tau_\theta\} \quad (94)$$

where  $\hat{\omega} = \sum_r \omega_r \hat{P}_r$ . Assuming the high-temperature approximation, the thermal correction term is  $\hat{\Theta} = \hat{\Gamma} \omega \tau_\theta$ . The effect of adding this correction term is to expand the equation of motion of various longitudinal magnetization modes by adding the normalized unit operator  $\frac{1}{2}\mathbf{1}$ . For example, for a two spin system  $IS$ , the equation of motion in the absence of RF is given by:

$$\frac{d}{dt} \begin{pmatrix} \langle \frac{1}{2}\mathbf{1} \rangle \\ \langle I_z \rangle \\ \langle S_z \rangle \\ \langle 2I_z S_z \rangle \end{pmatrix} = \begin{pmatrix} 0 & 0 & 0 & 0 \\ \theta_I & -\rho_I & -\sigma_{IS} & -\delta_I \\ \theta_S & -\sigma_{IS} & -\rho_S & -\delta_S \\ \theta_{IS} & -\delta_I & -\delta_S & -\rho_{IS} \end{pmatrix} \begin{pmatrix} \langle \frac{1}{2}\mathbf{1} \rangle \\ \langle I_z \rangle \\ \langle S_z \rangle \\ \langle 2I_z S_z \rangle \end{pmatrix} \quad (95)$$

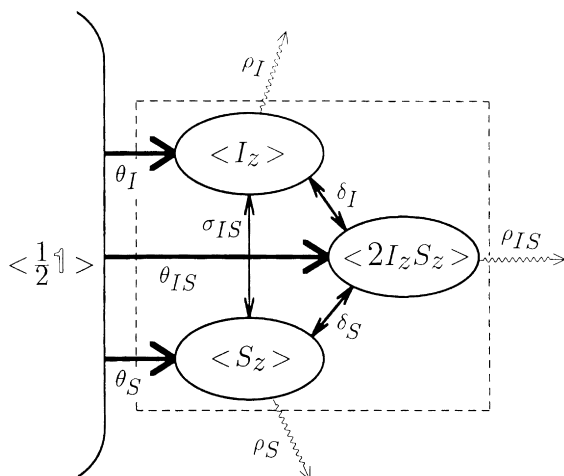


Fig. 27. Physical interpretation of the Homogeneous Master equation (Eq. (95)) for the two-spin system. The expectation values of the four spin-operators  $(\frac{1}{2}\mathbf{1})$ ,  $I_z$ ,  $S_z$  and  $2I_z S_z$  constitute reservoirs. The three terms  $\theta_I$ ,  $\theta_S$  and  $\theta_{IS}$  represent the creation of spin order by polarization from the environment. The  $\rho$  terms represent the self relaxation rate of each mode,  $\sigma$  the cross-relaxation and  $\delta$  the cross-correlation rates, respectively. [Reproduced with permission from M.H. Levitt, L. Di Bari, Bull. Magn. Reson. 16 (1994) 94.]

The three new elements of the relaxation matrix are:

$$\begin{aligned} \theta_I &= -\frac{1}{2}(\rho_I \omega_I^0 + \sigma_{IS} \omega_S^0) \tau_\theta \\ \theta_S &= -\frac{1}{2}(\sigma_{IS} \omega_I^0 + \rho_S \omega_S^0) \tau_\theta \\ \theta_{IS} &= -\frac{1}{2}(\delta_I \omega_I^0 + \delta_S \omega_S^0) \tau_\theta \end{aligned} \quad (96)$$

where  $\omega_I^0$  and  $\omega_S^0$  are the Larmor frequencies of the two species. The zeroes in the top row indicate that the expectation value of  $\langle \frac{1}{2}\mathbf{1} \rangle$ , which represents the amount of spin disorder, does not change with time.

A pictorial representation of the dynamics of Eq. (95) is shown in Fig. 27. The relaxation dynamics appears as a unidirectional flow from left to right in the picture. The physical significance of this “flow” is as follows. The “reservoirs” enclosed by the dotted line contains “spin-order”, which can be redistributed internally by  $\sigma$  and  $\delta$  terms. The object on the left contains the large  $\langle \frac{1}{2}\mathbf{1} \rangle$  term, that is the disorder of the spin system. The three arrows labeled  $\theta_I$ ,  $\theta_S$  and  $\theta_{IS}$  indicate conversion of spin disorder into spin order, that is a decrease in spin-entropy due to the polarizing influence of the finite temperature molecular environment. These three terms therefore take into account

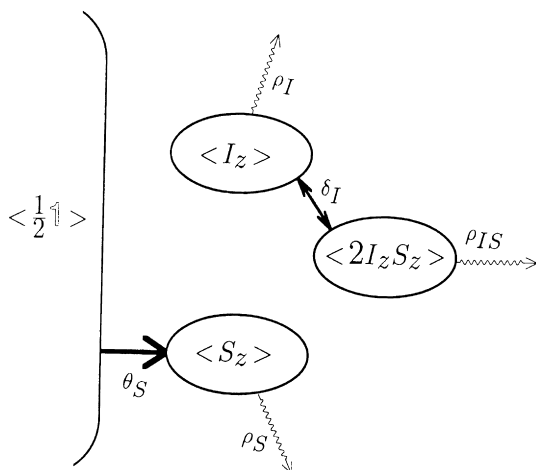


Fig. 28. Relaxation dynamics in the presence of rapid  $\pi$  pulses on the  $I$ -spins. The effective relaxation superoperator is factored into a *gerade* subspace  $\{\langle \frac{1}{2}1 \rangle, \langle S_Z \rangle\}$  and an *ungerade* subspace  $\{\langle I_Z \rangle, \langle 2I_Z S_Z \rangle\}$ . [Reproduced with permission from M.H. Levitt, L. Di Bari, Bull. Magn. Reson. 16 (1994) 94.]

the spin-bath correlations. The three wiggly arrows marked  $\rho_I$ ,  $\rho_S$  and  $\rho_{IS}$  indicate dissipation of spin order, that is creation of spin entropy. These arrows do not need to “go anywhere” since the destruction of order is an irreversible process. Thermal equilibrium is established when the expectation values  $\langle I_Z \rangle$ ,  $\langle S_Z \rangle$  and  $\langle 2I_Z S_Z \rangle$  reach steady-state values such that as much spin energy is created as is destroyed.

### 3.5.2. Isolation of coupling networks by application of RF pulses

The advantage of the above picture becomes clear when  $\pi$  pulses are applied rapidly to the system. If evenly spaced strong  $\pi$  pulses are applied rapidly (in times shorter than the relaxation time of the various spin orders), Levitt and Di Bari have shown that the spin operators transform under these pulses, yielding, for example, for  $\pi$  pulses only on  $I$  spins, the following transformations [214,215],  $\frac{1}{2}1 \rightarrow \frac{1}{2}1$ ;  $I_Z \rightarrow -I_Z$ ;  $S_Z \rightarrow S_Z$ ;  $2I_Z S_Z \rightarrow 2I_Z S_Z$ . These operators are then separated out into two subspaces, *gerade* subspace (operators which do not change sign) and *ungerade* subspace (which change sign). For rapid pulsing

$$\left( \frac{\tau}{4} - \pi_I - \frac{\tau}{2} - \pi_I - \frac{\tau}{4} \right)_n$$

with interval  $\tau \ll T_1$ , these two subspaces evolve

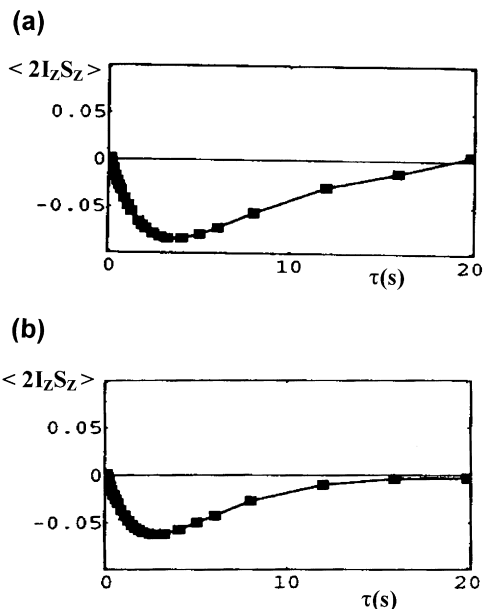


Fig. 29. Experimental results for  $^{13}\text{C}$ -labeled chloroform at a proton frequency of 200 MHz. (a) The experiment uses two phase-cycled  $\pi/2$  pulses on the  $I$  spins: These select the contribution from initial  $\langle I_Z \rangle$  polarization at the beginning of the mixing period  $\tau$ . A  $\pi/2$  pulse on the  $S$ -spins at the end of the  $\tau$  period allows the detection of  $\langle S_Z \rangle$  and  $\langle 2I_Z S_Z \rangle$ . As there is a single  $\pi$  pulse on the  $I$  spin, there is no manipulation of the relaxation network. (b) Two  $I$ -spin  $\pi$  pulses are added at  $\tau/4$  and  $3\tau/4$ , which isolates the *ungerade* space with  $\langle I_Z \rangle$  and  $\langle 2I_Z S_Z \rangle$ . [Reproduced with permission from M.H. Levitt, L. Di Bari, Bull. Magn. Reson. 16 (1994) 94.]

independently of each other breaking the links between them. For example as shown in Fig. 28, under rapid  $\pi$  pulses on  $I$  spin, the *gerade* subspace contains only the terms  $\langle \frac{1}{2}1 \rangle$  and  $\langle S_Z \rangle$ , which are coupled to each other by  $\theta_S$  and *ungerade* subspace  $\langle I_Z \rangle$  and  $\langle 2I_Z S_Z \rangle$ , which are coupled to each other by  $\delta_I$  and not connected to the *gerade* subspace. The dynamics in the *gerade* space is that  $\langle S_Z \rangle$  gets polarized at the rate  $\theta_S$  and dissipates at the rate  $\rho_S$ . The dynamics of the *ungerade* space is that  $\langle I_Z \rangle$  and  $\langle 2I_Z S_Z \rangle$  are coupled by  $\delta_I$  and dissipate via  $\rho_I$  and  $\rho_{IS}$ , respectively. The evolution of the two-spin order  $\langle 2I_Z S_Z \rangle$  has been measured by two separate experiments: (i) in which there are no  $\pi$  pulses on  $I$  spin during relaxation and two pathways namely,  $\langle I_Z \rangle \xrightarrow{\rho_{IS}} \langle S_Z \rangle \xrightarrow{\delta_S} \langle 2I_Z S_Z \rangle$  and  $\langle I_Z \rangle \xrightarrow{\delta_I} \langle 2I_Z S_Z \rangle$  contribute [Fig. 29(a)]; (ii) in which only the later pathway contributes as the *ungerade* space is isolated by a

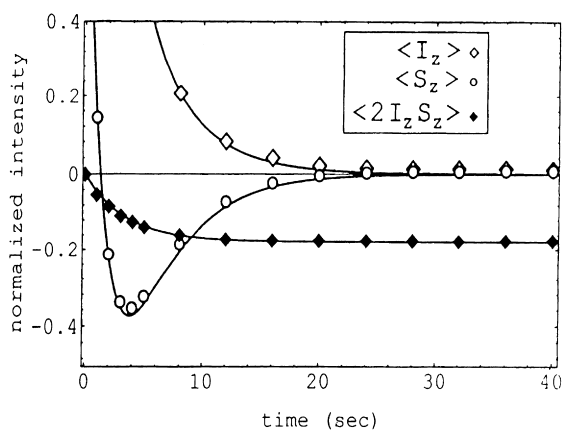


Fig. 30. Experimental results for  $^{13}\text{C}$ -labeled chloroform at a proton frequency of 200 MHz, on rapid application of simultaneous  $\pi$  pulses on both proton ( $I$ ) and  $^{13}\text{C}$  ( $S$ ) spins. The *ungerade* space consists of  $\langle I_z \rangle$  and  $\langle S_z \rangle$ , which are coupled by  $\sigma_{IS}$ .  $\langle I_z \rangle$  and  $\langle S_z \rangle$  saturate from their equilibrium value to zero, with  $\langle S_z \rangle$  showing NOE transfer at intermediate times. The *gerade* space consists of  $\langle (1/2)1 \rangle$  and  $\langle 2I_z S_z \rangle$ , which are coupled by  $\theta_I$ . The two-spin order gets polarized from  $\langle (1/2)1 \rangle$  and decays by  $\rho_{IS}$  reaching a steady state value. [Reproduced with permission from M.H. Levitt, L. Di Bari, Phys. Rev. Lett. 69 (1992) 3124.]

series of  $\pi$  pulses on  $I$  spin during relaxation [Fig. 29(b)]. The observed maximum magnitude and the rates of build-up of  $\langle 2I_z S_z \rangle$  in the two experiments are clearly different.

The case when  $\pi$  pulses are applied to both the spins, the *gerade* space contains  $\langle \frac{1}{2}1 \rangle$  and  $\langle 2I_z S_z \rangle$  and the *ungerade* space contains  $\langle I_z \rangle$  and  $\langle S_z \rangle$ . The dynamics of the *ungerade* space is purely dissipative. Order is transferred from  $\langle I_z \rangle$  to  $\langle S_z \rangle$  with the cross-relaxation rate  $\sigma_{IS}$  accompanied by dissipation of both the Zeeman orders by rate constants  $\rho_I$  and  $\rho_S$  (Fig. 30). This describes a normal transient nuclear Overhauser experiment, with the difference that cross-correlation is eliminated in the dynamics of the *ungerade* space. This experiment thus can be used for monitoring NOE, without cross-correlations in two-spin systems.

The dynamics of the *gerade* subspace is also quite interesting. The two spin order  $\langle 2I_z S_z \rangle$  instead of building up and decreasing, is created and spin locked to a steady-state value (Fig. 31), governed by the input rate  $\theta_{IS}$  and dissipation rate  $\rho_{IS}$ , yielding:

$$\langle 2I_z S_z \rangle^{SS} = \frac{\theta_{IS}}{2\rho_{IS}}. \quad (97)$$

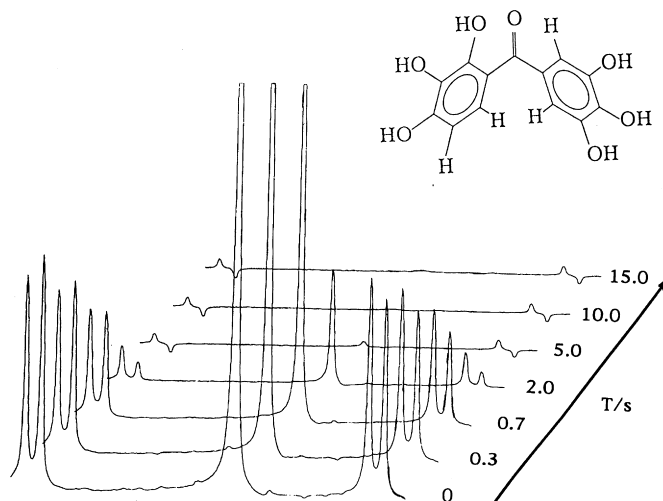


Fig. 31. Experimental  $^1\text{H}$  spectra for exifone at a frequency of 300 MHz, when the  $\pi$  pulses are applied to all the protons with a cycle period of  $\tau = 50$  ms. The normal  $^1\text{H}$  spectrum (lowest plot) shows a four-line AX pattern from the ortho and meta protons on one of the aromatic rings and a strong singlet from the two equivalent ortho protons on the other ring. The topmost spectrum is in the steady state, after the application of many hundreds of  $\pi$  pulses. The two-spin order due to CSA–dipole cross-correlation is small, but not negligible. [Reproduced with permission from M.H. Levitt, L. Di Bari, Bull. Magn. Reson. 16 (1994) 94.]

Using  $\theta_{IS}$  from Eq. (96) and the fact that  $\langle S_Z \rangle^{\text{eq}} = -(1/4)\omega_S^0\tau_\theta$ , one obtains:

$$\frac{\langle 2I_Z S_Z \rangle^{\text{SS}}}{\langle S_Z \rangle^{\text{eq}}} = \frac{\delta_I \omega_I^0 + \delta_S \omega_S^0}{\rho_{IS} \omega_S^0}. \quad (98)$$

Such steady-state two-spin orders have also been observed in a three- [178] and four-spin systems [197] and are shown in Figs. 32 and 33, respectively. In some cases (for example, Figs. 31 and 32), very small cross-correlations have been detected by this method [178,214].

In this section, we have discussed the effect of cross-correlations on longitudinal relaxation. Cross-correlations have a first-order multiplet effect on longitudinal relaxation, such that different lines of a resolved multiplet have differential relaxation as well as NOE. Cross-correlations also have a second order (both in time and magnitude) net effect, which exists even for unresolved multiplets (or non-J-coupled spins) and which cannot be suppressed easily. The net effect of cross-correlations, in general, leads to non-exponential or multi-exponential longitudinal relaxation. The net effect on NOE has been analyzed in detail. It is also found that cross-correlations contribute to longitudinal relaxation of weakly coupled spins, in the absence of RF fields, via the spectral densities only at Larmor frequency. Therefore, for biomolecules for which  $\omega\tau_c$  tends to be greater than one, the effects of cross-correlations decrease progressively. For this reason, experiments have been designed to monitor relaxation in presence of RF fields which will be discussed in Section 5. Alternatively, attention is being focused on effects of cross-correlations in transverse relaxation, where cross-correlations also contribute via spectral densities at zero frequency, which become significant for  $\omega\tau_c \gg 1$ . In the next section, we discuss the effect of cross-correlations on transverse relaxation.

#### 4. Cross-correlations in transverse relaxation

It has been known from the early days of NMR that cross-correlations affect longitudinal as well as transverse relaxation [106,121,217,218]. In this section, the effects of cross-correlation on the transverse relaxation of single-quantum coherence (SQC) and multiple-quantum coherence of coupled spin systems

are discussed in detail. Differential line broadening (DLB) is the earliest signature of the effects of cross-correlations on transverse relaxation [217–221]. From the “kite” structure of the Redfield relaxation matrix (Fig. 1), as stated in Section 2.1.1, the time evolution of the diagonal and off-diagonal elements of the density matrix are completely decoupled in the absence of RF fields. Each single- or multiple-quantum order of the off-diagonal elements also evolves independent of the other orders. In general, the time evolution of the off-diagonal elements can be written, neglecting the dynamic frequency shift as:

$$\frac{d\sigma(t)}{dt} = (-i\mathcal{H} + R)\sigma(t) \quad (99)$$

where  $\sigma(t)$  is a vector for the off-diagonal elements of the density matrix,  $\mathcal{H}$  the time-independent Hamiltonian and  $R$  the relaxation superoperator. The formal solution of Eq. (99) is given by:

$$\sigma(t) = e^{(-i\mathcal{H} + R)t} \sigma(0). \quad (100)$$

However, the solution is not straight forward if  $\mathcal{H}$  and  $R$  do not commute since it requires diagonalization of non-Hermitian complex matrices. Eq. (100) simplifies under the condition that the differences in the diagonal elements of  $\mathcal{H}$  are large compared to the off-diagonal elements of  $R$ . Under the secular approximation, the  $R$  matrix, becomes block diagonal, as represented by the dashed lines in Fig. 1, such that the time evolution of all coherences of same order are coupled within themselves, but decoupled from coherences of different order. Further simplification is obtained when all coherences within the same order are also well resolved such that:

$$\begin{aligned} & |(\mathcal{H}_{\alpha\alpha} - \mathcal{H}_{\alpha'\alpha'}) - (\mathcal{H}_{\beta\beta} - \mathcal{H}_{\beta'\beta'})| \\ & = |\omega_{\alpha\alpha'} - \omega_{\beta\beta'}| \gg R_{\alpha\alpha'\beta\beta'} \end{aligned} \quad (101)$$

In such cases,  $R_{\alpha\alpha'\beta\beta'}$  can be neglected and one obtains single- exponential decay rate for each coherence of frequency  $\omega_{\alpha\alpha'}$ , given by the diagonal elements  $R_{\alpha\alpha'\alpha\alpha'}$ . This is known as the simple-line approximation. Transverse relaxation thus strongly depends on whether the simple-line approximation holds or not. When it does not hold, the evolution of various coherences of the same order remain coupled and leads to multi-exponential transverse relaxation. In the case of partially resolved multiplets, the situation is complex. In Section 4.2, we will be discussing the linewidths of

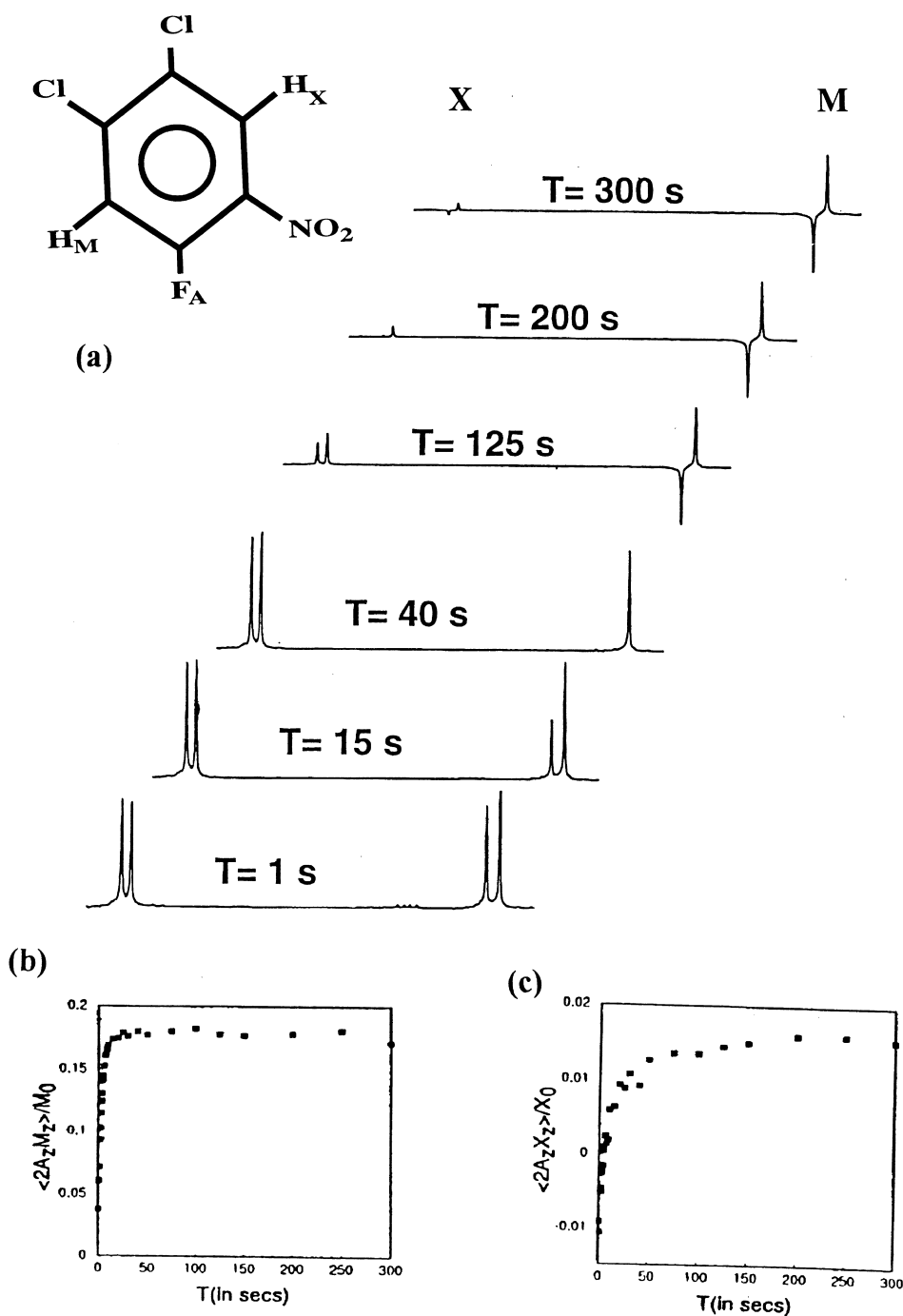


Fig. 32. (a) Experimental  $^1H$  spectra at 400 MHz for 1,2-dichloro-4-fluoro-5-nitrobenzene dissolved in  $CDCl_3$ , recorded when  $\pi$  pulses are applied on both  $^{19}F$  and  $^1H$  nuclei with a  $\tau$  delay of 500 ms between the pulses. The last trace shows the steady state spectrum. The two-spin order for the  $M$ -spin is large whereas that of the  $X$ -spin is small, due to the weak dipolar interaction between  $A$  and  $X$  spins. (b) Normalized buildup of the two-spin order  $\langle 2A_z M_z \rangle$  for the  $M$ -spin. (c) Same as (b) for the  $X$ -spin. The steady state value of this two-spin order is small, but not negligible. [Reproduced with permission from Kavita Dorai, Anil Kumar (unpublished results).]

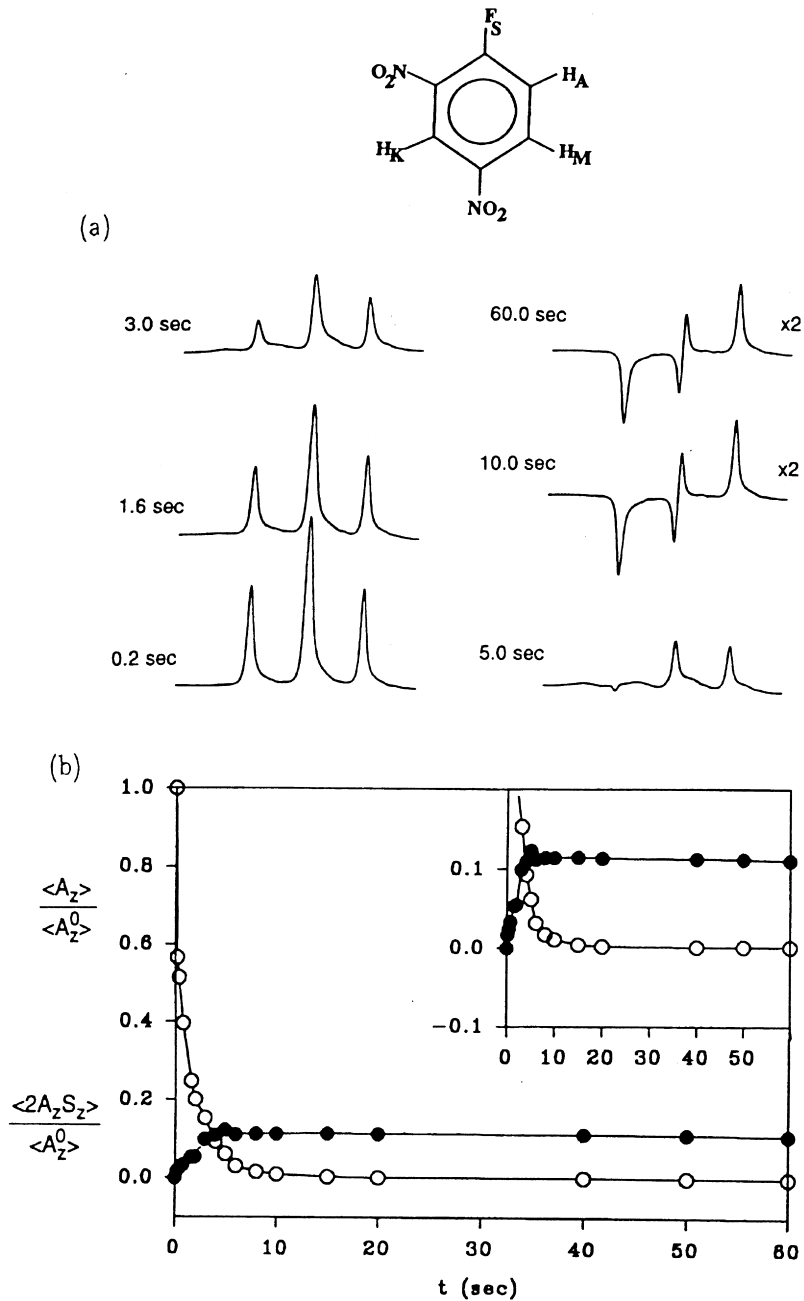


Fig. 33. (a) Experimental  $A$ -spin part of the  $^1\text{H}$  spectrum at 400 MHz of 1-fluoro, 2,4-dinitrobenzene (Fig. 22) in  $\text{CDCl}_3$ , recorded with  $\pi$  pulses on  $^{19}\text{F}$  and  $^1\text{H}$  spins, with pulse duration of 200 ms between the pulses. Some of the spectra are multiplied by a factor 2 as indicated. (b) Normalized decay and buildup of the single  $\langle A_Z \rangle$  (open circles) and two-spin order  $\langle 2A_Z S_Z \rangle$  (filled circles) for the  $A$ -spin. The insert shows the plots on an expanded scale. [Reproduced with permission from R.C.R. Grace, Anil Kumar, J. Magn. Reson. A 115 (1995) 87.]

various coherences of several spin systems under the “simple-line approximation”. However, before discussing these linewidths, a brief description of transverse relaxation in the absence of the simple-line approximation is given in the following section.

#### 4.1. Time evolution of transverse coherence in the absence of simple-line approximation

For a two-spin system AX, the time evolution of the four SQCs from Eq. (99) is given by:

$$\frac{d}{dt} \begin{pmatrix} \sigma_{12}(t) \\ \sigma_{34}(t) \\ \sigma_{13}(t) \\ \sigma_{24}(t) \end{pmatrix} = \left[ -i \begin{pmatrix} \omega_{12} & & & \\ & \omega_{34} & & \\ & & \omega_{13} & \\ & & & \omega_{24} \end{pmatrix} + \begin{pmatrix} R_{1212} & R_{1234} & R_{1213} & R_{1224} \\ R_{3412} & R_{3434} & R_{3413} & R_{3424} \\ R_{1312} & R_{1334} & R_{1313} & R_{1324} \\ R_{2412} & R_{2434} & R_{2413} & R_{2424} \end{pmatrix} \right] \begin{pmatrix} \sigma_{12}(t) \\ \sigma_{34}(t) \\ \sigma_{13}(t) \\ \sigma_{24}(t) \end{pmatrix}. \quad (102)$$

Here  $\omega_{12} = \Omega_A + \frac{1}{2}J$ ;  $\omega_{34} = \Omega_A - \frac{1}{2}J$ ;  $\omega_{13} = \Omega_X + \frac{1}{2}J$  and  $\omega_{24} = \Omega_X - \frac{1}{2}J$  and in general the evolution of each coherence is multi-exponential. However, if  $|\Omega_A - \Omega_X| \gg R_{12ij}, R_{34ij}$ , for  $i, j = 1, 3$  and  $2, 4$ , then the above equation takes the block structure for A and X parts by neglecting the off-diagonal elements of R between the A and X parts, namely  $R_{1213}, R_{1224}, R_{1334}$  and  $R_{2434}$ . The time evolution of the A part, for example, can then be written as [222,223]:

$$\frac{d}{dt} \begin{pmatrix} \sigma_{12}(t) \\ \sigma_{34}(t) \end{pmatrix} = \left[ -i \begin{pmatrix} \omega_{12} & \\ & \omega_{34} \end{pmatrix} + \begin{pmatrix} D_1 & C \\ C & D_2 \end{pmatrix} \right] \times \begin{pmatrix} \sigma_{12}(t) \\ \sigma_{34}(t) \end{pmatrix} \quad (103)$$

with a similar equation for the X part. Here  $D_1 = R_{1212}$ ,  $D_2 = R_{3434}$  and  $C = R_{1234}$ . Eq. (103) can be further transformed into normal modes of spin A using the transformation

$$U = \frac{1}{\sqrt{2}} \begin{pmatrix} 1 & -1 \\ 1 & 1 \end{pmatrix}, \quad (104)$$

yielding the time evolution of the sum mode  $\sigma_{12} + \sigma_{34} = A_+$  and the difference mode  $\sigma_{12} - \sigma_{34} = 2A_+X_z$  as:

$$\frac{d}{dt} \begin{pmatrix} A_+ \\ 2A_+X_z \end{pmatrix} = \begin{pmatrix} \frac{1}{2}(D_1 + D_2) + C - i\Omega_A & \frac{1}{2}(D_1 - D_2) - \frac{1}{2}J \\ \frac{1}{2}(D_1 - D_2) - \frac{1}{2}J & \frac{1}{2}(D_1 + D_2) - C - i\Omega_A \end{pmatrix} \times \begin{pmatrix} A_+ \\ 2A_+X_z \end{pmatrix} \quad (105)$$

The time evolution of this equation can be examined under the following conditions.

- Case (i)  $J = 0$ . In this case, the two A spin coherences are degenerate and only the sum modes can be excited by a RF pulse applied to the system in equilibrium. If in addition cross-correlations are absent then  $D_1 = D_2$  and the sum mode cannot be converted into the difference mode and decays with a single time constant given by  $\frac{1}{2}(D_1 + D_2) + C$ . If however,  $D_1 \neq D_2$ , the difference mode can be created and both the sum and the difference modes remain coupled, with their relaxation being biexponential. Since the difference mode  $2A_+X_z$ , is a “A spin coherence antiphase with respect to spin X”, a  $90^\circ$  pulse on A and X can convert it into  $2A_zX_+$ , which is a “X-spin coherence antiphase with respect to spin A”. Such coherence transfers have been observed and given the name “relaxation allowed coherence transfers (RACT)” [222,223]. These will be further discussed for the AX case in Section 4.2.1.1.
- Case (ii)  $J \gg |D_1 - D_2|$ . In this case, while the sum mode can be created by a selective pulse on one of the spins, the difference mode can be created by either a selective pulse on one of the transitions or by time evolution of the sum mode. Even when one of the modes is created, both the sum and difference modes oscillate rapidly between each other due to large J and decay with an average time constant, given by the average of the diagonal elements of Eq. (105), that is by  $(D_1 + D_2)$  and the term C can be neglected. Going back to Eq. (103), it is seen that in such a case (in which C can be neglected) each off-diagonal element of  $\sigma$

decays exponentially with a single time constant. This is the justification for the simple-line approximation mentioned earlier. In this case, the Redfield matrix has a ‘kite’ structure with each off-diagonal element of  $\sigma_{\alpha\alpha'}$  evolving independently of all others with a single time constant  $R_{\alpha\alpha'\alpha\alpha'}$ , which has contributions also from cross-correlations. However, the sum and difference modes will relax biexponentially like case (i) above, if J-coupling to the other spin is removed by decoupling.

- Case (iii)  $J \approx |D_1 - D_2|$ . This is the case of partially resolved multiplets. In such cases Eqs. (103) and (105) do not simplify and have to be solved numerically with the effects of cross-correlations as an integral part of the solution [223].

#### 4.2. Time evolution of transverse coherence under the simple-line approximation

In the following sections, the linewidths of SQC and multiple-quantum coherences of various spin systems under the simple-line approximation in the presence of cross-correlations are outlined. The spin systems considered are: (i) heteronuclear AX [196,217,219,224–229]; (ii) homonuclear AB [129,230]; (iii) heteronuclear AMX [230,231]; (iv) homonuclear ABX [232–234]; (v) heteronuclear AX<sub>2</sub>

#### 4.2.1. Cross-correlations in the heteronuclear AX spin system

The linewidths of various coherences of a heteronuclear two-spin system under the simple-line approximation [196,217,219,224–229] in which all the coherences (single- and multiple-quantum) are well resolved, can be written in a compact notation developed by Kumar and Kumar [232,233] as:

$$-\vec{R} = \sum_{n=0}^2 \{a(n\omega)J_a(n\omega) + c(n\omega)J_c(n\omega)\} \quad (106)$$

where  $\vec{R}$  is a column vector representing the linewidths of various coherences,  $J_a(n\omega)$  are column vectors of auto-correlation spectral densities at various frequencies ( $n = 0$  for zero frequency and difference between two Larmor frequencies,  $n = 1$  for Larmor and  $n = 2$  for sum of two Larmor frequencies), and  $J_c(n\omega)$  are the column vectors of cross-correlation spectral densities. The matrices  $a(n\omega)$  and  $c(n\omega)$  connect the spectral densities to the various linewidths. For the heteronuclear AX system, considering CSA and dipolar interactions as the relaxation mechanisms, the linewidths of the two A spin SQCs ( $R_{1212} = R_A^\alpha$  and  $R_{3434} = R_A^\beta$ ), the AX zero ( $R_{2323} = R_{AX}^{ZQ}$ ) and the DQC ( $R_{1414} = R_{AX}^{DQ}$ ) are given in the notation of Eq. (106) by<sup>2</sup> [232]:

$$\begin{aligned} - \begin{pmatrix} R_{1212}^{SQ} \\ R_{3434}^{SQ} \\ R_{2323}^{ZQ} \\ R_{1414}^{DQ} \end{pmatrix} &= - \begin{pmatrix} R_A^\alpha \\ R_A^\beta \\ R_{AX}^{ZQ} \\ R_{AX}^{DQ} \end{pmatrix} = \frac{1}{6} \begin{pmatrix} 4 & 1 & 16 & 0 \\ 4 & 1 & 16 & 0 \\ 0 & 2 & 16 & 16 \\ 0 & 0 & 16 & 16 \end{pmatrix} \begin{pmatrix} J_{AXAX}(0) \\ J_{AXAX}(\omega_A - \omega_X) \\ J_{AA}(0) \\ J_{XX}(0) \end{pmatrix} + \frac{1}{2} \begin{pmatrix} 1 & 1 & 4 & 4 \\ 1 & 1 & 4 & 4 \\ 1 & 1 & 4 & 4 \\ 1 & 1 & 4 & 4 \end{pmatrix} \begin{pmatrix} J_{AXAX}(\omega_A) \\ J_{AXAX}(\omega_X) \\ J_{AA}(\omega_A) \\ J_{XX}(\omega_X) \end{pmatrix} \\ &+ \begin{pmatrix} 1 & 0 & 0 \\ 1 & 0 & 0 \\ 0 & 0 & 0 \\ 2 & 0 & 0 \end{pmatrix} \begin{pmatrix} J_{AXAX}(\omega_A + \omega_X) \\ J_{AA}(2\omega_A) \\ J_{XX}(2\omega_X) \end{pmatrix} + \frac{8}{3} \begin{pmatrix} -1 & 0 & 0 \\ 1 & 0 & 0 \\ 0 & 0 & -2 \\ 0 & 0 & 2 \end{pmatrix} \begin{pmatrix} J_{A,AX}(0) \\ J_{X,AX}(0) \\ J_{A,X}(0) \end{pmatrix} + 2 \begin{pmatrix} -1 & 0 & 0 \\ 1 & 0 & 0 \\ 0 & 0 & 0 \\ 0 & 0 & 0 \end{pmatrix} \begin{pmatrix} J_{A,AX}(\omega_A) \\ J_{X,AX}(\omega_X) \\ J_{A,X}(\omega_A) \end{pmatrix} \quad (107) \end{aligned}$$

[121,128], and (vi) heteronuclear AX<sub>3</sub> [121,129]. The cross-correlations, which are considered are CSA–dipole and CSA–CSA for two-spin systems and additionally dipole–dipole cross-correlations for three- and higher-order spin systems.

<sup>2</sup> Negative sign on transverse relaxation rates indicate decay rates. In this review, this sign has been shifted to the left-hand side in all equations.

The auto-correlation spectral densities (first three terms on the right-hand side) contribute equal widths to all the SQCs, but contribute unequal widths to the zero-quantum coherence (ZQC) and double-quantum coherence (DQC) via  $J_{AXAX}(\omega_A \pm \omega_X)$ . While  $J_{AXAX}(\omega_A - \omega_X)$  contributes to zero- and not to double-quantum linewidths,  $J_{AXAX}(\omega_A + \omega_X)$  contributes to double- and not to zero-quantum linewidths. While  $J_{AA}(0)$  contributes equally to all SQC and MQC,  $J_{XX}(0)$  contributes to AX ZQC and DQC but not to A spin SQC. CSA(A)–dipole(AX) cross-correlations,  $J_{A,AX}(0)$  and  $J_{A,AX}(\omega_A)$  contribute equal and opposite differential effects to A spin SQC. On the other hand, the CSA(A)–CSA(X) cross-correlation  $J_{A,X}(0)$  does not contribute to the time evolution of SQC but contributes a differential effect to the ZQ and DQ coherences [235]. It may be noted that there is no adiabatic dipolar contribution to ZQC and DQC, as  $J_{A,AX}(0)$  and  $J_{X,AX}(0)$  do not contribute to ZQC and DQC.  $J_{X,AX}(0, \omega_X)$  does not affect the A spin SQC as well as ZQC and DQC. It will however affect the X-spin SQC. Furthermore, the linewidths of the two X spin SQC can be obtained from the above equation, by interchanging the spin labels A and X in the spectral densities.

It may be mentioned here that while the cross-correlations add to the linewidth of one of the components of the A doublet, they subtract from the other, decreasing its linewidth. Thus in an isolated AX spin system in large molecules, where only the spectral densities at zero frequency contribute (for example, in  $^{15}\text{N}-^1\text{H}_\text{N}$  pairs, with complete deuteration of all non-labile protons in large proteins), if the cross-correlation contribution  $(8/3)J_{A,AX}(0)$  is nearly equal to the auto-correlation contribution  $[(5/6)J_{AXAX}(0) + (8/3)J_{AA}(0)]$ , the narrow component will become extremely sharp. This extremely interesting line-narrowing feature of cross-correlations is present in all the spin systems to be discussed in later sections and has recently been exploited by Wüthrich et al. [369] to detect exclusively the narrow components in large proteins, via an experiment named TROSY, which will be discussed in detail in Section 7.6.

Under the break down of the simple-line approximation, there are two situations to be considered. Case (i)  $|\Omega_A - \Omega_X| \gg R$  and  $J = 0$ ; in this case, the A and X spins are two singlets, respectively, at  $\Omega_A$  and  $\Omega_X$ . Case (ii)  $\Omega_A = \Omega_X$ ; in this case, the AX spin system reduces to  $A_2$ . In both these cases, the above analyses

are not valid. In case (i), Eq. (102) is factored into two  $2 \times 2$  blocks, one for each A and X spin (see Eq. (103)). The various relaxation elements for the A spin are obtained as:

$$\begin{aligned} \frac{1}{2}(D_1 + D_2) &= D = \frac{1}{2}(R_{1212} + R_{3434}) = (R_A^\alpha + R_A^\beta)/2 \\ &= -\frac{1}{2}[\frac{4}{3}J_{AXAX}(0) + \frac{1}{3}J_{AXAX}(\omega_A - \omega_X) + \frac{16}{3}J_{AA}(0) \\ &\quad + J_{AXAX}(\omega_A) + J_{AXAX}(\omega_X) + 4J_{AA}(\omega_A) \\ &\quad + 4J_{XX}(\omega_X) + 2J_{AXAX}(\omega_A + \omega_X)] \\ \frac{1}{2}(D_1 - D_2) &= \frac{1}{2}[\frac{16}{3}J_{A,AX}(0) + 4J_{A,AX}(\omega_A)] \\ C &= R_{1234} = -\frac{1}{2}J_{AXAX}(\omega_A) + 2J_{AA}(\omega_A) \end{aligned} \quad (108)$$

In case (ii) where the AX spin system collapses to  $A_2$ , only the sum mode  $A_X + X_X$  can be created and observed. One has to retain all the terms in Eq. (102) and transform the equation to sum and difference modes and the sum mode decays multi-exponentially in the presence of cross-correlations [236].

*4.2.1.1. Coherence transfer via cross-correlations.* As stated earlier, cross-correlations can lead to coherence transfer from one spin to another. In order to examine the coherence transfer from spin A to spin X either by J-coupling or by cross-correlations, it is best to recast the density matrix analysis into “Product–Operator” form. One can define product operators such as  $A_X$ ,  $A_Y$ ,  $2A_XX_Z$  and  $2A_YX_Z$ , which are related in a straightforward manner to  $A_+$ ,  $A_-$  and  $2A_\pm X_Z$ . If one creates  $A_X$  magnetization at  $t = 0$ , it evolves under the chemical shift  $\Omega_A$  and the J coupling and decays due to transverse relaxation. Assuming the simple-line approximation (neglecting C in Eq. (103))  $A_X$  evolves into [222,223]:

$$\begin{aligned} \sigma(t) &= A_X \frac{1}{2} [\exp\{D_1 t\} + \exp\{D_2 t\}] \cos(\pi J_{AX} t) \cos(\Omega_A t) \\ &\quad + 2A_Y X_Z \frac{1}{2} [\exp\{D_1 t\} + \exp\{D_2 t\}] \sin(\pi J_{AX} t) \cos(\Omega_A t) \\ &\quad + 2A_X X_Z \frac{1}{2} [\exp\{D_1 t\} - \exp\{D_2 t\}] \cos(\pi J_{AX} t) \cos(\Omega_A t) \\ &\quad + A_Y \frac{1}{2} [\exp\{D_1 t\} - \exp\{D_2 t\}] \sin(\pi J_{AX} t) \cos(\Omega_A t) \\ &\quad + \text{sin modulated terms,} \end{aligned} \quad (109)$$

where  $D_1, D_2$  are defined by Eq. (108). This shows that  $A_X$  will evolve into  $2A_YX_Z$ , the well known antiphase term created by J-coupling, as well as into  $2A_XX_Z$ , arising from cross-correlations and into  $A_Y$  by the combined effect of the two. The interesting part is that cross-correlations also contribute to antiphase terms (which can give rise to coherence transfer). The antiphase term created by cross-correlations is  $90^\circ$  out-of-phase with that created by J-coupling.

In the absence of J-coupling and the presence of cross-correlations, the above analysis is not valid and one has to retain the off-diagonal terms in Eq. (103). The result is obtained as [223]:

$$\begin{aligned} \sigma(t) = & A_X \frac{1}{2} [(1 + \sin \alpha_A) \exp\{\lambda_A t\} \\ & + (1 - \sin \alpha_A) \exp\{\mu_A t\}] \cos(\Omega_A t) \\ & + 2A_X X_Z \frac{1}{2} \cos \alpha_A [\exp\{\lambda_A t\} \\ & - \exp\{\mu_A t\}] \cos(\Omega_A t) \\ & + \text{sin modulated terms,} \end{aligned} \quad (110)$$

where

$$\begin{aligned} \lambda_A &= D + \frac{1}{2}(D_1 - D_2) \cos \alpha_A + C \sin \alpha_A \\ \mu_A &= D - \frac{1}{2}(D_1 - D_2) \cos \alpha_A - C \sin \alpha_A \\ \tan \alpha_A &= 2C/(D_1 - D_2) \end{aligned} \quad (111)$$

This shows that the antiphase term can be created even in the absence of J-coupling, but in the presence of cross-correlations. An antiphase term easily leads to coherence transfer by the use of appropriately phased non-selective  $90^\circ$  pulses on both spins. Such coherence transfers have been observed experimentally using 2D NMR and have been termed as relaxation allowed coherence transfer (RACT) [222,223,237]. They point out that one could observe a cross-peak in a COSY experiment arising from cross-correlations even in the absence of J-coupling. The antiphase term can also lead to multiple-quantum excitation and gives rise to relaxation allowed multiple-quantum coherences in the absence of J-coupling [237]. Such peaks have also been experimentally observed and exploited, the details of which will be outlined in Section 4.3.4.

**4.2.1.2. Operator method for description of relaxation.** The case of cross-correlations in a heteronuclear two-spin system (with special emphasis to  $^{15}\text{N}$ - $^1\text{H}$  spin system) has been treated in detail by Goldman [238], who has shown by explicit calculations that the doublet components of each spin relax differentially due to cross-correlation between CSA of  $^{15}\text{N}$  spins and the dipolar relaxation with the protons attached to it. Goldman has utilized the elegant “operator” method of Abragam [1] for calculating the expectation values of various operators and in turn the linewidths of various transitions or time evolution of transverse modes and the longitudinal relaxation of various transitions or longitudinal modes. This method has been utilized by several workers to measure the CSA of amide nitrogen-15 [239], amide proton [240,241] and  $^{13}\text{C}$ -carbon [242], in enriched proteins, as well as to study local anisotropic motions involving nuclei of peptide backbone [243–245]. These and many other studies utilizing the Goldman operator method form a significant use of cross-correlations in labeled biomolecules and will be reviewed in Section 7.2. The operator method, which is applicable not only for heteronuclear systems, but also for weakly coupled homonuclear systems, is discussed briefly in Appendix A.

#### 4.2.2. Cross-correlations in strongly coupled two-spin system AB

The effect of cross-correlations in the presence of strong coupling has been investigated for a homonuclear two spin-(1/2) system (AB) [234]. There are four SQCs, one DQC and one ZQC, in this spin system. The linewidths of the two “A” spin SQCs ( $R_{1313}^{\text{SQ}}, R_{2424}^{\text{SQ}}$ ) and the ZQC and DQCs ( $R_{2323}^{\text{ZQ}}, R_{1414}^{\text{DQ}}$ ) under the simple-line approximation (all coherences are well resolved,  $\delta_{AB}, J_{AB} \gg R$ ) can be written in a compact notation as [234]:

$$\begin{aligned} -\vec{R} = & \sum_{n=0}^2 \{ [a(n\omega) + a'(n\omega)] \vec{J}_a(n\omega) \\ & + [c(n\omega) + c'(n\omega)] \vec{J}_c(n\omega) \} \end{aligned} \quad (112)$$

The vector  $\vec{R}$  represents the linewidths of various non-degenerate SQCs as well as the ZQC and DQC and the right-hand side contains the auto

$[J_a(n\omega)]$  and cross  $[J_c(n\omega)]$  correlation spectral densities for two relaxation mechanisms namely mutual dipolar interactions between the two spins and the CSA relaxation. The coefficient matrices  $a$ ,  $a'$ ,  $c$ , and  $c'$  connect the spectral densities to the linewidths.  $a$  and  $c$  contain, respectively, the auto- and cross-correlation coefficients under weak coupling and  $a'$  and  $c'$  contain additional contributions to these coefficients arising exclusively from strong coupling. Thus under weak coupling ( $\theta = 0$ ) all elements of  $a'$  and  $c'$  are zero. This notation thus clearly separates out the contributions of auto- and cross-correlation spectral densities at each frequency and that of the strong couplings to the linewidths of various coherences of the spin system. The result is obtained as [234]:

$$\begin{aligned}
& - \begin{pmatrix} R_{1313}^{\text{SQ}} \\ R_{2424}^{\text{SQ}} \\ R_{2323}^{\text{ZQ}} \\ R_{1414}^{\text{DQ}} \end{pmatrix} = - \begin{pmatrix} R_A^\alpha \\ R_A^\beta \\ R_{AB}^{\text{ZQ}} \\ R_{AB}^{\text{DQ}} \end{pmatrix} = \frac{1}{6} \begin{pmatrix} 5 & 16 & 0 \\ 5 & 16 & 0 \\ 2 & 16 & 16 \\ 0 & 16 & 16 \end{pmatrix} \begin{pmatrix} J_{ABAB}(0) \\ J_{AA}(0) \\ J_{BB}(0) \end{pmatrix} + \begin{pmatrix} 1 & 2 & 2 \\ 1 & 2 & 2 \\ 1 & 2 & 2 \\ 1 & 2 & 2 \end{pmatrix} \begin{pmatrix} J_{ABAB}(\omega) \\ J_{AA}(\omega) \\ J_{BB}(\omega) \end{pmatrix} \\
& + \begin{pmatrix} 1 & 0 & 0 \\ 1 & 0 & 0 \\ 0 & 0 & 0 \\ 2 & 0 & 0 \end{pmatrix} \begin{pmatrix} J_{ABAB}(2\omega) \\ J_{AA}(2\omega) \\ J_{BB}(2\omega) \end{pmatrix} + \frac{2}{3} \begin{pmatrix} -\sin 2\theta & 2(\cos 2\theta - 1) & -2(\cos 2\theta - 1) \\ \sin 2\theta & 2(\cos 2\theta - 1) & -2(\cos 2\theta - 1) \\ \sin^2 2\theta & 2(\cos^2 2\theta - 1) & 2(\cos^2 2\theta - 1) \\ 0 & 0 & 0 \end{pmatrix} \begin{pmatrix} J_{ABAB}(0) \\ J_{AA}(0) \\ J_{BB}(0) \end{pmatrix} \\
& + \frac{1}{2} \begin{pmatrix} -\sin 2\theta & 0 & 0 \\ \sin 2\theta & 0 & 0 \\ 0 & 0 & 0 \\ 0 & 0 & 0 \end{pmatrix} \begin{pmatrix} J_{ABAB}(\omega) \\ J_{AA}(\omega) \\ J_{BB}(\omega) \end{pmatrix} + \frac{8}{3} \begin{pmatrix} -1 & 0 & 0 \\ 1 & 0 & 0 \\ 0 & 0 & -2 \\ 0 & 0 & 2 \end{pmatrix} \begin{pmatrix} J_{A,AB}(0) \\ J_{B,AB}(0) \\ J_{A,B}(0) \end{pmatrix} + 2 \begin{pmatrix} -1 & 0 & 0 \\ 1 & 0 & 0 \\ 0 & 0 & 0 \\ 0 & 0 & 0 \end{pmatrix} \begin{pmatrix} J_{A,AB}(\omega) \\ J_{B,AB}(\omega) \\ J_{A,B}(\omega) \end{pmatrix} \\
& + \frac{2}{3} \begin{pmatrix} -(2 \cos 2\theta + \sin 2\theta - 2) & (2 \cos 2\theta + \sin 2\theta - 2) & 0 \\ (2 \cos 2\theta + \sin 2\theta - 2) & -(2 \cos 2\theta + \sin 2\theta - 2) & 0 \\ 2 \sin 2\theta \cos 2\theta & -6 \sin 2\theta \cos 2\theta & 8 \sin^2 2\theta \\ 0 & 0 & 0 \end{pmatrix} \begin{pmatrix} J_{A,AB}(0) \\ J_{B,AB}(0) \\ J_{A,B}(0) \end{pmatrix} \\
& + 2 \begin{pmatrix} \sin^2 \theta & -\sin^2 \theta & -\sin 2\theta \\ -\sin^2 \theta & \sin^2 \theta & \sin 2\theta \\ 0 & 0 & 0 \\ 0 & 0 & 0 \end{pmatrix} \begin{pmatrix} J_{A,AB}(\omega) \\ J_{B,AB}(\omega) \\ J_{A,B}(\omega) \end{pmatrix} \tag{113}
\end{aligned}$$

From the above equation the following conclusions are derived:

(i) The DQC, which is the highest quantum coherence in a two-spin system is not influenced by strong coupling.

(ii) Weak coupling without cross-correlations (only first three terms contribute).

The two SQCs of spin  $A$  have equal linewidths while ZQC and DQC have unequal widths from the spectral densities  $J_{ABAB}(0)$  and  $J_{ABAB}(2\omega)$ .  $J_{ABAB}(0)$  contributes to ZQC but not to DQC whereas  $J_{ABAB}(2\omega)$  does not contribute to ZQC but contributes to DQC (in conformity with AX analysis given by Eq. (107)) [224–229].

(iii) Weak coupling with cross-correlations (only

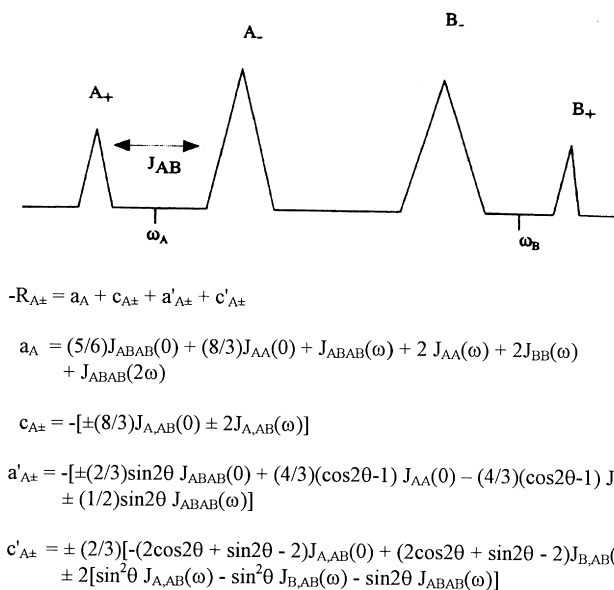


Fig. 34. Schematic diagram showing the differential line broadening in a homonuclear  $AB$  spin system. Linewidths of  $B_+$  and  $B_-$  can be obtained by interchanging the labels  $A$ ,  $B$ .  $a_A$  and  $c_A$  are the contributions from auto and cross-correlations, respectively, in the weak coupling limit.  $a'_A$  and  $c'_A$  are the contributions from auto and cross-correlations, respectively, exclusively from strong coupling. In the weak coupling limit, the primed quantities ( $a'_A$  and  $c'_A$ ) do not contribute to the linewidths [234].

the first three terms and the sixth and seventh terms contribute).

In this case, the two SQC of spin  $A$  have unequal linewidths due to the equal and opposite contribution of cross-correlation spectral densities  $J_{A,AB}(0)$  and  $J_{A,AB}(\omega)$  which do not contribute to DQC and ZQC. Cross-correlation spectral density between the two CSA,  $J_{A,B}(0)$  contributes equal and opposite (differential) linewidth to ZQC and DQC without contributing to SQC (as in  $AX$  case as well; Eq. (107)).

(iv) Strong coupling without cross-correlations (only the first five terms contribute).

Strong coupling brings additional linewidths to the various coherences.  $J_{ABAB}(0)$  and  $J_{ABAB}(\omega)$  give differential linewidths to the two SQC while  $J_{AA}(0)$  and  $J_{BB}(0)$  cause equal broadening. Only spectral densities at zero frequency give additional contribution to zero-quantum linewidth.

(v) Strong coupling with cross-correlations (all terms contribute).

SQC have additional unequal contribution to the linewidth from all cross-correlation spectral densities at zero and  $\omega$  frequencies except

$J_{A,B}(0)$ . ZQC has contributions from all zero-frequency cross-correlation spectral densities.

From the above, it may be concluded that either strong coupling or cross-correlation makes the linewidths of the SQC unequal. This is shown schematically in Fig. 34. The linewidths of the other two SQC ( $R_{1212}$  and  $R_{3434}$ ) which may be termed as spin ‘ $B$ ’ coherences are obtained by interchanging the labels of spin  $A$  and  $B$  as well as the sign of the  $\theta$  terms in Eq. (113). It is noticed that the cross-correlation between the CSA of the two spins  $J_{A,B}$  makes a differential contribution under the weak coupling approximation to ZQC and DQC, and under strong coupling to the two SQCs. This cross-correlation term is independent of the distance between the two spins and therefore has been termed as a “remote” and is discussed in detail in Section 4.4.1 [234].

#### 4.2.3. Cross-correlations in heteronuclear three-spin system ( $AMX$ )

The presence of dipole–dipole cross-correlations requires a minimum of three coupled spins and its

effect on the decay rates (linewidths) of SQC and multiple-quantum coherence has been investigated by several workers [222,228–230]. In the following section, the results for dipole–dipole, CSA–dipole and CSA–CSA cross-correlations are summarized using a weakly coupled heteronuclear three-spin system  $AMX$  [each spin-(1/2)]. The labeling of the states and the coherences is given in Fig. 2. The

SQC and multiple-quantum coherences are treated in two subsections.

*4.2.3.1. Single-quantum coherences.* The linewidths or the decay rates of the four ‘A’ spin SQCs of the  $AMX$  spin system under the simple-line approximation are obtained in the notation of Eq. (107) as [234]:

$$\begin{aligned}
 & - \begin{pmatrix} R_{1414} \\ R_{2626} \\ R_{3737} \\ R_{5858} \end{pmatrix} = - \begin{pmatrix} R_A^{\alpha\alpha} \\ R_A^{\alpha\beta} \\ R_A^{\beta\alpha} \\ R_A^{\beta\beta} \end{pmatrix} = \frac{1}{6} \begin{pmatrix} 4 & 4 & 0 & 1 & 1 & 0 \\ 4 & 4 & 0 & 1 & 1 & 2 \\ 4 & 4 & 0 & 1 & 1 & 2 \\ 4 & 4 & 0 & 1 & 1 & 0 \end{pmatrix} \begin{pmatrix} J_{AMAM}(0) \\ J_{AXAX}(0) \\ J_{MXMX}(0) \\ J_{AMAM}(\omega_A - \omega_M) \\ J_{AXAX}(\omega_A - \omega_X) \\ J_{MXMX}(\omega_M - \omega_X) \end{pmatrix} \\
 & + \frac{1}{2} \begin{pmatrix} 1 & 1 & 1 & 1 & 1 & 1 \\ 1 & 1 & 1 & 1 & 1 & 1 \\ 1 & 1 & 1 & 1 & 1 & 1 \\ 1 & 1 & 1 & 1 & 1 & 1 \end{pmatrix} \begin{pmatrix} J_{AMAM}(\omega_A) \\ J_{AMAM}(\omega_M) \\ J_{AXAX}(\omega_A) \\ J_{AXAX}(\omega_X) \\ J_{MXMX}(\omega_M) \\ J_{MXMX}(\omega_X) \end{pmatrix} + \begin{pmatrix} 1 & 1 & 2 \\ 1 & 1 & 0 \\ 1 & 1 & 0 \\ 1 & 1 & 2 \end{pmatrix} \begin{pmatrix} J_{AMAM}(\omega_A + \omega_M) \\ J_{AXAX}(\omega_A + \omega_X) \\ J_{MXMX}(\omega_M + \omega_X) \end{pmatrix} \\
 & + \frac{8}{3} \begin{pmatrix} 1 & 0 & 0 \\ 1 & 0 & 0 \\ 1 & 0 & 0 \\ 1 & 0 & 0 \end{pmatrix} \begin{pmatrix} J_{AA}(0) \\ J_{MM}(0) \\ J_{XX}(0) \end{pmatrix} + 2 \begin{pmatrix} 1 & 1 & 1 \\ 1 & 1 & 1 \\ 1 & 1 & 1 \\ 1 & 1 & 1 \end{pmatrix} \begin{pmatrix} J_{AA}(\omega_A) \\ J_{MM}(\omega_M) \\ J_{XX}(\omega_X) \end{pmatrix} + \frac{4}{3} \begin{pmatrix} 1 & 0 & 0 \\ -1 & 0 & 0 \\ -1 & 0 & 0 \\ 1 & 0 & 0 \end{pmatrix} \begin{pmatrix} J_{AMAX}(0) \\ J_{AMMX}(0) \\ J_{AXMX}(0) \end{pmatrix} \\
 & + \begin{pmatrix} 1 & 0 & 0 \\ -1 & 0 & 0 \\ -1 & 0 & 0 \\ 1 & 0 & 0 \end{pmatrix} \begin{pmatrix} J_{AMAX}(\omega_A) \\ J_{AMMX}(\omega_M) \\ J_{AXMX}(\omega_X) \end{pmatrix} + \frac{8}{3} \begin{pmatrix} -1 & -1 & 0 & 0 & 0 & 0 \\ -1 & 1 & 0 & 0 & 0 & 0 \\ 1 & -1 & 0 & 0 & 0 & 0 \\ 1 & 1 & 0 & 0 & 0 & 0 \end{pmatrix} \begin{pmatrix} J_{A,AM}(0) \\ J_{A,AX}(0) \\ J_{M,AM}(0) \\ J_{M,MX}(0) \\ J_{X,AX}(0) \\ J_{X,MX}(0) \end{pmatrix} \\
 & + 2 \begin{pmatrix} -1 & -1 & 0 & -1 & 0 & -1 \\ -1 & 1 & 0 & 1 & 0 & -1 \\ 1 & -1 & 0 & -1 & 0 & 1 \\ 1 & 1 & 0 & 1 & 0 & 1 \end{pmatrix} \begin{pmatrix} J_{A,AM}(\omega_A) \\ J_{A,AX}(\omega_A) \\ J_{M,AM}(\omega_M) \\ J_{M,MX}(\omega_M) \\ J_{X,AX}(\omega_X) \\ J_{X,MX}(\omega_X) \end{pmatrix}. \tag{114}
 \end{aligned}$$

The first three terms represent, respectively, the zero, single- and double-quantum dipole–dipole auto-correlation spectral densities. The next two terms represent zero- and single-quantum CSA auto-correlation spectral densities, respectively. These terms are followed by the zero- and single-quantum dipolar cross-correlation spectral densities. The last two terms represent the zero- and single-quantum CSA–dipole cross-correlation spectral densities. CSA–CSA cross-correlations do not contribute to the linewidths of the SQC of weakly coupled spins. The linewidths of  $M$  and  $X$  SQCs can be obtained by symmetry, by interchanging the labels. From Eq. (114), the following results can be summarized.

1. *Auto-correlation contributions*: All the four  $A$  spin SQCs have equal contributions from auto-correlation spectral densities, except the remote zero [ $J_{MXMX}(\omega_M - \omega_X)$ ] and the double [ $J_{MXMX}(\omega_M + \omega_X)$ ] quantum spectral densities, which contribute different linewidths to the inner and the outer SQCs, retaining pairwise symmetry in the linewidths. Zero frequency remote auto-correlations [namely  $J_{MXMX}(0)$ ,  $J_{MM}(0)$  and  $J_{XX}(0)$ ] do not contribute to the decay of  $A$ -spin SQCs. On the other hand, remote single-quantum auto-correlation spectral densities at  $\omega$  [ $J_{MXMX}(\omega_M)$ ,  $J_{MXMX}(\omega_X)$ ,  $J_{MM}(\omega_M)$  and  $J_{XX}(\omega_X)$ ] contribute equal widths to all the linewidths of the SQCs. These remote auto-correlations are present only in the presence of  $J$ -coupling and the secular approximation. If  $J$ -couplings are absent, the transitions become degenerate and the secular approximation is no longer valid. In such situations, only the sum mode can be excited, the time evolution of which is free of

remote auto-correlations. If one of the couplings is zero (say,  $J_{AX} = 0$ ), then one of the remote CSA auto-correlation term [ $J_{XX}(\omega_X)$ ] drops out.

2. *Cross-correlation contributions*: Cross-correlations contribute only differential linewidths (equal and opposite) to the SQCs with no net contribution. While dipolar cross-correlations maintain symmetry between outer and inner coherences, each CSA–dipole cross-correlation has pairwise symmetry for different pairs. Thus in the presence of several cross-correlations, all the four coherences may have different linewidths. Dipole–dipole cross-correlations in which  $A$  is the common spin, only contribute to the linewidths of  $A$  spin SQC in the three-spin system. CSA–dipole cross-correlations at zero frequency only have contributions involving the CSA of spin  $A$  and dipolar of  $AM$  and  $AX$ . Four out of the possible six single-quantum CSA–dipole cross-correlations contribute equal but opposite linewidths to the various  $A$  spin coherences. The last two cross-correlation spectral densities namely  $J_{M,MX}(\omega_M)$  and  $J_{X,MX}(\omega_X)$  can be termed as “remote” and have a first-order contribution to the resolved  $A$  spin multiplet. There is no contribution of cross-correlation spectral densities at  $2\omega$  to these linewidths [234].

4.2.3.2. *Multiple quantum coherences*. The linewidths of two ZQCs, two DQCs of  $AM$  spins and the triple-quantum coherence (TQC) contain the totality of information on MQC of this system. The linewidths of the remaining ZQC and DQC can be generated by interchanging the spin labels. These linewidths are given by [234]:

$$- \begin{pmatrix} R_{1717}^{\text{DQ}} \\ R_{2828}^{\text{DQ}} \\ R_{3434}^{\text{ZQ}} \\ R_{5656}^{\text{ZQ}} \\ R_{1818}^{\text{TQ}} \end{pmatrix} = - \begin{pmatrix} R_{AM}^{\text{DQ},\alpha} \\ R_{AM}^{\text{DQ},\beta} \\ R_{AM}^{\text{ZQ},\alpha} \\ R_{AM}^{\text{ZQ},\beta} \\ R_{AMX}^{\text{TQ}} \end{pmatrix} = \frac{1}{6} \begin{pmatrix} 0 & 4 & 4 & 0 & 1 & 1 \\ 0 & 4 & 4 & 0 & 1 & 1 \\ 0 & 4 & 4 & 2 & 1 & 1 \\ 0 & 4 & 4 & 2 & 1 & 1 \\ 0 & 0 & 0 & 0 & 0 & 0 \end{pmatrix} \begin{pmatrix} J_{AMAM}(0) \\ J_{AXAX}(0) \\ J_{MXMX}(0) \\ J_{AMAM}(\omega_A - \omega_M) \\ J_{AXAX}(\omega_A - \omega_X) \\ J_{MXMX}(\omega_M - \omega_X) \end{pmatrix}$$

$$\begin{aligned}
& + \frac{1}{2} \begin{pmatrix} 1 & 1 & 1 & 1 & 1 & 1 \\ 1 & 1 & 1 & 1 & 1 & 1 \\ 1 & 1 & 1 & 1 & 1 & 1 \\ 1 & 1 & 1 & 1 & 1 & 1 \\ 1 & 1 & 1 & 1 & 1 & 1 \end{pmatrix} \begin{pmatrix} J_{AMAM}(\omega_A) \\ J_{AMAM}(\omega_M) \\ J_{AXAX}(\omega_A) \\ J_{AXAX}(\omega_X) \\ J_{MXMX}(\omega_M) \\ J_{MXMX}(\omega_X) \end{pmatrix} + \begin{pmatrix} 2 & 1 & 1 \\ 2 & 1 & 1 \\ 0 & 1 & 1 \\ 0 & 1 & 1 \\ 2 & 2 & 2 \end{pmatrix} \begin{pmatrix} J_{AMAM}(\omega_A + \omega_M) \\ J_{AXAX}(\omega_A + \omega_X) \\ J_{MXMX}(\omega_M + \omega_X) \end{pmatrix} \\
& + \frac{8}{3} \begin{pmatrix} 1 & 1 & 0 \\ 1 & 1 & 0 \\ 1 & 1 & 0 \\ 1 & 1 & 0 \\ 1 & 1 & 1 \end{pmatrix} \begin{pmatrix} J_{AA}(0) \\ J_{MM}(0) \\ J_{XX}(0) \end{pmatrix} + 2 \begin{pmatrix} 1 & 1 & 1 \\ 1 & 1 & 1 \\ 1 & 1 & 1 \\ 1 & 1 & 1 \end{pmatrix} \begin{pmatrix} J_{AA}(\omega_A) \\ J_{MM}(\omega_M) \\ J_{XX}(\omega_X) \end{pmatrix} + \frac{4}{3} \begin{pmatrix} 0 & 0 & 1 \\ 0 & 0 & 1 \\ 0 & 0 & -1 \\ 0 & 0 & -1 \\ 0 & 0 & 0 \end{pmatrix} \begin{pmatrix} J_{AMAX}(0) \\ J_{AMMX}(0) \\ J_{AXMX}(0) \end{pmatrix} \\
& + \begin{pmatrix} 0 & 0 & 1 \\ 0 & 0 & 1 \\ 0 & 0 & -1 \\ 0 & 0 & -1 \\ 1 & 1 & 1 \end{pmatrix} \begin{pmatrix} J_{AMAX}(\omega_A) \\ J_{AMMX}(\omega_M) \\ J_{AXMX}(\omega_X) \end{pmatrix} + \frac{8}{3} \begin{pmatrix} 0 & -1 & 0 & -1 & 0 & 0 \\ 0 & 1 & 0 & 1 & 0 & 0 \\ 0 & -1 & 0 & -1 & 0 & 0 \\ 0 & 1 & 0 & 1 & 0 & 0 \\ 0 & 0 & 0 & 0 & 0 & 0 \end{pmatrix} \begin{pmatrix} J_{A,AM}(0) \\ J_{A,AX}(0) \\ J_{M,AM}(0) \\ J_{M,MX}(0) \\ J_{X,AX}(0) \\ J_{X,MX}(0) \end{pmatrix} \\
& + \frac{8}{3} \begin{pmatrix} -1 & -1 & 0 \\ 1 & 1 & 0 \\ 1 & 1 & 0 \\ -1 & -1 & 0 \\ 0 & 0 & 0 \end{pmatrix} \begin{pmatrix} J_{A,MX}(0) \\ J_{M,AX}(0) \\ J_{X,AM}(0) \end{pmatrix} + 2 \begin{pmatrix} 0 & -1 & 0 & -1 & 0 & 0 \\ 0 & 1 & 0 & 1 & 0 & 0 \\ 0 & -1 & 0 & -1 & 0 & 0 \\ 0 & 1 & 0 & 1 & 0 & 0 \\ 0 & 0 & 0 & 0 & 0 & 0 \end{pmatrix} \begin{pmatrix} J_{A,AM}(\omega_A) \\ J_{A,AX}(\omega_A) \\ J_{M,AM}(\omega_M) \\ J_{M,MX}(\omega_M) \\ J_{X,AX}(\omega_X) \\ J_{X,MX}(\omega_X) \end{pmatrix} \\
& + \frac{16}{3} \begin{pmatrix} 1 & 0 & 0 \\ 1 & 0 & 0 \\ -1 & 0 & 0 \\ -1 & 0 & 0 \\ 1 & 1 & 1 \end{pmatrix} \begin{pmatrix} J_{A,M}(0) \\ J_{A,X}(0) \\ J_{M,X}(0) \end{pmatrix}
\end{aligned} \tag{115}$$

From this equation the following results are obtained:

1. *Auto-correlation contributions*: All dipolar auto-correlation spectral densities at the Larmor frequencies of various spins contribute equal widths to all multiple-quantum coherences (second term on RHS). At zero frequency (first term),  $J_{AXAX}(0)$ ,  $J_{MXMX}(0)$ , and  $J_{MXMX}(\omega_M - \omega_X)$ ,  $J_{AXAX}(\omega_A - \omega_X)$  contribute equal widths to *AM* DQC and ZQCs whereas  $J_{AMAM}(\omega_A - \omega_M)$  contributes only to ZQCs.  $J_{AMAM}(0)$  does not contribute to *AM* DQC and ZQC. None of the dipolar spectral densities at zero frequency contribute to TQC. At the sum of the two Larmor frequencies (third term), auto-correlation dipolar spectral densities  $J_{AXAX}(\omega_A + \omega_X)$  and  $J_{MXMX}(\omega_M + \omega_X)$  contribute equal widths to the *AM* DQC and ZQC with  $J_{AMAM}(\omega_A + \omega_M)$  contributing only to DQC. TQC has equal contribution from all the three spectral densities at the sum of the two Larmor frequencies. All the three CSA auto-correlation spectral densities at zero and Larmor frequencies (fourth and fifth terms) contribute equal widths to all the multiple-quantum coherences except that there is no contribution from  $J_{XX}(0)$  to *AM* DQC and ZQC.

2. *Cross-correlation contributions*: Dipolar cross-correlation spectral density  $J_{AXMX}$  at frequencies zero and  $\omega_X$  contribute equal and opposite widths to the *AM* DQCs and ZQCs, respectively, with no contribution from the other two cross-correlation spectral densities (sixth and seventh terms). TQC, on the other hand, has equal contribution from all the three spectral densities at the three Larmor frequencies. Similarly CSA–CSA cross-correlation spectral density  $J_{A,M}(0)$  contributes equal and opposite widths to the *AM* DQCs and ZQCs, respectively (last term). TQC has equal contribution from all the three CSA–CSA cross-correlation spectral densities at the zero frequency. Only two CSA–dipole cross-correlation spectral densities  $J_{A,AX}$  and  $J_{M,MX}$  at zero and Larmor frequencies contribute differential widths to

the *AM* DQCs and ZQCs with no contributions from the remaining spectral densities (eighth and tenth terms).

#### 4.2.4. Dipole–dipole cross-correlations in a strongly coupled homonuclear three-spin system *ABX*

In order to study the effects associated with strong coupling in the presence of dipole–dipole cross-correlations, an analysis has been reported in the literature, calculating the complete transverse relaxation matrix for a homonuclear *ABX* spin system [232]. Only dipole–dipole cross-correlations have been included in this study and these results are given in Sections 4.2.4.1–4.2.4.4.<sup>3</sup>

4.2.4.1. *Single-quantum coherences*. The decay rates for the various coherences in the *ABX* case contain contributions from auto-correlation spectral densities  $J_{ABAB}$ ,  $J_{AXAX}$  and  $J_{BXXB}$  and cross-correlation spectral densities  $J_{ABAX}$ ,  $J_{ABBX}$  and  $J_{AXBX}$  each at frequencies 0,  $\omega$  and  $2\omega$ . The notation and labeling of states used in the preceding section for the heteronuclear case is continued here with *B* replacing *M*. The number of spectral densities is reduced since  $\omega_A = \omega_B = \omega_X = \omega$ . The strong coupling parameters  $\theta_{\pm}$  has the usual definitions [246]. Separating out the contributions of strong coupling into primed quantities (see Eq. (112)), one can write the contribution of the various spectral densities to the linewidths of the four ‘*A*’ coherences (mixed *AB* in strong coupling situation) as [232]:

$$-\vec{R}_A = \sum_{n=0}^2 \{ [a_A(n\omega) + a'_A(n\omega)] \vec{J}_a(n\omega) + [c_A(n\omega) + c'_A(n\omega)] \vec{J}_c(n\omega) \} \quad (116)$$

This equation, when expanded in terms of the spectral

<sup>3</sup> The decay rates of the various SQCs and multiple-quantum coherences of an *ABX* spin system, where *X* is a heteronucleus and considering relaxation via both CSA and dipolar interactions have also been calculated [Rangeet Bhattacharyya, R.C.R. Grace and Anil Kumar, unpublished results available on request via e-mail].

densities, is given by:<sup>4</sup>

$$\begin{aligned}
-\begin{pmatrix} R_{1414} \\ R_{2626} \\ R_{3737} \\ R_{5858} \end{pmatrix} &= -\begin{pmatrix} R_A^{\alpha\alpha} \\ R_A^{\alpha\beta} \\ R_A^{\beta\alpha} \\ R_A^{\beta\beta} \end{pmatrix} = \frac{1}{6} \begin{pmatrix} 5 & 5 & 0 \\ 5 & 5 & 2 \\ 5 & 5 & 2 \\ 5 & 5 & 0 \end{pmatrix} \begin{pmatrix} J_{ABAB}(0) \\ J_{AXAX}(0) \\ J_{BXXB}(0) \end{pmatrix} + \begin{pmatrix} 1 & 1 & 1 \\ 1 & 1 & 1 \\ 1 & 1 & 1 \\ 1 & 1 & 1 \end{pmatrix} \begin{pmatrix} J_{ABAB}(\omega) \\ J_{AXAX}(\omega) \\ J_{BXXB}(\omega) \end{pmatrix} \\
&+ \begin{pmatrix} 1 & 1 & 2 \\ 1 & 1 & 0 \\ 1 & 1 & 0 \\ 1 & 1 & 2 \end{pmatrix} \begin{pmatrix} J_{ABAB}(2\omega) \\ J_{AXAX}(2\omega) \\ J_{BXXB}(2\omega) \end{pmatrix} + \frac{4}{3} \begin{pmatrix} 1 & 0 & 0 \\ -1 & 0 & 0 \\ -1 & 0 & 0 \\ 1 & 0 & 0 \end{pmatrix} \begin{pmatrix} J_{ABAX}(0) \\ J_{ABBX}(0) \\ J_{AXBX}(0) \end{pmatrix} + \begin{pmatrix} 1 & 0 & 0 \\ -1 & 0 & 0 \\ -1 & 0 & 0 \\ 1 & 0 & 0 \end{pmatrix} \begin{pmatrix} J_{ABAX}(\omega) \\ J_{ABBX}(\omega) \\ J_{AXBX}(\omega) \end{pmatrix} \\
&+ \frac{1}{6} \begin{pmatrix} -8c_{+s_+} & -5s_+^2 & 5s_+^2 \\ -8c_{-s_-} & -3s_-^2 & 3s_-^2 \\ 8c_{+s_+} & -3s_+^2 & 3s_+^2 \\ 8c_{-s_-} & -5s_-^2 & 5s_-^2 \end{pmatrix} \begin{pmatrix} J_{ABAB}(0) \\ J_{AXAX}(0) \\ J_{BXXB}(0) \end{pmatrix} + \begin{pmatrix} -c_{+s_+} & 0 & 0 \\ -c_{-s_-} & 0 & 0 \\ c_{+s_+} & 0 & 0 \\ c_{-s_-} & 0 & 0 \end{pmatrix} \begin{pmatrix} J_{ABAB}(\omega) \\ J_{AXAX}(\omega) \\ J_{BXXB}(\omega) \end{pmatrix} \\
&+ \begin{pmatrix} 0 & s_+^2 & -s_+^2 \\ 0 & -s_-^2 & s_-^2 \\ 0 & -s_+^2 & s_+^2 \\ 0 & s_-^2 & -s_-^2 \end{pmatrix} \begin{pmatrix} J_{ABAB}(2\omega) \\ J_{AXAX}(2\omega) \\ J_{BXXB}(2\omega) \end{pmatrix} + \frac{1}{3} \begin{pmatrix} -2s_+(c_+ + 2s_+) & -2s_+(c_+ - 2s_+) & -c_{+s_+} \\ 2s_-(c_- + 2s_-) & 2s_-(c_- - 2s_-) & -c_{-s_-} \\ -2s_+(c_+ - 2s_+) & -2s_+(c_+ + 2s_+) & c_{+s_+} \\ 2s_-(c_- - 2s_-) & 2s_-(c_- + 2s_-) & c_{-s_-} \end{pmatrix} \begin{pmatrix} J_{ABAX}(0) \\ J_{ABBX}(0) \\ J_{AXBX}(0) \end{pmatrix} \\
&+ \begin{pmatrix} -s_+^2 & s_+^2 & -c_{+s_+} \\ s_-^2 & -s_-^2 & -c_{-s_-} \\ s_+^2 & -s_+^2 & c_{+s_+} \\ -s_-^2 & s_-^2 & c_{-s_-} \end{pmatrix} \begin{pmatrix} J_{ABAX}(\omega) \\ J_{ABBX}(\omega) \\ J_{AXBX}(\omega) \end{pmatrix} + 2 \begin{pmatrix} 0 & 0 & -c_{+s_+} \\ 0 & 0 & -c_{-s_-} \\ 0 & 0 & c_{+s_+} \\ 0 & 0 & c_{-s_-} \end{pmatrix} \begin{pmatrix} J_{ABAX}(2\omega) \\ J_{ABBX}(2\omega) \\ J_{AXBX}(2\omega) \end{pmatrix} \tag{117}
\end{aligned}$$

From this equation it is seen that for

(i) Weak coupling without cross-correlations (only the first three terms contribute).

This part is identical to the weakly coupled *AMX* case (Eq. (114)) and restates that the linewidths are unequal due to the contributions from remote auto-correlation spectral densities  $J_{BXXB}(0)$  and  $J_{BXXB}(2\omega)$ . All the other spectral densities have

equal contribution to all the four coherences.  $J_{BXXB}(0)$  and  $J_{BXXB}(2\omega)$  contribute equal amount to the outer and inner lines in such a way that they have symmetrical widths.

(ii) Weak coupling with cross-correlations (the first five terms contribute).

This is also identical to the *AMX* case and confirms that the linewidths are additionally unequal due to the unequal contributions from the spectral densities  $J_{ABAX}(0)$  and  $J_{ABAX}(\omega)$  (Eq. (115)). However, the symmetry is maintained in the outer and inner linewidths. All the other dipole–dipole cross-correlations have zero contribution to the linewidths [223,228–232].

<sup>4</sup> The results given in Ref. [232] have errors in strong coupling contributions from spectral densities at zero frequency, which are corrected here. Some of the coefficient matrices have also been simplified. The conclusions of Ref. [232] remain unchanged.

(iii) Strong coupling without cross-correlations (the first three and the sixth, seventh and eighth terms contribute).

An additional contribution from strong coupling comes from all the auto-correlation spectral densities at zero frequency, but the spectral densities at  $\omega$  contribute only via  $J_{ABAB}(\omega)$  and at  $2\omega$  via  $J_{AXAX}(2\omega)$  and  $J_{BXXB}(2\omega)$ . Here all the linewidths are unequal without any symmetry. Strong coupling is known to introduce differences in linewidths of  $AB$  spin system making the inner and outer linewidths unequal [Ref. [1], p. 509]. These results indicate that the introduction of the third spin makes all the linewidths unequal under strong coupling, even in the absence of cross-correlations.

(iv) Strong coupling with cross-correlations (all the terms contribute).

Additional contribution comes from all cross-correlation spectral densities at zero and  $\omega$  frequencies, and at  $2\omega$ , only  $J_{AXBX}(2\omega)$  contributes. All linewidths are unequal and there is no symmetry.

The linewidths of ‘B’ coherences are obtained by interchanging labels ‘A’ and ‘B’ in Eq. (117) and in the definitions of  $\theta_{\pm}$  and a consequent substitution of  $c_{\pm} = -c_{\mp}$  in the primed matrices of Eq. (117) assuming that the four ‘B’ transitions are arranged in the order 1–3, 2–5, 4–7 and 6–8.

For ‘X’ spin SQCs, an equation similar to Eq. (117) can be written having [232]<sup>5</sup>

$$\begin{aligned}
 & - \begin{pmatrix} R_{1212} \\ R_{3535} \\ R_{4646} \\ R_{7878} \\ R_{3636} \\ R_{4545} \end{pmatrix} = - \begin{pmatrix} R_X^{\alpha\alpha} \\ R_X^{\alpha\beta} \\ R_X^{\beta\alpha} \\ R_X^{\beta\beta} \\ R_X^{\alpha\beta \rightarrow \beta\alpha} \\ R_X^{\beta\alpha \rightarrow \alpha\beta} \end{pmatrix} = \frac{1}{6} \begin{pmatrix} 0 & 5 & 5 \\ 2 & 5 & 5 \\ 2 & 5 & 5 \\ 0 & 5 & 5 \\ 2 & 0 & 2 \\ 2 & 2 & 0 \end{pmatrix} \begin{pmatrix} J_{ABAB}(0) \\ J_{AXAX}(0) \\ J_{BXXB}(0) \end{pmatrix} + \begin{pmatrix} 1 & 1 & 1 \\ 1 & 1 & 1 \\ 1 & 1 & 1 \\ 1 & 1 & 1 \\ 1 & 1 & 1 \\ 1 & 1 & 1 \end{pmatrix} \begin{pmatrix} J_{ABAB}(\omega) \\ J_{AXAX}(\omega) \\ J_{BXXB}(\omega) \end{pmatrix} \\
 & + \begin{pmatrix} 2 & 1 & 1 \\ 0 & 1 & 1 \\ 0 & 1 & 1 \\ 2 & 1 & 1 \\ 0 & 2 & 0 \\ 0 & 0 & 2 \end{pmatrix} \begin{pmatrix} J_{ABAB}(2\omega) \\ J_{AXAX}(2\omega) \\ J_{BXXB}(2\omega) \end{pmatrix} + \frac{4}{3} \begin{pmatrix} 0 & 0 & 1 \\ 0 & 0 & -1 \\ 0 & 0 & -1 \\ 0 & 0 & 1 \\ 0 & 0 & 0 \\ 0 & 0 & 0 \end{pmatrix} \begin{pmatrix} J_{ABAX}(0) \\ J_{ABBX}(0) \\ J_{AXBX}(0) \end{pmatrix} + \begin{pmatrix} 0 & 0 & 1 \\ 0 & 0 & -1 \\ 0 & 0 & -1 \\ 0 & 0 & 1 \\ -1 & 1 & -1 \\ 1 & -1 & -1 \end{pmatrix} \begin{pmatrix} J_{ABAX}(\omega) \\ J_{ABBX}(\omega) \\ J_{AXBX}(\omega) \end{pmatrix} \\
 & + \frac{1}{6} \begin{pmatrix} 0 & 0 & 0 \\ -8c_+s_+c_-s_- & (s_+^2 - s_-^2) - 2(s_s^2 + s_d^2) & -(s_+^2 - s_-^2) - 2(s_s^2 + s_d^2) \\ -8c_+s_+c_-s_- & -(s_+^2 - s_-^2) - 2(s_s^2 + s_d^2) & (s_+^2 - s_-^2) - 2(s_s^2 + s_d^2) \\ 0 & 0 & 0 \\ 8c_+s_+c_-s_- & (s_+^2 + s_-^2) + 2(s_s^2 + s_d^2) & (s_+^2 + s_-^2) + 2(s_s^2 + s_d^2) \\ 8c_+s_+c_-s_- & -(s_+^2 + s_-^2) + 2(s_s^2 + s_d^2) & +(s_+^2 + s_-^2) + 2(s_s^2 + s_d^2) \end{pmatrix} \begin{pmatrix} J_{ABAB}(0) \\ J_{AXAX}(0) \\ J_{BXXB}(0) \end{pmatrix}
 \end{aligned}$$

<sup>5</sup> See footnote 4 following Eq. (117).

$$\begin{aligned}
& + \begin{pmatrix} 0 & 0 & 0 \\ (c_+s_+ + c_-s_-) & 0 & 0 \\ -(c_+s_+ + c_-s_-) & 0 & 0 \\ 0 & 0 & 0 \\ (c_+s_+ - c_-s_-) & 0 & 0 \\ -(c_+s_+ - c_-s_-) & 0 & 0 \end{pmatrix} \begin{pmatrix} J_{ABAB}(\omega) \\ J_{AXAX}(\omega) \\ J_{BXXB}(\omega) \end{pmatrix} + \begin{pmatrix} 0 & 0 & 0 \\ 0 & -(s_+^2 - s_-^2) & (s_+^2 - s_-^2) \\ 0 & (s_+^2 - s_-^2) & -(s_+^2 - s_-^2) \\ 0 & 0 & 0 \\ 0 & -(s_+^2 + s_-^2) & (s_+^2 + s_-^2) \\ 0 & (s_+^2 + s_-^2) & -(s_+^2 + s_-^2) \end{pmatrix} \begin{pmatrix} J_{ABAB}(2\omega) \\ J_{AXAX}(2\omega) \\ J_{BXXB}(2\omega) \end{pmatrix} \\
& + \frac{1}{3} \begin{pmatrix} 0 & 0 & 0 \\ 2c_d s_d & -2c_d s_d & (c_+s_+ + c_-s_-) + 2(s_s^2 + s_d^2) \\ 2c_d s_d & -2c_d s_d & -(c_+s_+ + c_-s_-) + 2(s_s^2 + s_d^2) \\ 0 & 0 & 0 \\ -2c_d s_d & 2c_d s_d & (c_+s_+ - c_-s_-) - 2(s_s^2 + s_d^2) \\ -2c_d s_d & 2c_d s_d & -(c_+s_+ - c_-s_-) - 2(s_s^2 + s_d^2) \end{pmatrix} \begin{pmatrix} J_{ABAX}(0) \\ J_{ABBX}(0) \\ J_{AXBX}(0) \end{pmatrix} \\
& + \begin{pmatrix} 0 & 0 & 0 \\ (s_+^2 - s_-^2) & -(s_+^2 - s_-^2) & (c_+s_+ + c_-s_-) \\ -(s_+^2 - s_-^2) & (s_+^2 - s_-^2) & -(c_+s_+ + c_-s_-) \\ 0 & 0 & 0 \\ (s_+^2 + s_-^2) & -(s_+^2 + s_-^2) & (c_+s_+ - c_-s_-) \\ -(s_+^2 + s_-^2) & (s_+^2 + s_-^2) & -(c_+s_+ - c_-s_-) \end{pmatrix} \begin{pmatrix} J_{ABAX}(\omega) \\ J_{ABBX}(\omega) \\ J_{AXBX}(\omega) \end{pmatrix} \\
& + 2 \begin{pmatrix} 0 & 0 & 0 \\ 0 & 0 & (c_+s_+ + c_-s_-) \\ 0 & 0 & -(c_+s_+ + c_-s_-) \\ 0 & 0 & 0 \\ 0 & 0 & (c_+s_+ - c_-s_-) \\ 0 & 0 & -(c_+s_+ - c_-s_-) \end{pmatrix} \begin{pmatrix} J_{ABAX}(2\omega) \\ J_{ABBX}(2\omega) \\ J_{AXBX}(2\omega) \end{pmatrix} \tag{118}
\end{aligned}$$

where  $s_s = \sin(\theta_+ + \theta_-)$ ,  $s_d = \sin(\theta_+ - \theta_-)$ ,  $c_s = \cos(\theta_+ + \theta_-)$  and  $c_d = \cos(\theta_+ - \theta_-)$ .

The linewidth vector on the LHS here is arranged in such a way that in the weak coupling limit the last two three-spin-one-quantum coherences namely 3,6 and 4,5 have zero intensity and the remaining four SQCs have equal intensity and are arranged in the order of increasing frequency with the two coherences

between the pure states 1,2 and 7,8 being the first and the fourth.

Under various limits, the results yield the following analyses. In the weak coupling limit, without cross-correlation the first four 'X' coherences have finite and equal intensity and have linewidth differences coming only from the remote auto-correlation spectral densities  $J_{ABAB}(0)$  and  $J_{ABAB}(2\omega)$  whereas all the

other spectral densities have equal contribution to the four ‘X’ coherences [232,234]. This results in symmetrical differential linewidths for the outer and the inner lines.

In the weak coupling limit with cross-correlations, the linewidths are additionally unequal due to contributions from the spectral densities  $J_{AXBX}(0)$  and  $J_{AXBX}(\omega)$  with no contribution from all the other cross-correlation spectral densities. Symmetry is maintained between the outer and the inner linewidths. The last two coherences namely  $3 \rightarrow 6$  and  $4 \rightarrow 5$  have unequal widths due to auto and cross-correlations [228–232]. However, they have zero intensity in the weak coupling limit.

In the strong coupling limit without cross-correlations, strong coupling brings unequal contribution from all auto-correlation spectral densities at zero frequency and the spectral densities  $J_{ABAB}(\omega)$ ,  $J_{AXAX}(2\omega)$ ,  $J_{BXXB}(2\omega)$  to the linewidths of the mixed ‘X’ coherences. The two ‘X’ coherences between pure states namely  $1 \rightarrow 2$  and  $7 \rightarrow 8$  have no contribution from strong coupling. The last two coherences have finite intensity and unequal widths.

Under the situation of strong coupling with cross-correlations, all the linewidths of the mixed coherences are unequal due to all the cross-correlation spectral densities at the frequencies 0 and  $\omega$  and the spectral density  $J_{AXBX}(2\omega)$  contributing to them. The two coherences involving the pure states ( $1 \rightarrow 2$  and  $7 \rightarrow 8$ ) have no contribution from strong coupling and have identical widths, which are different from the other mixed transitions.

**4.2.4.2. Double-quantum coherences.** For the ABX case, there are six DQCs. Linewidths for these coherences have also been obtained in a manner similar to SQCs. Contribution from strong coupling and cross-correlation can be separated out as before and the relaxation matrix elements can be expressed by an equation similar to Eq. (117) as [232]:

$$\begin{aligned} \bar{R}_{DQ} = & - \sum_{n=0}^2 \{ [a_{DQ}(n\omega) + a'_{DQ}(n\omega)] \bar{J}_a(n\omega) \\ & + [c_{DQ}(n\omega) + c'_{DQ}(n\omega)] \bar{J}_c(n\omega) \} \end{aligned} \quad (119)$$

This equation when expanded, yields:<sup>6</sup>

$$\begin{aligned} - \begin{pmatrix} R_{1717} \\ R_{2828} \\ R_{1515} \\ R_{4848} \\ R_{1616} \\ R_{3838} \end{pmatrix} = & - \begin{pmatrix} R_{AB}^{DQ,\alpha} \\ R_{AB}^{DQ,\beta} \\ R_{BX}^{DQ,\alpha} \\ R_{BX}^{DQ,\beta} \\ R_{AX}^{DQ,\alpha} \\ R_{AX}^{DQ,\beta} \end{pmatrix} = \frac{5}{6} \begin{pmatrix} 0 & 1 & 1 \\ 0 & 1 & 1 \\ 1 & 1 & 0 \\ 1 & 1 & 0 \\ 1 & 0 & 1 \\ 1 & 0 & 1 \end{pmatrix} \begin{pmatrix} J_{ABAB}(0) \\ J_{AXAX}(0) \\ J_{BXXB}(0) \end{pmatrix} + \begin{pmatrix} 1 & 1 & 1 \\ 1 & 1 & 1 \\ 1 & 1 & 1 \\ 1 & 1 & 1 \\ 1 & 1 & 1 \\ 1 & 1 & 1 \end{pmatrix} \begin{pmatrix} J_{ABAB}(\omega) \\ J_{AXAX}(\omega) \\ J_{BXXB}(\omega) \end{pmatrix} \\ + \begin{pmatrix} 2 & 1 & 1 \\ 2 & 1 & 1 \\ 1 & 1 & 2 \\ 1 & 1 & 2 \\ 1 & 2 & 1 \\ 1 & 2 & 1 \end{pmatrix} \begin{pmatrix} J_{ABAB}(2\omega) \\ J_{AXAX}(2\omega) \\ J_{BXXB}(2\omega) \end{pmatrix} + \frac{4}{3} \begin{pmatrix} 0 & 0 & 1 \\ 0 & 0 & 1 \\ 1 & 0 & 0 \\ 1 & 0 & 0 \\ 0 & 1 & 0 \\ 0 & 1 & 0 \end{pmatrix} \begin{pmatrix} J_{ABAX}(0) \\ J_{ABBX}(0) \\ J_{AXBX}(0) \end{pmatrix} + \begin{pmatrix} 0 & 0 & 1 \\ 0 & 0 & 1 \\ 1 & 0 & 0 \\ 1 & 0 & 0 \\ 0 & 1 & 0 \\ 0 & 1 & 0 \end{pmatrix} \begin{pmatrix} J_{ABAX}(\omega) \\ J_{ABBX}(\omega) \\ J_{AXBX}(\omega) \end{pmatrix} \end{aligned}$$

<sup>6</sup> See footnote 4 following Eq. (117).

$$\begin{aligned}
& + \frac{1}{6} \begin{pmatrix} 0 & 0 & 0 \\ 0 & 0 & 0 \\ 8c_{-s_-} & -5s_-^2 & 5s_-^2 \\ -8c_{+s_+} & -5s_+^2 & 5s_+^2 \\ -8c_{-s_-} & 5s_-^2 & -5s_-^2 \\ 8c_{+s_+} & 5s_+^2 & -5s_+^2 \end{pmatrix} \begin{pmatrix} J_{ABAB}(0) \\ J_{AXAX}(0) \\ J_{BXXB}(0) \end{pmatrix} + \begin{pmatrix} 0 & 0 & 0 \\ 0 & 0 & 0 \\ c_{-s_-} & 0 & 0 \\ -c_{+s_+} & 0 & 0 \\ -c_{-s_-} & 0 & 0 \\ c_{+s_+} & 0 & 0 \end{pmatrix} \begin{pmatrix} J_{ABAB}(\omega) \\ J_{AXAX}(\omega) \\ J_{BXXB}(\omega) \end{pmatrix} \\
& + \begin{pmatrix} 0 & 0 & 0 \\ 0 & 0 & 0 \\ 0 & s_-^2 & -s_-^2 \\ 0 & s_+^2 & -s_+^2 \\ 0 & -s_-^2 & s_-^2 \\ 0 & -s_+^2 & s_+^2 \end{pmatrix} \begin{pmatrix} J_{ABAB}(2\omega) \\ J_{AXAX}(2\omega) \\ J_{BXXB}(2\omega) \end{pmatrix} + \frac{1}{3} \begin{pmatrix} 0 & 0 & 0 \\ 0 & 0 & 0 \\ 2s_-(c_- - 2s_-) & 2s_-(c_+ + 2s_-) & c_{-s_-} \\ -2s_+(c_+ + 2s_+) & -2s_+(c_+ - 2s_+) & -c_{+s_+} \\ -2s_-(c_- - 2s_-) & -2s_-(c_- + 2s_-) & -c_{-s_-} \\ 2s_+(c_+ + 2s_+) & 2s_+(c_+ - 2s_+) & c_{+s_+} \end{pmatrix} \begin{pmatrix} J_{ABAX}(0) \\ J_{ABBX}(0) \\ J_{AXBX}(0) \end{pmatrix} \\
& + \begin{pmatrix} 0 & 0 & 0 \\ 0 & 0 & 0 \\ -s_-^2 & s_-^2 & c_{-s_-} \\ -s_+^2 & s_+^2 & -c_{+s_+} \\ s_-^2 & -s_-^2 & -c_{-s_-} \\ s_+^2 & -s_+^2 & c_{+s_+} \end{pmatrix} \begin{pmatrix} J_{ABAX}(\omega) \\ J_{ABBX}(\omega) \\ J_{AXBX}(\omega) \end{pmatrix} + 2 \begin{pmatrix} 0 & 0 & 0 \\ 0 & 0 & 0 \\ 0 & 0 & c_{-s_-} \\ 0 & 0 & -c_{+s_+} \\ 0 & 0 & -c_{-s_-} \\ 0 & 0 & c_{+s_+} \end{pmatrix} \begin{pmatrix} J_{ABAX}(2\omega) \\ J_{ABBX}(2\omega) \\ J_{AXBX}(2\omega) \end{pmatrix}. \tag{120}
\end{aligned}$$

Here the coherences are arranged as ‘AB’(1–7, 2–8), ‘BX’(1–5, 4–8) and ‘AX’(1–6, 3–8) DQCs, respectively (Fig. 2). The two AB DQCs are between pure states and hence have no contribution from strong coupling. An analysis of the linewidths of these DQCs reveals the following:

(I) *In the weak coupling limit without cross-correlations.* This is identical to the AMX case, except that a homonuclear spin system is considered. Linewidths are not equal but follow a symmetry pattern. All the auto-correlation spectral densities at the Larmor frequency contribute equally to all the DQCs. Only two out of the three auto-correlation spectral densities at zero frequency contribute to the linewidth of each DQC with  $J_{ABAB}(0)$ ,  $J_{AXAX}(0)$  and  $J_{BXXB}(0)$  not contributing to AB, AX and BX DQCs, respectively. While all the auto-correlation

spectral densities at  $2\omega$  contribute to the linewidth of all DQCs,  $J_{ABAB}(2\omega)$ ,  $J_{AXAX}(2\omega)$  and  $J_{BXXB}(2\omega)$  contribute a larger amount (twice as large) to AB, AX and BX DQCs, respectively. Thus both the DQCs of each pair of spin have equal widths, not equal to the widths of the coherences of the other pairs of spins in this case [227].

(II) *Weak coupling with cross-correlations.* Inclusion of cross-correlations within the weak coupling approximation adds additional widths to the various DQCs with the above mentioned symmetry pattern preserved, the same way as in the AMX case. Only one cross-correlation spectral density each at zero and  $\omega$  contributes to the linewidths of each pair of the DQCs such that only  $J_{AXBX}$  contributes to AB,  $J_{ABAX}$  to BX and  $J_{ABBX}$  to AX DQCs, respectively. None of the cross-correlation spectral densities at  $2\omega$

contribute to the linewidths of the DQCs of weakly coupled spins [227,232].

(III) In the strong coupling situation without cross-correlations, the four DQCs between the mixed states have additional contributions compared to case (I) to linewidths with no change in the linewidths of the  $AB$  DQCs (namely 1,7 and 2,8 coherences). While all the auto-correlation spectral densities at zero frequency contribute, only one spectral density at  $\omega$ , namely  $J_{ABAB}(\omega)$  and two at frequency  $2\omega$  namely  $J_{AXAX}(2\omega)$  and  $J_{BXXB}(2\omega)$  contribute additional and unequal widths to the remaining four DQCs. Thus in this limit the two DQCs between pure states have equal widths with all others being different.

(IV) Inclusion of cross-correlation with strong

coupling does not affect the linewidths of the DQCs between pure states but brings additional and unequal contributions to the remaining four DQCs from all the cross-correlation spectral densities at 0 and  $\omega$  and from  $J_{AXBX}(2\omega)$  at  $2\omega$ .

4.2.4.3. *Zero-quantum coherences.* For the three-spin  $ABX$  case, there are six ZQCs whose linewidths can also be expressed as [232]:

$$-\bar{R}_{ZQ} = \sum_{n=0}^2 \{ [a_{ZQ}(n\omega) + a'_{ZQ}(n\omega)] \bar{J}_a(n\omega) + [c_{ZQ}(n\omega) + c'_{ZQ}(n\omega)] \bar{J}_c(n\omega) \} \quad (121)$$

This equation can be reexpressed in terms of spectral densities as:<sup>7</sup>

$$\begin{aligned} & - \begin{pmatrix} R_{3434} \\ R_{5656} \\ R_{2323} \\ R_{6767} \\ R_{2424} \\ R_{5757} \end{pmatrix} = - \begin{pmatrix} R_{AB}^{ZQ,\alpha} \\ R_{AB}^{ZQ,\beta} \\ R_{BX}^{ZQ,\alpha} \\ R_{BX}^{ZQ,\beta} \\ R_{AX}^{ZQ,\alpha} \\ R_{AX}^{ZQ,\beta} \end{pmatrix} = \frac{1}{6} \begin{pmatrix} 2 & 5 & 5 \\ 2 & 5 & 5 \\ 5 & 5 & 2 \\ 5 & 5 & 2 \\ 5 & 2 & 5 \\ 5 & 2 & 5 \end{pmatrix} \begin{pmatrix} J_{ABAB}(0) \\ J_{AXAX}(0) \\ J_{BXXB}(0) \end{pmatrix} + \begin{pmatrix} 1 & 1 & 1 \\ 1 & 1 & 1 \\ 1 & 1 & 1 \\ 1 & 1 & 1 \\ 1 & 1 & 1 \\ 1 & 1 & 1 \end{pmatrix} \begin{pmatrix} J_{ABAB}(\omega) \\ J_{AXAX}(\omega) \\ J_{BXXB}(\omega) \end{pmatrix} \\ & + \begin{pmatrix} 0 & 1 & 1 \\ 0 & 1 & 1 \\ 1 & 1 & 0 \\ 1 & 1 & 0 \\ 1 & 0 & 1 \\ 1 & 0 & 1 \end{pmatrix} \begin{pmatrix} J_{ABAB}(2\omega) \\ J_{AXAX}(2\omega) \\ J_{BXXB}(2\omega) \end{pmatrix} + \frac{4}{3} \begin{pmatrix} 0 & 0 & -1 \\ 0 & 0 & -1 \\ -1 & 0 & 0 \\ -1 & 0 & 0 \\ 0 & -1 & 0 \\ 0 & -1 & 0 \end{pmatrix} \begin{pmatrix} J_{ABAX}(0) \\ J_{ABBX}(0) \\ J_{AXBX}(0) \end{pmatrix} + \begin{pmatrix} 0 & 0 & -1 \\ 0 & 0 & -1 \\ -1 & 0 & 0 \\ -1 & 0 & 0 \\ 0 & -1 & 0 \\ 0 & -1 & 0 \end{pmatrix} \begin{pmatrix} J_{ABAX}(\omega) \\ J_{ABBX}(\omega) \\ J_{AXBX}(\omega) \end{pmatrix} \\ & + \frac{1}{6} \begin{pmatrix} 8c_+^2s_+^2 & -8c_+^2s_+^2 & -8c_+^2s_+^2 \\ 8c_-^2s_-^2 & -8c_-^2s_-^2 & -8c_-^2s_-^2 \\ 8c_+s_+ & -3s_+^2 & 3s_+^2 \\ -8c_-s_- & -3s_-^2 & 3s_-^2 \\ -8c_+s_+ & 3s_+^2 & -3s_+^2 \\ 8c_-s_- & 3s_-^2 & -3s_-^2 \end{pmatrix} \begin{pmatrix} J_{ABAB}(0) \\ J_{AXAX}(0) \\ J_{BXXB}(0) \end{pmatrix} + \begin{pmatrix} 0 & 0 & 0 \\ 0 & 0 & 0 \\ c_+s_+ & 0 & 0 \\ -c_-s_- & 0 & 0 \\ -c_+s_+ & 0 & 0 \\ c_-s_- & 0 & 0 \end{pmatrix} \begin{pmatrix} J_{ABAB}(\omega) \\ J_{AXAX}(\omega) \\ J_{BXXB}(\omega) \end{pmatrix} \end{aligned}$$

<sup>7</sup> See footnote 4 following Eq. (117).

$$\begin{aligned}
& + \begin{pmatrix} 0 & 0 & 0 \\ 0 & 0 & 0 \\ 0 & -s_+^2 & s_+^2 \\ 0 & -s_-^2 & s_-^2 \\ 0 & s_+^2 & -s_+^2 \\ 0 & s_-^2 & -s_-^2 \end{pmatrix} \begin{pmatrix} J_{ABAB}(2\omega) \\ J_{AXAX}(2\omega) \\ J_{BXXB}(2\omega) \end{pmatrix} + \frac{1}{3} \begin{pmatrix} -4c_+s_+(c_+^2 - s_+^2) & 4c_+s_+(c_+^2 - s_+^2) & 8c_+^2s_+^2 \\ 4c_-s_-(c_-^2 - s_-^2) & -4c_-s_-(c_-^2 - s_-^2) & 8c_-^2s_-^2 \\ -2s_+(c_+ - 2s_+) & -2s_+(c_+ + 2s_+) & c_+s_+ \\ 2s_-(c_- + 2s_-) & 2s_-(c_- - 2s_-) & -c_-s_- \\ 2s_+(c_+ - 2s_+) & 2s_+(c_+ + 2s_+) & -c_+s_+ \\ -2s_-(c_- + 2s_-) & -2s_-(c_- - 2s_-) & c_-s_- \end{pmatrix} \begin{pmatrix} J_{ABAX}(0) \\ J_{ABBX}(0) \\ J_{AXBX}(0) \end{pmatrix} \\
& + \begin{pmatrix} 0 & 0 & 0 \\ 0 & 0 & 0 \\ s_+^2 & -s_+^2 & c_+s_+ \\ s_-^2 & -s_-^2 & -c_-s_- \\ -s_+^2 & s_+^2 & -c_+s_+ \\ -s_-^2 & s_-^2 & c_-s_- \end{pmatrix} \begin{pmatrix} J_{ABAX}(\omega) \\ J_{ABBX}(\omega) \\ J_{AXBX}(\omega) \end{pmatrix} + 2 \begin{pmatrix} 0 & 0 & 0 \\ 0 & 0 & 0 \\ 0 & 0 & c_+s_+ \\ 0 & 0 & -c_-s_- \\ 0 & 0 & -c_+s_+ \\ 0 & 0 & c_-s_- \end{pmatrix} \begin{pmatrix} J_{ABAX}(2\omega) \\ J_{ABBX}(2\omega) \\ J_{AXBX}(2\omega) \end{pmatrix} \quad (122)
\end{aligned}$$

Here also the coherences are arranged as ‘AB’, ‘BX’ and ‘AX’ ZQCs, respectively. All the six coherences are between mixed states and hence they all have strong coupling character in them. From these matrices, it is seen that in the weak coupling limit each ZQC of a pair has equal width and not equal to the other pairs, both with or without cross-correlations. In the strong coupling limit, all the widths are unequal. While none of the cross-correlation spectral densities at  $2\omega$  contribute to the linewidths in the weak coupling limit,  $J_{AXBX}(2\omega)$  alone contributes in the strong coupling limit. In the weak coupling limit, the contribution of cross-correlations to the linewidths of ZQCs is equal and opposite to their contribution to DQCs [since  $c_{ZQ}(n\omega) = -c_{DQ}(n\omega)$ ].

**4.2.4.4. Triple-quantum coherence.** The linewidth of the TQC of the ABX spin system is obtained as [232]:

$$\begin{aligned}
R_{AMX}^{\text{TQ}} = R_{1818} = & (1 \quad 1 \quad 1) \begin{pmatrix} J_{ABAB}(\omega) \\ J_{AXAX}(\omega) \\ J_{BXXB}(\omega) \end{pmatrix} \\
& + (2 \quad 2 \quad 2) \begin{pmatrix} J_{ABAB}(2\omega) \\ J_{AXAX}(2\omega) \\ J_{BXXB}(2\omega) \end{pmatrix} + (1 \quad 1 \quad 1) \begin{pmatrix} J_{ABAX}(\omega) \\ J_{ABBX}(\omega) \\ J_{AXBX}(\omega) \end{pmatrix} \quad (123)
\end{aligned}$$

It has contributions from auto-correlation spectral densities at  $\omega$  and  $2\omega$  and from cross-correlation spectral densities at  $\omega$  only. The linewidth of this coherence is free from strong coupling effects even in the presence of cross-correlations.

#### 4.2.5. AX<sub>2</sub> spin system

Such a spin system is often formed by isolated methylene carbons with their directly attached equivalent protons. The carbon (A spin) spectrum consists of a 1:2:1 triplet with three equispaced transitions between symmetric eigenstates and a transition between two antisymmetric states overlapping with the central symmetric transition. While the decay of the outer isolated transitions follow the simple-line approximation and are given by single exponentials, the inner overlapped transitions decay as two independent exponentials, which cannot be independently observed. For the central transition, one can monitor the sum and difference modes.

Several workers have treated this case and have included the dipole–dipole cross-correlations [121,228,229,247]. The decay rates for the two outer transitions (1,2) and (7,8) are equal and are given by  $R_{1212}$  and  $R_{7878}$ , respectively. For the central transitions

(3,6) and (4,5) one obtains:

$$\frac{d}{dt} \begin{pmatrix} M_+ \\ M_- \end{pmatrix} = \begin{pmatrix} \rho_1 & \sigma_{12} \\ \sigma_{12} & \rho_2 \end{pmatrix} \begin{pmatrix} M_+ \\ M_- \end{pmatrix} \quad (124)$$

where  $M_+$  gives the sum mode and  $M_-$  the difference mode, and  $\rho$  and  $\sigma$  are given by [229]:

$$\begin{aligned} \rho_1 &= (1/2)(R_{3636} + R_{4545} + 2R_{3645}) \\ \rho_2 &= (1/2)(R_{3636} + R_{4545} - 2R_{3645}) \\ \sigma_{12} &= (1/2)(R_{3636} - R_{4545}) \end{aligned} \quad (125)$$

The expressions for various  $R$ 's are obtained as:

$$\begin{aligned} - \begin{pmatrix} R_{1212} \\ R_{3636} \\ R_{4545} \end{pmatrix} &= \frac{1}{3} \begin{pmatrix} 4 & 1 & 3 & 3 & 6 \\ 2 & 1 & 3 & 3 & 6 \\ 2 & 1 & 3 & 3 & 6 \end{pmatrix} \begin{pmatrix} J_{AXAX}(0) \\ J_{AXAX}(\omega_A - \omega_X) \\ J_{AXAX}(\omega_A) \\ J_{AXAX}(\omega_X) \\ J_{AXAX}(\omega_A + \omega_X) \end{pmatrix} \\ &+ \frac{1}{3} \begin{pmatrix} 4 & 0 & 3 & 0 & 0 & 3 & 6 \\ -2 & 1 & -3 & -3 & 6 & 6 & 0 \\ -2 & -1 & -3 & -3 & -6 & 0 & 0 \end{pmatrix} \\ &\times \begin{pmatrix} J_{AXAX'}(0) \\ J_{AXAX'}(\omega_A - \omega_X) \\ J_{AXAX'}(\omega_A) \\ J_{AXAX'}(\omega_X) \\ J_{AXAX'}(\omega_A + \omega_X) \\ J_{XX'XX'}(\omega_X) \\ J_{XX'XX'}(2\omega_X) \end{pmatrix}. \end{aligned} \quad (126)$$

and

$$R_{3645} = R_{4536} = -\frac{2}{3}[J_{AXAX}(0) - J_{AXAX'}(0)]. \quad (127)$$

The first term on RHS of Eq. (126) contains the dipolar auto-correlation and the second term the dipole–dipole cross-correlation spectral densities. The two outer transitions have identical decay rates, due to dipole–dipole auto and cross-correlation contributions. They are different if CSA–dipole contributions are included [228]. For the inner transitions, the sum

mode decays biexponentially since  $R_{3636}$  and  $R_{4545}$  differ due to auto-correlation spectral density  $J_{XX'XX'}(\omega_X)$  and cross-correlation spectral densities,  $J_{AXAX'}(\omega_A - \omega_X)$  and  $J_{AXAX'}(\omega_A + \omega_X)$ . However, in the long correlation limit, when only  $J(0)$ 's survive, the difference disappears and the sum mode of inner transitions decays with a single exponential. Under this condition, the inner and outer lines become Lorentzians, whose linewidths differ only due to cross-correlation  $J_{AXAX'}(0)$ . (Under this limit,  $R_{1212} = (4/3)[J_{AXAX}(0) + J_{AXAX'}(0)]$  and the decay rate of  $M_+$  is given by  $(4/3)[J_{AXAX}(0) + J_{AXAX'}(0)]$ .)

#### 4.2.6. $AX_3$ spin system

A typical  $AX_3$  spin system which is often encountered is the methyl group  $^{13}\text{CH}_3$ . The  $A$  spin carbon multiplet is a quartet, in the intensity ratio, 1:3:3:1. The complete analyses for such a system is given in Refs. [175,228–230,248–251]. In the long correlation limit, where  $J_{AXAX}(0)$  spectral density terms dominate the transverse relaxation, the relaxation rates for the outer and inner transitions are given by [229]:

$$R_{\text{IN/OUT}} = -[2J_{AXAX}(0) \mp 4J_{AXAX'}(0)] \quad (128)$$

Here  $J_{AXAX}(0)$  is the auto-correlation spectral density for the internuclear  $^1\text{H}-^{13}\text{C}$  vector evaluated at zero frequency, and  $J_{AXAX'}(0)$  is the three-spin cross-correlation spectral density, where  $X, X'$  share the same  $A$  spin. Hence from these equations, it can be seen that for  $\omega\tau_c \gg 1$ , the inner and outer lines decay with single exponentials which differ from each other due to cross-correlations.

In the presence of CSA( $^{13}\text{C}$ )–dipole cross-correlations, all the four transitions of the  $A$  spin have different linewidths. The linewidths of the two outer transitions are given by [252]:

$$\begin{aligned} \left(\frac{1}{T_2}\right)_{\pm} &= \frac{8}{3}J_{AA}(0) + 2J_{AXAX}(0) + 4J_{AXAX'}(0) \\ &\mp 8J_{A,AX}(0) + 2J_{AA}(\omega_A) + \frac{3}{2}J_{AXAX}(\omega_A) \\ &+ \frac{3}{2}J_{AXAX'}(\omega_A) \mp 6J_{A,AX}(\omega_A) \\ &+ \frac{1}{2}J_{AXAX}(\omega_A - \omega_X) + \frac{3}{2}J_{AXAX}(\omega_X) \\ &+ 3J_{AXAX}(\omega_A + \omega_X) + 3J_{XX'XX'}(\omega_X) \\ &+ 3J_{XX'XX''}(\omega_X) + 6J_{XX'XX'}(2\omega_X) \end{aligned} \quad (129)$$

The differential width between the outermost components  $(1/T_2)_- - (1/T_2)_+$  depends upon the cross-correlations and equals  $16J_{A,AX}(0) + 12J_{A,AX}(\omega_A)$ . In the absence of CSA–dipole cross-correlations, the outer components are identical in width and shape, yet they differ in width and shape from the inner components. The inner components each are degenerate transitions, and have multi-exponential relaxation with only the sum mode being observable.

#### 4.2.7. Spin-(1/2) coupled to spin > (1/2) system

Consider the scalar coupled two-spin system where spin  $I = 1/2$  and spin  $S > (1/2)$ . Assuming that the relaxation of spin  $S$  is governed by an axially symmetric quadrupolar interaction, and spin  $I$  is relaxed directly by the  $I$ – $S$  dipolar interaction and an electronic shielding anisotropy, the relaxation rate,  $(1/T_2)_{s,m}$ , of each transition of the  $I$  [spin-(1/2)] spin, is given by [64,253–255]:

$$\begin{aligned} \left(\frac{1}{T_2}\right)_{s,m} = & \left[ \frac{2}{s(2s-1)} \right]^2 \{ [s(s+1)(4m^2+1) \\ & - m^2(4m^2+5)] J^Q(\omega_s) + \{ [s(s+1) \\ & - (m^2+1)]^2 + 3m^2 - 1 \} J^Q(2\omega_s) \} \\ & + \left[ \frac{8m}{s(2s-1)} \right] [2s(s+1) \\ & - 2m^2 - 1] J^{Q,CSA_s}(\omega_s) \\ & + \frac{8}{3} [m^2 J_{ISIS}(0) + J_{II}(0) - 2m J_{I,IS}(0)]. \end{aligned} \quad (130)$$

Here  $J^Q$  are the quadrupolar auto-correlation terms,  $J^{Q,CSA_s}$  the cross-correlation between quadrupole and CSA of  $S$  spin,  $J_{ISIS}$  is the  $IS$ -dipolar and  $J_{II}$  the CSA of the  $I$  spin auto-correlation terms, while  $J_{I,IS}$  is the CSA( $I$ )–dipole( $IS$ ) cross-correlation term. In Eq. (130), only adiabatic (zero frequency) terms have been included for the CSA and dipole auto and cross-correlations. While the CSA( $I$ ) auto-correlation contributes equal widths to all the transitions of spin  $I$ , all other auto and cross-correlation terms contribute differentially. The cross-correlation between quadrupolar and dipolar relaxation contributes to the dynamic frequency shift (see Eq. (188)) and not to the linewidth of  $I$  spin transitions.

### 4.3. Experimental observation of transverse cross-correlations

As seen from the above analyses, cross-correlations lead to DLB/line narrowing. The same effect can lead to coherence transfer from one spin to another, also known as RACT. In this section, we first deal with DLB observations and later with RACT. The same effect also leads to transverse relaxation optimized spectroscopy (TROSY), which will be discussed in Section 7.6.

#### 4.3.1. Direct observations of differential line broadening

The possibility of observing DLB in coupled spin-(1/2), spin-(1/2) AX systems was discussed first by Shimizu [3]. An effort to observe this effect was done by Mackor and McLean, where they used  $\text{CH}_2\text{FCl}_2$  as a model compound [217,219]. They found that the longitudinal relaxation is different for the two lines in the high-resolution  $^{19}\text{F}$  NMR spectrum but could not see any DLB effects.

Quantitative evidence of DLB was given by Farrar and Quintero-Arcaya, where they observed DLB in both the  $^{19}\text{F}$  and  $^{31}\text{P}$  spectra of fluorophosphate anion,  $\text{PFO}_3^{2-}$  [256,257]. Fig. 35 summarizes their

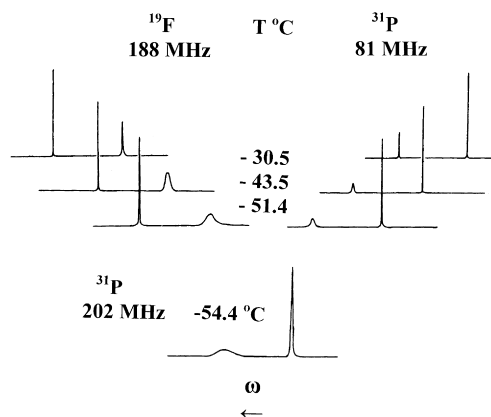


Fig. 35.  $^{31}\text{P}$  and  $^{19}\text{F}$  NMR spectra of fluorophosphate ( $\text{PFO}_3^{2-}$ ) anion at different temperatures and magnetic field values. The peak heights for the various doublets are quite different, but in each case the integrated intensities of each of the pair of lines are equal. The DLB is due to cross-correlation between the CSA and dipolar relaxation mechanisms. The DLB increases with the strength of the magnetic field. [Reproduced with permission from Ref. [256].]

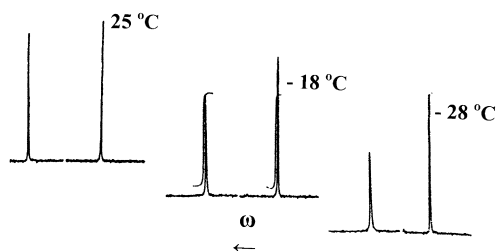


Fig. 36. Coupled carbon-13 NMR spectra of the acetylenic carbon of phenylacetylene in a 1:1 mixture of acetone- $d_6$  and ethylene glycol- $d_6$ , at +25, -18 and -28°C. The spectra were recorded at 90 MHz. The high frequency line is broader than the low frequency line due to CSA-dipole cross-correlations. The DLB effects increase as the temperature decreases. A similar DLB effect was also observed for the *para* carbon in the ring, but the effect is more pronounced for the acetylenic carbon. This is because the principal axis of the CSA tensor is coincident with the dipolar vector for the acetylenic carbon. [Reproduced with permission from T.C. Farrar, B.R. Adams, G.C. Grey, R.A. Quintero-Arcaya, Q. Zuo, J. Am. Chem. Soc. 108 (1986) 8190.]

results. They further concluded that the observation of differential transverse relaxation is made possible if the following criteria are satisfied:

- The magnitude of the CSA must be comparable to the intramolecular dipolar interaction [256,257]. Hence, nuclei having a wide range of chemical shifts, such as  $^{31}\text{P}$ ,  $^{195}\text{Pt}$ ,  $^{77}\text{Se}$ ,  $^{19}\text{F}$ ,  $^{29}\text{Si}$ ,  $^{15}\text{N}$  and  $^{13}\text{C}$  [252,258–260] are expected to display DLB in their coupled NMR spectra.
- The DLB will increase with the strength of the magnetic field.
- The observation of DLB requires relatively slow molecular motions or long correlation times ( $\omega\tau_c \gg 1$ ). Therefore, spin systems embedded in macromolecules or adsorbed on high surface area materials are likely candidates to exhibit DLB.
- DLB will be masked by the presence of intermolecular dipolar interactions.

Some other early observations of DLB involve the observation of such effects for protons in slowly moving large biomolecules (such as t-RNA) by Guéron et al. [191]. Another instance is the differential line widths in the phosphorous doublet in the phosphonium ion  $[\text{HP}(\text{CH}_3)_3^+]$  when adsorbed in H-Y zeolite [256]. Farrar et al. have showed that the linewidths of the various  $^{13}\text{C}$  doublets in

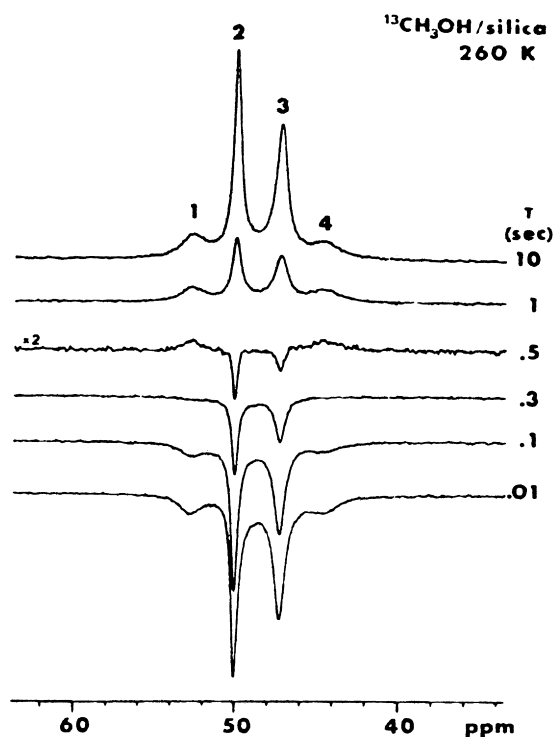


Fig. 37. Inversion-recovery  $^{13}\text{C}$  spectra of methanol adsorbed on silica recorded using Bruker CXP-200 spectrometer with magic-angle spinning (MAS) at 260 K. The 0.5 s spectrum is multiplied by 2 to emphasize the difference in the recovery of the inner and outer lines. The differences in the linewidths of the multiplet result from the effects of cross-correlation on the transverse relaxation. The differential recovery results from the effects of cross-correlation on longitudinal relaxation. [Reproduced with permission from C.J. Hartzell, P.C. Stein, T.J. Lynch, L.G. Werbelow, W.L. Earl, J. Am. Chem. Soc. 111 (1989) 5114.]

phenylacetylene are differentially broadened due to CSA-dipole cross-correlations and they also observed an increase in the DLB with decreasing temperature (Fig. 36) [258]. Hertzell et al. have observed both DLB and differential longitudinal relaxation effects arising from cross-correlations in the  $^{13}\text{C}$  spectrum of methanol adsorbed on silica (Fig. 37) [252]. These cross-correlation effects can provide a detailed description of molecular dynamics and anisotropic interactions at the molecular level. The relative magnitudes of dipolar and CSA interactions as well as the degree of CSA-dipole and dipole-dipole cross-correlations have been determined. It has been shown in this paper that the

cross-correlations which give rise to both DLB and longitudinal multi-spin orders, can be used to determine the absolute signs of various spin couplings and position the principal axes of the spin interaction. The evolution of multi-spin order is extremely sensitive to motional anisotropies and can be used to study highly anisotropic systems where conventional NMR relaxation studies normally would not work. There are many recent DLB studies which will be discussed in Section 7.

#### 4.3.2. Motional information from non-axial CSA and dipole cross-correlations

Fischer et al. [243], have carried out a detailed study of motional aspects of the protein *E. coli*, flavodoxin. In an earlier study, they had measured several relaxation parameters for the peptide-plane carbonyl and nitrogen nuclei, and a poor correlation between the general order parameters of  $C'-C_\alpha$  vector and the N–NH vector was interpreted as evidence for local anisotropic motion [244]. In the present study [243] the cross-correlation between the  $C'$  CSA and  $C'-C_\alpha$  dipolar interaction was measured from the differences in the intensities of the single-quantum  $C'$  doublet split by  $J_{^{13}C'-^{13}C_\alpha}$ , in a constant time 3D experiment, for several residues of the  $^{13}C$ – $^{15}N$  labeled protein. The formalism of Daragan and Mayo [245], has been extended to include cross-correlation between non-axial CSA and dipolar relaxation to account for the dynamics of the  $C'-C_\alpha$  vector and N–NH vector and the CSA tensor components, which behave differently under anisotropic motion. A detailed motional model has been fitted to this data to characterize the internal motion along the  $C'-C_\alpha$  and N–NH axes for each residue [243].

#### 4.3.3. Break down of coherence transfer rules in equivalent spin systems

Coherence transfer rules have been introduced in 2D NMR, assuming that transverse relaxation can be ignored [49]. These rules remain valid in the presence of auto-correlated transverse relaxation but break down in the presence of cross-correlations, because of the unequal decay of degenerate coherences [261–263]. The transfer rules imply that in a  $p$ -quantum filtered correlation spectroscopy ( $p$ QF-COSY) of  $AX_2$  and  $AX_3$  spin systems, no cross peaks should be observed for  $p > 2$ . This is because according to the

predictions, in systems with magnetically equivalent spins ( $AX_2$ ,  $AX_3$ ) it is not possible to transfer SQC of the  $X$  spins into multiple-quantum coherence involving more than one  $X$  spin. Müller et al. have found that in contrast to the prediction based on these selection rules, SQCs of the  $X$  spins in  $AX_n$  groups can be transferred into multiple-quantum coherence involving several  $X$  spins, due to the unequal transverse relaxation of degenerate  $X$  spin SQCs in the course of the evolution period [261]. This multi-exponential  $T_2$  relaxation, arising due to cross-correlations, can lead to the appearance of forbidden cross peaks in 2D NMR spectra, which have been observed, for example in the 4QF-COSY spectra of the protein, BPTI as shown in Fig. 38 [261]. Müller has suggested a new multiple-quantum 2D NMR method to monitor the combined effects of multi-exponential relaxation, due to longitudinal and transverse cross-correlations [264,265]. The experiment employs the pulse sequence  $\pi$ – $\tau$ – $\beta_\phi$ – $t_1$ – $\beta'_\phi$ –acq. In this experiment the non-selective  $\pi$  pulse inverts the magnetization which relaxes multi-exponentially during  $\tau$  and creates multi-spin longitudinal orders due to cross-correlations. At the end of  $\tau$  period,  $\beta$ -pulse converts these multi-spin orders into multiple-quantum coherences, which evolve during  $t_1$  and are reconverted into detectable SQCs by a  $\beta'$  pulse. The experiment was performed on BPTI. Skew-diagonal peaks exhibit lineshapes characteristic of multi-exponential  $T_1$  and  $T_2$  relaxation along the two frequency axes. The appearance of remote peaks in coupled spin systems requires only longitudinal relaxation to be non-exponential. Fig. 39 shows the cross-sections of selected peaks from the 2D spectrum of BPTI obtained with the pulse sequence listed above which is a 3Q-MERCY (multi-exponential relaxation spectroscopy) spectrum (only three-quantum coherence is selected during  $t_1$ ). These cross-sections clearly demonstrate the manifestations of multi-exponential longitudinal and transverse relaxation. Müller has further observed multiple-quantum coherences up to an order of 5 in the  $A_5$  spin systems of the organometallic  $\pi$ -complex ferrocene in the absence of J-coupling via multi-exponential relaxation due to cross-correlations [266].

#### 4.3.4. Relaxation-allowed coherence transfer

Another important development in the experimental observation of cross-correlations in transverse

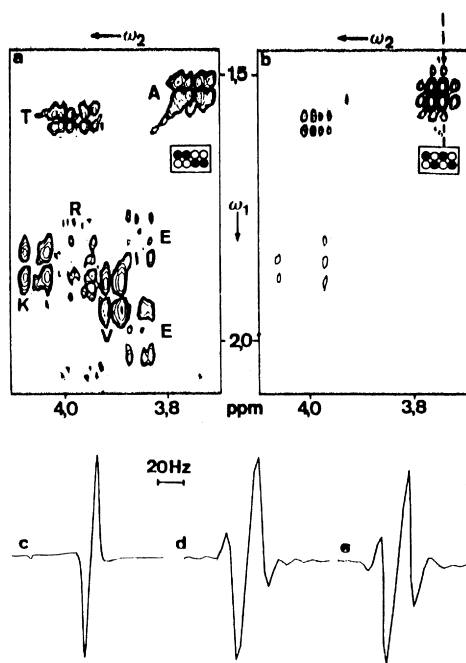


Fig. 38. Phase-sensitive (a) 2QF-COSY and (b) 4QF-COSY spectra of basic pancreatic trypsin inhibitor (BPTI, 20 mM in D<sub>2</sub>O, pD = 4.6,  $T = 36^\circ\text{C}$ ). The regions shown contain the cross-peaks between H <sub>$\alpha$</sub>  and H <sub>$\beta$</sub>  of (A) alanine-25, (K) lysine-26, (R) arginine-53, (V) valine-34 and (E) glutamate-49, as well as the H <sub>$\beta$</sub>  and H <sub>$\gamma$</sub>  cross peak of (T) threonine-54. In (b), all these cross peaks should disappear, but the signals due to A and T survive because of multi-exponential transverse relaxation effects, due to cross-correlations. The inserts show the sign patterns of the cross peaks of A (filled and open symbols representing positive and negative signals, respectively). The pattern of the forbidden cross peak in (b) is in antiphase with respect to all multiplet components. The spectra were obtained with a Bruker AM-360 spectrometer; spectral width 3030 Hz in both dimensions, data matrices with 2048  $\times$  600 points before and 4k  $\times$  4k after zero filling; 32 and 256 scans per  $t_1$  value for (a) and (b), respectively; filtration with shifted sine-bell ( $\phi = \pi/16$  in  $\omega_1$  and  $\pi/8$  in  $\omega_2$ ). (c) Simulated antiphase doublet, where each component consists of the difference of two Lorentzians with time-constants of 0.2 and 0.125 s. (d) Same as (c) but with limited digitization and sine-bell multiplication as in the experiment. (e) Cross-section taken from the experimental “forbidden” alanine cross peak in 4QF-COSY parallel to  $\omega_1$ , as indicated by dashed line in (b). Note the qualitative agreement of (d) and (e). [Reproduced with permission from N. Müller, G. Bodenhausen, K. Wüthrich, R.R. Ernst, J. Magn. Reson. 65 (1985) 531.]

relaxation was that connected with RACT peaks in 2D spectra, particularly COSY type of experiments, even in the absence of J-coupling. Wimperis and Bodenhausen observed that coherence transfer can be

induced by a single RF pulse between two spins that are not scalar coupled which in turn gives rise to cross peaks in COSY spectra [222]. This phenomenon arises from multi-exponential  $T_2$  relaxation that can arise from cross-correlations between two dipolar interactions. Fig. 40 shows schematic spectra that correspond to (a) a conventional 1D spectrum with a four-line multiplet of spin A in a linear  $M-A-K$  spin system with  $J_{AM} > J_{AK} > 0$ ; (b) the same multiplet antiphase with respect to spin K, which corresponds to the appearance of the multiplet in a cross-section through a COSY spectrum if it had arisen from a non-zero J-coupling,  $J_{AK}$ ; (c) the same antiphase multiplet for  $J_{AK} \rightarrow 0$  in which the outer and inner lines do not have the same line width due to dipole-dipole cross-correlations and it is this multiplet structure that one expects for a cross-section through a relaxation allowed cross peak: two lines in antiphase with respect to a spin that would merely play a passive role in normal coherence transfer. The experimental COSY spectrum of umbelliferone (Fig. 41) reveals a cross peak between the spins A and K although the scalar coupling  $J_{AK}$  is much less than the linewidth [222]. They have further discussed the implications for COSY spectra by considering a four spin-1/2 system  $M-A \cdots K-X$  where the dotted line indicates the presence of a time-dependent dipolar coupling without scalar interactions and solid lines indicate the simultaneous presence of a resolved scalar coupling and a time-dependent dipolar coupling [223]. Experimental evidence for such RACT peaks is shown in Fig. 42 [223]. These cross peaks appear due to dipole-dipole cross-correlations. However, CSA-dipole cross-correlations can also lead to RACT peaks.

Even if cross-correlations were not present there could be differences in the linewidth of the various transitions of the multiplets of a weakly coupled spin system with three or more relaxation coupled spins [see Eq. (114); contributions of  $J_{MXMX}(\omega_A \pm \omega_X)$ ]. In these cases RACT peaks can appear in the absence of cross-correlations.

#### 4.4. Remote cross-correlations

Cross-correlations between two interactions that do not explicitly depend upon the distance from the spin of interest have been termed as “remote”

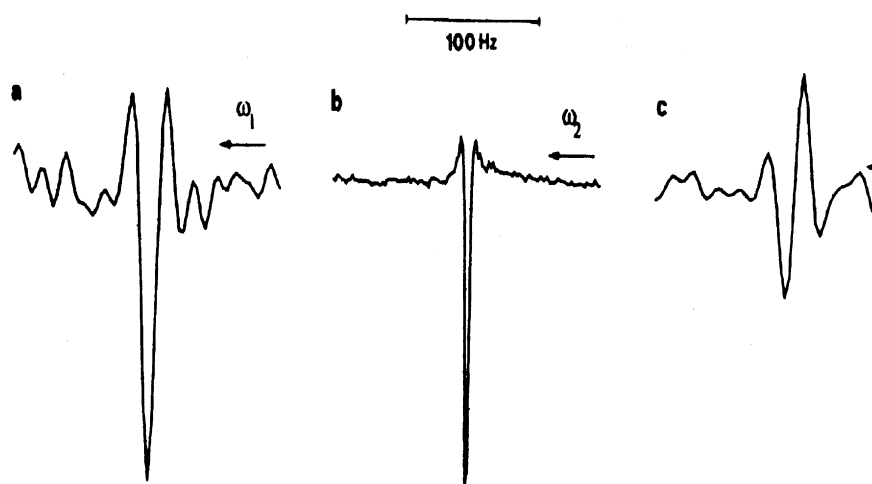


Fig. 39. Cross-sections of selected peaks from the 2D multi-exponential relaxation spectroscopy (MERCY) proton spectrum of BPTI at 400 MHz (36°C, 18 mM in  $^2\text{H}_2\text{O}$ , pH = 4.7). Three-quantum coherence is selected during  $t_1$ . For these plots, the spectrum was re-transformed without window multiplication. In (a), the vertical cross-section of the Met-52 singlet exhibits sidelobes, of a sign opposite to the central lobe, that are obvious manifestations of multi-exponential longitudinal relaxation during  $\tau$ . The horizontal cross-section (b) is also flanked by such lobes, which however reflect multi-exponential transverse relaxation. The antiphase doublet between the methyl and  $\alpha$ -protons of Ala-58 is shown in (c) along the  $\omega_1$  dimension. The sidelobes are due to the longitudinal relaxation. [Reproduced with permission from N. Müller, Chem. Phys. Lett. 131 (1986) 218.].

[222,233,235]. The term “remote” is not confined to cross-correlations since there are also “remote” auto-correlations. The “remote” terms affect both longitudinal as well as transverse relaxation. In this section, we confine the discussion to contributions of “remote” cross-correlations to transverse relaxation. Like all cross-correlations, “remote” terms also contribute differential line broadening to various transitions of a spin, in the case of resolved transitions and to multi-exponential transverse relaxation in the case of unresolved, overlapping or degenerate transitions.

Examples of “remote” cross-correlations are cross terms (i) between CSA of two different spins in a molecule, (ii) between CSA of spin  $i$  and dipolar interaction between spins  $j$  and  $k$ , (iii) between CSA of spins  $j$  or  $k$  and dipolar interaction between spins  $j$  and  $k$ , affecting the linewidths of spin  $i$ , (iv) cross terms between two pairs of dipolar interactions with no common spin among them and (v) cross-terms between two dipolar interaction among spins  $i, j$  and  $j, k$  affecting spin  $m$ . While such cross terms do not depend explicitly on the distance of the spins from the spin of interest, they do depend on the geometric disposition of the spins. For example, the CSA( $i$ )–CSA( $j$ ) cross-term depends on the angle between

the orientation of the two tensors (see Eq. (43)) and dipole( $ij$ )–dipole( $kl$ ) cross-term depends on the angle between the two dipolar vectors (see Eq. (44)). Similarly CSA( $i$ )–dipole( $jk$ ) cross-term depends on the angle between the orientation of the CSA tensor with respect to the dipolar vector (Eq. (42)).

It has been shown [233,235] that the remote cross-correlations have a first-order contribution, which is a differential effect between SQC or multiple-quantum coherence. To excite the multiple quanta as well as to observe the first order differential effect, well resolved J-couplings are needed between the spins of interest. In the absence of J-coupling, the first-order contribution cancels and the remote cross-correlations give rise to a second-order effect, which becomes observable only in the presence of some direct cross-correlations. In the following, some results are reproduced to highlight the above conclusions [233], by specific examples of AX, AMX and AMKX spin systems.

#### 4.4.1. Remote CSA–CSA cross-correlations

The possibility of a CSA–CSA cross correlated relaxation was first mentioned by Vold and Vold [59]. Later Werbelow [83], Konrat and Sterk [227] and recently Kumar and Kumar [233] showed that

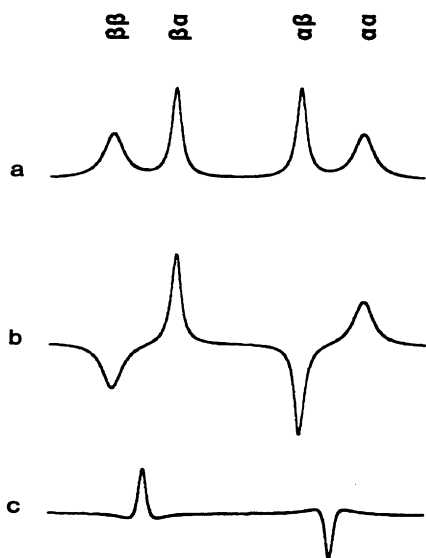


Fig. 40. Schematic A-spin multiplets for a linear three weakly scalar-coupled spin-1/2 nuclei, with the four lines labeled  $\alpha\alpha$ ,  $\alpha\beta$  etc., according to the states of the coupling partners. In (a), it is assumed that  $J_{AM} > J_{AK} > 0$ ; the linewidth differences are due to the (positive) cross-correlation spectral density  $J_{AMAK}$ . In (b), the multiplet is shown in antiphase with respect to spin  $K$ , but with the same linewidths. In the limit of  $J_{AK} = 0$ , case (b) is converted into case (c). This corresponds to a cross-section through a relaxation-allowed cross-peak in a 2D correlation spectrum (“COSY”). These schematics are also applicable to the case where the linewidth differences would arise from the remote auto-correlation spectral density  $J_{MKMK}$ . [Reproduced with permission from S. Wimperis, G. Bodenhausen, Chem. Phys. Lett. 140 (1987) 41].

the CSA–CSA cross-correlations contribute a DLB effect on ZQC and DQC. This contribution to DLB is contained in Eqs. (107), (113) and (115). The spectral densities,  $J_{A,X}(n\omega)$  the remote CSA(A)–CSA(X) cross-correlations, do not contribute to the linewidths of SQCs in weakly coupled spins, but contribute a DLB effect to the ZQC and DQC through  $J_{A,X}(0)$  in AX spin systems (Eq. (107)), and to DQ(AM) and ZQ(AM) through  $J_{A,M}(0)$  in an AMX spin system (Eq. (115)). Since the excitation of the ZQC and DQC requires the presence of a resolved J-coupling between the spins, the cross terms between CSA of spins  $i$  and  $j$  can contribute only when they are nearby in a covalent network and have a resolved J-coupling. This ensures that only “scalar coupled” spins have a contribution from CSA–CSA cross-correlations [233].

The cross-correlation between  $^{15}\text{N}$  and  $^{13}\text{C}$  chemical shift anisotropies has been recently observed while measuring the differences in the relaxation rates of the ZQC and DQC of these two spins in a constant time 2D HNC0 experiment in a doubly labeled protein binase (12.3 kDa) [267]. Two experiments were performed. In experiment (A) (Fig. 43), at the beginning of the constant period ( $2\Delta$ ), the two spin coherence  $N_x C_x$  is created, which is the sum of ZQC and DQC. The  $C_\alpha$  carbon is decoupled by a selective  $180^\circ$  pulse in the middle of the  $\Delta$  period. Each ZQC and DQC is split into doublets by the coupling to the amide proton. The evolution of each doublet is interchanged by a  $180^\circ$  pulse in the middle of the  $\Delta$  period and an average relaxation of each coherence order is obtained, retaining the simple-line approximation. From Eq. (115), it can be seen that the CSA–dipole cross-correlations, which give differential relaxation of the doublets of ZQC and DQC cancel out and the average decay rates of ZQC and DQC differ by the CSA–CSA and a dipole–dipole cross-correlation at zero frequency. In addition, the difference contains some auto- and cross-terms from high-frequency spectral densities. Retaining only the zero-frequency spectral densities, one obtains, from the ratio of ZQC and DQC in a decoupled HNC0 experiment

$$(2\Delta)^{-1} \ln\left(\frac{I_{ZQ}}{I_{DQ}}\right) = J_{\text{NH,CH}}(0) + J_{\text{N,C}}(0). \quad (131)$$

In the second experiment (B) (Fig. 43), the above two contributions, have been separated out by creating a TQC  $4H_x N_x C_x$  at the beginning of the  $2\Delta$  period, but the evolution of only the ZQC and DQC between N-15 and C-13 is monitored. The generation of TQC ensures that the adiabatic contribution involving the dipolar interaction between the three spins [ $J_{\text{NH,CH}}(0)$ ] is eliminated [267]. Consequently in experiment (B)

$$(2\Delta)^{-1} \ln\left(\frac{I_{ZQ}}{I_{DQ}}\right) = J_{\text{N,C}}(0). \quad (132)$$

From these experiments (Fig. 44), both  $J_{\text{N,C}}(0)$  as well as  $J_{\text{NH,CH}}(0)$  were obtained for all the residues in the protein (Fig. 45). The CSA–CSA cross-correlation rates were found to vary between  $+1.2$  and  $-5.2 \text{ s}^{-1}$ , with an average value of  $-2.3 \pm 1.4 \text{ s}^{-1}$ , and  $J_{\text{NH,CH}}(0)$  varies between  $-0.1$  and  $-3.8 \text{ s}^{-1}$ , with

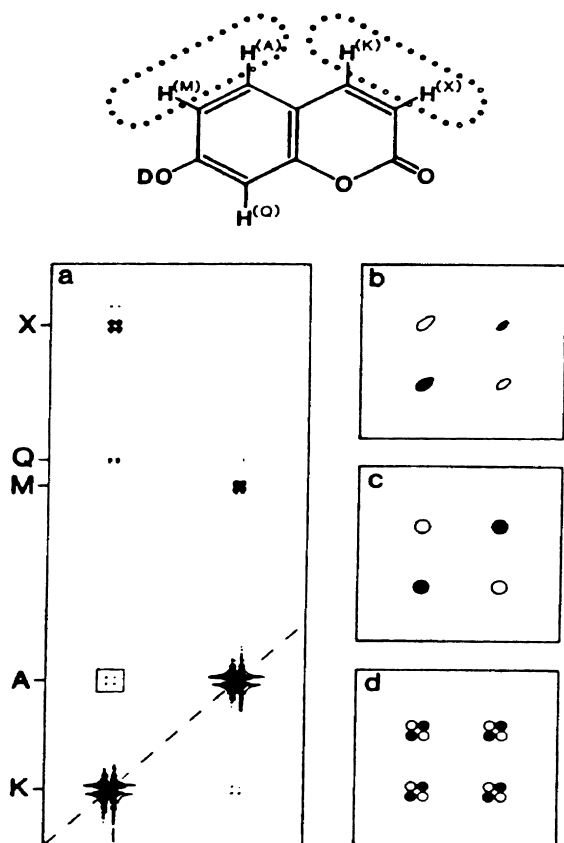


Fig. 41. (a) Partial 2D COSY proton spectrum of an isotropic solution of umbelliferone in a mixture of  $D_2O$ ,  $(CD_3)_2SO$  and  $(CD_3)_2CO$  (2:2:1 by volume). The spectrum was recorded with the usual procedures ( $\pi/2$  mixing pulse) at 223 K and at 400 MHz on a Bruker AM-400 spectrometer. The relevant four-spin subsystem has been emphasized by dotted envelopes in the molecule. The scalar coupling  $J_{AK}$  is negligible with respect to the linewidths, but  $J_{AM}$  and  $J_{KX}$  are not. The cross-correlation spectral densities  $J_{AMAK}$  and  $J_{AKKX}$  are large due to spatial proximity and a roughly linear arrangement. The relaxation-allowed  $A$ – $K$  cross-peak multiplet centered at  $\omega_1 = \Omega_A$  and  $\omega_2 = \Omega_K$  (framed in (a)) is enlarged in (b), where it can be compared with the schematic pattern expected for RACT shown in (c). The signals in this rectangular pattern are separated by  $J_{AM}$  in  $\omega_1$  and  $J_{KX}$  in  $\omega_2$ . The pattern that would result from a hypothetical well-behaved transfer due to  $J_{AK}$  is shown in (d). Positive signals have been rendered by filled contours in (b), (c) and (d). [Reproduced with permission from S. Wimperis, G. Bodenhausen, Chem. Phys. Lett. 140 (1987) 41.]

an average value of  $-2.0 \pm 0.8 \text{ s}^{-1}$ . While the average values for both the cross-correlations are within expected theoretical values, the variation is outside experimental error. These variations have been

assigned to local anisotropic internal motion as well as variations of the magnitude of the CSA tensors and the angles between them [267].

Norwood et al. have also measured the cross-correlation between  $^1H_N$  and  $^{15}N$  CSA tensors, by measuring the differential relaxation of the ZQC and DQC of the amide proton and nitrogen in perdeuterated,  $^{15}N$ -labeled human-dynamic-light-chain-1 protein [268]. They have also considered only the zero-frequency spectral densities, since  $\omega\tau_c \gg 1$  is satisfied. Their experiment has the additional advantage that the zero frequency dipole–dipole cross-correlation terms with all other non-bonded protons are negligible since all other spins (protons as well as  $^{15}N$ ) are far away from the  $^{15}N$ – $^1H$  bonded pair. Therefore the difference in the zero- and double-quantum relaxation rates is exclusively due to CSA–CSA cross-correlations. This has been measured for the  $^1H$ – $^{15}N$  group of Glutamine 27 of the protein and a value of  $1.01 \pm 0.14 \text{ s}^{-1}$  is obtained for this cross-correlation. Using  $\Delta\sigma_N$  and the angle between the orientation of the two tensors as measured by Tjandra et al. [239] a reasonable estimate of  $\Delta\sigma_{H_N} = 5.06 \pm 0.73 \text{ ppm}$  has been obtained.

#### 4.4.2. Remote CSA–dipole cross-correlations

These cross-correlations show up in three-spin systems and can be analysed from the results for the  $AMX$  spin system contained in Eqs. (114) and (115). The linewidths of  $A$ -spin SQCs (Eq. (114)) have a differential contribution from remote cross-correlations  $J_{M,MX}(\omega_M)$  and  $J_{X,MX}(\omega_X)$ , both of which are independent of the distances of spins  $M$  and  $X$  from spin  $A$ . The result of Eq. (114) is valid only under the condition of simple-line approximation, which requires resolved  $J_{AM}$  and  $J_{AX}$  couplings, as shown in the Appendix of Ref. [233]. In the absence of these  $J$ -couplings, the first-order contribution cancels and these remote cross-correlations contribute a second-order effect, but only in the presence of direct cross-correlations  $J_{A,AM}$  or  $J_{A,AX}$  [233]. Similarly for the multiple-quantum coherences, the linewidths of which are contained in Eq. (115), it is seen that the  $AM$  ZQC and DQC have a first-order differential line broadening contribution from remote cross-correlations  $J_{A,MX}(0)$ ,  $J_{M,AX}(0)$  and  $J_{A,M}(0)$ .

In a recent experiment using doubly ( $^{13}C$ ,  $^{15}N$ ) and fully enriched human ubiquitin, Brutscher et al. have

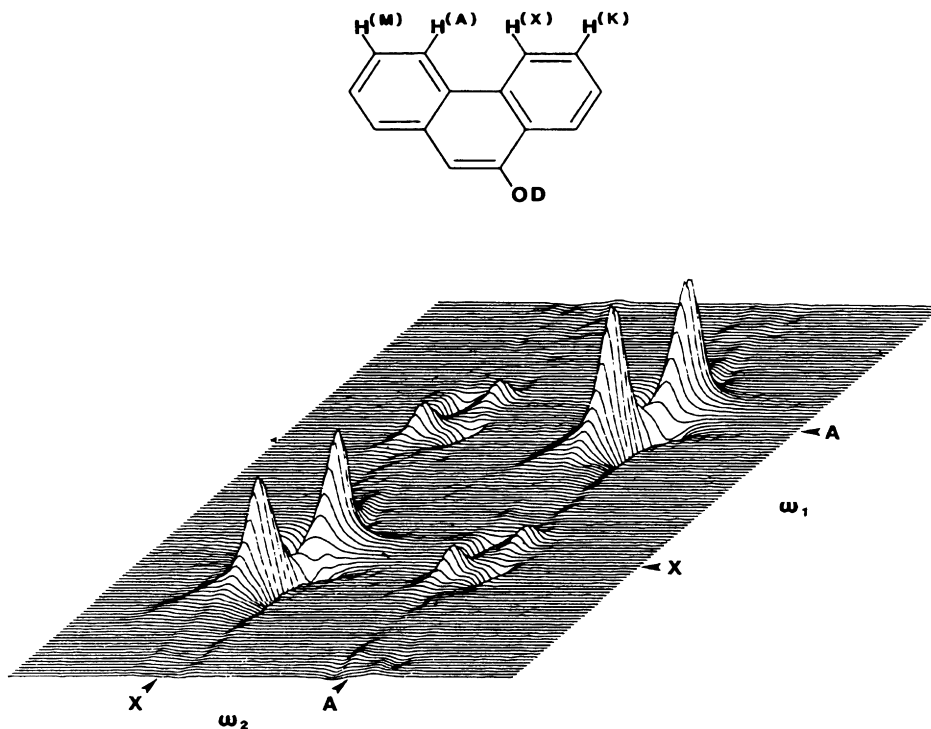


Fig. 42. Stack plot of a double-quantum filtered COSY proton spectrum at 400 MHz of 9-phenanthrol showing relaxation allowed cross-peaks resulting from cross-correlation between dipolar interactions. Two symmetrically disposed  $A$ – $X$  cross-peak multiplets can clearly be seen, indicating RACT between  $A$  and  $X$ . The diagonal multiplets centered at  $(\omega_1, \omega_2) = (\Omega_A, \Omega_A)$  and  $(\Omega_X, \Omega_X)$  show passive splittings because of the scalar couplings  $J_{AM}$  and  $J_{KX}$ , respectively. The relaxation-allowed  $A$ – $X$  cross-peak multiplets centered at  $(\omega_1, \omega_2) = (\Omega_A, \Omega_X)$  (in the back) and  $(\Omega_X, \Omega_A)$  (in front) appear even though the scalar coupling  $J_{AX}$  is negligible. The antiphase splittings of the relaxation-allowed cross-peak multiplets also result from the passive couplings. Thus, the multiplet centered at  $(\omega_1, \omega_2) = (\Omega_X, \Omega_A)$  is split by  $J_{KX}$  in  $\omega_1$  and by  $J_{AM}$  in  $\omega_2$ . The intensity of the  $A$ – $X$  cross-peak multiplet is approximately 25% of that of the diagonal peak, indicating a large effect of cross-correlation on the transverse relaxation of the  $A$  and  $X$  spins. [Reproduced with permission from S. Wimperis, G. Bodenhausen, Mol. Phys. 66 (1989) 897.]

utilized the differences in  $^{15}\text{N}$ – $^{13}\text{C}'$  zero- and double-quantum decay rates to measure “remote” cross-correlations, involving the three spins,  $^{15}\text{N}$  and  $^{13}\text{C}'$  and the amide proton nuclei of the peptide plane [269]. The spectral densities,  $J_{N,NH_N}$  and  $J_{C',C'H_N}$  have been termed as direct and  $J_{N,C'H_N}$  and  $J_{C',NH_N}$  as remote cross-correlations. It is shown (also follows from Eq. (115)) that the decay rates of the two ZQCs and two DQCs differ due to CSA–dipole ( $CSA, d$ ) cross-correlations which in turn differ from each other by “remote” CSA–dipole cross-correlations and are given by:

$$R_{DQ}^c = R_{CSA,d}^{c(d)} + R_{CSA,d}^{c(r)}$$

$$R_{ZQ}^c = R_{CSA,d}^{c(d)} - R_{CSA,d}^{c(r)}$$

$$R_{CSA,d}^{c(d)} = R_{N,NH_N} + R_{C',C'H_N}$$

$$R_{CSA,d}^{c(r)} = R_{N,C'H_N} + R_{C',NH_N} \quad (133)$$

From Eq. (115), it is seen that

$$R_{i,ik} = -\frac{8}{3}J_{i,ik}(0) + 2J_{i,ik}(\omega_i)$$

$$R_{i,jk} = -\frac{8}{3}J_{i,jk}(0) \quad (134)$$

Thus by measuring the relative intensities of the ZQ and DQ doublets in a constant time experiment (Fig. 46), they obtained  $R_{DQ}^{\text{cross}}$  and  $R_{ZQ}^{\text{cross}}$ , the difference and sum of which then yields information on the direct cross-correlation,  $R_{CSA,d}^{c(d)}$  and remote cross-correlation,  $R_{CSA,d}^{c(r)}$ . These rates have been measured for 48 peptide planes in the protein. It is found that  $R_{CSA,d}^{c(d)}$

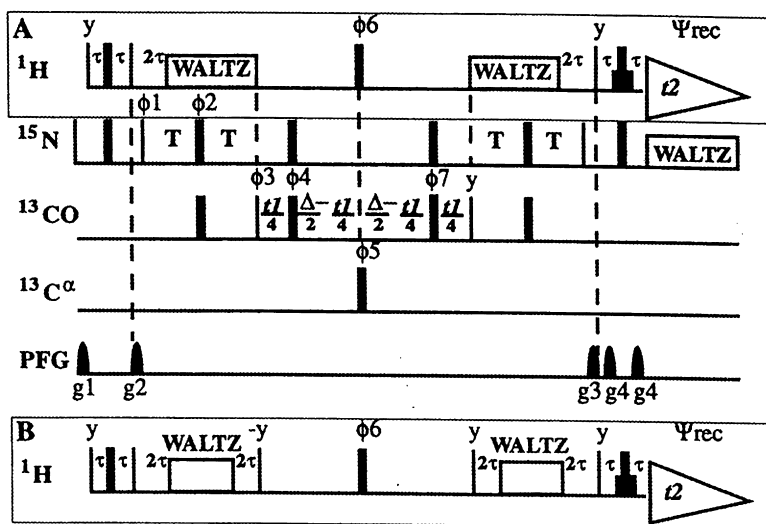


Fig. 43. (A) Pulse sequence for the determination of transverse  $^{13}\text{C}\text{O}$  and  $^{15}\text{N}$  CSA–CSA cross-correlation rates ( $\Gamma_{\text{N,C}}$ ) and  $^1\text{H}^{\text{N}}-^{15}\text{N}$  and  $^1\text{H}^{\text{N}}-^{13}\text{C}\text{O}$  dipole–dipole cross-correlation rates ( $\Gamma_{\text{HN,HC}}$ ). Narrow and thin bars represent  $90^\circ$  and  $180^\circ$  pulses, respectively. Unless specified otherwise, pulse phases are along the  $x$ -axis. The durations of the  $^{13}\text{C}\text{O}$  and  $^{13}\text{C}\alpha$  pulses have been optimized not to interfere with each other. Pulsed field gradients are half-sine-bell shaped with 1 ms duration and strengths of  $g_1 = 20$  G/cm,  $g_2 = 40$  G/cm,  $g_3 = 30$  G/cm and  $g_4 = 50$  G/cm. The delays are:  $\tau = 2.7$  ms,  $T = 11.0$  ms and  $\Delta = 22$  ms. States-TPPI [8] quadrature detection is achieved by incrementing  $\phi_2$  so that cross peaks at  $\omega_c \pm \omega_N$  were observed. To reduce the resonance overlap between double- and zero-quantum cross peaks, the  $^{15}\text{N}$  carrier frequency was shifted to the edge of the  $^{15}\text{N}$  spectral envelope during the chemical shift evolution.  $^{15}\text{N}$  decoupling during  $t_2$  was achieved with a 1.25 kHz WALTZ-16 decoupling sequence. Water suppression was achieved with a WATERGATE scheme. (B) The pulse scheme is identical to (A) except for the two delays  $2\tau$  ( $\tau = 2.7$  ms) and two  $90^\circ$  proton pulses just before and after the chemical shift evolution period  $\Delta$ . Details of phase cycling are contained in Ref. [267] [Reproduced with permission from M. Pellecchia, Y. Pang, L. Wang, A.V. Kurochkin, Anil Kumar, E.R.P. Zuiderweg, J. Am. Chem. Soc. 121 (1999) 9165].

varies between 0.7 and  $6.3 \text{ s}^{-1}$ , whereas  $R_{\text{CSA,d}}^{\text{c(r)}}$  varies between  $-3.0$  and  $0.5 \text{ s}^{-1}$ . The four smallest  $R_{\text{CSA,d}}^{\text{c(d)}}$  are found in the flexible C-terminus region. From the rather weak overall correlation between  $R_{\text{CSA,d}}^{\text{c(d)}}$  and  $R_{\text{CSA,d}}^{\text{c(r)}}$ , it has been concluded that these two cross-correlation parameters carry complementary information about CSA tensors and about anisotropic internal and overall motion of the protein [269].

Remote CSA–dipole cross-correlations have also been measured by Yang et al. [270], involving the  $^{13}\text{C}\alpha-^1\text{H}\alpha$  dipolar interaction and the  $^{13}\text{C}'$  (carbonyl) CSA. The method relies on measurement of the peak intensities of the multiplet components of the zero- and double-quantum  $^{13}\text{C}\alpha-^{13}\text{C}'$  coherences, in a manner identical to the above described experiment. The experiments have been carried out on the fully doubly labeled ( $^{13}\text{C}$ ,  $^{15}\text{N}$ ) protein ubiquitin. The experiment is a HN(CO)CA scheme, in which the proton magnetization is transferred to  $^{15}\text{N}$  and then to  $\text{C}'$  and  $\text{C}\alpha$  carbons and back to proton via nitrogen.

During an evolution step,  $^{13}\text{C}\alpha-^{13}\text{C}'$  DQC and ZQC are allowed to evolve with  $\pi$  pulses on  $^{15}\text{N}$ , decoupling the  $^{15}\text{N}$  spin with splitting due to protons being active. The linewidths of the two DQC and ZQCs (following Eq. (115)) can be written as:

$$\begin{aligned}
 R_{\text{AM}}^{\text{DQ},\alpha} &= R_{\text{a}}^{\text{DQ}} + R_{\text{AXMX}}(0, \omega_X) + R_{\text{CSA,d}}^{\text{c(d)}} + R_{\text{CSA,d}}^{\text{c(r)}} \\
 &\quad + R_{\text{CSA,CSA}}(0) \\
 R_{\text{AM}}^{\text{DQ},\beta} &= R_{\text{a}}^{\text{DQ}} + R_{\text{AXMX}}(0, \omega_X) - R_{\text{CSA,d}}^{\text{c(d)}} - R_{\text{CSA,d}}^{\text{c(r)}} \\
 &\quad + R_{\text{CSA,CSA}}(0) \\
 R_{\text{AM}}^{\text{ZQ},\alpha} &= R_{\text{a}}^{\text{ZQ}} - R_{\text{AXMX}}(0, \omega_X) + R_{\text{CSA,d}}^{\text{c(d)}} - R_{\text{CSA,d}}^{\text{c(r)}} \\
 &\quad - R_{\text{CSA,CSA}}(0) \\
 R_{\text{AM}}^{\text{ZQ},\beta} &= R_{\text{a}}^{\text{ZQ}} - R_{\text{AXMX}}(0, \omega_X) - R_{\text{CSA,d}}^{\text{c(d)}} + R_{\text{CSA,d}}^{\text{c(r)}} \\
 &\quad - R_{\text{CSA,CSA}}(0)
 \end{aligned} \tag{135}$$

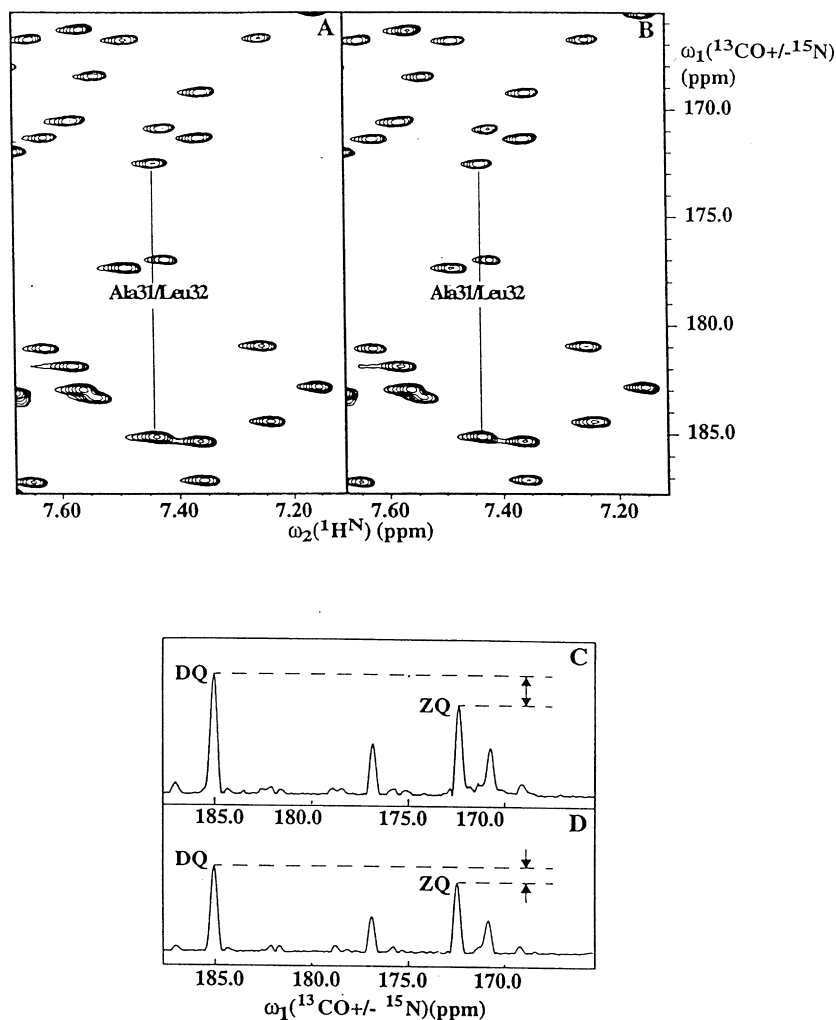


Fig. 44. (A) and (B) are, respectively, parts of the spectra of the double-zero quantum and modified triple quantum 2D-constant time experiments recorded with two different pulse schemes given in Fig. 43. (C) and (D) show traces along  $\omega_1$  taken at the resonance of the residue Leu-32 from the spectra in (A) and (B), respectively. The spectra were acquired at 303 K on a Bruker AMX-500 spectrometer, with a 1.0 mM sample of  $^{15}\text{N}$ ,  $^{13}\text{C}$ -labeled binase (12.3 kDa) from *Bacillus intermedius*. [Reproduced with permission from M. Pellecchia, Y. Pang, L. Wang, A.V. Kurochkin, Anil Kumar, E.R.P. Zuiderweg, J. Am. Chem. Soc. 121 (1999) 9165.].

where  $X$  is the proton spin and  $A$  and  $M$  are  $^{13}\text{C}'$  spins. The intensity ratios of the DQC and ZQC in the constant time ( $T$ ) experiment are obtained as:<sup>8</sup>

$$\frac{(I_{\text{DQ},\alpha} \cdot I_{\text{ZQ},\beta})}{(I_{\text{DQ},\beta} \cdot I_{\text{ZQ},\alpha})} = \frac{\exp(R_{\text{DQ},\alpha} T) \cdot \exp(R_{\text{ZQ},\beta} T)}{\exp(R_{\text{DQ},\beta} T) \cdot \exp(R_{\text{ZQ},\alpha} T)}$$

$$= \exp[(R_{\text{DQ},\alpha} - R_{\text{DQ},\beta})T] \cdot \exp[(R_{\text{ZQ},\alpha} - R_{\text{ZQ},\beta})T] \quad (136)$$

Taking the logarithm, one obtains:

$$\frac{1}{T} \ln \left( \frac{I_{\text{DQ},\alpha} \cdot I_{\text{ZQ},\beta}}{I_{\text{DQ},\beta} \cdot I_{\text{ZQ},\alpha}} \right) = R_{\text{CSA,d}}^{c(r)}$$

$$= R_{^{13}\text{C}', ^{13}\text{C}^{\alpha}-^1\text{H}} + R_{^{13}\text{C}^{\alpha}, ^{13}\text{C}'-^1\text{H}}. \quad (137)$$

The cross-correlation  $R_{^{13}\text{C}^{\alpha}, ^{13}\text{C}'-^1\text{H}}$  has been neglected in this study, since the CSA of  $^{13}\text{C}^{\alpha}$  is small and  $^{13}\text{C}'-^1\text{H}$  distance is large. The measured

<sup>8</sup> All  $R$ 's are negative numbers, see footnote following Eq. (107).

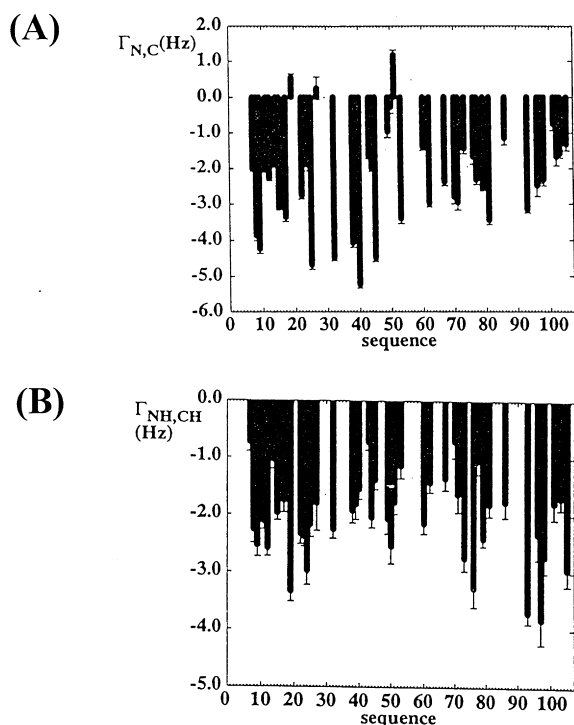


Fig. 45. Dependence of (A) the  $^{15}\text{N}$ – $^{13}\text{C}$  CSA–CSA cross-correlation rates ( $\Gamma_{\text{N,C}}$ ), and (B) the  $^1\text{H}$ – $^{15}\text{N}$  and  $^1\text{H}$ – $^{13}\text{C}$  dipole–dipole cross-correlation rates ( $\Gamma_{\text{NH,CH}}$ ) for the various amino acid sequence measured for the protein binase (12.3 kDa) for well-resolved cross peaks. The error bars were estimated from the signal to noise ratio as well as from spectral density terms at higher frequencies and from magnetic field inhomogeneities, are also indicated in the figure. [Reproduced with permission from M. Pellecchia, Y. Pang, L. Wang, A.V. Kurochkin, Anil Kumar, E.R.P. Zuiderweg, J. Am. Chem. Soc. 121 (1999) 9165.]

$R_{^{13}\text{C}',^{13}\text{C}^{\alpha-1}\text{H}}$  has been directly related to a non-axial CSA tensor (following Goldman [238]), assuming rigid and isotropic overall tumbling with a correlation time  $\tau_c$ , as:

$$R_{^{13}\text{C}',^{13}\text{C}^{\alpha-1}\text{H}} = \frac{4}{15} \hbar \omega_c \gamma_C \gamma_H r_{\text{HC}}^{-3} \tau_c f(\sigma_X, \sigma_Y, \sigma_Z) \quad (138)$$

where

$$f(\sigma_X, \sigma_Y, \sigma_Z) = \frac{1}{2} [\sigma_X (3 \cos^2 \theta_X - 1) + \sigma_Y (3 \cos^2 \theta_Y - 1) + \sigma_Z (3 \cos^2 \theta_Z - 1)] \quad (139)$$

where  $\theta_X$ ,  $\theta_Y$  and  $\theta_Z$  are the angles that the principal axes of the CSA tensor make with the internuclear  $^{13}\text{C}^{\alpha-1}\text{H}$  axis. Assuming a standard peptide plane

geometry and the CSA tensor as measured in a solid state study by Teng et al. [271], the angles have been related to the dihedral angle  $\psi$ . The measured cross-correlation rate and the derived dihedral angle  $\psi$  correlates well with the calculated values in the two proteins. In the case of the glycine residue, each ZQ and DQ coherence is split into triplets and the ratio of intensities of most upfield and downfield lines have been used to measure the cross-correlation rates.

In a subsequent study, Yang et al. [272] have utilized the idea of measuring the average relaxation rate of  $\text{DQ}_{\alpha}$  and  $\text{ZQ}_{\beta}$  components which resonate at  $\omega_{\text{C}'} \pm \omega_{\text{C}^{\alpha}} - \pi J_{\text{CH}}$  and the average rate of  $\text{DQ}_{\beta}$  and  $\text{ZQ}_{\alpha}$  components which resonate at  $\omega_{\text{C}'} \pm \omega_{\text{C}^{\alpha}} + \pi J_{\text{CH}}$ . This is achieved by simultaneous interchange of  $\text{DQ}_{\alpha} \leftrightarrow \text{ZQ}_{\beta}$  and  $\text{DQ}_{\beta} \leftrightarrow \text{ZQ}_{\alpha}$  by application of  $\pi$  pulses on  $^1\text{H}$  and  $^{13}\text{C}^{\alpha}$  midway between the  $T$  period of the experiment. It is claimed that since the cross-correlation rate has been obtained from the ratio of two, rather than four terms, the precision of the experiment has been improved.

#### 4.4.3. Remote dipole–dipole cross-correlation

4.4.3.1. *Single-quantum coherences.* The presence of remote dipole( $ij$ )–dipole( $kl$ ) cross-correlations requires a coupled four-spin system  $\text{AMKX}$  [233]. It has been shown that the eight  $A$ -spin SQCs differ in linewidths due to direct [ $J_{\text{AMAX}}(0, \omega)$ ,  $J_{\text{AMAX}}(0, \omega)$  and  $J_{\text{AKAX}}(0, \omega)$ ] as well as remote [ $J_{\text{MKMX}}(\omega)$ ,  $J_{\text{MKKX}}(\omega)$  and  $J_{\text{MXKX}}(\omega)$ ] dipole–dipole cross-correlations, under the simple-line approximation when all the eight coherences are resolved. The result can be summarized by the following equation:

$$R_{A\alpha\alpha\alpha}^c = R_{A\beta\beta\beta}^c = +R_{\text{AMAX}}^{c(d)} + R_{\text{AMAX}}^{c(d)} + R_{\text{AKAX}}^{c(d)} + R_{\text{MKMX}}^{c(r)} + R_{\text{MKKX}}^{c(r)} + R_{\text{MXKX}}^{c(r)}$$

$$R_{A\alpha\alpha\beta}^c = R_{A\beta\beta\alpha}^c = +R_{\text{AMAX}}^{c(d)} - R_{\text{AMAX}}^{c(d)} - R_{\text{AKAX}}^{c(d)} - R_{\text{MKMX}}^{c(r)} - R_{\text{MKKX}}^{c(r)} + R_{\text{MXKX}}^{c(r)}$$

$$R_{A\alpha\beta\alpha}^c = R_{A\beta\alpha\beta}^c = -R_{\text{AMAX}}^{c(d)} + R_{\text{AMAX}}^{c(d)} - R_{\text{AKAX}}^{c(d)} - R_{\text{MKMX}}^{c(r)} + R_{\text{MKKX}}^{c(r)} - R_{\text{MXKX}}^{c(r)}$$

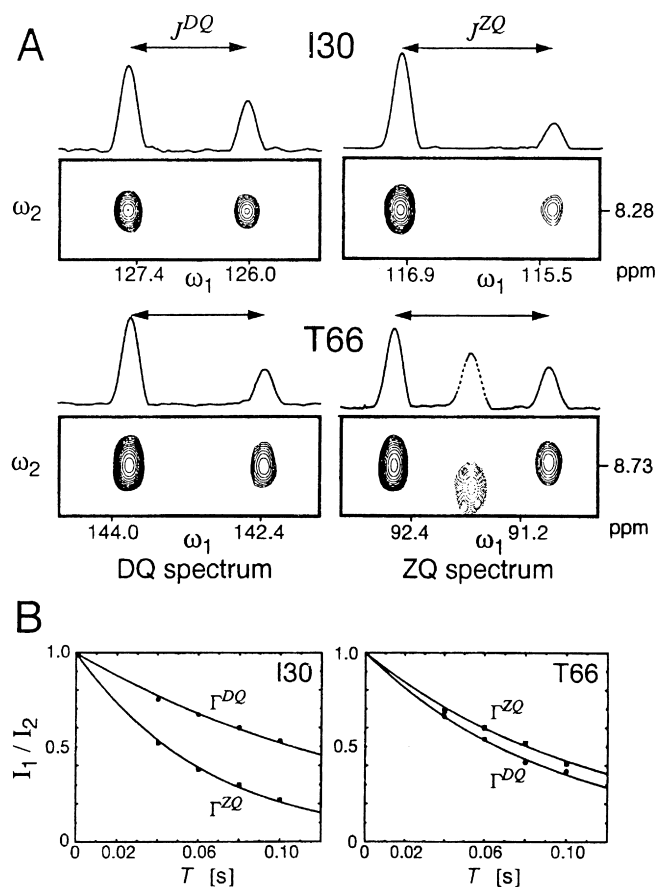


Fig. 46. Experimental results of the 2D ZQ/DQ HNCQ(H) experiment applied to human ubiquitin at 300 K and  $B_0$  field strength of 14.1 T. Quadrature detection on  $^{15}\text{N}$  was used in  $\omega_1$  and the  $^{13}\text{C}'$  demodulation frequency was shifted to 182.5 ppm by time-proportional phase incrementation. In (A), contour plots of ZQ and DQ cross-peak doublets are shown for the peptide plane between Lys 29 and Ile 30 and between Ser 65 and Thr 66 with the constant period of time evolution,  $T = 80$  ms, where  $\omega_1$  ( $^{15}\text{N}$  ppm) corresponds to the ZQ/DQ dimension and  $\omega_2$  to the  $\text{H}^{\text{N}}$  frequency. Projections are drawn along the cross correlated relaxation-active ZQ/DQ frequency domain  $\omega_1$  ( $^{15}\text{N}$  ppm scale). (B) Plot of ratio of intensities of the doublets of double and zero-quantum peaks as a function of the constant evolution period  $T$ . [Reproduced with permission from B. Brutscher, N.R. Skrynnikov, T. Bremi, R. Bruschweiler, R.R. Ernst, J. Magn. Reson. 130 (1998) 346].

$$\begin{aligned}
 R_{A\beta\alpha\alpha}^{\text{c}} = R_{A\alpha\beta\beta}^{\text{c}} = & -R_{AMAK}^{\text{c(d)}} - R_{AMAX}^{\text{c(d)}} + R_{AKAX}^{\text{c(d)}} \\
 & + R_{MKMX}^{\text{c(r)}} - R_{MKKX}^{\text{c(r)}} - R_{MXKX}^{\text{c(r)}}.
 \end{aligned}
 \tag{140}$$

Both the remote and direct cross-correlations give rise to first-order differential line broadening, while maintaining the symmetry of the pattern. If one of the couplings is zero, the first-order contribution cancels. For example if  $J_{AX} = 0$ , transitions in which the  $X$  spin changes state will overlap and cancel the

contributions of  $R_{AMAX}^{\text{c(d)}}$ ,  $R_{AKAX}^{\text{c(d)}}$ ,  $R_{MKMX}^{\text{c(r)}}$  and  $R_{MKKX}^{\text{c(r)}}$  yielding:

$$\begin{aligned}
 R_{A\alpha\alpha\alpha}^{\text{c}} = R_{A\beta\beta\beta}^{\text{c}} = R_{A\alpha\alpha\beta}^{\text{c}} = R_{A\beta\beta\alpha}^{\text{c}} \\
 = +R_{AMAK}^{\text{c(d)}} + R_{MXKX}^{\text{c(r)}} \\
 R_{A\alpha\beta\alpha}^{\text{c}} = R_{A\beta\alpha\beta}^{\text{c}} = R_{A\beta\alpha\alpha}^{\text{c}} = R_{A\alpha\beta\beta}^{\text{c}} \\
 = -R_{AMAK}^{\text{c(d)}} - R_{MXKX}^{\text{c(r)}}.
 \end{aligned}
 \tag{141}$$

Differences in the linewidths yield a sum of these two cross-correlations one of which is the remote

contribution for spin  $A$ . However, this contribution is also observable only under the condition that both  $\mathbf{J}_{AM}$  and  $\mathbf{J}_{AK}$  are unequal and yield well resolved quartet [233].

**4.4.3.2. Double-quantum coherences.** The linewidths of  $^{15}\text{N}_i\text{--}^{13}\text{C}_j$  DQCs have been studied in a four-spin system consisting of  $\text{H--}^{15}\text{N--CO--}^{13}\text{C}_\alpha\text{--H}$ . There are four DQCs whose linewidths are given by [273]:

$$\begin{aligned} R_{\alpha\alpha} &= R^a + R_{\text{CSA},d_i}^c + R_{\text{CSA},d_j}^c + R_{d_i,d_j}^c \\ R_{\beta\alpha} &= R^a - R_{\text{CSA},d_i}^c + R_{\text{CSA},d_j}^c - R_{d_i,d_j}^c \\ R_{\alpha\beta} &= R^a + R_{\text{CSA},d_i}^c - R_{\text{CSA},d_j}^c - R_{d_i,d_j}^c \\ R_{\beta\beta} &= R^a - R_{\text{CSA},d_i}^c - R_{\text{CSA},d_j}^c + R_{d_i,d_j}^c \end{aligned} \quad (142)$$

where the subscripts  $\alpha$  and  $\beta$  reflect the spin states of the protons attached to nitrogen and carbon, respectively, the indices  $d_i$  and  $d_j$  refer to  $\text{N--H}^{\text{N}}$  and  $\text{C--H}^{\text{C}}$  dipolar vectors, respectively.  $R^a$  contains the auto-correlation contribution to the double-quantum linewidths, which are all identical. The  $R_{\text{CSA},d_i}^c$  and  $R_{\text{CSA},d_j}^c$  terms describe the sum of all interactions due to CSA–dipole cross-correlated relaxation for the  $d_i$ th and  $d_j$ th dipolar vectors, respectively.  $R_{d_i,d_j}^c$  is the cross-correlation contribution from  $\text{N--H}^{\text{N}}$  and  $\text{C--H}^{\text{C}}$  dipolar vectors. This cross-correlation is strongly dependent on the angle  $\theta$  between these two dipolar vectors (Fig. 47). Experimental observation of these four DQCs in a constant time experiment has been carried out by Reif et al. [273], which yields intensities strongly dependent on this angle (Fig. 48). The various rate constants have been calculated by measuring the intensities of the four DQCs by the following equations:

$$\begin{aligned} R_{d_i,d_j}^c &= \frac{1}{4T} \ln \left[ \frac{I(\alpha\beta)\dot{I}(\beta\alpha)}{I(\alpha\alpha)\dot{I}(\beta\beta)} \right] \\ R_{\text{CSA},d_i}^c &= \frac{1}{4T} \ln \left[ \frac{I(\alpha\beta)\dot{I}(\beta\beta)}{I(\alpha\alpha)\dot{I}(\beta\alpha)} \right] \\ R_{\text{CSA},d_j}^c &= \frac{1}{4T} \ln \left[ \frac{I(\beta\beta)\dot{I}(\beta\alpha)}{I(\alpha\alpha)\dot{I}(\alpha\beta)} \right] \end{aligned} \quad (143)$$

The dipole–dipole cross-correlation  $R_{d_i,d_j}^c$  is given

by:

$$R_{d_i,d_j}^c = \frac{8}{5} \left( \frac{\gamma_{\text{H}}\gamma_{\text{C}}}{r_{\text{NH}_i}^3} \right) \left( \frac{\gamma_{\text{H}}\gamma_{\text{C}}}{r_{\text{CH}_j}^3} \right) \left( \frac{\mu_0\hbar}{4\pi} \right)^2 \frac{1}{2} (3 \cos^2 \theta_{d_i,d_j} - 1) \quad (144)$$

where  $\theta_{d_i,d_j}$  is the angle between the two dipolar vectors  $d_i$  and  $d_j$ . Assuming the planarity of the peptide bond, angle  $\theta_{d_i,d_j}$  depends on the torsion angle  $\psi$  according to the equation,  $\cos \theta_{d_i,d_j} = 0.163 + 0.819 \cos(\psi - 119)$ . The torsion angle  $\psi$  has been estimated from this methodology for rhodniin, a 11 kDa protein, for all the peptide planes along the backbone. The extracted torsion angle  $\psi$  agrees very well with the various known secondary structure elements of this protein. This new methodology has proved quite useful in extracting the structural parameters of proteins in solution.

In the above study, four values of  $\psi$  are consistent with the measured value of  $\theta_{d_i,d_j}$ . It has been recently shown by Yang and Kay [274,275] that, if in addition to measuring the cross-correlation between  $^{13}\text{C}^{\alpha-1}\text{H}^{\alpha}$  and  $^{15}\text{N--}^1\text{H}_{\text{N}}$  dipolar interactions, one also measures the cross-correlation between the  $^{13}\text{C}^{\alpha-1}\text{H}^{\alpha}$  dipolar interaction and  $^{13}\text{C}'$  (carbonyl) CSA, the ambiguity in  $\psi$  can be reduced to two from four. In order to derive this rate, the ratio of  $R_{\text{CSA},d_i}^c$  and  $R_{\text{CSA},d_j}^c$  as given by the second and third equations of Eq. (142) has to be used. The other dipole–dipole cross-correlation between  $\text{H}_{\text{N--C}_\alpha}$  and  $\text{H}_\alpha\text{--N}$  has been found to be negligible in both these studies.

Pelupessy et al. [276] have recently proposed a pair of complimentary 2D experiments which enable one to determine the effects of cross-correlation between  $^{13}\text{C}^{\alpha}\text{--H}^{\alpha}$  and  $^{15}\text{N--H}^{\text{N}}$  dipolar interactions on the relaxation of the antiphase multiple-quantum coherence  $4\text{N}_x\text{C}_x^{\alpha}\text{C}_z'$ . This allows one to reduce the constant time  $T$ , in the experiment by Reif et al., thus making these schemes applicable to larger biomolecules. In the 3D experiments, however, short constant time evolution periods lead to limited digital resolution in the zero- and double-quantum dimension, thus hampering their actual use. By this method, the duration of the relaxation interval  $T$  is not dictated by the necessity to resolve the lines of the multiplet in the third dimension. Furthermore, if the signals overlap in HSQC spectra, the dispersion of the cross peaks

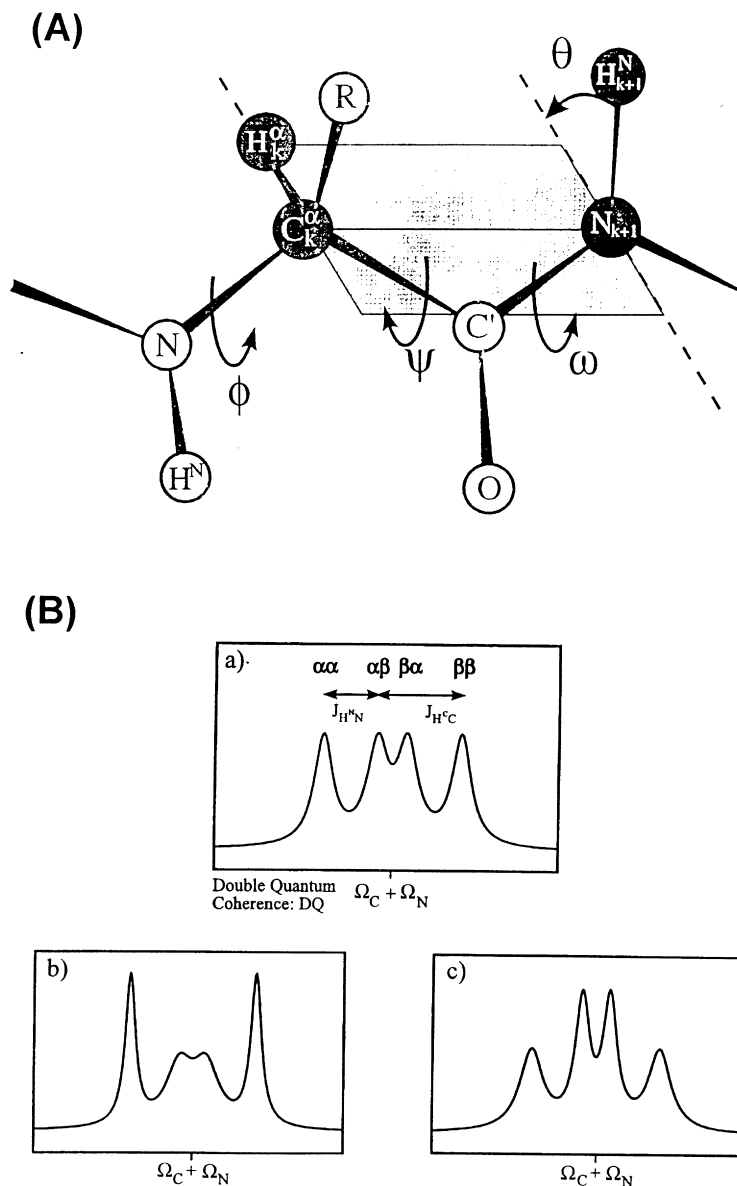


Fig. 47. (A) Pictorial representation of the angle  $\theta$  between the dipolar vectors  $C_k^\alpha-H_k^\alpha$  and  $N_{k+1}-H_{k+1}^N$ . (B) Calculated  $C_k^\alpha-N_{k+1}$  double-quantum spectra (a) in the absence of dipole-dipole cross-correlations; in the presence of the  $C_k^\alpha-H_k^\alpha/N_{k+1}-H_{k+1}^N$  dipole-dipole cross-correlation with angle (b)  $\theta = 90^\circ$  and (c)  $\theta = 0^\circ$ . The signal in the double-quantum dimension is split due to the  $^1J_{HN}$  and the  $^1J_{CH}$ -couplings.  $\alpha\alpha$ ,  $\alpha\beta$ ,  $\beta\alpha$  and  $\beta\beta$  denote the proton spin states of  $H_\alpha$  and  $H^N$ , respectively. [Reproduced with permission from B. Reif, M. Henning, C. Griesinger, Science 276 (1997) 1230.].

can be improved by inserting an additional evolution period to allow precession of the carbonyl  $^{13}C'$  nuclei, which have favorable relaxation properties [276].

#### 4.5. Cross-correlations involving quadrupolar nuclei

The interference effects involving the quadrupolar interaction are documented in the literature

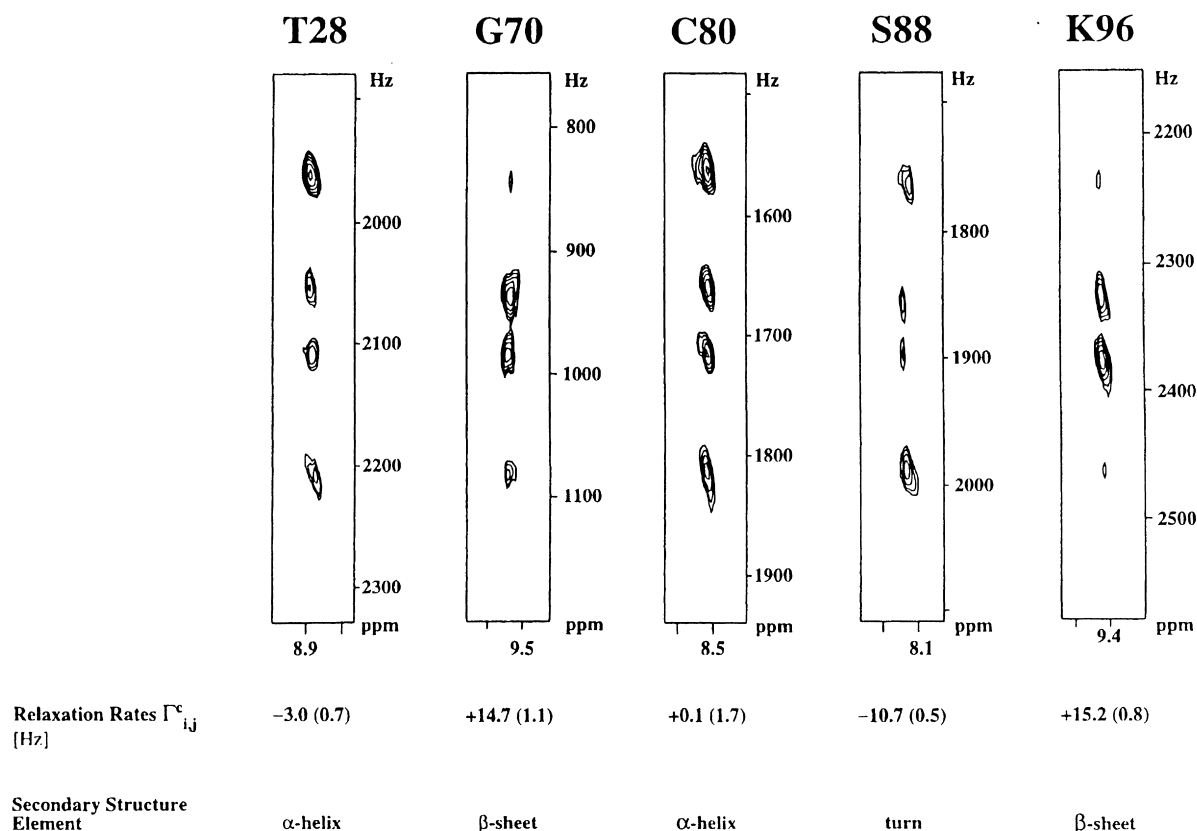


Fig. 48. Experimentally observed peak shapes for selected residues in rhodniin. The  $H^N$  chemical shift (600 MHz) of residue  $k + 1$  is given on the horizontal axis. Double-quantum coherences which evolve between the nuclei  $C_k^{\alpha}$  and  $N_{k+1}$  are represented on the vertical axis. Deviations from the intensity ratio (1:1:1) that would be found without cross-correlated relaxation can clearly be seen. Two residues within an  $\alpha$ -helical (T28 and C80) as well as two residues within a  $\beta$ -sheet (G70 and K96), together with one residue from a turn motive (S88) are shown. The mean relaxation rates  $R_{d,d_j}^c$  in Hz as extracted according to Eq. (142) and their standard deviations are given below each residue. [Reproduced with permission from B. Reif, M. Henning, C. Griesinger, Science 276 (1997) 1230.]

[277–294]. An early experimental study that observed the presence of quadrupolar–quadrupolar cross-correlation was by Vold et al. in 1980 in which they monitored deuterium relaxation in a 10 mol% solution of  $CD_2Cl_2$  in Merck liquid crystal phase V [284,285]. The experiments involved measurements of spin–lattice deuteron relaxation in a  $CD_2$  group, combined with 2D measurements of single- and double-quantum spin-echo decay rates. Six spectral densities, three for auto-correlation and three for cross-correlation, could be determined in this experiment. Another example in which dipole–quadrupolar cross-correlations have been

observed in a spin-1 coupled to spin-(1/2) system, in a nematic phase is shown in Fig. 49 [286]. The recovery of the two lines with different relaxation is ascribed to dipole–quadrupolar cross-correlation. The detailed theory for the longitudinal relaxation using normal modes in the presence of both dipolar and quadrupolar relaxation mechanisms, including their cross-correlations is given in this paper. It may be noted that dipole–quadrupolar cross-correlations do not give rise to a differential line broadening and only give rise to a differential longitudinal relaxation [287,288].

Cross-correlation between CSA and quadrupolar

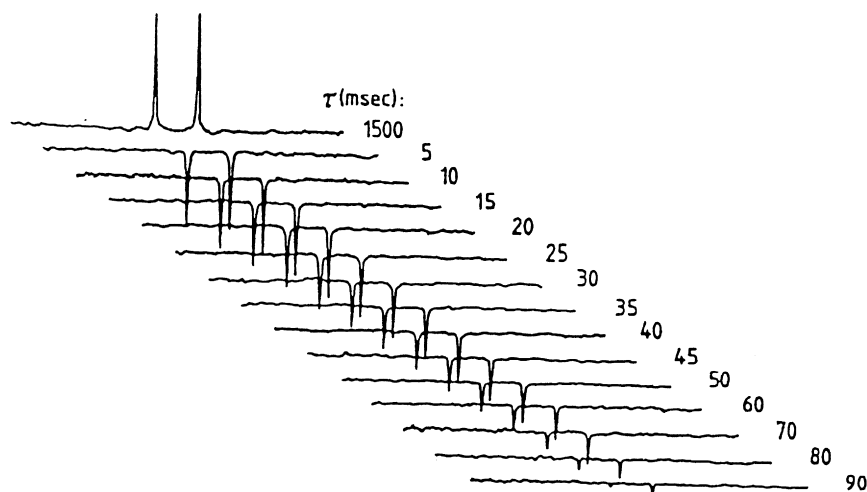


Fig. 49. Initial rate inversion recovery experiments of  $\text{CHDCl}_2$  in the nematic liquid crystal ZLI-1167 obtained on a JEOL FX60Q FTNMR spectrometer at a temperature of  $26^\circ\text{C}$ . The experiments were performed selectively on one part of the quadrupole doublet in the  $^2\text{H}$  NMR spectrum. [Reproduced with permission from J. Voigt, J.P. Jacobsen, J. Chem. Phys. 78 (1983) 1693.]

interactions can give rise to DLB, in spin-(1/2) nuclei coupled to quadrupolar nuclei, as theoretically shown by Gutowsky and Vold [289], and Werbelow et al. [290,291]. Granger et al. have observed in tetrahedral clusters with a phosphorus ligand bound to a cobalt atom,  $\text{HFeCo}_3(\text{CO})_{11}\text{L}$ , that the  $^{31}\text{P}$  spectra of some clusters exhibit a remarkable asymmetry in the line shapes [292]. This asymmetry was the first experimental confirmation of the CSA–quadrupole cross-correlations. Since the CSA–quadrupole cross-correlations depend on these two tensor orientations, Elbayed et al. have calculated the line shapes for three different cases, namely coincident-axially symmetric, non-coincident-axially symmetric and general non-coincident quadrupolar and CSA tensors in such systems [293].

Recently, Werbelow et al. have measured the quadrupolar–quadrupolar cross-correlation in a spin-(1/2) coupled to spin-1 system, via ‘spying’ spin-(1/2) nuclei [294]. In the  $^{13}\text{C}$  multiplets of deuterated ethylene glycol, it was observed that the apparent heights of the multiplet components do not obey the simple pentet pattern due to DLB. This broadening in the pentet was attributed to the cross-correlation between the two quadrupolar interactions.

## 5. Cross-correlations in the presence of a radio frequency field

It was shown in Section 3 that cross-correlations contribute to longitudinal relaxation via spectral densities only at the Larmor frequency. Thus the effect of cross-correlations in longitudinal relaxation as well as on the NOE of slowly tumbling molecules for which  $\omega\tau_c \gg 1$  is minimal. However, in Section 4, it was shown that cross-correlations contribute to transverse relaxation via spectral densities also at other frequencies, including zero. Bull [61,295, 296], therefore suggested that the relaxation experiments be performed in the presence of large RF fields (the so-called rotating frame experiments). The RF field mixes the evolution of longitudinal and transverse relaxation enhancing the effect of cross-correlations. Such experiments have gained popularity from several other considerations as well and many experiments have been developed such as TOCSY [297,298], HOHAHA [299], CAMELSPIN [300] and ROESY [301], exploiting both the coherence transfer and the relaxation studies in the presence of strong RF fields. A detailed review on relaxation in the rotating frame in liquids has been published recently by Bull [61], which includes in detail the effect of cross-correlations. We will therefore restrict

this review to a few introductory remarks and some simple cases to illustrate the effect of cross-correlations in the presence of RF fields and refer the reader to the above review for further details of various spin systems. The discussion here closely follows the ideas contained in Bull's original article [295] and an experimental study by Burghardt et al. [211].

### 5.1. Theory

Application of a steady off-resonance (offset =  $\Delta\omega$ ) RF field of strength  $\omega_1 = \gamma H_1$  along the  $X$ -axis, yields an effective field in the  $XZ$  plane in the rotating frame given by:

$$\omega_{\text{eff}} = \sqrt{(\Delta\omega)^2 + (\omega_1)^2} \quad (145)$$

at an angle  $\theta$  from the  $Z$ -direction given by:

$$\theta = \tan^{-1}\left(\frac{\omega_1}{\Delta\omega}\right) \quad (146)$$

If  $\omega_{\text{eff}} \gg R$ , the various relaxation matrix elements, then it can be shown that the total magnetization can be resolved into two components, one spin-locked along the effective field and the other perpendicular to it and that the dynamics of the magnetization locked along the effective field is decoupled from the magnetization transverse to it [211]. Under this assumption, the density matrix is described by the product of nuclear spin operators directed along and perpendicular to the corresponding effective fields. The magnetization components transverse to the effective field perform Torrey oscillations about the effective field and decay (if the RF field is sufficiently inhomogeneous) and can be ignored [302]. The magnetization of each nucleus is thus locked along its effective field, whose relaxation becomes a mixture of the relaxation of the longitudinal and the transverse components.

The transformation to the effective field of each spin also leads to the transformation of the operators and one can define spin operators in the rotating frame (with primes) for each spin as [211]:

$$\begin{pmatrix} I_{X'}^A \\ I_{Y'}^A \\ I_{Z'}^A \end{pmatrix} = \begin{pmatrix} \cos \theta_A & 0 & -\sin \theta_A \\ 0 & 1 & 0 \\ \sin \theta_A & 0 & \cos \theta_A \end{pmatrix} \begin{pmatrix} I_X^A \\ I_Y^A \\ I_Z^A \end{pmatrix}. \quad (147)$$

The time evolution of the longitudinal spin operators in the rotating frame then follows an equation of motion similar to the laboratory frame case except all the quantities are replaced by primes [295]. For example, for a two-spin system ( $AX$ ), the equation of motion is given by [211]:

$$-\frac{d}{dt} \begin{pmatrix} \langle I_{Z'}^A \rangle \\ \langle I_{Z'}^X \rangle \\ \langle 2I_{Z'}^A I_{Z'}^X \rangle \end{pmatrix} = \begin{pmatrix} \rho'_A & \sigma'_{AX} & \delta'_{A,AX} \\ \sigma'_{AX} & \rho'_X & \delta'_{X,AX} \\ \delta'_{A,AX} & \delta'_{X,AX} & \rho'_{AX} \end{pmatrix} \times \begin{pmatrix} \langle \Delta I_{Z'}^A \rangle \\ \langle \Delta I_{Z'}^X \rangle \\ \langle 2\Delta I_{Z'}^A I_{Z'}^X \rangle \end{pmatrix} \quad (148)$$

where  $\Delta$  represents the deviation from thermal equilibrium and the relaxation parameters  $\rho'$ ,  $\sigma'$  and  $\delta'$ , respectively, represent the self-relaxation rate of each mode, the cross relaxation rate between modes of the same order and the cross-correlation rate between modes of different order, in the respective rotating frames. While the RF field is assumed to be strong enough to redefine the secular and non-secular terms (by decoupling the longitudinal and transverse operators in the rotating frame), it is assumed to be not strong enough to perturb the fundamental relaxation process. This later assumption holds if  $(\gamma H_1)\tau_c \ll 1$  [295], a condition satisfied for all practical purposes. Under this assumption, all the spectral densities defined earlier (Section 2.2.5) remain unchanged. However, the way the spectral densities influence the dynamics of the magnetization is modified. They need to be transformed into rotating frame along with the spin operators. The following sections provide a discussion of the dynamics of the various spin systems in the rotating frame in the presence of cross-correlations.

### 5.2. Effect of CSA–dipole cross-correlations for an $AX$ spin system

For the homonuclear two-spin system  $AX$ , when the two spins  $A$  and  $X$  are selectively spin locked along the  $\theta_A$  and  $\theta_X$  the various elements of Eq. (148), are

obtained as [211]:

$$\begin{aligned}
 \begin{pmatrix} \rho'_A \\ \rho'_X \\ \rho'_{AX} \\ \sigma'_{AX} \end{pmatrix} &= \begin{pmatrix} [\frac{1}{2} \sin^2 \theta_A + \frac{1}{3}] & \frac{8}{3} \sin^2 \theta_A & 0 \\ [\frac{1}{2} \sin^2 \theta_X + \frac{1}{3}] & 0 & \frac{8}{3} \sin^2 \theta_X \\ \frac{1}{6} [4 \sin^2(\theta_A + \theta_X) + \cos^2 \theta_A \sin^2 \theta_X + \sin^2 \theta_A \cos^2 \theta_X] & \frac{8}{3} \sin^2 \theta_A & \frac{8}{3} \sin^2 \theta_X \\ \frac{1}{3} [2 \sin \theta_A \sin \theta_X - \cos \theta_A \cos \theta_X] & 0 & 0 \end{pmatrix} \begin{pmatrix} J_{AXAX}(0) \\ J_{AA}(0) \\ J_{XX}(0) \end{pmatrix} \\
 &+ \begin{pmatrix} [\frac{1}{2} \sin^2 \theta_A + 1] & 2(\cos^2 \theta_A + 1) & 0 \\ [\frac{1}{2} \sin^2 \theta_X + 1] & 0 & 2(\cos^2 \theta_X + 1) \\ \frac{1}{2} [1 + 2 \cos^2(\theta_A + \theta_X) + \cos(\theta_A + \theta_X) \cos(\theta_A - \theta_X)] & 2(\cos^2 \theta_A + 1) & 2(\cos^2 \theta_X + 1) \\ \sin \theta_A \sin \theta_X & 0 & 0 \end{pmatrix} \\
 &\times \begin{pmatrix} J_{AXAX}(\omega) \\ J_{AA}(\omega) \\ J_{XX}(\omega) \end{pmatrix} + \begin{pmatrix} \cos^2 \theta_A + 1 & 0 & 0 \\ \cos^2 \theta_X + 1 & 0 & 0 \\ (1 - \cos^2 \theta_A \cos^2 \theta_X) & 0 & 0 \\ 2 \cos \theta_A \cos \theta_X & 0 & 0 \end{pmatrix} \begin{pmatrix} J_{AXAX}(2\omega) \\ J_{AA}(2\omega) \\ J_{XX}(2\omega) \end{pmatrix} + \begin{pmatrix} \sin^2 \theta_A & 0 \\ 0 & \sin^2 \theta_X \\ \sin^2 \theta_A & \sin^2 \theta_X \\ 0 & 0 \end{pmatrix} \begin{pmatrix} J_A(0) \\ J_X(0) \end{pmatrix} \\
 &+ \begin{pmatrix} 1 + \cos^2 \theta_A & 0 \\ 0 & 1 + \cos^2 \theta_X \\ 1 + \cos^2 \theta_A & 1 + \cos^2 \theta_X \\ 0 & 0 \end{pmatrix} \begin{pmatrix} J_A(\omega) \\ J_X(\omega) \end{pmatrix}. \tag{149}
 \end{aligned}$$

The last two terms  $J_i(n\omega)$  represent spectral densities arising from random field mechanisms, while the other spectral densities have their usual meaning. It is noted that both  $\rho'$  and  $\sigma'$  continue to depend on auto-correlation spectral densities even in the rotating frame. The cross-correlation rates which connect the single spin operators to the two spin operators are obtained as [211]:

$$\begin{aligned}
 \begin{pmatrix} \delta'_{A,AX} \\ \delta'_{X,AX} \end{pmatrix} &= -\frac{4}{3} \begin{pmatrix} (2 \sin^2 \theta_A \cos \theta_X + \sin \theta_A \sin \theta_X \cos \theta_A) & 0 \\ 0 & (2 \sin^2 \theta_X \cos \theta_A + \sin \theta_A \sin \theta_X \cos \theta_X) \end{pmatrix} \begin{pmatrix} J_{A,AX}(0) \\ J_{X,AX}(0) \end{pmatrix} \\
 &- 2 \begin{pmatrix} (\cos^2 \theta_A \cos \theta_X + \cos \theta_X - \sin \theta_A \sin \theta_X \cos \theta_A) & 0 \\ 0 & (\cos^2 \theta_X \cos \theta_A + \cos \theta_A - \sin \theta_A \sin \theta_X \cos \theta_X) \end{pmatrix} \begin{pmatrix} J_{A,AX}(\omega) \\ J_{X,AX}(\omega) \end{pmatrix} \tag{150}
 \end{aligned}$$

Here  $\delta'_{i,j}$  represents the cross-correlation rate between even and odd order modes arising from cross terms between CSA of spin  $i$  with the dipolar vector  $ij$ . The above equation shows that the spectral densities at zero frequency also contribute to the cross-correlation rates and their contribution disappears for  $\theta_A = \theta_X = 0$  (lab frame). The CSA of spin  $A$  contributes to the CSA–dipole cross-correlation rate  $\delta'_{A,AX}$ , which connects the

single spin order of spin A to the two spin order, but not to  $\delta'_{X,AX}$ , which connects the single spin order of spin X to the two-spin order. Similarly, the CSA of spin X contributes to  $\delta'_{X,AX}$  and not to  $\delta'_{A,AX}$ .

If the spin-locking field has different values at different spins, then either a spin or a group of spins can be selectively spin locked [296]. In the case of homonuclear spins, this requires careful adjustment of the frequency and the amplitude of the RF field. The above description using the prime notation has the dual advantage that (i) it is similar to the longitudinal relaxation description, (ii) it can be continuously taken from the rotating frame description to the laboratory frame by continuous change of angles  $\theta_A$  and  $\theta_X$ . Indeed this description is completely valid for different values of  $\theta_A$  and  $\theta_X$  including selective spin lock of different spins. Some special cases of selective spin locking are discussed below.

### 5.2.1. No spin locking

This corresponds to a situation in which  $\theta_A = \theta_X = 0$ . The above parameters reduce to laboratory frame values and relaxation is purely longitudinal and Eq. (149) reduces to the truncated Eq. (61) describing the longitudinal relaxation of AX spin system in the absence of RF field [42,45].

### 5.2.2. Selective spin locking

When the magnetization of A spin is selectively spin locked, that is  $\theta_A = 90^\circ$  and  $\theta_X = 0$ , then from Eq. (149) it is seen that  $I_{Z'}^A = I_X^A$ ,  $I_{Z'}^X = I_Z^X$  and  $2I_{Z'}^A I_{Z'}^X = 2I_X^A I_Z^X$  and relaxation is a mixture of longitudinal and transverse relaxation. Furthermore, Eqs. (149) and (150) given above simplify, respectively, to [211]:

$$\begin{pmatrix} \rho'_A \\ \rho'_X \\ \rho'_{AX} \\ \sigma'_{AX} \end{pmatrix} = \frac{1}{6} \begin{pmatrix} 5 & 16 & 0 \\ 2 & 0 & 0 \\ 5 & 16 & 0 \\ 0 & 0 & 0 \end{pmatrix} \begin{pmatrix} J_{AXAX}(0) \\ J_{AA}(0) \\ J_{XX}(0) \end{pmatrix} + \frac{1}{2} \begin{pmatrix} 3 & 4 & 0 \\ 2 & 0 & 8 \\ 1 & 4 & 8 \\ 0 & 0 & 0 \end{pmatrix} \begin{pmatrix} J_{AXAX}(\omega) \\ J_{AA}(\omega) \\ J_{XX}(\omega) \end{pmatrix}$$

$$\begin{aligned} & + \begin{pmatrix} 1 & 0 & 0 \\ 2 & 0 & 0 \\ 1 & 0 & 0 \\ 0 & 0 & 0 \end{pmatrix} \begin{pmatrix} J_{AXAX}(2\omega) \\ J_{AA}(2\omega) \\ J_{XX}(2\omega) \end{pmatrix} + \begin{pmatrix} 1 & 0 \\ 0 & 0 \\ 1 & 0 \\ 0 & 0 \end{pmatrix} \begin{pmatrix} J_A(0) \\ J_X(0) \end{pmatrix} \\ & + \begin{pmatrix} 1 & 0 \\ 0 & 2 \\ 1 & 2 \\ 0 & 0 \end{pmatrix} \begin{pmatrix} J_A(\omega) \\ J_X(\omega) \end{pmatrix} \end{aligned} \quad (151)$$

and

$$\begin{aligned} \begin{pmatrix} \delta'_{A,AX} \\ \delta'_{X,AX} \end{pmatrix} &= -\frac{8}{3} \begin{pmatrix} 1 & 0 \\ 0 & 0 \end{pmatrix} \begin{pmatrix} J_{A,AX}(0) \\ J_{X,AX}(0) \end{pmatrix} \\ & - 2 \begin{pmatrix} 1 & 0 \\ 0 & 0 \end{pmatrix} \begin{pmatrix} J_{A,AX}(\omega) \\ J_{X,AX}(\omega) \end{pmatrix} \end{aligned} \quad (152)$$

It can be seen from these equations that the cross-relaxation rate  $\sigma'_{AX}$  and the cross-correlation rate  $\delta'_{X,AX}$  are zero and only the cross-correlation rate  $\delta'_{A,AX}$  is finite. It does not vanish even in the slow motion limit (since  $J_{A,AX}(0)$  contributes). Since in this case,  $\sigma'_{AX} = 0$ , the transfer of magnetization from one spin to another is exclusively by cross-correlation which can be measured accurately [211].

### 5.2.3. Spin locking both spins A and X

For this case,  $\theta_A = \theta_X = 90^\circ$ , and as seen from Eq. (149), relaxation is purely transverse. This state is obtained by applying a high power spin locking RF field on both the spins. The different relaxation rates, given by Eq. (149) reduce to:

$$\begin{aligned} \begin{pmatrix} \rho'_A \\ \rho'_X \\ \rho'_{AX} \\ \sigma'_{AX} \end{pmatrix} &= \frac{1}{6} \begin{pmatrix} 5 & 16 & 0 \\ 5 & 0 & 16 \\ 0 & 16 & 16 \\ 4 & 0 & 0 \end{pmatrix} \begin{pmatrix} J_{AXAX}(0) \\ J_{AA}(0) \\ J_{XX}(0) \end{pmatrix} \\ & + \frac{1}{2} \begin{pmatrix} 3 & 4 & 0 \\ 3 & 0 & 4 \\ 2 & 4 & 4 \\ 2 & 0 & 0 \end{pmatrix} \begin{pmatrix} J_{AXAX}(\omega) \\ J_{AA}(\omega) \\ J_{XX}(\omega) \end{pmatrix} \end{aligned}$$

$$\begin{aligned}
& + \begin{pmatrix} 1 & 0 & 0 \\ 1 & 0 & 0 \\ 1 & 0 & 0 \\ 0 & 0 & 0 \end{pmatrix} \begin{pmatrix} J_{AXAX}(2\omega) \\ J_{AA}(2\omega) \\ J_{XX}(2\omega) \end{pmatrix} \\
& + \begin{pmatrix} 1 & 0 \\ 0 & 1 \\ 1 & 1 \\ 0 & 0 \end{pmatrix} \begin{pmatrix} J_A(0) \\ J_X(0) \end{pmatrix} + \begin{pmatrix} 1 & 0 \\ 0 & 1 \\ 1 & 1 \\ 0 & 0 \end{pmatrix} \begin{pmatrix} J_A(\omega) \\ J_X(\omega) \end{pmatrix}, \\
\end{aligned} \tag{153}$$

and the cross-correlation rates go to zero.<sup>9</sup> Hence in the rotating frame, when all the interacting spins are spin-locked, the partial conversion of  $I_Z^A$  to  $2I_Z^A I_Z^X$  and vice versa is not possible. On the other hand, it has been shown that by spin-locking all the spins along the magic angle ( $\theta_A = \theta_X = 54^\circ 44'$ ), the contribution of  $J(0)$  to the cross-correlation rate is maximum. Therefore, one can choose this value for for obtaining the maximum contribution of cross-correlation in

biomolecular NMR. Such experiments have been carried out using double quantum filtered tilted ROESY [192].

In the above analyses, it is assumed that the J-coupling is small compared to the RF field strength and that the effective field direction and magnitude are equal for all the transitions of a spin multiplet. The cases where different transitions of a multiplet have different effective field value and direction have been treated by Bull [61].

### 5.3. Effect of cross-correlations for an AMX spin system

The general case of selective spin locking of each spin of an AMX spin system with different angles of spin-lock  $\theta_A$ ,  $\theta_M$  and  $\theta_X$  is treated here in order to study the effect of CSA–dipole and dipole–dipole cross-correlations in the presence of RF fields. Following the method outlined above for the two-spin case, the equation of motion of the longitudinal modes in the rotating frame is obtained as:

$$-\frac{d}{dt} \begin{pmatrix} E \\ A'_Z(t) \\ M'_Z(t) \\ X'_Z(t) \\ 2A'_Z M'_Z(t) \\ 2A'_Z X'_Z(t) \\ 2M'_Z X'_Z(t) \\ 4A'_Z M'_Z X'_Z(t) \end{pmatrix} = \begin{pmatrix} 0 & 0 & 0 & 0 & 0 & 0 & 0 & 0 \\ 0 & \rho'_A & \sigma'_{AM} & \sigma'_{AX} & \delta'_{A,AM} & \delta'_{A,AX} & 0 & \delta'_{AMAX} \\ 0 & \sigma'_{AM} & \rho'_M & \sigma'_{MX} & \delta'_{M,AM} & 0 & \delta'_{M,MX} & \delta'_{AMMX} \\ 0 & \sigma'_{AX} & \sigma'_{MX} & \rho'_X & 0 & \delta'_{X,AX} & \delta'_{X,MX} & \delta'_{AXMX} \\ 0 & \delta'_{A,AM} & \delta'_{M,AM} & 0 & \rho'_{AM} & \delta'_{AMAX} + \sigma'_{MX} & \delta'_{AMMX} + \sigma'_{AX} & \delta'_{A,AX} + \delta'_{M,MX} \\ 0 & \delta'_{A,AX} & 0 & \delta'_{X,AX} & \delta'_{AMAX} + \sigma'_{MX} & \rho'_{AX} & \delta'_{AXMX} + \sigma'_{AM} & \delta'_{A,AM} + \delta'_{X,MX} \\ 0 & 0 & \delta'_{M,MX} & \delta'_{X,MX} & \delta'_{AMMX} + \sigma'_{AX} & \delta'_{AXMX} + \sigma'_{AM} & \rho'_{MX} & \delta'_{M,AM} + \delta'_{X,AX} \\ 0 & \delta'_{AMAX} & \delta'_{AMMX} & \delta'_{AXMX} & \delta'_{A,AX} + \delta'_{M,MX} & \delta'_{A,AM} + \delta'_{X,MX} & \delta'_{M,AM} + \delta'_{X,AX} & \rho'_{AMX} \end{pmatrix}$$

<sup>9</sup> The absence of  $\delta_{A,AX}$  in the case when both the spins are spin-locked with  $\theta_A = \theta_X = 90^\circ$  is in agreement with Section 3.5.2; where also the CSA-dipole cross correlations do not come into play, when  $\pi$  pulses are applied to both the spins, decoupling the dynamics of the gerade ( $2\langle I_Z S_Z \rangle$ ,  $\frac{1}{2}1$ ) and the ungerade ( $\langle I_Z \rangle$ ,  $\langle S_Z \rangle$ ) spaces.

$$\times \begin{pmatrix} E \\ A'_Z(t) - A_Z^{I0} \\ M'_Z(t) - M_Z^{I0} \\ X'_Z(t) - X_Z^{I0} \\ 2A'_Z M'_Z(t) \\ 2A'_Z X'_Z(t) \\ 2M'_Z X'_Z(t) \\ 4A'_Z M'_Z X'_Z(t) \end{pmatrix} \tag{154}$$

The various self- and cross-relaxation rates stated in the above relaxation matrix are given by [61,211]:

$$\begin{pmatrix} \rho'_A \\ \rho'_{AM} \\ \rho'_{AMX} \\ \sigma'_{AM} \end{pmatrix} = \begin{pmatrix} \frac{1}{3} + \frac{1}{2} \sin^2 \theta_A & \frac{1}{3} + \frac{1}{2} \sin^2 \theta_A & 0 \\ \zeta'_{AM}(0) & \frac{1}{3} + \frac{1}{2} \sin \theta_A & \frac{1}{3} + \frac{1}{2} \sin \theta_M \\ \zeta'_{AM}(0) & \zeta'_{AX}(0) & \zeta'_{MX}(0) \\ \frac{1}{3} [2 \sin \theta_A \sin \theta_M - \cos \theta_A \cos \theta_M] & 0 & 0 \end{pmatrix} \begin{pmatrix} J_{AMAM}(0) \\ J_{AXAX}(0) \\ J_{MXMX}(0) \end{pmatrix} \\
 + \begin{pmatrix} 1 + \frac{1}{2} \sin^2 \theta_A & 1 + \frac{1}{2} \sin^2 \theta_A & 0 \\ \zeta'_{AM}(\omega) & 1 + \frac{1}{2} \sin^2 \theta_A & 1 + \frac{1}{2} \sin^2 \theta_M \\ \zeta'_{AM}(\omega) & \zeta'_{AX}(\omega) & \zeta'_{MX}(\omega) \\ \sin \theta_A \sin \theta_M & 0 & 0 \end{pmatrix} \begin{pmatrix} J_{AMAM}(\omega) \\ J_{AXAX}(\omega) \\ J_{MXMX}(\omega) \end{pmatrix} \\
 + \begin{pmatrix} 1 + \cos^2 \theta_A & 1 + \cos^2 \theta_A & 0 \\ \zeta'_{AM}(2\omega) & 1 + \cos^2 \theta_A & 1 + \cos^2 \theta_M \\ \zeta'_{AM}(2\omega) & \zeta'_{AX}(2\omega) & \zeta'_{MX}(2\omega) \\ 2 \cos \theta_A \cos \theta_M & 0 & 0 \end{pmatrix} \begin{pmatrix} J_{AMAM}(2\omega) \\ J_{AXAX}(2\omega) \\ J_{MXMX}(2\omega) \end{pmatrix} \\
 + \frac{8}{3} \begin{pmatrix} \sin^2 \theta_A & 0 & 0 \\ \sin^2 \theta_A & \sin^2 \theta_M & 0 \\ \sin^2 \theta_A & \sin^2 \theta_M & \sin^2 \theta_X \\ 0 & 0 & 0 \end{pmatrix} \begin{pmatrix} J_{AA}(0) \\ J_{MM}(0) \\ J_{XX}(0) \end{pmatrix} \\
 + 2 \begin{pmatrix} 1 + \cos^2 \theta_A & 0 & 0 \\ 1 + \cos^2 \theta_A & 1 + \cos^2 \theta_M & 0 \\ 1 + \cos^2 \theta_A & 1 + \cos^2 \theta_M & 1 + \cos^2 \theta_X \\ 0 & 0 & 0 \end{pmatrix} \begin{pmatrix} J_{AA}(\omega) \\ J_{MM}(\omega) \\ J_{XX}(\omega) \end{pmatrix} \tag{155}$$

where

$$\begin{aligned} \zeta'_{AM}(0) &= \frac{1}{6} [4 \sin^2(\theta_A + \theta_M) + \cos^2 \theta_A \sin^2 \theta_M \\ &\quad + \sin^2 \theta_A \cos^2 \theta_M] \\ \zeta'_{AM}(\omega) &= \frac{1}{2} [1 + 2 \cos^2(\theta_A + \theta_M) \\ &\quad + \cos(\theta_A + \theta_M) \cos(\theta_A - \theta_M)] \\ \zeta'_{AM}(2\omega) &= 1 - \cos^2 \theta_A \cos^2 \theta_M \end{aligned} \tag{156}$$

The cross-correlation rates are given by:

$$\begin{aligned} \delta'_{A,AM} &= -\frac{4}{3} (2 \sin^2 \theta_A \cos \theta_M \\ &\quad + \cos \theta_A \sin \theta_A \sin \theta_M) J_{A,AM}(0) \\ &\quad - 2(\cos^2 \theta_A \cos \theta_M + \cos \theta_M \\ &\quad - \cos \theta_A \sin \theta_A \sin \theta_M) J_{A,AM}(\omega) \end{aligned} \tag{157}$$

$$\begin{aligned}
\delta'_{AMAX} &= \frac{1}{3}(2 \sin \theta_A \cos \theta_M + \cos \theta_A \sin \theta_M) \\
&\times (2 \sin \theta_A \cos \theta_X + \cos \theta_A \sin \theta_X) J_{AMAX}(0) \\
&+ [\cos \theta_M \cos \theta_X + \cos(\theta_A + \theta_M)] \\
&\times \cos(\theta_A + \theta_X) J_{AMAX}(\omega) \\
&+ \sin \theta_M \sin \theta_X (1 + \cos^2 \theta_A) J_{AMAX}(2\omega)
\end{aligned} \tag{158}$$

The expressions for the other auto- and cross-correlation rates can be obtained by changing the subscript indices appropriately. The effect of various selective spin-locking experiments is discussed in the following:

### 5.3.1. Case (i): when $\theta_A = \theta_M = \theta_X = 0$

This condition reduces the relaxation to purely longitudinal relaxation and the expression for the various relaxation rates reduces to the lab frame expression given in Eqs. (63) and (64):

### 5.3.2. Case (ii): when $\theta_A = 90^\circ$ , $\theta_M = \theta_X = 0$

This situation corresponds to a selective spin lock of the A-spin and the other spins are unaffected by the spin locking field. The expression for the various self-relaxation rates given by Eq. (155), simplifies to:

$$\begin{aligned}
\begin{pmatrix} \rho'_A \\ \rho'_{AM} \\ \rho'_{AMX} \end{pmatrix} &= \frac{1}{6} \begin{pmatrix} 5 & 5 & 0 \\ 5 & 5 & 2 \\ 5 & 5 & 0 \end{pmatrix} \begin{pmatrix} J_{AMAM}(0) \\ J_{AXAX}(0) \\ J_{MXMX}(0) \end{pmatrix} \\
&+ \frac{1}{2} \begin{pmatrix} 3 & 3 & 0 \\ 1 & 3 & 2 \\ 1 & 1 & 4 \end{pmatrix} \begin{pmatrix} J_{AMAM}(\omega) \\ J_{AXAX}(\omega) \\ J_{MXMX}(\omega) \end{pmatrix} + \begin{pmatrix} 1 & 1 & 0 \\ 1 & 1 & 2 \\ 1 & 1 & 0 \end{pmatrix} \\
&\times \begin{pmatrix} J_{AMAM}(2\omega) \\ J_{AXAX}(2\omega) \\ J_{MXMX}(2\omega) \end{pmatrix} + \frac{8}{3} \begin{pmatrix} 1 & 0 & 0 \\ 1 & 0 & 0 \\ 1 & 0 & 0 \end{pmatrix} \begin{pmatrix} J_{AA}(0) \\ J_{MM}(0) \\ J_{XX}(0) \end{pmatrix} \\
&+ 2 \begin{pmatrix} 1 & 0 & 0 \\ 1 & 2 & 0 \\ 1 & 2 & 2 \end{pmatrix} \begin{pmatrix} J_{AA}(\omega) \\ J_{MM}(\omega) \\ J_{XX}(\omega) \end{pmatrix}.
\end{aligned} \tag{159}$$

The cross-relaxation and cross-correlation rates are

given by [211]:

$$\begin{aligned}
\sigma'_{AM} &= 0 \\
\delta'_{A,AM} &= -\frac{8}{3} J_{A,AM}(0) - 2J_{A,AM}(\omega) \\
\delta'_{AMAX} &= \frac{4}{3} J_{AMAX}(0) + J_{AMAX}(\omega)
\end{aligned} \tag{160}$$

These equations show that while cross-relaxation rates from the spin locked spin to non-spin-locked spins are zero ( $\sigma'_{AX}$  is also zero) the single spin-order of the spin-locked spin, can be converted to the two- or three-spin orders by the cross-correlation rates at zero frequency. Thus these cross-correlation rates can be observed even when  $\omega\tau_c \gg 1$ .

### 5.3.3. Case (iii): when $\theta_A = \theta_M = 90^\circ$ and $\theta_X = 0$

This is a situation in which the spins A and M are selectively spin locked, while the X-spin remains unaffected by the spin locking field. The self-relaxation rates are given by:

$$\begin{aligned}
\begin{pmatrix} \rho'_A \\ \rho'_{AM} \\ \rho'_{AMX} \end{pmatrix} &= \frac{5}{6} \begin{pmatrix} 1 & 1 & 0 \\ 0 & 1 & 1 \\ 0 & 1 & 1 \end{pmatrix} \begin{pmatrix} J_{AMAM}(0) \\ J_{AXAX}(0) \\ J_{MXMX}(0) \end{pmatrix} \\
&+ \frac{1}{2} \begin{pmatrix} 3 & 3 & 0 \\ 2 & 3 & 3 \\ 2 & 1 & 1 \end{pmatrix} \begin{pmatrix} J_{AMAM}(\omega) \\ J_{AXAX}(\omega) \\ J_{MXMX}(\omega) \end{pmatrix} + \begin{pmatrix} 1 & 1 & 0 \\ 1 & 1 & 1 \\ 1 & 1 & 1 \end{pmatrix} \\
&\times \begin{pmatrix} J_{AMAM}(2\omega) \\ J_{AXAX}(2\omega) \\ J_{MXMX}(2\omega) \end{pmatrix} + \frac{8}{3} \begin{pmatrix} 1 & 0 & 0 \\ 1 & 1 & 0 \\ 1 & 1 & 0 \end{pmatrix} \begin{pmatrix} J_{AA}(0) \\ J_{MM}(0) \\ J_{XX}(0) \end{pmatrix} \\
&+ 2 \begin{pmatrix} 1 & 0 & 0 \\ 1 & 1 & 0 \\ 1 & 1 & 2 \end{pmatrix} \begin{pmatrix} J_{AA}(\omega) \\ J_{MM}(\omega) \\ J_{XX}(\omega) \end{pmatrix}.
\end{aligned} \tag{161}$$

The cross-relaxation and cross-correlation rates are given by:

$$\begin{aligned}
\sigma'_{AM} &= \frac{2}{3} J_{AMAM}(0) + J_{AMAM}(\omega), \\
\delta'_{A,AM} &= 0, \\
\delta'_{AMAX} &= 0, \\
\sigma'_{AX} &= \sigma'_{MX} = 0.
\end{aligned} \tag{162}$$

Under a doubly selective spin-locking case, cross-correlations involving the dipolar interactions between the spin-locked spins, become zero. Hence this provides a method of measuring the cross-relaxation rate (NOE) between two spins without the interference of spin diffusion as well as cross-correlation effects.

#### 5.3.4. Case (iv): when $\theta_A = \theta_M = \theta_X = 90^\circ$

Under this condition, all three interacting spins are spin locked and the relaxation is purely transverse. The various self-relaxation rates are given by:

$$\begin{aligned} \begin{pmatrix} \rho'_A \\ \rho'_{AM} \\ \rho'_{AMX} \end{pmatrix} &= \frac{5}{6} \begin{pmatrix} 1 & 1 & 0 \\ 0 & 1 & 1 \\ 0 & 0 & 0 \end{pmatrix} \begin{pmatrix} J_{AMAM}(0) \\ J_{AXAX}(0) \\ J_{MXMX}(0) \end{pmatrix} \\ &+ \frac{1}{2} \begin{pmatrix} 3 & 3 & 0 \\ 2 & 3 & 3 \\ 2 & 2 & 2 \end{pmatrix} \begin{pmatrix} J_{AMAM}(\omega) \\ J_{AXAX}(\omega) \\ J_{MXMX}(\omega) \end{pmatrix} + \begin{pmatrix} 1 & 1 & 0 \\ 1 & 1 & 1 \\ 1 & 1 & 1 \end{pmatrix} \\ &\times \begin{pmatrix} J_{AMAM}(2\omega) \\ J_{AXAX}(2\omega) \\ J_{MXMX}(2\omega) \end{pmatrix} + \frac{8}{3} \begin{pmatrix} 1 & 0 & 0 \\ 1 & 1 & 0 \\ 1 & 1 & 1 \end{pmatrix} \begin{pmatrix} J_{AA}(0) \\ J_{MM}(0) \\ J_{XX}(0) \end{pmatrix} \\ &+ 2 \begin{pmatrix} 1 & 0 & 0 \\ 1 & 1 & 0 \\ 1 & 1 & 1 \end{pmatrix} \begin{pmatrix} J_{AA}(\omega) \\ J_{MM}(\omega) \\ J_{XX}(\omega) \end{pmatrix}. \end{aligned} \quad (163)$$

The cross-relaxation and cross-correlation rates are given by:

$$\begin{aligned} \sigma'_{AM} &= \frac{2}{3} J_{AMAM}(0) + J_{AMAM}(\omega) \\ \delta'_{A,AM} &= 0 \\ \delta'_{AMAX} &= J_{AMAX}(\omega) + J_{AMAX}(2\omega). \end{aligned} \quad (164)$$

Here, the CSA–dipole cross-correlations go to zero. In the NOE experiment, if there is any multiplet effect, it will be due to dipole–dipole cross-correlations.

#### 5.4. Experimental observations

Rotating frame cross-correlations were observed using selective spin-locking fields by Burghardt et al. [211]. They observed the CSA–dipole cross-

correlations by selective spin locking using the pulse sequence shown in Fig. 50(a). Transverse magnetization  $I_X^A$  is initially excited using a self-refocusing  $270^\circ$ , on-resonance Gaussian pulse [303]. During the subsequent spin lock pulse which is applied along the X-axis, the  $I_X^A$  term may be regarded as an operator  $I_Z^A$ . It is the rotating-frame relaxation of this term, which is of interest. This term relaxes via the CSA–dipole cross-correlation to the two spin order term,  $2I_Z^A I_Z^X$  (equivalent to  $2I_X^A I_Z^X$  in the lab frame). At the end of the spin locking period  $\tau_{SL}$ , this term ( $2I_X^A I_Z^X$ ) is separated from the in-phase term  $I_X^A$ , by applying two Gaussian  $270^\circ$  pulses, the first at the chemical shift  $\Omega_A$ , to convert  $2I_X^A I_Z^X$  into  $2I_Z^A I_Z^X$ , and the second at the chemical shift  $\Omega_X$  to create  $2I_Z^A I_X^X$ . The single-spin operator terms are excluded by doing a phase cycle on the three pulses along with the receiver. Fig. 51 shows the experimentally observed build-up and decay of the antiphase two-spin order in exifone recorded with the sequence of Fig. 50(a), including a hard purging pulse, before the spin-locking period.

Using selective pulses, the rotating frame dipole–dipole cross-correlation rate was measured in a three spin system using the pulse sequence shown in Fig. 50(b) [211]. Fig. 52 shows the 2D multiplets of *N*-methylleucine, the 4th residue in the cyclic undecapeptide cyclosporin-A, for various mixing times. Fig. 53 shows the 1D build up and decay of the three-spin order for the same leucine that is shown in Fig. 52. Brüschweiler et al. [210] have observed the three-spin order using the tilted rotating frame (3QF T-ROESY) experiment on BPTI for a spin-locking angle of  $\theta = 35^\circ$  (Fig. 54). The 3QF-NOESY spectrum is also shown for comparison. It is seen that there are many more cross peaks in the 3QF-T-ROESY spectrum than the 3QF-NOESY. This is due to cross-correlation at zero frequency showing up in the T-ROESY.

Brüschweiler et al. have also extended the selective spin locking to a fluorine–proton system, in which the two spins are locked in orthogonal directions, naming the experiment ortho-ROESY [304]. Cross-correlations lead to an antiphase peak, the amplitude of which is sensitive to the magnitude of the spin-locking field, the various cross-correlations and the correlation time of the molecular reorientation. From a detailed analysis of the results of experiment on 1-fluoro-1,1,2,2-tetrachloroethane in a 1:5 mixture with benzene- $d_6$ , it is shown that the cross peak

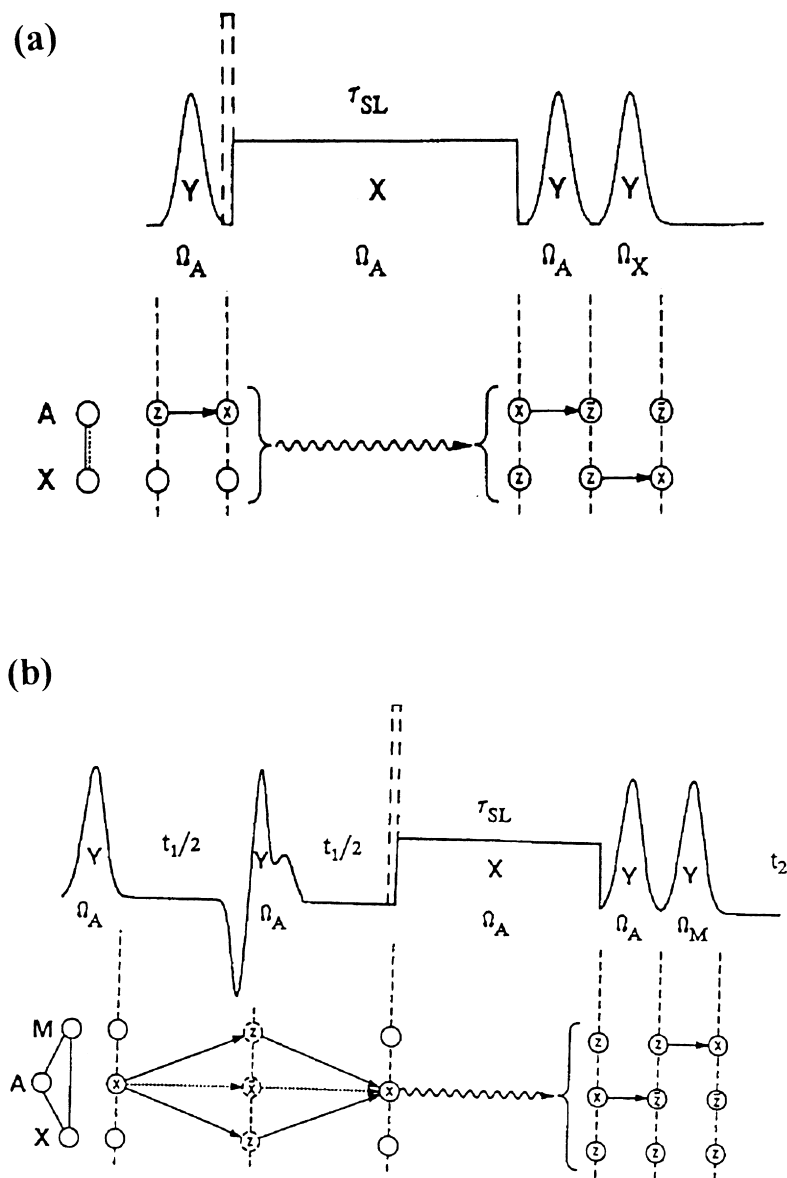


Fig. 50. (a) Pulse sequence for the 1D experimental observation of CSA–dipole cross-correlation using selective spin locking. The Gaussian pulses typically have a duration of 30 ms with a peak RF amplitude of 55 Hz to provide an on-resonance flip angle of  $270^\circ$ . The RF amplitude of the spin locking field is typically 40 Hz. The RF frequencies and phases are indicated ( $\Omega_A$  implies that the pulse is applied at the chemical shift of spin A). In the laboratory frame product operator evolution graphs, shown at the bottom of (a) and (b), the conversion of  $I_X^A = I_Z^A$  into  $2I_X^A I_Z^X = 2I_Z^A I_Z^X$ , represented by a wavy arrow, is due to cross-correlation between CSA of spin A and the dipolar interaction between A and X. (b) Pulse sequence for 2D spectroscopy with selective spin locking, suitable for a system with three or more spins. The Gaussian pulse in the middle of the evolution period refocuses all the scalar couplings. In the product operator evolution graph, the wavy arrow represents the partial conversion of  $I_Z^A$  into  $4I_Z^A I_Z^M I_Z^X$ , due to cross-correlation between the fluctuations of the AX and AM dipolar interactions. [Reproduced with permission from I. Burghardt, R. Konrat, G. Bodenhausen, Mol. Phys. 75 (1992) 467.]

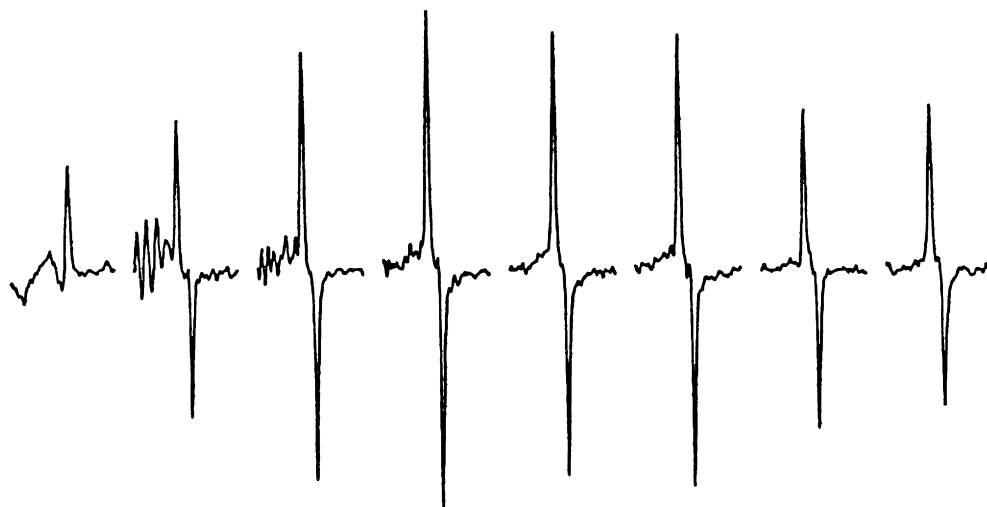
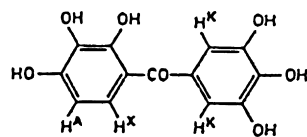


Fig. 51. Experimental build-up of two-spin order in the tilted frame,  $2I_Z^A I_Z^X$ , involving the two protons  $H^A$  and  $H^X$  in exifone, obtained with the pulse sequence of Fig. 50(a), including a hard purging pulse. The spin locking interval was varied between 1 and 900 ms. The spectra were recorded at 303 K with a Bruker AM-400 spectrometer equipped with a selective excitation unit, using a sample dissolved in  $[^2H_6]$  DMSO without degassing. [Reproduced with permission from I. Burghardt, R. Konrat, G. Bodenhausen, Mol. Phys. 75 (1992) 467].

observed in this case is largely due to cross correlated fluctuation between the scalar coupling and the isotropic chemical shift in a system undergoing *trans/gauche* reorientation. This is an extremely interesting work, which shows by explicit theoretical and experimental analysis, that time dependent correlated fluctuations of isotropic  $J$  and isotropic chemical shift can lead to two-spin orders.

Poppe and Halbeek have observed differential relaxation of the anomeric protons of  $\alpha$ - and  $\beta$ - $[1-^{13}C]$ -D-glucose during the non-selective proton spin-lock in proton–carbon system (ortho-ROESY experiment) and during a selective proton spin-lock (SLOESY experiment). The observed features in the spectrum are due to CSA (proton) and dipolar ( $^1H$ – $^{13}C$ ) cross-correlations. The experiments were performed under the condition  $\omega_1 \tau_c \approx 1$ , in order to enhance the cross-correlations [305]. Varma et al. [306] have recently shown that in higher spin systems ( $n \geq 4$ ), if the spin-locking fields are very weak, the

residual scalar interactions can give rise to three-spin order terms, which are difficult to distinguish from the three spin order terms arising from dipole–dipole cross-correlations. On the other hand, if the spin-locking fields are strong enough to make the scalar couplings ineffective, new complications arise due to the interaction of the RF field with the passive spins [306].

## 6. Dynamic frequency shift

It has been mentioned in Section 2 that the relaxation matrix  $F$  has real and imaginary parts (Eq. (12)). The real part gives rise to relaxation, which has been discussed in detail, in Sections 3–5. The imaginary part, gives rise to a small frequency shift, known as the dynamic frequency shift (DFS). While the DFS has been known in the literature for a long time and was introduced in the context of the semiclassical

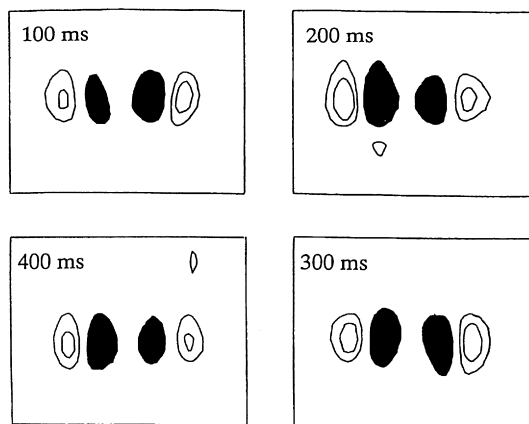


Fig. 52. Two-dimensional three-quantum filtered spectra of the cyclic undecapeptide, obtained with a selective spin lock applied to the protons  $H^{\alpha}$  and  $H^{\beta}$  of the *N*-methylleucine-4th residue cyclosporin-A for the duration from 100 to 400 ms. The spectra were recorded at 303 K with a Bruker AM 400 spectrometer using a degassed solution in  $CDCl_3$ . The spectral widths are 128 and 256 Hz in  $\omega_1$  and  $\omega_2$ , respectively (only  $20 \times 40$  Hz shown).  $64 \times 512$  data points were recorded, zero-filled to  $128 \times 1k$ . A Lorentzian-to-Gaussian lineshape transformation ( $LB = -1.5$ ,  $GB = 0.08$ ) was applied before Fourier transformation. [Reproduced with permission from I. Burghardt, R. Konrat, G. Bodenhausen, Mol. Phys. 75 (1992) 467.]

theory of relaxation by Abragam [1], it has gained importance in recent years due to contributions from cross-correlations. Both auto and cross-correlation spectral densities contribute to DFS, but manifest in the spectra in a different manner. Auto-correlations contribute equal DFS to all transitions of a spin, giving rise to a net DFS, indistinguishable from a chemical shift and therefore difficult to establish experimentally. Cross-correlations, on the other hand, give rise to differential effects on various transitions. In the simplest case of a doublet, the effect is often equal and opposite on the two transitions, making DFS indistinguishable from a change in coupling value, and again difficult to establish experimentally, except via careful measurement of the splitting as a function of magnetic field [307]. In the case of a triplet or higher multiplets, which may have unequal DFS on various transitions (arising from cross-correlations) the symmetry of the multiplet is broken, giving rise to unequivocal experimental evidence of the existence of DFS. This latter type therefore needs a minimum of three coupled spin-(1/2) system or a spin-(1/2) coupled to spin  $> (1/2)$  and

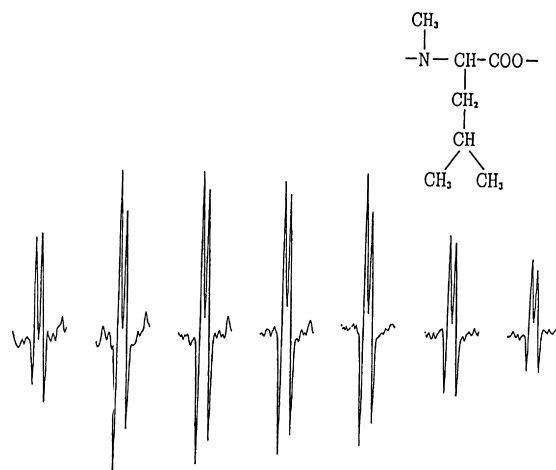


Fig. 53. One-dimensional multiplets of the *N*-methylleucine-4th residue in cyclosporin-A, obtained with the 1D selective spin locking shown in Fig. 50(a), without the purging pulse. The spin locking interval was varied from 20 to 750 ms. [Reproduced with permission from I. Burghardt, R. Konrat, G. Bodenhausen, Mol. Phys. 75 (1992) 467.]

needs resolved or partially resolved multiplets [308–310].

It can be seen that in the case of non-overlapping non-degenerate transitions, ( $|\omega_{\alpha\alpha'} - \omega_{\beta\beta'}| \gg \Gamma_{\alpha\alpha'\beta\beta'}$ , the simple-line approximation) the summation on the RHS of Eq. (20) reduces to only one term, namely,  $\Gamma_{\alpha\alpha'\alpha\alpha'}$ , which contributes to the time evolution of the off-diagonal element  $\sigma_{\alpha\alpha'}$ , which has a frequency  $\omega_{\alpha\alpha'}$ , an exponential decay rate  $R_{\alpha\alpha'\alpha\alpha'}$  and a DFS  $L_{\alpha\alpha'\alpha\alpha'}$ . However, in the limit  $|\omega_A - \omega_X| \gg J_{AX} \gg \Gamma_{\alpha\alpha'\beta\beta'}$ , the coupled evolution of the two *A* transitions of an *AX* spin system, can be written from Eq. (12) and Eq. (21) as:

$$\frac{d}{dt} \begin{pmatrix} \sigma_{12}(t) \\ \sigma_{34}(t) \end{pmatrix} = - \left[ i \begin{pmatrix} \omega_{12} + \delta_{12} & 0 \\ 0 & \omega_{34} + \delta_{34} \end{pmatrix} + \begin{pmatrix} R_{1212} & R_{1234} \\ R_{1234} & R_{3434} \end{pmatrix} \right] \begin{pmatrix} \sigma_{12}(t) \\ \sigma_{34}(t) \end{pmatrix}. \quad (165)$$

Here use is made of the fact that  $R_{\alpha\alpha'\beta\beta'} = R_{\beta\beta'\alpha\alpha'}$  and that  $L_{\alpha\alpha'\beta\beta'}$  is negligible, and  $\omega_{12} = \omega_A + \frac{1}{2}J_{AX}$  and  $\omega_{34} = \omega_A - \frac{1}{2}J_{AX}$  and  $\delta_{\alpha\alpha'} = L_{\alpha\alpha'\alpha\alpha'}(\omega)$ . Eq. (165) can be discussed in two limits. In the first limit, if  $J_{AX} \gg R_{1234}$ , the contribution of  $R_{1234}$  is negligible

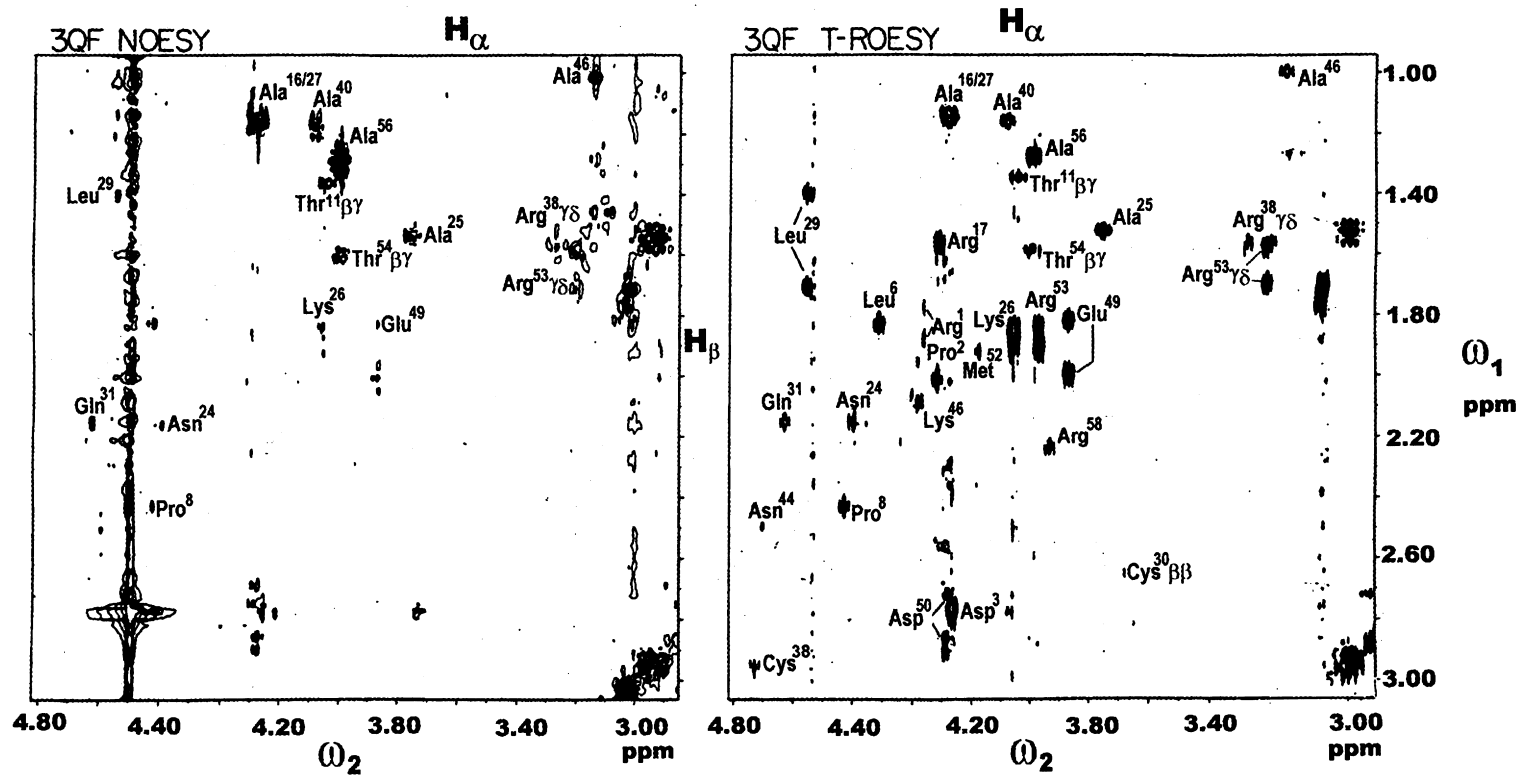


Fig. 54. Proton NMR spectra of a 20 mM solution of basic pancreatic trypsin inhibitor in  $D_2O$  at  $pD = 4.6$  recorded with a RF field strength  $\gamma B_1/2\pi = 6100$  Hz and irradiation effectively 14.3 ppm at lower field from the middle of the spectrum. 1024 experiments with 60 transients each were recorded. (a) 3QF NOESY (500 MHz),  $B_1 = 0$ ,  $\theta = 0$  at 305 K. The water resonance ridge at  $\omega_2 = 4.7$  ppm is plotted at a four times higher level than the rest of the spectrum. (b) 3QF T-ROESY with  $\theta = 35^\circ$  (600 MHz) at 300 K. The  $H_\beta$ - $H_\alpha$  cross peak region is shown, which also includes some other cross peaks. The water resonance was suppressed by presaturation. [Reproduced with permission from R. Brüschweiler, C. Griesinger, R.R. Ernst, J. Am. Chem. Soc. 111 (1989) 8034.]

and each coherence  $\omega_{12}$  and  $\omega_{34}$  evolve independently of each other by a single time constant given by  $R_{1212}$  or  $R_{3434}$ . The DFS also makes a contribution to the shift of each line. The imaginary part of auto-correlation spectral densities contributes equal values to  $\delta_{12}$  and  $\delta_{34}$  while the imaginary part of cross-correlation spectral densities makes equal and opposite contributions to  $\delta_{12}$  and  $\delta_{34}$ , exactly in the manner  $R_{1212}$  and  $R_{3434}$  differ from each other via the real part of cross-correlation spectral densities. This results in a modified splitting given by  $J + (\delta_{12} - \delta_{34})$ . In the limit,  $J$  is zero, the two transitions overlap and their time evolution gets coupled. In such a case, one can monitor the time evolution of the sum ( $\sigma_{12} + \sigma_{34}$ ) and difference ( $\sigma_{12} - \sigma_{34}$ ) modes. In this circumstance, the imaginary part of cross-correlation spectral densities cancels out and the DFS is obtained only from the imaginary part of auto-correlation term, which can at best shift slightly the resonance frequency and is indistinguishable from a chemical shift change. In the intermediate case when  $J \sim R_{1234}$ , the full equation has to be solved and one obtains numerical solutions [311]. Similar analysis can be carried out for higher order spin systems. In the following, we point out the DFS of various spin systems in the simple-line approximation, assuming all transitions and coherences to be well resolved.

Before that the functional form of the DFS and its manifestation under various motional limits is briefly discussed.

### 6.1. Functional form of the dynamic frequency shift

Following Eq. (12),  $K(\omega)$ , the DFS is the sine transform of the correlation function  $G(\tau)$  and can be written as:

$$K_{\mu\nu}(\omega) = \int_0^{\infty} G_{\mu\nu}(\tau) \sin(\omega\tau) d\tau, \quad (166)$$

where  $G_{\mu\nu}(\tau)$  is the correlation function of the lattice part of the interactions containing both auto-correlations ( $\mu = \nu$ ) and cross-correlations ( $\mu \neq \nu$ ). For isotropically tumbling molecules  $K_{\mu\nu}(\omega)$  is obtained as [64]:

$$K_{\mu\nu}(\omega) = \frac{1}{2} C_{\mu} C_{\nu} (3 \cos^2 \chi_{\mu\nu} - 1) \left[ \frac{\omega\tau_c^2}{1 + (\omega\tau_c)^2} \right] \quad (167)$$

where  $\tau_c$  is the correlation time,  $\chi_{\mu\nu}$  the angle between the principal axes of the tensor interaction  $\mu$  and  $\nu$  with  $C_{\mu}$  and  $C_{\nu}$  being the constants indicating the strength of each interaction. This should be compared with the real part of the spectral densities which govern the relaxation of the spin and which are given by [58]:

$$J_{\mu\nu}(\omega) = \frac{1}{2} C_{\mu} C_{\nu} (3 \cos^2 \chi_{\mu\nu} - 1) \left[ \frac{\tau_c}{1 + (\omega\tau_c)^2} \right]. \quad (168)$$

Eqs. (167) and (168) indicate that the real and the imaginary parts of the spectral densities differ only by a multiplicative factor  $\omega\tau_c$ . Thus the analytical expressions for DFS are similar to the linewidths of the various coherences, except for the multiplicative factor  $\omega\tau_c$  and the absence of adiabatic (zero frequency) contributions to DFS. The dependence of these spectral densities on  $\tau_c$  has been studied by Fouques and Werbelow (Fig. 55) [312]. They show that for isotropic reorientations, the DFS becomes comparable to the linewidth for  $\omega\tau_c \approx 1$  and shows up prominently. For the short correlation time limit  $\omega\tau_c \ll 1$ , the DFS is much smaller in magnitude compared to the real part of the spectral densities. In this limit, one obtains well resolved multiplets, since the linewidths are small, but the DFS is negligible. On the other hand, for the long correlation limit  $\omega\tau_c \gg 1$ , the DFS reaches a saturation value. The non-adiabatic contributions to the linewidth  $J(\omega)$  and  $J(2\omega)$  decrease, but the adiabatic contribution  $J(0)$  increases linearly, yielding broad lines, masking the multiplet structure. In cases, where the adiabatic contribution to linewidths is negligible, such as heteronuclear dipolar interaction, the DFS becomes important in this limit, as well. Anisotropic and internal motions, in general, reduce the magnitude of DFS [312].

### 6.2. Dynamic frequency shift for various spin systems

In this section, the DFS in various spin-(1/2) systems is discussed, within the limit of the ‘‘simple-line approximation’’, such that there are no degenerate transitions. A special case of degenerate transitions of three equivalent spins ( $A_3$ ) will also be considered.

#### 6.2.1. Two unlike spin-1/2 system (AX)

Considering all the four single-quantum transitions

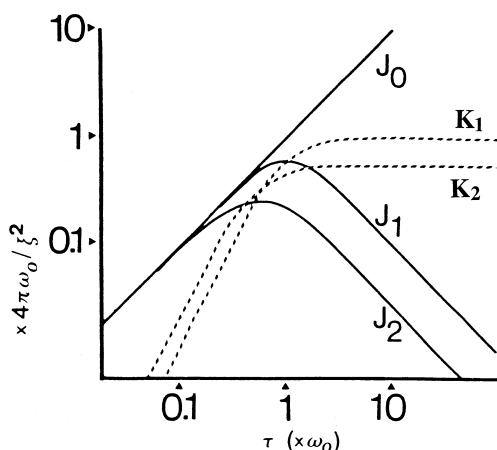


Fig. 55. Plot of  $J_0(0)$ ,  $J_1(\omega_0)$ ,  $J_2(2\omega_0)$ ,  $K_1(\omega_0)$  and  $K_2(2\omega_0)$  measured in units of  $4\pi\omega_0/\xi^2$  versus the reorientational correlation time  $\tau$ , measured in units of  $\omega_0$ . Here  $\xi$  is the strength of the interaction. [Reproduced with permission from C.E.M. Fouques, L.G. Werbelow, Can. J. Chem. 57 (1979) 2329].

to be well resolved, the off-diagonal elements  $R_{\alpha\alpha'\beta\beta'}$  and  $L_{\alpha\alpha'\beta\beta'}$  have negligible influence. Under this secular approximation, the DFS follows a result which is similar to the real part of  $\Gamma$  given in Section 4.2.1, except that the zero-frequency (adiabatic) contributions to the DFS are absent. Considering the relaxation of the spin system to be governed by the CSA of each spin and the mutual dipolar interaction, the frequencies of the two single-quantum transitions of spin  $A$  can be written as:

$$\omega_A + L_{\text{auto}}^A \pm \left(\frac{1}{2}J_{AX} + L_{\text{cross}}^A\right) \quad (169)$$

where  $L_{\text{auto}}^A$  is obtained neglecting the adiabatic contributions, as [64,314]:

$$-L_{\text{auto}}^A = \frac{1}{6}K_{AXAX}(\omega_A - \omega_X) + \frac{1}{2}K_{AXAX}(\omega_A) + K_{AXAX}(\omega_A + \omega_X) + 2K_{AA}(\omega_A) \quad (170)$$

and the cross-correlation contribution as:

$$L_{\text{cross}}^A = 2K_{A,AX}(\omega_A) + 2K_{X,AX}(\omega_X). \quad (171)$$

The DFS for the  $X$ -spin transitions can be obtained by interchanging the indices  $A$  and  $X$  in the above equations. The cross-correlation contribution is identical for both the spins, but the auto-correlation contribution is different on the two spins [307,313–316].

The double and zero quantum coherences also have

DFS but only from auto-correlation terms respectively given by [64]:

$$-L_{AX}^{\text{DQ}} = \frac{1}{2}[K_{AXAX}(\omega_A) + K_{AXAX}(\omega_X)] + 2K_{AXAX}(\omega_A + \omega_X) + 2[K_{AA}(\omega_A) + K_{XX}(\omega_X)] \quad (172)$$

and

$$-L_{AX}^{\text{ZQ}} = \frac{1}{2}[K_{AXAX}(\omega_A) - K_{AXAX}(\omega_X)] + \frac{1}{3}K_{AXAX}(\omega_A - \omega_X) + 2[K_{AA}(\omega_A) - K_{XX}(\omega_X)] \quad (173)$$

For homonuclear weakly coupled spins,  $\omega_A \approx \omega_X = \omega$ , and the contribution from  $K_{AXAX}(\omega_A - \omega_X)$  to auto-correlations vanishes both for SQ and ZQ cases (Eqs. (170) and (173)).

These shifts, for single as well as for MQ coherence, are typically less than 1 Hz and are difficult to establish as arising due to DFS, since they are indistinguishable from the chemical shift. However, the change in  $J$  value (or the doublet separation) could be identified due to DFS by making field-dependent  $J$  measurement, provided CSA and dipolar interactions are the major contributors to the relaxation and their cross term is significant in magnitude [307].

### 6.2.2. Three spin-1/2 system (AMX)

For a weakly coupled heteronuclear three spin-(1/2) system (AMX), with all three quartets well resolved ( $J_{AM} \neq J_{AX} \neq J_{MX} \gg$  linewidths), such that the simple-line approximation holds, the DFS contributions to the four 'A'-spin single-quantum transitions are obtained, as [64,317]:

$$\begin{aligned} \omega_A^{\alpha\alpha} &= L_{\text{auto}}^A + J_{AMX} + 2K_{AM} + 2K_{AX} \\ \omega_A^{\alpha\beta} &= L_{\text{auto}}^A - J_{AMX} + 2K_{AM} - 2K_{AX} \\ \omega_A^{\beta\alpha} &= L_{\text{auto}}^A - J_{AMX} - 2K_{AM} + 2K_{AX} \\ \omega_A^{\beta\beta} &= L_{\text{auto}}^A + J_{AMX} - 2K_{AM} - 2K_{AX}. \end{aligned} \quad (174)$$

While auto-correlations contribute identical shifts to

all the  $A$ -spin transitions given by:

$$\begin{aligned}
 -L_{\text{auto}}^A &= \frac{1}{6}[K_{AMAM}(\omega_A - \omega_M) + K_{AXAX}(\omega_A - \omega_X)] \\
 &+ \frac{1}{2}[K_{AMAM}(\omega_A) + K_{AXAX}(\omega_A)] \\
 &+ [K_{AMAM}(\omega_A + \omega_M) + K_{AXAX}(\omega_A + \omega_X)] \\
 &+ 2K_{AA}(\omega_A), \quad (175)
 \end{aligned}$$

the cross-correlations contribute differential shifts, breaking the symmetry of the multiplets. The contribution of dipole–dipole cross-correlations to DFS, following Brüschweiler, is given by [317]:

$$J_{AMX} = -[K_{AMAX}(\omega_A) + K_{AMMX}(\omega_M) + K_{AXMX}(\omega_X)] \quad (176)$$

and the CSA–dipole cross-correlation contribution is given by (to be published):

$$K_{ij} = K_{i,jj}(\omega_i) + K_{j,ij}(\omega_j) \quad (177)$$

All the three dipole–dipole cross-correlations contribute equal and opposite DFS to inner and outer transitions of  $A$ -spin multiplet, breaking the symmetry of the multiplet. Similarly, the CSA–dipole cross-correlations also contribute differential shifts.

It can be shown that the contribution of the DFS to the various spin systems can be added as a modification to the spin Hamiltonian (to be published) and the above result for the contributions of dipole–dipole and CSA–dipole cross-correlations to single-quantum transitions of spin-(1/2) system can be generalized, into the following spin Hamiltonian:

$$\mathcal{H}_{\text{DFS}}^{\text{cross}} = 4 \sum_{i < j < k} J_{ijk} I_{Zi} I_{Zj} I_{Zk} + 4 \sum_{i < j} K_{ij} I_{Zi} I_{Zj} \quad (178)$$

where [317]

$$J_{ijk} = -[K_{ijik}(\omega_i) + K_{ijjk}(\omega_j) + K_{ikjk}(\omega_k)], \quad (179)$$

and  $K_{ij}$  is given by Eq. (177).

Thus, in general, the presence of cross-correlations break the symmetry of a multiplet, leading to unequivocal evidence for the existence of DFS. However, it is possible that some CSA–dipole cross-correlations retain the symmetry of the multiplet, while changing the  $J$ .

### 6.2.3. Three identical spin-(1/2) system ( $A_3$ )

All the single-quantum transitions of this spin

system are degenerate, with the eigenstates being grouped into a quartet and two doublets belonging, respectively, to the irreducible representations  $E$ ,  $A_1$  and  $A_2$  of the  $C_{3v}$  symmetry group.

Werbelow has given expressions for the DFS for the SQ transitions of the quartet manifold as well as for the doubly degenerate manifolds. The DFS of these degenerate transitions, in the presence of CSA–dipole and dipole–dipole cross-correlations are different [308,313]. While  $J$ -coupling does not lift the degeneracy of these transitions, the DFS could. However, the simple-line approximation would not be valid in this case.

## 6.3. Dynamic frequency shifts for quadrupolar nuclei

### 6.3.1. Spin-1 system

The DFS of the two single quantum coherences for a system of isolated  $I$  spins (spin-1) relaxed by intramolecular anisotropic shieldings and quadrupolar interactions are given by [64]:

$$\begin{aligned}
 \Omega_{1,0} &= -[2K^{QI}(\omega_I) + 4K^{QI}(2\omega_I) + 2K^{\text{CSA}_I}(\omega_I) \\
 &+ 12K^{QI,\text{CSA}_I}(\omega_I)] \quad (180)
 \end{aligned}$$

$$\begin{aligned}
 \Omega_{0,-1} &= -[2K^{QI}(\omega_I) + 4K^{QI}(2\omega_I) + 2K^{\text{CSA}_I}(\omega_I) \\
 &- 12K^{QI,\text{CSA}_I}(\omega_I)]. \quad (181)
 \end{aligned}$$

The DFS difference between these two coherences:

$$\Omega_{1,0} - \Omega_{0,-1} = -[24K^{QI,\text{CSA}_I}(\omega_I)] \quad (182)$$

depends on the cross-correlation between quadrupolar and CSA relaxation.

The DFS of the double quantum coherence is given by [64]:

$$\Omega_{1,-1} = -[4K^{QI}(\omega_I) + 8K^{QI}(2\omega_I) + 4K^{\text{CSA}_I}(\omega_I)]. \quad (183)$$

and is dependent only on auto-correlation terms. The relaxation rate of the double quantum coherence given by:

$$\begin{aligned}
 (1/T_2)_{1,-1} &= 4J^{QI}(\omega_I) + 8J^{QI}(2\omega_I) + (32/3)J^{\text{CSA}_I}(0) \\
 &+ 4J^{\text{CSA}_I}(\omega_I) \quad (184)
 \end{aligned}$$

which has no adiabatic quadrupolar contribution. In this case, if the extreme narrowing condition fails, the

DFS will be larger than the homogeneous linewidth. The maximum DFS of the double quantum coherence is given by  $(3/20)(e^2q_1Q_I/h)^2/\omega_I$  and may exceed 1 kHz for a deuteron. This suggests that for quadrupolar nuclei, DFS of significant order to be measurable can be anticipated [64].

### 6.3.2. General case of spin $I > 1$

As seen in Section 6.3.1 (spin  $I = 1$  case), the auto-correlation contribution to the DFS can be significant for quadrupolar nuclei. The constant  $e^2qQ/h$  for most of the quadrupolar nuclei ranges from 0.2 to 5 MHz and the DFS from quadrupole relaxation range from one to several kHz. This is the main reason for the interest in DFS in quadrupolar nuclei with subsequent observation of the same in various systems [318–326]. It may be noted that even in such cases the DFS will not be pronounced in regions away from the  $T_1$  minimum, where it will be smaller than the adiabatic linewidth [326]. The DFS,  $\Omega_{m,m-n}$  for the specific component  $|m\rangle \rightarrow |m-n\rangle$  of the  $n$  quantum coherence for an arbitrary spin  $I$  (either integer or half-integer) is given by [327]:

$$\Omega_{m,m-n} = \left[ \frac{8n}{I^2(2I-1)^2} \right] \times \left\{ \left[ -I(I+1) + 6m(m-n) + 2n^2 + \frac{1}{4} \right] \times K^{Q_I}(\omega_I) + [I(I+1) - 3m(m-n) - n^2 - \frac{1}{2}]K^{Q_I}(2\omega_I) \right\}. \quad (185)$$

Using the above equation, the DFS for various transitions of nuclei with  $I < (9/2)$  have been tabulated and plotted [for  $I = (5/2)$  and  $(3/2)$ , Fig. 56]. This figure clearly exemplifies the fact that the DFS reveals itself outside the extreme narrowing regime that is in the long correlation limit, for the cases in which the adiabatic contributions to linewidths are absent.

The DFS due to the cross-correlation between quadrupolar and other interactions can become prominent even when there are dominant quadrupolar interactions. For example, the DFS associated with the cross-correlation between quadrupolar and CSA is

given by [64]:

$$\Omega_{m,m-n} = \left[ \frac{-12n(2m-n)}{I(2I-1)} \right] K^{Q_I,CSA_I}(\omega_I). \quad (186)$$

### 6.4. Dynamic frequency shifts of $I = 1/2$ spins scalar coupled to efficiently relaxed quadrupolar spins ( $S$ )

Efficiently relaxed quadrupolar nuclei can dissipate single quantum coherences of coupled spin-1/2 nuclei via scalar relaxation of the second kind [328–331]. Cross-correlation between the quadrupolar, CSA and dipolar relaxation can result in a differential shift of multiplet components that are comparable to the multiplet splittings themselves. This section discusses the effect on the line shape features of spin-1/2 nuclei arising from the cross-correlation induced DFS from  $J$ -coupled, efficiently relaxed quadrupolar nuclei.

The spin-1/2 line shape function:

$$\mathbf{F}(\omega) = \text{Re} \int_0^\infty \langle \mathbf{I}_+(t) \mathbf{I}_-(0) \rangle \exp(-i\omega t) dt, \quad (187)$$

is calculated from the expression [1,332]:

$$\mathbf{F}(\omega) = \text{Re} \sum_{m=-s}^s \sum_{m'=-s}^s (\mathbf{A}^{-1}(\omega))_{m,m'} \quad (188)$$

where  $\mathbf{A}$  is a  $(2s+1) \times (2s+1)$  symmetric matrix, with  $s$  being the spin quantum number of the quadrupolar spin. The matrix elements of  $\mathbf{A}$  are given by [313,332]:

$$A_{m,m} = i(\omega_I - \omega - mJ + \Omega_{s,m}) - (1/T_2)_{s,m} \quad (189)$$

$$\begin{aligned} A_{m,m-1} &= A_{m-1,m} = A_{-m,-m+1} = A_{-m+1,-m} \\ &= [2(s-m+1)(s+m)(2m-1)^2s^{-2} \\ &\quad \times (2s-1)^{-2}] J^{Q_s}(\omega_s) \end{aligned} \quad (190)$$

$$\begin{aligned} A_{m,m-2} &= A_{-m,-m+2} = A_{m-2,m} = A_{-m+2,-m} \\ &= [2(s-m+1)(s-m+2)(s+m-1) \\ &\quad \times (s+m)s^{-2}(2s-1)^{-2}] J^{Q_s}(2\omega_s) \end{aligned} \quad (191)$$

In the above,  $J$  is the  $I$ - $S$  scalar coupling constant, and

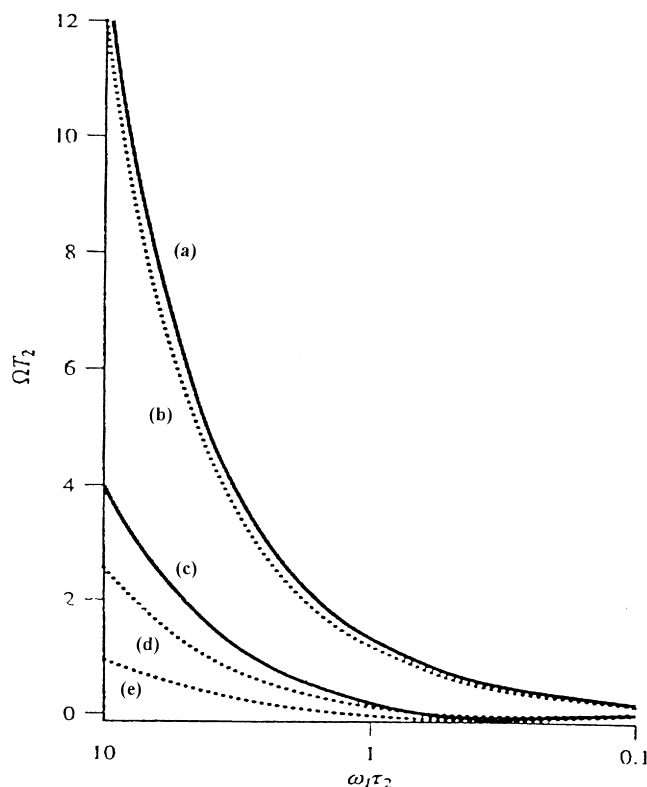


Fig. 56. Plot of the quadrupole-induced dynamic frequency shift  $\Omega_{mm'}$  measured in units of  $(1/T_2)_{mm'}$  for various coherences having no adiabatic linewidth contribution. The parameter  $\Omega T_2$  equals the DFS/halfwidth-at-halfheight ratio. Only the magnitude and not the sign of the shift is considered. The solid curves (a) and (c) are for  $I = (3/2)$  and the dotted curves (b), (d) and (e) are for  $I = (5/2)$  spins. The various transitions are (a)  $\Omega_{3/2,-3/2}$  ( $I = \frac{3}{2}$ ) (b)  $\Omega_{5/2,-5/2}$  ( $I = \frac{5}{2}$ ) (c)  $\Omega_{1/2,-1/2}$  ( $I = \frac{3}{2}$ ) (d)  $\Omega_{1/2,-1/2}$  ( $I = \frac{5}{2}$ ) (e)  $\Omega_{3/2,-3/2}$  ( $I = \frac{5}{2}$ ). [Reproduced with permission from L.G. Werbelow, R.E. London, Conc. Magn. Reson. 8 (1996) 325].

$\omega_I = \gamma_I B_0$ . The DFS is obtained as [313,332]:

$$\Omega_{s,m} = \frac{\gamma_I}{|\gamma_I|} \left[ \frac{4}{s(2s-1)} \right] [s(s+1) - 3m^2] K^{Q_S \cdot D_{IS}}(\omega_S) \quad (192)$$

Simulations of the  $^{13}\text{C}$  line shape for a  $^{13}\text{C}$ - $^2\text{H}$  spin system for various values of the rotational correlation time  $\tau$  are shown in Fig. 57 [313]. It is seen from Fig. 57 that under extreme narrowing conditions, the expected symmetric triplet is obtained. The multiplet structure collapses near the  $T_1$  minimum. In the slow motion regime, the multiplet structure reappears with a markedly noncentrosymmetric line shape. Experimentally such nonsymmetric lineshapes have been observed (Fig. 58) in  $^{13}\text{C}_\alpha$  triplets in an  $^1\text{H}$ - $^{13}\text{C}$

correlation spectrum of monodeuterated glycine residues in a small protein, *E. coli* thioredoxin, in the absence of  $^2\text{H}$  decoupling [283]. The observed DFS arises through cross-correlations between dipolar and quadrupolar relaxation. Simulation of similar line-shape features have been reported for various spin systems, namely  $^{13}\text{C}$ - $^{11}\text{B}$  [332], (Fig. 59), and  $^{31}\text{P}$ - $^{17}\text{O}$  [332] (Figs. 60 and 61). Figs. 60 and 61 contain simulations with varying quadrupolar coupling and magnetic field strengths. From these figures, it is evident that the multiplet resolution increases at slower correlation times and/or higher magnetic field strengths. The former in any case depends on various other relaxation mechanisms like dipolar interactions with other spins and CSA contributions. These simulated patterns obtained

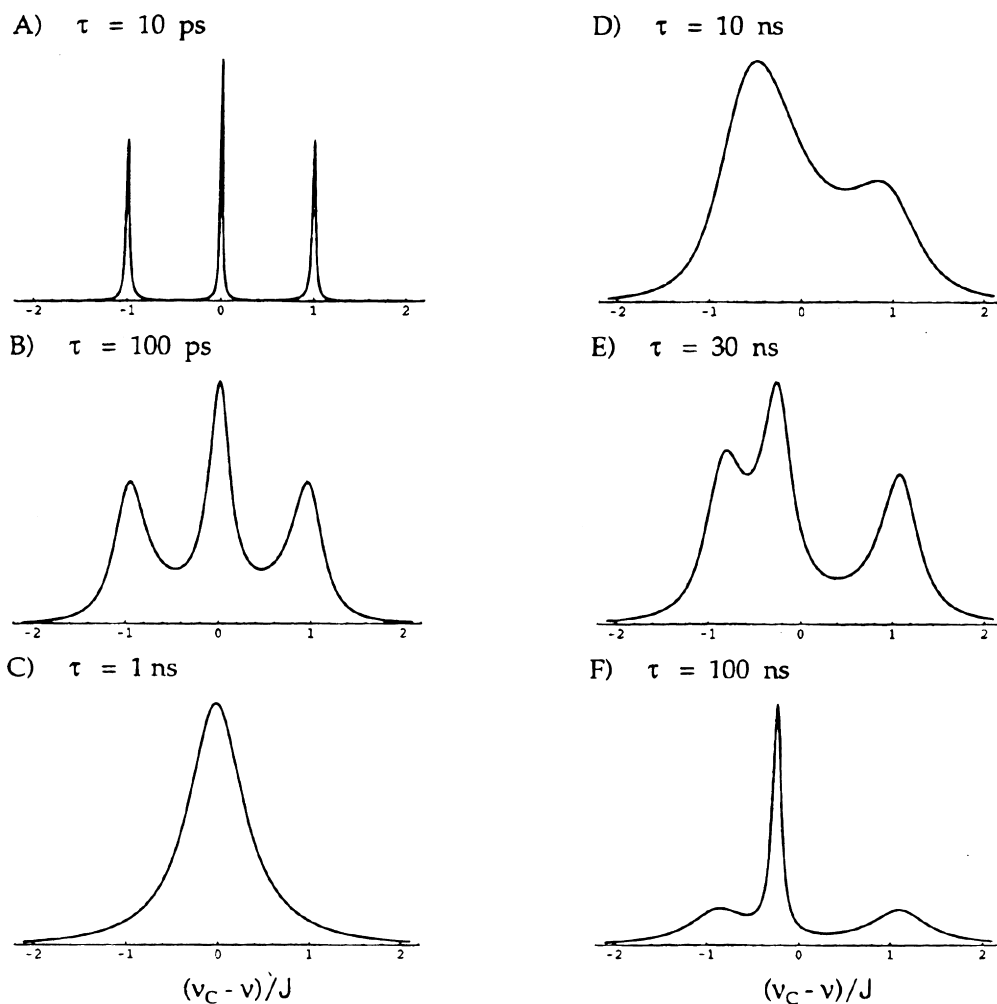


Fig. 57. Spectral simulations of the  $^{13}\text{C}$  spectra for the  $^{13}\text{C}$ - $^2\text{H}$  spin grouping. The  $^{13}\text{C}$ - $^2\text{H}$  dipole-dipole coupling constant was +3.6 kHz ( $r_{\text{CD}} = 1.09 \text{ \AA}$ ,  $^1J_{\text{CD}}$  was +20 Hz and quadrupole coupling constant +170 kHz, are based upon commonly accepted values. It is also assumed that the dipolar and quadrupolar interaction are completely correlated [ $J^{\text{Q-D}}(\omega) = \{J^{\text{Q}}(\omega)J^{\text{D}}(\omega)\}^{\frac{1}{2}}$ ] and the applied field strength is 11.75 T. Simulations (A) through (F) correspond to isotropic reorientation with a correlation time  $\tau = 10 \text{ ps}$ ,  $100 \text{ ps}$ ,  $1 \text{ ns}$ ,  $10 \text{ ns}$ ,  $30 \text{ ns}$  and  $100 \text{ ns}$ , respectively. [Reproduced with permission from L.G. Werbelow, R.E. London, Conc. Magn. Reson. 8 (1996) 325].

from an appropriate blend of structural and dynamic parameters range from highly resolved spectra with anomalous intensity distributions and unequal peak separations, to partially collapsed spectra showing linewidth asymmetries arising from DFS due to cross-correlations. The sensitivity of these lineshapes to structural and dynamical parameters provides an elegant way for investigating the motional characteristics of the corresponding spin systems.

The simulations listed above carry additional attraction because many of the recent developments in high resolution multi-dimensional NMR methods for the determination of structure of biomolecules employ extensively  $^{13}\text{C}$ ,  $^{15}\text{N}$  and  $^2\text{H}$  labeling of the molecules [307,332–336]. These labeled spin systems will have fragments containing spin-1/2 spin-1 which are directly bonded to each other and they may have a J-coupling interaction between them. Although the

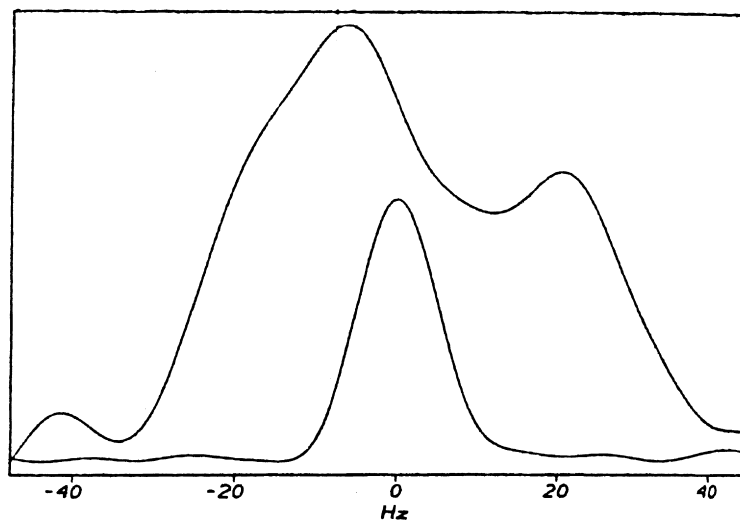


Fig. 58. Upper trace:  $F_1$  slice of a  $^2\text{H}$ -coupled  $^2\text{H}$ - $^{13}\text{C}$  HSQC spectrum of  $[2-^2\text{H}_\alpha, 2-^{13}\text{C}]$  glycine enriched *E. coli* thioredoxin drawn through the Gly-74 resonance. Lower trace: The corresponding  $F_1$  slice obtained using broad-band  $^2\text{H}$  decoupling (attenuated six-fold relative to the  $^2\text{H}$ -coupled spectrum). These spectra were obtained at 14.1 T under conditions corresponding to a 8.1 ns correlation time. [Reproduced with permission from R.E. London, D.M. LeMaster, L.G. Werbelow, *J. Am. Chem. Soc.* 116 (1994) 8400.]

J-couplings can be masked by the quadrupolar interactions, there could be a residual line broadening. This broadening could be reduced by RF irradiation in the vicinity of the resonance of the quadrupolar nucleus. Murali and Rao [311] have extensively studied the lineshapes of a spin-1/2 nucleus coupled to a quadrupolar nucleus (of spin-1) subjected to RF irradiation, in the presence of a cross-correlation induced DFS (Fig. 62). For the system they have considered, DFS with respect to the spin-spin multiplet arise from the dipole-quadrupole cross-correlation terms of the spin ( $S = 1$ ) and from the CSA-dipole cross-correlation term of spin [ $I = (1/2)$ ]. This figure shows that the DFS causes asymmetric multiplet patterns, which collapse under RF irradiation, along with disappearance of the DFS.

### 6.5. Experimental observations of the dynamic frequency shifts

It has been observed that there is a considerable line narrowing of  $^{13}\text{C}_\alpha$  resonances on perdeuteration of proteins calcineurin B [316] and thioredoxin [333]. The  $^2\text{H}$ -coupled  $^{13}\text{C}$  multiplets in these proteins exhibit asymmetrical patterns (Fig. 58), which have been

explained as due to dipole-quadrupole cross-correlation induced DFS [283]. The  $^{13}\text{C}$  spectrum of perdeuterated glycerol (Fig. 63) consists of a triplet for the central methine carbon, which broadens when the temperature is lowered from 333 K, and collapses to a broad singlet at around 293 K, the temperature corresponding to the  $T_1$  minimum of deuterium. On further lowering of temperature, the lines become narrow again, showing an asymmetric triplet between 283 and 268 K. These features have been reproduced via simulations and ascribed to CSA-quadrupole cross-correlation induced DFS [315].

One of the earliest observations of DFS in NMR is by Marshall et al. [337] by a lineshape analysis of  $^{23}\text{Na}$  in an aqueous sodium laurate/lauric acid solution. For a spin-3/2 nuclei, the theoretical spectrum (Fig. 64), has two transitions of different chemical shifts and widths. The narrow component arises from  $(1/2) \rightarrow -(1/2)$  transition, while the broad component arises from  $(3/2) \rightarrow (1/2)$  and  $-(1/2) \rightarrow -(3/2)$  transitions. The chemical shift is due to different DFS. Marshall et al. [337] observed that the asymmetry in the composite peak in Fig. 64 is difficult to establish experimentally since it cannot be distinguished from a small phase misadjustment and

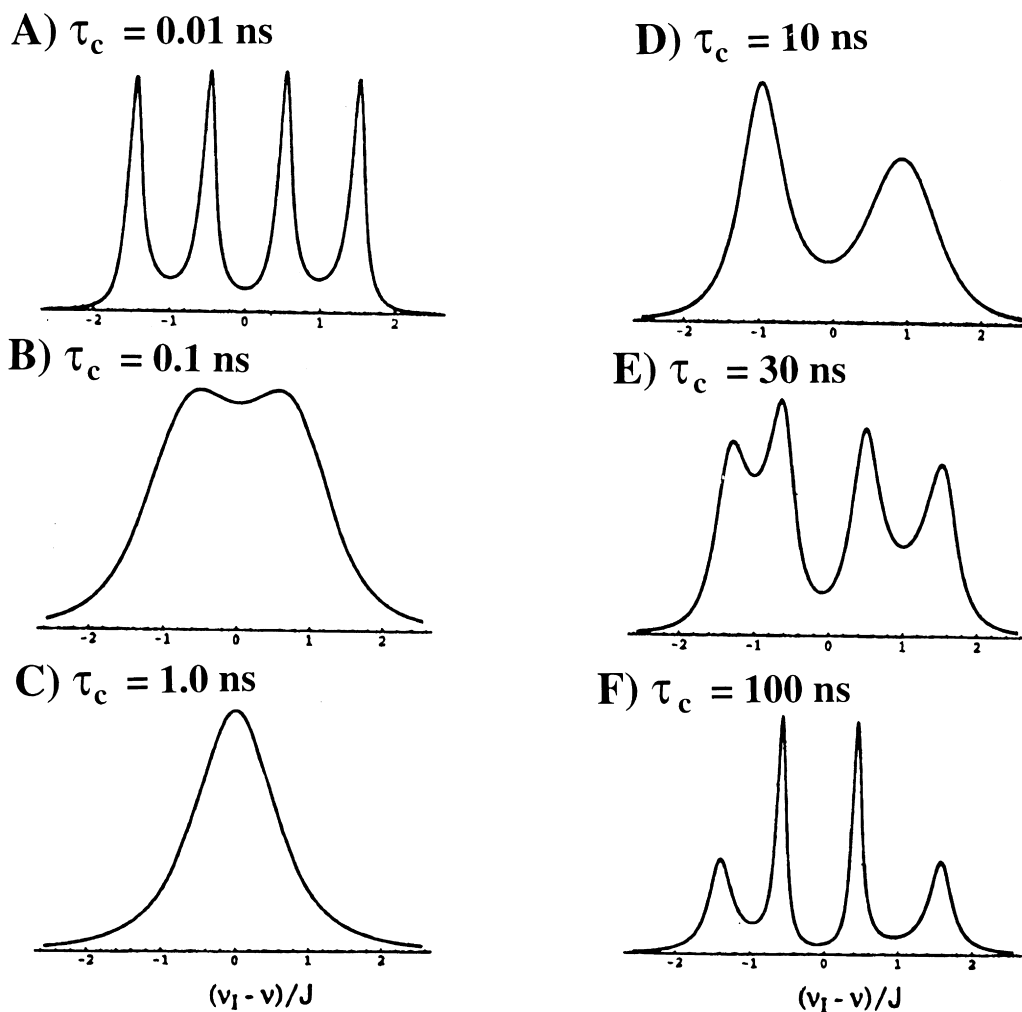


Fig. 59. Spectral simulations of the  $^{13}\text{C}$  spectra for a directly bonded boron nucleus. The  $^{11}\text{B}$ – $^{13}\text{C}$  dipole–dipole coupling constant ( $\gamma_{\text{C}}\gamma_{\text{B}}r_{\text{CB}}^{-3}/2\pi = +2.55$  kHz),  $^1\text{J}_{\text{BC}}$  scalar coupling constant (+60 Hz) and quadrupole coupling constant, ( $e^2qQ_{\text{C}}/h = +1$  MHz) are based upon literature values. The assumed field strength is 11.75 T. It is assumed that the dipolar and quadrupolar interactions are completely correlated. Shielding anisotropies are assumed to be negligible. Simulations (A)–(F) correspond to isotropic reorientation with  $\tau_{\text{c}} = 10$  ps, 100 ps, 1 ns, 30 ns and 100 ns, respectively. [Reproduced with permission from L.G. Werbelow, G. Pouzard, *J. Phys. Chem.* 85 (1981) 3887.]

could be overlooked. They have used the extraordinary sensitivity of the dispersion vs. absorption (DISPA) plot, to highlight deviations from a Lorentzian line shape, substantiating the existence of two chemically shifted peaks. The DISPA plot of the  $^{23}\text{Na}$  spectrum of ordinary NaCl in  $\text{D}_2\text{O}$  [Fig. 65(a)] is reflective of a near Lorentzian shape. On the other hand, the DISPA plot for the sodium ion spectrum in a

laurate/lauric acid mixture [Fig. 65(b)] deviates significantly from Lorentzian shape, yielding an asymmetric composite peak, establishing the DFS.

Tromp et al. [318] have shown that the observation and quantification of the DFS by an analysis of line-shape can be complemented by the calculation of the shift from the field dependent relaxation rates. The lineshape analysis is done for  $^{23}\text{Na}$  in an isotropic

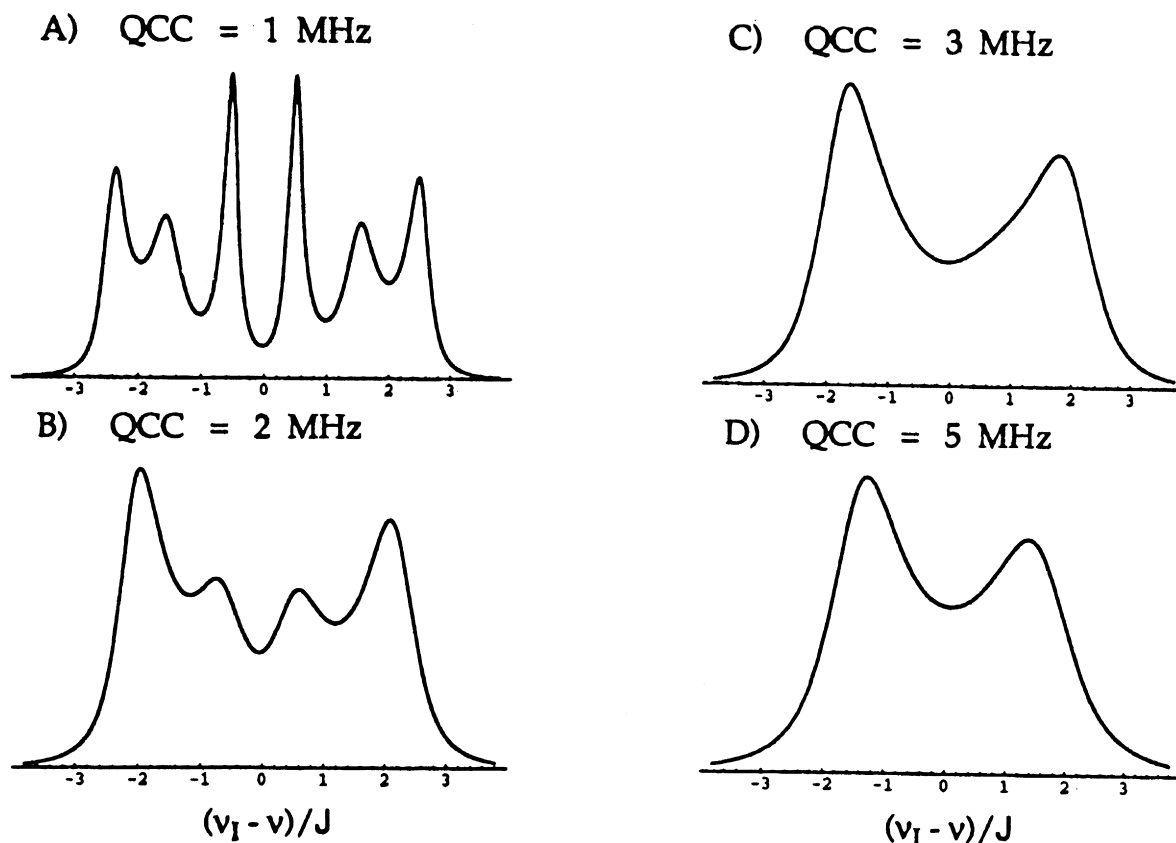


Fig. 60. Spectral simulations of the  $^{31}\text{P}$  spectra for a directly bonded oxygen-17 nucleus. The  $^{17}\text{O}$ - $^{31}\text{P}$  dipole-dipole coupling constant ( $\gamma_{\text{P}}\gamma_{\text{O}}r_{\text{PO}}^{-3}\hbar/2\pi = 2.0$  kHz), and  $^1\text{J}_{\text{PO}}$  scalar coupling constant (200 Hz) are typical. The applied field strength is taken as 11.75 T. It is assumed that the dipolar and quadrupolar interaction are completely correlated  $\{J^{\text{Q,D}}(\omega) = [J^{\text{Q}}(\omega)J^{\text{D}}(\omega)]^{1/2}\}$  and motions are isotropic with a correlation time of 30 ns. Shielding anisotropies are assumed negligible. Simulations (A)–(D) correspond to quadrupole couplings,  $e^2qQ_s/h$  of +1, +2, +3 and +5 MHz, respectively. [Reproduced with permission from L.G. Werbelow, G. Pouzard, J. Phys. Chem. 85 (1981) 3887.]

medium of crosslinked aqueous NaPSS (sodium polystyrene sulfonate) in which the sodium relaxation is far from the extreme narrowing limit. They have also systematically observed the field dependence of the DFS. The measurement of the DFS for single quantum coherences has been difficult since the shifts are comparable to the linewidths. However, in  $I = (3/2)$  systems, it has been theoretically shown that the DFS for triple quantum coherence can be larger than its linewidth, allowing clear observation of DFS [338]. Eliav et al. [339,340] have presented the experimental observation of a triple quantum DFS in solution. The DFS was measured on the triple quantum spectrum of  $^{23}\text{Na}$  in 4,7,13,16,21-pentaoxa-1,10-diazabi-

cyclo[8.8.5] tricosane, dissolved in glycerol. The relaxation times of the triple quantum coherence and the triple quantum DFS were measured by the 2D pulse sequence,  $90^\circ - \tau/2 - 180^\circ - \tau/2 - 90^\circ - t_1 - 90^\circ - t_2$  (acq). They have observed that the DFS is larger at the lower temperature where the decay rate is smaller. Recently another interesting experimental observation of DFS is the  $^{13}\text{C}$  triplet of doubly labeled D-glucose complexed to *E. coli* periplasmic glucose/galactose receptor, and it is shown that an asymmetrical triplet can arise due to DFS from cross-correlation between the  $^{13}\text{C}$ - $^2\text{H}$  dipolar interaction and the quadrupolar relaxation of deuterium (Fig. 66) [341].

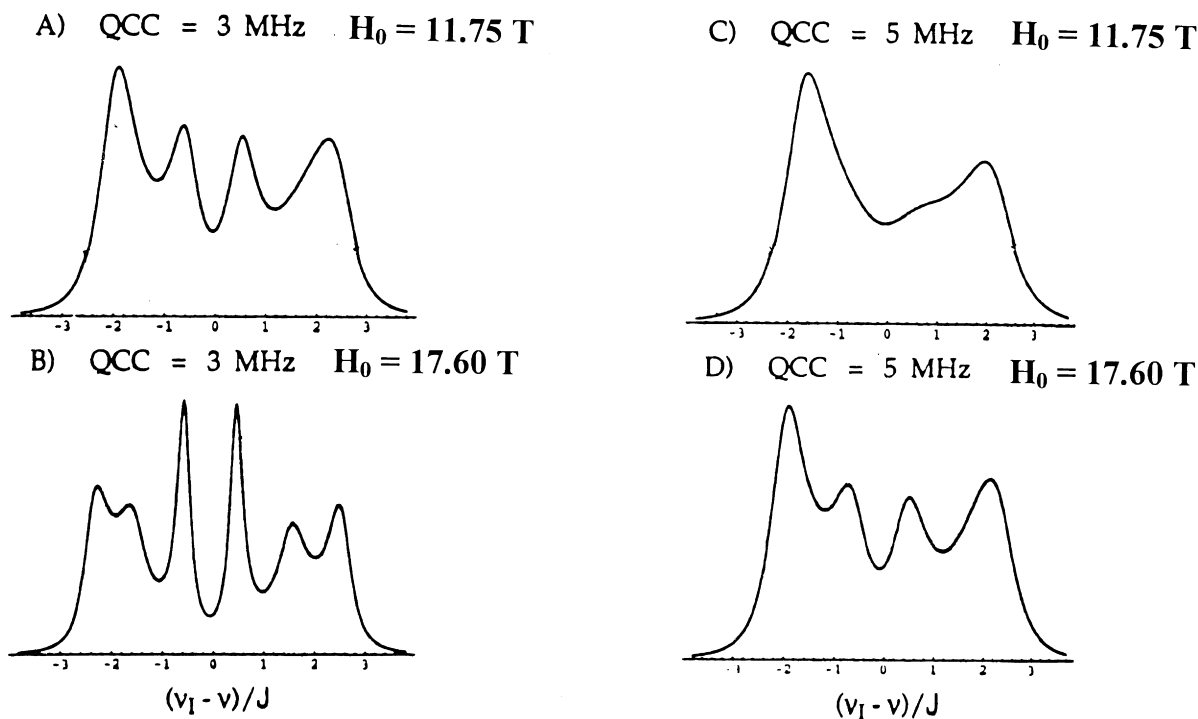


Fig. 61. Spectral simulations of the  $^{31}\text{P}$  spectra for a directly bonded  $^{17}\text{O}$  nucleus. An isotropic correlation time of 100 ns is assumed. Other relevant parameters are as indicated in Fig. 60. For (A)  $e^2qQ_s/h = +3$  MHz,  $B_0 = 11.75$  T; for (B)  $e^2qQ_s/h = +3$  MHz,  $B_0 = 17.60$  T; for (C)  $e^2qQ_s/h = +5$  MHz,  $B_0 = 11.75$  T; for (D)  $e^2qQ_s/h = +5$  MHz,  $B_0 = 17.60$  T. [Reproduced with permission from L.G. Werbelow, G. Pouzard, *J. Phys. Chem.* 85 (1981) 3887].

## 7. Other recent developments

Cross-correlations have gained significant interest in recent years with the advent of high-field spectrometers. At the high fields produced by superconducting magnets, the CSA has increased proportionally and its cross-correlation with dipolar interactions has become routinely observable. A large number of studies are directed towards DLB and narrowing produced by cross-correlations in single as well as multiple quantum coherences in  $^{13}\text{C}$ ,  $^{15}\text{N}$ ,  $^2\text{H}$  labeled biomolecules. Major attention is focused on spectral densities at zero frequencies, which increase in value for large molecules in the long correlation limit. Furthermore, the large CSA tensors of  $^{13}\text{C}$  and  $^{15}\text{N}$  at high fields are contributing significantly to cross-correlations with dipolar relaxation. Recently, there have been several observations of cross-correlations from Curie relaxation in paramagnetic proteins, at

high fields. Some of the recent experimental results are discussed in the following sections.

### 7.1. Cross-correlations in paramagnetic molecules

Cross-correlation between dipole–dipole relaxation and paramagnetic relaxation can play an important role in paramagnetic proteins [342,343]. Anomalous cross peaks have been observed in the COSY spectra of metalloproteins containing paramagnetic species and they were attributed to cross-correlation between the interproton dipole–dipole interaction and the Curie spin relaxation (CSR) (Fig. 67) [344]. These cross peaks in COSY spectra in the absence of scalar coupling arise from cross-correlation induced coherence transfer and can be distinguished from scalar coupling cross peaks by their phase with respect to the diagonal. While similar relaxation-induced cross peaks have been reported

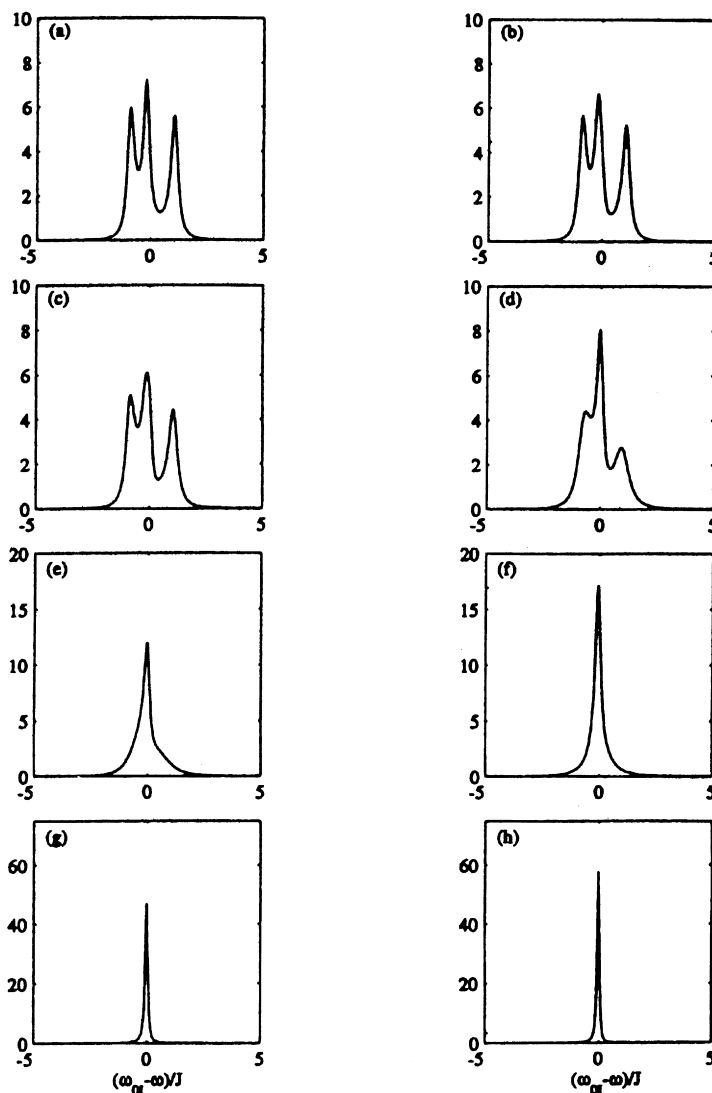


Fig. 62. Simulated  $^{13}\text{C}$  spectra of a  $^{13}\text{C}$ - $^2\text{H}$  spin system with the dynamic frequency shifts arising from the quadrupole-dipole cross-correlation included. The spectra were plotted as a function of  $(\omega_{0I} - \omega)/J$ . The parameters used in the simulation are  $J/2\pi(^{13}\text{C}-^2\text{H}) = 22$  Hz,  $\tau_c = 20$  ns,  $e^2qQ = 1.1 \times 10^6 \text{ s}^{-1}$  and the proton Larmor frequency was set at 600 MHz. The irradiation amplitudes  $\nu_r = \omega_r/2\pi$  in (a) 0, (b) 11, (c) 22, (d) 50, (e) 100, (f) 150, (g) 500 and (h) 1000 Hz. Note that the vertical scales are not the same in all the figures. [Reproduced with permission from N. Murali, B.D.N. Rao, J. Magn. Reson. A 118 (1996) 202.]

due to other cross-correlations, they can be quite pronounced for paramagnetic compounds even when the NMR signals are broad. Hence the report of COSY cross peaks even for linewidths as large as 500–1000 Hz should be taken as a caveat.

Bertini et al. have shown that CSR is often the dominant source of proton line broadening in para-

magnetic macromolecules and it effectively acts as a CSA relaxation mechanism [345–348]. The CSR mechanism is due to the dipolar coupling of each nucleus with the time-averaged electron magnetic moment induced by the external magnetic field. It may be noted that like CSA, the CSR also increases with the magnetic field and becomes quite prominent

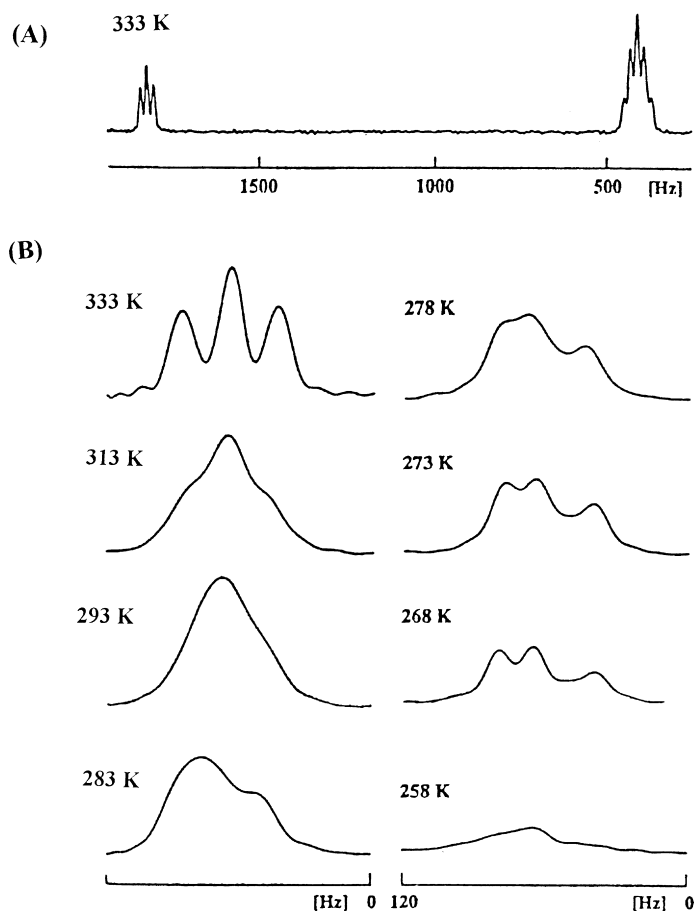


Fig. 63.  $^{13}\text{C}$  natural abundance spectrum of glycerol- $\text{d}_8$  at various temperatures at a magnetic field strength corresponding to a 600 MHz proton Larmor frequency. (A) Complete spectrum at 333 K. (B) Spectral region of the methine triplet in the temperature range from 333 to 258 K. Spectra were recorded with the spectrometer in the unlocked mode; therefore the reference frequency is arbitrary. A total of 32 transients were recorded per spectrum. [Reproduced with permission from S. Grzesiek, Ad Bax, J. Am. Chem. Soc. 116 (1994) 10196.]

at high magnetic fields. They also found that although cross-correlation effects are the largest when the CSR and dipolar interactions are nearly equal, they remain significant up to a ratio of 100. They have critically surveyed the literature reporting the observation of COSY cross peaks in paramagnetic metalloproteins and found that the ratio of the relaxation-induced effect to the scalar effect could be as high as 700. True scalar cross peaks may be expected for small metalloproteins, if the electron spin multiplicity is small and the scalar coupling constant is large. It may be noted that the relaxation-induced peaks are a rich source of structural and geometric information.

Maler et al. have investigated the influence of para-

magnetic cross-correlation effects on the longitudinal relaxation of small molecules, such as *cis*-chloroacrylic acid in solution in the presence of  $\text{Ni}^{2+}$  ions with the two olefinic protons constituting an isolated AX spin system [349]. Differential relaxation was observed in the presence of nickel ions due to cross-correlations between dipole–dipole and CSR [349]. In an interesting study, it is shown that the change of  $J$  due to cross-correlation induced DFS between CSR and dipole–dipole relaxation can interfere with the change in splittings due to small residual dipolar couplings arising from slight orientations of paramagnetic proteins in high field [350]. This study points out that these should be carefully discriminated. In

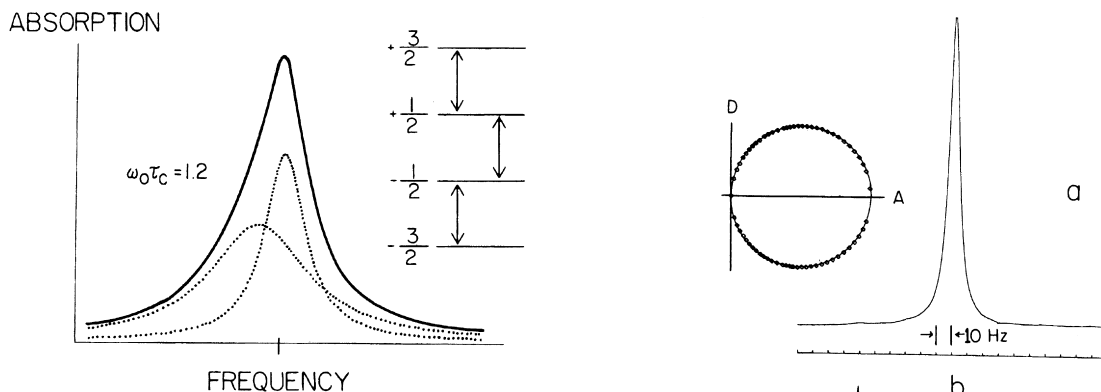


Fig. 64. Energy-level diagram (right) and single-quantum NMR spectrum (left) for a spin-(3/2) nucleus with rotational correlation time  $\tau_c = 1.2/\omega_0 = 15$  ns for  $^{23}\text{Na}$  at 7.0 T. The narrow component line arises from the  $-(1/2)$  to  $(1/2)$  transition and the broad component from the  $+(1/2)$  to  $+(3/2)$  and  $-(3/2)$  to  $-(1/2)$  transitions. Note the distinct chemical shift difference between the broad and the narrow transitions. [Reproduced with permission from A.G. Marshall, T. Cottrell, L.G. Werbelow, *J. Am. Chem. Soc.* 104 (1982) 7665.]

another recent study of uniformly  $^{15}\text{N}$ -labeled cytochrome  $\text{C}_3$ , the relative linewidths of the doublet peaks of the  $^{15}\text{N}$ -coupled imido proton of the coordinated imidazole group were reversed on oxidation (Fig. 68) [351]. This inversion has been explained by the interference between the electron–proton dipolar and  $^{15}\text{N}$ – $^1\text{H}$  dipolar interactions. Such an effect can be used to assign the imido protons of the coordinated imidazole groups in heme proteins. The electron–proton dipolar cross-correlation is thus another source of structural information in the investigation of paramagnetic proteins [352–354].

## 7.2. Determination of chemical shift anisotropy

The CSA of various nuclei in peptides has been determined with the help of solid-state NMR techniques [355–357]. In solution, by measuring the CSA–dipole cross-correlation rate one can determine the CSA. Recently, many groups have measured the  $^{15}\text{N}$ ,  $^{13}\text{C}$  and  $^1\text{H}$  CSA in several proteins by monitoring the differential relaxation of the spin multiplets.

### 7.2.1. $^{15}\text{N}$ CSA measurements

Dalvit [358] demonstrated the feasibility of transfer

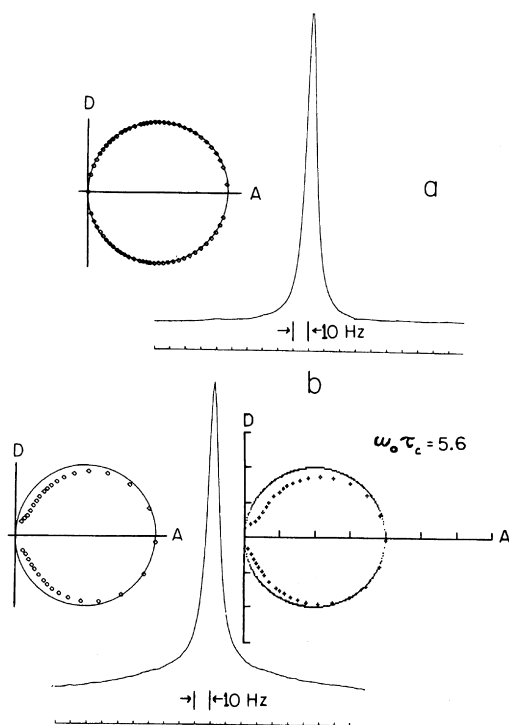


Fig. 65. (a) Experimental  $^{23}\text{Na}$  NMR spectrum and its corresponding DISPA plot for 1.0 M NaCl in  $\text{D}_2\text{O}$ , obtained from Fourier transformation of an unapodized 4096-point time-domain data set at a spectrometer frequency of 79.388 MHz, with a  $90^\circ$  excitation pulse (44  $\mu\text{s}$ ), for one cycle of an 8-pulse phase-alternating sequence. The close fit of the experimental data to the DISPA reference circle indicates a near-perfect Lorentzian line shape. (b) Experimental  $^{23}\text{Na}$  NMR spectrum and its corresponding DISPA plot (left) for 120 mM NaCl, 20 mM sodium laurate and 5 mM lauric acid in aqueous (15%  $\text{D}_2\text{O}$ ) solution. The sample was milky white, with a sodium laurate concentration of about twice the critical micelle concentration for 0.1 M NaCl solutions of sodium laurate. Detection was as in (a), except for a  $20^\circ$  excitation pulse width. The experimental DISPA plot (left) closely matches with that computed for  $\omega_0\tau_c = 5.6$  (right). [Reproduced with permission from A.G. Marshall, T. Cottrell, L.G. Werbelow, *J. Am. Chem. Soc.* 104 (1982) 7665.]

of polarization from  $^1\text{H}$  to  $^{15}\text{N}$  arising from cross-correlation between the proton CSA and proton–nitrogen dipolar relaxation mechanisms in a fully  $^{15}\text{N}$  labeled protein. The proton magnetization was initially spin locked during which the single spin order of the proton  $I_X$  was partially converted into  $2I_X S_Z$  via the CSA( $^1\text{H}$ )–dipole( $^1\text{H}$ – $^{15}\text{N}$ ) cross-correlation, which was detected in a 2D HSQC experiment. A large

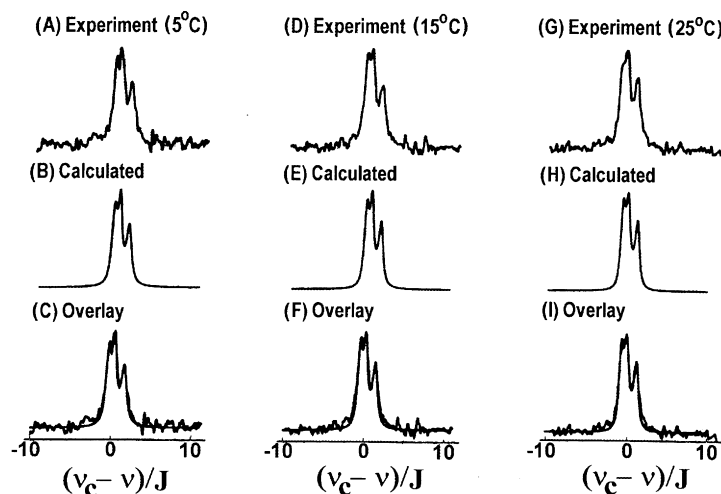


Fig. 66. Simulation of the observed  $^{13}\text{C}$  triplet arising from its coupling to deuterium of D-[1- $^{13}\text{C}$ , 1- $^2\text{H}$ ] glucose complexed with *E. coli* periplasmic glucose/galactose receptor. A, D and G are the experimental spectra, recorded respectively at 5, 15 and 25°C and at 125 MHz. B, E and H are the corresponding simulated spectra. C, F and I show the overlaps confirming the DFS arising from the cross-correlation between the  $^{13}\text{C}$ – $^2\text{H}$  dipolar interaction and the deuteron quadrupolar relaxation, in these systems. For other details see Ref. [341]. [Reproduced with permission from S.A. Gabel, L.A. Luck, L.G. Werbelow, R.E. London, *J. Magn. Reson.* 128 (1997) 101.]

number of cross peaks with varying intensity, indicative of variation in the magnitude and direction of the CSA tensor with respect to the dipolar axis, were observed.

Tjandra et al. [239] measured the  $^{15}\text{N}$  CSA tensor in uniformly  $^{15}\text{N}$ -enriched human ubiquitin utilizing the cross-correlation between the  $^{15}\text{N}$ -CSA and  $^{15}\text{N}$ – $^1\text{H}$  dipolar relaxation. The experiment is essentially a HSQC ( $^{15}\text{N}$ – $^1\text{H}$  correlation) experiment, with a relaxation period  $2\Delta$  inserted before the  $^{15}\text{N}$  evolution period during which the CSA–dipole cross-correlation converts the antiphase  $^{15}\text{N}$  magnetization into inphase  $^{15}\text{N}$  magnetization. Two spectra were recorded: one in which the operator terms arising from  $^{15}\text{N}$  CSA–dipole cross-correlation terms are selected (experiment A) and a reference experiment (B) in which they are suppressed (by combined use of additional pulses on the proton channel and gradients). The intensity ratio of the cross peaks in the two experiments has been shown to follow the relation:

$$\frac{I_A}{I_B} = \tanh(2\Delta\delta_{IS}), \quad (193)$$

where  $\delta_{IS}$  is the CSA–dipole cross-correlation in

which  $I = ^{15}\text{N}$  and  $S = ^1\text{H}$ . Significant variation in the intensities of the peaks as a function of residue number was observed. These were then reduced using a local order parameter to  $\text{CSA}^{\text{red}} = S^2(\sigma_{\parallel} - \sigma_{\perp})P_2(\cos \theta)$  where  $\theta$  is the angle between the principal axis of the CSA tensor and the dipolar vector,  $S^2$  is the generalized order parameter [359] and  $\Delta\sigma = (\sigma_{\parallel} - \sigma_{\perp})$  is the CSA anisotropy. The variation in observed intensity thus could be due to a variation in any of these parameters. The observed  $\text{CSA}^{\text{red}}/S^2$  shows a good correlation with the observed isotropic  $^{15}\text{N}$  chemical shift, indicating that the sum of the most shielded CSA tensor components is largely invariant to structural changes.

#### 7.2.2. $^1\text{H}$ CSA measurements

Tjandra and Bax have also measured the amide proton CSA in  $^{15}\text{N}$ -enriched ubiquitin and perdeuterated HIV-1-protease, by modifying the pulse scheme in two different ways [240]. In the first method, the relaxation delay  $2\Delta$  is incorporated in the proton evolution before transfer of magnetization to  $^{15}\text{N}$ , followed by a normal HSQC, experiment and as before a reference experiment is obtained by incorporating a  $\pi$  pulse on  $^{15}\text{N}$  during the period  $\Delta$ . The ratio

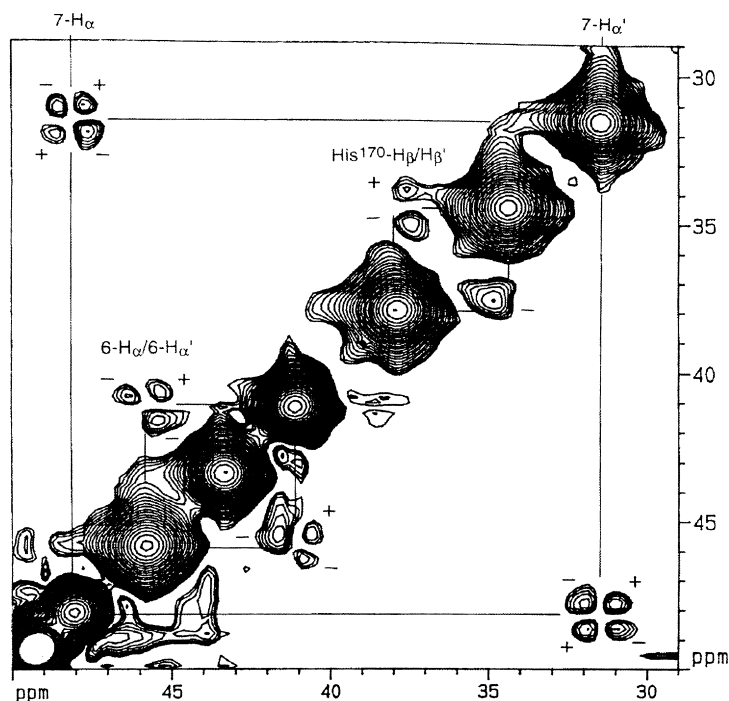


Fig. 67. Downfield region of the 360 MHz phase-sensitive COSY spectrum of horseradish peroxidase in  $D_2O$  at pH 7.0 and  $55^\circ C$ . The nearly absorptive antiphase cross peak between the well-resolved  $7-H_\alpha$  and  $7-H_{\alpha'}$  resonances shows the predominance of the cross-correlation effect between interproton dipolar relaxation and Curie spin relaxation (CSR). The slight asymmetry of the cross peak is due to non-negligible J-coupling effects. The diagonal peak is phased to be positive, and positive and negative components of the cross-peak multiplet are marked “+” and “-”, respectively. Cross peaks between  $His^{170}-C^\beta H$  and  $-C^\beta H'$  and between  $6-H_\alpha$  and  $6-H_{\alpha'}$  of the heme are distorted due to their proximity to the approximately 50 times more intense diagonal resonances. [Reproduced with permission from J. Qin, F. Delaglio, G.N. La Mar, A. Bax, *J. Magn. Reson. B* 102 (1993) 332.]

of the intensities follow the same hyperbolic tangent dependence as in Eq. (193). In a second experiment, they have utilized the constant time evolution period and expanded it to a 3D experiment. The advantage is that instead of running two experiments, with and without cross-correlations, one resolves the  $^{15}N$ -coupled proton doublet in the  $F_1$  dimension, the  $^{15}N$  chemical shift in  $F_2$ , and the  $^1H$  chemical shift in  $F_3$ . The ratio of the intensity of the components of the proton doublet is given by:

$$\frac{I_1}{I_2} = \exp(-4T\delta_{S,IS}), \quad (194)$$

where  $\delta_{S,IS}$  is the proton ( $S$ ) CSA and  $IS$  is the proton–nitrogen dipolar interaction. The measured proton CSA is found to be large in  $\beta$ -sheets and

considerably smaller in  $\alpha$ -helices. This has been correlated with the length of the hydrogen bond, which is longer in helices compared to  $\beta$ -sheet in these proteins (Fig. 69).

Tessari et al. [241] have also measured the amide proton CSA in  $^{15}N$ -labeled proteins using modified constant time HSQC experiments. The pulse schemes are shown in Fig. 70. The constant relaxation period is inserted in  $^{15}N$  evolution after INEPT transfer of polarization from proton to  $^{15}N$  in scheme A, in which the  $^{15}N$ -CSA,  $^{15}N$ – $^1H$  dipolar cross-correlation plays the role. In scheme B, the constant relaxation period is inserted before polarization transfer to  $^{15}N$ , such that the  $^1H$ -CSA,  $^1H$ – $^{15}N$  dipolar cross-correlation is active. The remaining part of the sequence is the same as the HSQC experiment. In each case, two

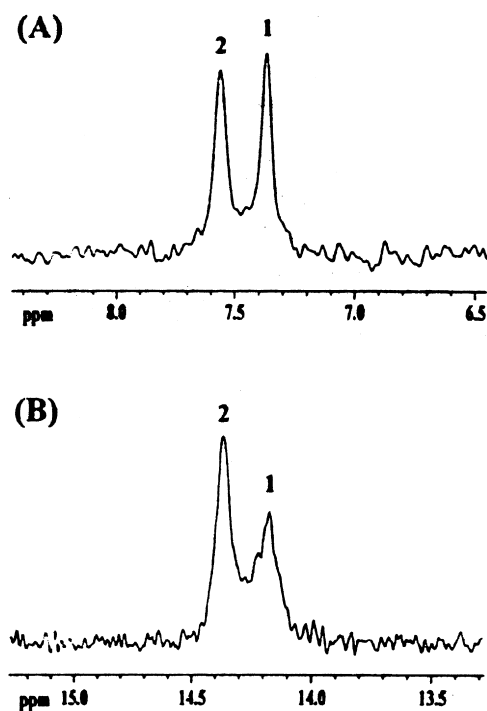


Fig. 68. Proton NMR spectra of the imidazole imido proton of His-52 of uniformly  $^{15}\text{N}$ -labeled cytochrome  $\text{C}_3$  from *Desulfovibrio vulgaris* Miyazaki F in the fully reduced (A) and fully oxidized (B) states. HMQC spectra were obtained with a Bruker AMX-500 MHz NMR spectrometer at  $30^\circ\text{C}$ . The protein was dissolved in a 20 mM phosphate buffer (90%  $^1\text{H}_2\text{O}/10\%$   $^2\text{H}_2\text{O}$ ), at (A) pH 7.0 and (B) pH 5.0. Partial slices for the proton dimension are presented. [Reproduced with permission from T. Ohmura, E. Harada, T. Fujiwara, G. Kawai, K. Watanabe, H. Akutsu, J. Magn. Reson. 131 (1998) 367.]

spectra are recorded: one in which the CSA–dipole cross-correlations are retained and a reference experiment in which they are suppressed. The ratio of the intensity of a peak in these two experiments yields:

$$\ln \frac{I_{\text{cross}}}{I_{\text{ref}}} = 4\Delta\delta_{i,j}, \quad (195)$$

where  $i$  is the CSA of the selected spin of experiment A or B. This linear dependence of the intensity ratio on  $\Delta$  and  $\delta_{i,j}$  is prone to less errors than the hyperbolic tangent dependence of Eq. (193). They found significant variation in  $\delta_{\text{H,HN}}$  as a function of residue number and much less variation for  $\delta_{\text{N,NH}}$ . The results

from  $^{15}\text{N}$  studies indicate a globular, well-structured, isotropic tumbling protein, displaying similar dynamics for most residues. On the other hand, the  $^1\text{H}$  CSA–dipole cross-correlation rate depends upon the CSA of the amide proton and also on the mobility of the H–N bond vector, which gives rise to the variation in  $\delta_{\text{H,HN}}$ .

### 7.2.3. $^{13}\text{C}_\alpha$ CSA measurements

Recently Tjandra and Bax have also measured the  $^{13}\text{C}_\alpha$  CSA in  $^{13}\text{C}$ ,  $^{15}\text{N}$  uniformly doubly labeled proteins, by monitoring the differential relaxation of the  $^{13}\text{C}_\alpha$ – $\{^1\text{H}\}$  doublet, due to cross-correlation between the  $^{13}\text{C}_\alpha$  CSA and  $^{13}\text{C}_\alpha$ – $^1\text{H}_\alpha$  dipolar relaxation [360]. The methodology followed is identical to the  $^{15}\text{N}$  CSA measurement outlined above, except that here the INEPT polarization transfer is first to  $^{13}\text{C}_\alpha$  carbon using selective carbon  $\text{C}_\alpha$  pulses. During the constant  $\text{C}_\alpha$  relaxation period  $\Delta$ , the carbonyl carbons ( $\text{C}'$ ) are decoupled by using a selective  $180^\circ$  pulse in the middle of the  $\Delta$  period. Furthermore, during  $^{13}\text{C}_\alpha$  evolution period, the protons are decoupled by Waltz decoupling. The  $^{13}\text{C}_\alpha$  coherence is further transferred to  $^{15}\text{N}$  and a  $^{15}\text{N}$ – $^1\text{H}$  HSQC spectrum is obtained in which the intensity of the cross peak in spectrum A is dependent on the  $^{13}\text{C}_\alpha$  CSA,  $^{13}\text{C}_\alpha$ – $^1\text{H}_\alpha$  dipolar cross-correlation and in the reference spectrum B, the cross-correlation is suppressed by the use of a  $180^\circ$  proton pulse applied appropriately during the  $\Delta$  period. As before, the intensity ratio in the two experiments is given by Eq. (193). In a 3D version the  $\Delta$  period also includes frequency labeling of the  $^{13}\text{C}_\alpha$ , with the central  $180^\circ$  pulse on  $^{13}\text{C}_\alpha$  moving in concert with  $t_1$ . In the 3D version the relative intensity of the  $^{13}\text{C}_\alpha$ – $\{^1\text{H}_\alpha\}$  doublet components are measured, which equals  $\exp(-4\Delta\delta_{i,IS})$ . Both the experiments were applied to samples of uniformly enriched  $^{13}\text{C}$ ,  $^{15}\text{N}$ -ubiquitin and calmodulin complexed to a 26 residue unlabeled peptide fragment (M13) of skeletal muscle myosin light chain kinase. Large variations in  $^{13}\text{C}_\alpha$  CSA were observed which correlates well with the various secondary structure elements. For example,  $\sigma_{\parallel}-\sigma_{\perp}$  for  $^{13}\text{C}_\alpha$  in  $\beta$ -sheets is obtained as  $27.1 \pm 4.3$  ppm, while for  $\alpha$ -helices it was found to be  $6.1 \pm 4.9$  ppm [360].

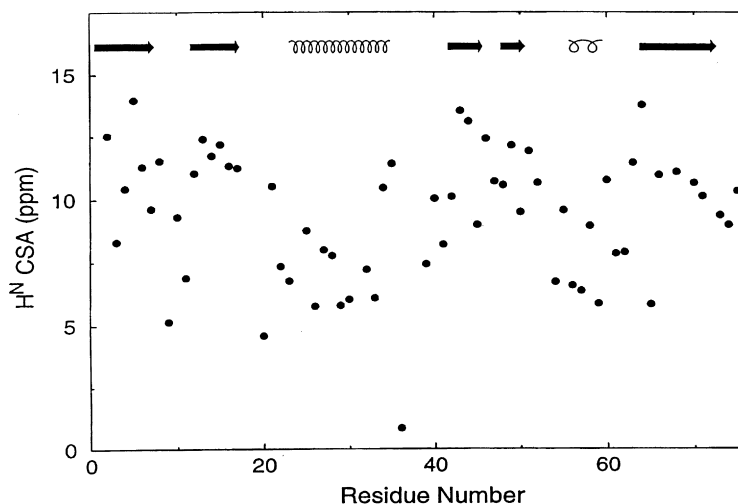


Fig. 69.  $H^N$  CSA calculated from the quantitative cross-correlation experiments, as a function of residue number for ubiquitin. The secondary structure of ubiquitin is marked at the top (solid arrow:  $\beta$ -sheet; small pitch coil:  $\alpha$ -helix; large pitch coil:  $3_{10}$ -helix). The CSA tensor is assumed to be axially symmetric with its unique axis collinear with the N–H bond direction. [Reproduced with permission from N. Tjandra, A. Bax, J. Am. Chem. Soc. 119 (1997) 8076.]

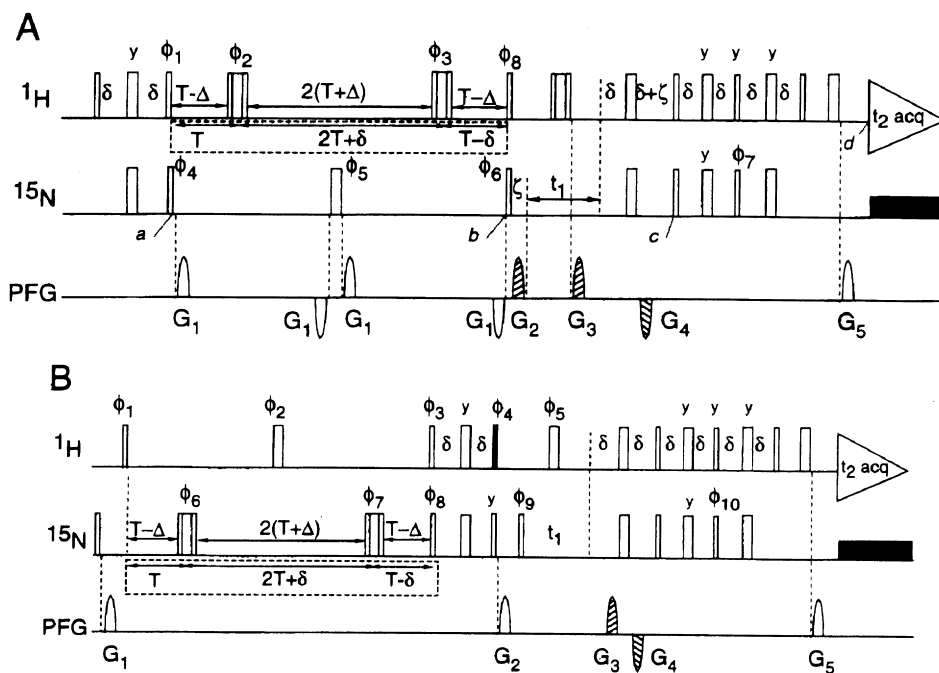


Fig. 70. Pulse sequence for quantitative measurement of (A)  $^{15}\text{N}$  CSA–dipole cross-correlations and (B)  $^1\text{H}$  N CSA–dipole cross-correlations. Narrow and wide bars denote pulses with a  $90^\circ$  and  $180^\circ$  flip angle, respectively. For both experiments, two variations of the pulse scheme are recorded selecting for magnetization arising from CSA–dipole pathways and a reference. For the reference experiment, the delays were chosen as indicated in the dashed boxes and the phase  $\phi_6$  (A) or  $\phi_3$  (B) was changed. All pulsed-field gradients (PFG) had a sine-bell shape and were applied along the Z-axis. [Reproduced with permission from M. Tessari, F.A.A. Mudler, R. Boelens, G.W. Vuister, J. Magn. Reson. 127 (1997) 128.]

### 7.3. Isolation of relaxation pathways by linear combination of various modes

#### 7.3.1. Longitudinal modes

Norwood et al. have utilized the idea of coadding the relaxation rates of various modes such that the relaxation of the sum is dependent only on the mutual dipolar relaxation of the two spins, free from all other relaxations, external to the two spins [361–363]. For longitudinal relaxation, this is shown by taking a three-spin system  $AMX$  [361]. The sum  $\rho_A + \rho_M - \rho_{AM}$  yields [see also Eq. (63)]:

$$\rho_A + \rho_M - \rho_{AM} = \left[\frac{2}{3}J_{AMAM}(\omega_A - \omega_M) + 4J_{AMAM}(\omega_A + \omega_M)\right] \quad (196)$$

This sum is only dependent on the mutual dipolar interaction between the two spins and is independent of all other auto and cross-correlation terms. Rates  $\rho_A$ ,  $\rho_M$  can be directly measured using selective inversion of  $A$  and  $M$  spins, under the initial rate approximation.  $\rho_{AM}$  can be measured using the sequence  $90_x^\circ(A) - \Delta - 90_y^\circ(A) - \tau - 90_{\phi+4}^\circ(A, M) - 90_{\phi 1}^\circ(A, M) - \text{Acq}(\phi_R)$ . The transverse magnetization of  $A(I_y^A)$  evolves into antiphase ( $2I_x^A I_z^M$ ) during  $\Delta$  and is converted into two-spin longitudinal order ( $2I_z^A I_z^M$ ) by the second  $90_y^\circ(A)$  pulse, which decays during  $\tau$  and is measured using a double quantum filter with appropriate phase cycle [361].

Dipolar relaxation of the three-spin systems can also be isolated from the rest of the spin by the following linear combinations [362] (see also Eq. (63)):

$$\begin{aligned} \rho_A + \rho_M + \rho_X - \rho_{AMX} = & \left[\frac{1}{3}J_{AMAM}(\omega_A - \omega_M) \right. \\ & + 2J_{AMAM}(\omega_A + \omega_M)] + \left[\frac{1}{3}J_{AXAX}(\omega_A - \omega_X) \right. \\ & + 2J_{AXAX}(\omega_A + \omega_X)] + \left[\frac{2}{3}J_{MXMX}(\omega_M - \omega_X) \right. \\ & + 2J_{MXMX}(\omega_M + \omega_X)] \end{aligned}$$

or

$$\begin{aligned} \rho_{AM} + \rho_X - \rho_{AMX} = & \left[\frac{1}{3}J_{AXAX}(\omega_A - \omega_X) \right. \\ & + 2J_{AXAX}(\omega_A + \omega_X)] + \left[\frac{2}{3}J_{MXMX}(\omega_M - \omega_X) \right. \\ & + 2J_{MXMX}(\omega_M + \omega_X)] \end{aligned} \quad (197)$$

Both these linear combinations isolate the mutual relaxation of a set of three spins, free of all cross-

correlations. However, while the first depends on all the three dipolar interactions, the later depends only on two of the dipolar interactions and is preferred.

#### 7.3.2. Transverse modes

Isolation of relaxation pathways can also be achieved by linear combination of transverse relaxation rates. For example, considering again the weakly coupled three-spin system  $AMX$ , one can monitor the relaxation rates of the sum modes of SQC, ZQC and DQC [362]. The following linear combination isolates the dipolar relaxation between spins  $A$  and  $M$ :

$$\begin{aligned} 2(\rho_{A^+}^{(1)} + \rho_{M^+}^{(1)}) - \rho_{2A^-M^-}^{(0)} - \rho_{2A^+M^+}^{(2)} \\ = \left[\frac{4}{3}J_{AMAM}(0) + \frac{1}{6}J_{AMAM}(\omega_A - \omega_M) + J_{AMAM}(\omega_A) \right. \\ \left. + J_{AMAM}(\omega_M) + J_{AMAM}(\omega_A + \omega_M)\right] \end{aligned} \quad (198)$$

where  $\rho_{A^+}^{(1)}$  is the self-relaxation rate of the sum mode of SQCs of spin  $A$ ,  $\rho_{A^+M^-}^{(0)}$  that of the ZQCs of  $A$  and  $M$  spins, and  $\rho_{A^+M^+}^{(2)}$  that of the DQCs [362]. This linear combination is again free of all cross-correlations. Another combination which exclusively depends on the dipole–dipole cross-correlation between the three spins, is given by:

$$\begin{aligned} \rho_{2A^-M^+}^{(0)} + \rho_{2A^+M^+}^{(2)} + \rho_{2M^+X^+}^{(2)} - \rho_{2A^+M^+X^+}^{(3)} - \rho_{A^+}^{(1)} - \rho_{M^+}^{(1)} - \rho_{X^+}^{(1)} \\ = \left[\frac{2}{3}J_{AMAX}(0) + \frac{1}{2}J_{AMAX}(\omega_A)\right](3 \cos^2 \theta_{AM,AX} - 1)/2 \\ + \left[\frac{2}{3}J_{AMMX}(0) + \frac{1}{2}J_{AMMX}(\omega_M)\right](3 \cos^2 \theta_{AM,MX} - 1)/2 \\ + \left[\frac{2}{3}J_{AXMX}(0) + \frac{1}{2}J_{AXMX}(\omega_X)\right](3 \cos^2 \theta_{AX,MX} - 1)/2. \end{aligned} \quad (199)$$

Excitation of multiple quantum coherences requires resolved couplings between the pair of involved spins. In such a circumstance, the measurement of ZQC, SQC and DQC sum modes presents practical problems and has to be done by taking into account the J-coupling evolution [362].

#### 7.3.3. Combination of longitudinal and transverse modes

In Eqs. (198) and (199), only the decay rates of the inphase transverse modes were considered. If the decay rate of antiphase transverse mode  $\rho_{2A^+M_z}$  is also measured, one can combine longitudinal and transverse mode relaxation rates in the following

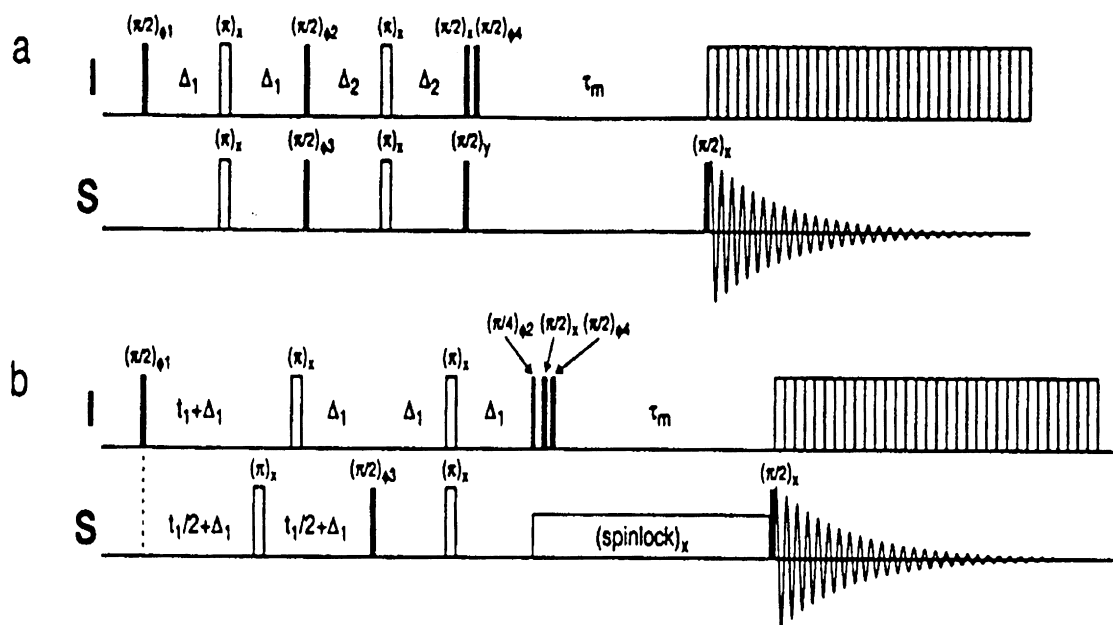


Fig. 71. Pulse sequences to measure the cross-relaxation rate constant  $\Gamma_{4S_z I_{z_1} I_{z_2} S_z}$ . (a) 1D version in the laboratory frame with a INEPT preparation sequence to generate the initial  $4S_z I_{z_1} I_{z_2}$  and (b) 2D version in the rotating frame, optimized for the observation of  $\text{CH}_2$  groups. The delays used are  $\Delta_1 = 1/(4J_{\text{CH}})$  and  $\Delta_2 = 1/(8J_{\text{CH}})$  for  $\text{CH}_2$  groups and  $\Delta_2 = 1/(4J_{\text{CH}})$  for  $\text{CH}_3$  groups. [Reproduced with permission from M. Ernst, R.R. Ernst, J. Magn. Reson. A 110 (1994) 202.]

manner:

$$\rho_{A^+} + \rho_{M_z} - \rho_{2A^+M_z} = \left[ \frac{1}{6} J_{AMAM} (\omega_A - \omega_M) + J_{AMAM} (\omega_M) + J_{AMAM} (\omega_A + \omega_M) \right]. \quad (200)$$

This rate is also free of other dipolar interactions as well as cross-correlations.

Experimental pulse schemes have been given for measuring the above rates [361–363].

#### 7.4. Dipole–dipole cross-correlations in $^{13}\text{CH}_2$ and $^{13}\text{CH}_3$ spin systems

Recently heteronuclear dipole–dipole cross-correlations which couple carbon single-spin-order ( $S_z$ ) to carbon–proton three-spin-order ( $4S_z I_{z_1} I_{z_2}$ ) in  $^{13}\text{CH}_2$  and  $^{13}\text{CH}_3$  spin systems have been utilized to characterize the side chain motion in biopolymers [364]. The technique has been applied to the cyclic decapeptide antamanide and to the protein human ubiquitin. This rate depends on the modulation details of the cross terms between  $SI_1$  and  $SI_2$  dipolar interactions. The

experimental data has, therefore, been compared with various motional models. The 1D experiments have been carried out using the pulse scheme of Fig. 71(a) and the 2D ROESY experiments using the pulse scheme of Fig. 71(b). Suppression of undesired terms at the beginning and the end of the mixing period is essential to monitor the small cross-correlation rates. In this case, the pathway  $\sigma(0) \propto \langle 4S_z I_{z_1} I_{z_2} \rangle \rightarrow \sigma(m) \propto \langle S_z \rangle$  has been utilized.

Fig. 72 shows the 1D spectra obtained using the scheme of Fig. 71(a) on  $^{13}\text{C}$  labeled antamanide dissolved in (a) chloroform at  $T = 280$  K and (b) acetone at  $T = 310$  K. The viscosity of chloroform,  $\eta = 0.651$  cP at 280 K while for acetone,  $\eta = 0.285$  cP at 310 K. Using Stoke's relation, the correlation times for isotropic reorientation are in the ratio [364]:

$$\frac{\tau_c(\text{chloroform at 280 K})}{\tau_c(\text{acetone at 310 K})} = 2.6 \quad (201)$$

Fig. 72 reveals that there are three classes of signals. (i) The Val-1 and Ala-4 methyl group signals are negative in (a) and positive in (b). (ii) The  $^{13}\text{CH}_2$

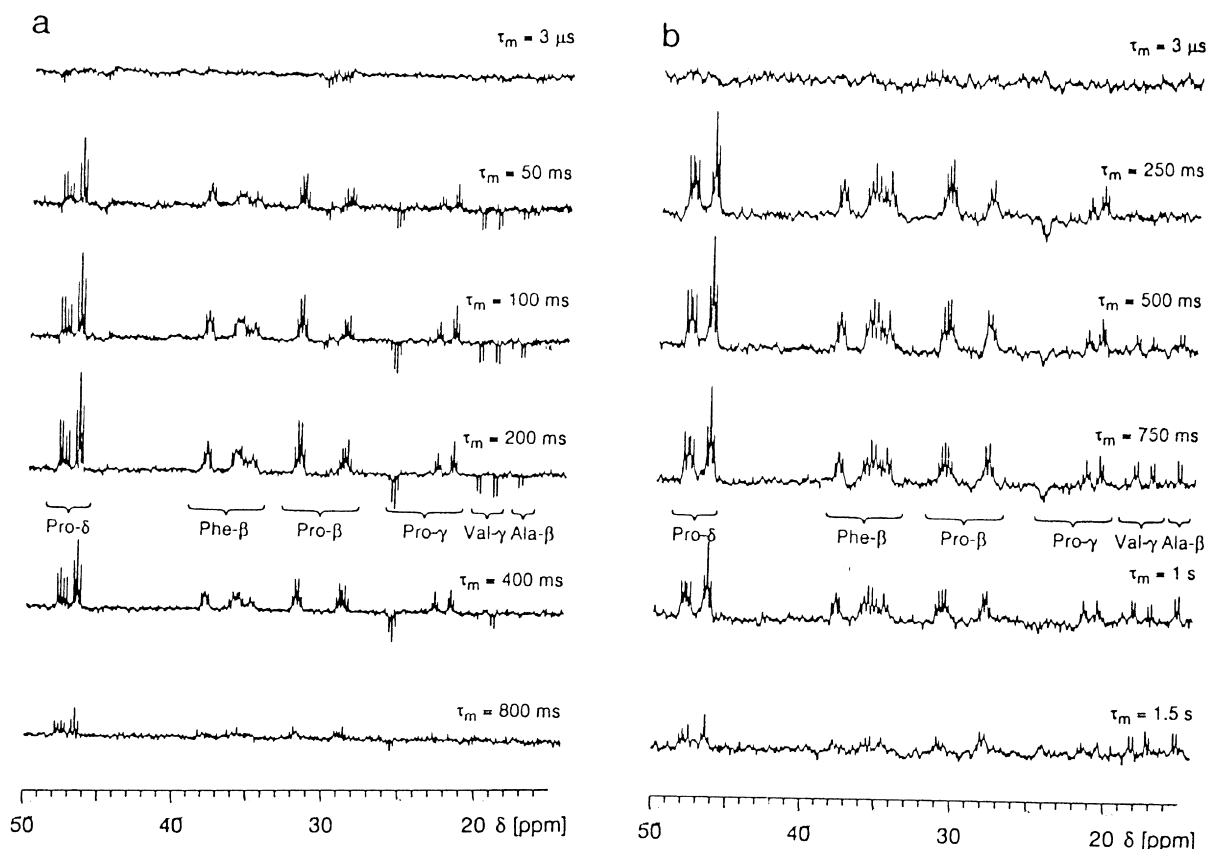


Fig. 72.  $\langle 4S_Z I_{1Z} I_{2Z} \rangle \rightarrow \langle S_Z \rangle$  cross-relaxation  $^{13}\text{C}$  spectra for fully  $^{13}\text{C}$ -labeled antamanide (a) in chloroform at  $T = 280\text{ K}$  and in (b) in acetone at  $T = 310\text{ K}$ , for six different mixing times  $\tau_m$ . The spectra have been recorded at  $150.8\text{ MHz}$   $^{13}\text{C}$  resonance frequency with the pulse sequence of Fig. 71(a) in the laboratory frame. The visible multiplet structure is due to  $^{13}\text{C}$ – $^{13}\text{C}$  J-coupling interactions. The chemical shift refers to  $\delta(\text{TMS}) = 0\text{ ppm}$ . [Reproduced with permission from M. Ernst, R.R. Ernst, J. Magn. Reson. A 110 (1994) 202.]

signals are negative in both for the  $\text{C}_\gamma\text{H}_2$  of Pro-2 and Pro-7, but rather weak in (b). (iii) Signals which are positive in both (for all the remaining residues). From these data and measured  $T_1$  values of  $\text{C}_\alpha$  resonances, upper and lower bounds have been obtained for the correlation times of internal motion for these residues.

Using  $^{13}\text{C}$ -labeled ubiquitin the 2D experiment has been carried out with the pulse scheme of Fig. 71(b). Most of the cross peaks for the  $^{13}\text{CH}_2$  are positive except for  $^{13}\text{C}_\beta\text{H}_2$  in Ser-57,  $^{13}\text{C}_\gamma\text{H}_2$  in Pro-37 and  $^{13}\text{C}_\gamma\text{H}_2$ ,  $^{13}\text{C}_\delta\text{H}_2$  and  $^{13}\text{C}_\epsilon\text{H}_2$  in Lysine residue at 6, 11, 29, 33, 48 and 63 positions. The positive cross-peaks of  $^{13}\text{CH}_2$  groups indicate slow rotation about the  $\chi_1$  angle with a correlation time  $\tau_i \approx 1.3\text{ ns}$ . The

negative cross peak for Pro- $\gamma$  indicates fast puckering motion with a large amplitude. The negative cross peaks of lysine side chains indicate a rapid and virtually unrestricted motion of these residues [364].

### 7.5. Combined use of transverse and longitudinal cross-correlations

Several groups have suggested measurement of longitudinal and transverse cross-correlation rates in independent experiments, on the same sample, to obtain motional parameters independent of structural attributes. The procedure is to measure the CSA–dipole cross-correlation rate  $\eta_{xy}$  for transfer of

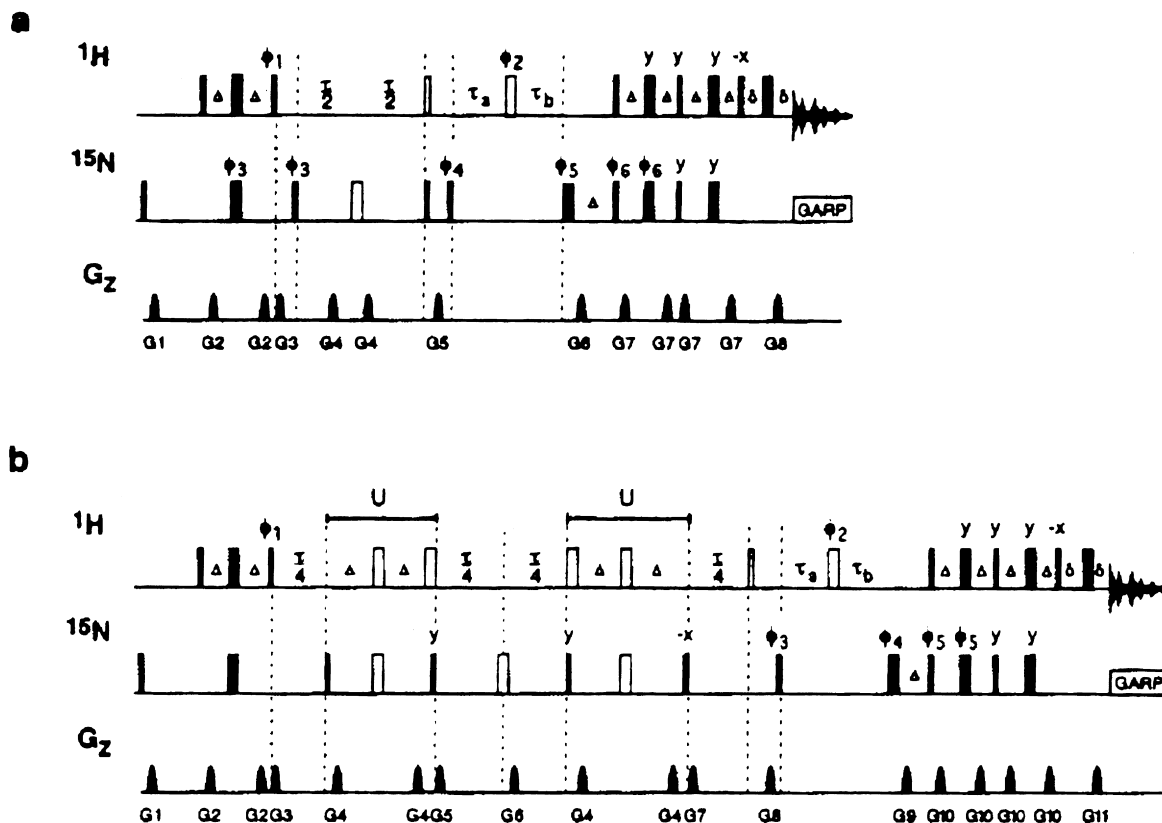


Fig. 73. Pulse sequences for the measurement of (a) transverse  $\eta_{xy}$  and (b) longitudinal  $\eta_z$   $^1\text{H}$ - $^{15}\text{N}$  dipolar/ $^{15}\text{N}$  CSA relaxation interference effects. Narrow and wide bars correspond to  $90^\circ$  and  $180^\circ$  pulses, respectively. Solid bars represent rectangular pulses, while open bars correspond to composite  $(90^\circ_x-90^\circ_y)90^\circ$  and composite  $(90^\circ_y-180^\circ_x-90^\circ_y)180^\circ$  pulses. All pulses are applied with phase  $x$  unless specified otherwise. Delay durations are  $\Delta = 2.67$  ms and  $\delta = 0.75$  ms. Two experiments are performed for each value of the relaxation period  $\tau$ . In the first experiment, the composite  $^1\text{H}$   $90^\circ$  pulse, designated by the narrow open bar is included,  $\tau_a = \Delta$  and  $\tau_b = \Delta + t_1/2$ . In the second experiment, the composite  $90^\circ$  pulse is absent,  $\tau_a = \Delta + t_1/2$  and  $\tau_b = t_1/2$ . [Reproduced with permission from C.D. Kroenke, J.P. Loria, L.K. Lee, M. Rance, A.G. Palmer III, J. Am. Chem. Soc. 120 (1998) 7905.]

inphase transverse magnetization  $\langle S_X \rangle$  (or  $\langle S_Y \rangle$ ) to antiphase coherence  $\langle 2I_Z S_X \rangle$  (or  $\langle 2I_Z S_Y \rangle$ ). The same CSA-dipole cross-correlation is also responsible for cross relaxation between longitudinal orders  $\langle S_Z \rangle$  and  $\langle 2I_Z S_Z \rangle$  with rate constant  $\eta_z$ . These rates for CSA-dipole cross-correlation in a two-spin system are given by [365]:

$$\eta_z = -4cdP_2(\cos \theta)J(\omega_S) \quad (202)$$

$$\eta_{xy} = -\frac{2}{3}cdP_2(\cos \theta)[4J(0) + 3J(\omega_S)]$$

Here  $c = (\gamma_S B_0 \Delta \sigma_S) / (\sqrt{30})$ ,  $d = (\sqrt{3} \mu_0 \hbar \gamma_I \gamma_S) / (4\pi r_{IS}^3 \sqrt{10})$  and  $cdP_2(\cos \theta)J(\omega_S) = J_{S,IS}(\omega_S)$  (Eq. (42)). These expressions can be obtained from Eqs.

(64) and (107), as well as being given in Eq. (A8). It is noted that while  $\eta_{xy}$  depends on both  $J(0)$  and  $J(\omega_S)$ ,  $\eta_z$  depends only on  $J(\omega_S)$ . The rates  $\eta_{xy}$  and  $\eta_z$  have been measured by using the following experiments. The rate  $\eta_{xy}$  is measured using the pulse scheme of Fig. 73(a). The proton magnetization ( $\langle I_Z \rangle$ ) is transferred to  $^{15}\text{N}$  by an INEPT transfer as  $\langle 2I_Z S_Y \rangle$  (or  $\langle 2N_Y H_Z \rangle$ ), which evolves during the  $\tau$  period and is converted to  $\langle S_Y \rangle$  (or  $\langle N_Y \rangle$ ) by the cross-correlation rate  $\eta_{xy}$ . The  $180^\circ$   $^{15}\text{N}$  pulse in the middle of  $\tau$  refocuses chemical shift and J-coupling evolutions, as well as averages the auto relaxation rates of the inphase and antiphase coherences. If  $\tau = n/J$ , then the effective evolution during the relaxation period

$\tau$  is given by:

$$\frac{d}{dt} \begin{pmatrix} \langle S_Y \rangle(\tau) \\ \langle 2I_Z S_Y \rangle(\tau) \end{pmatrix} = - \begin{pmatrix} \overline{R}_2 & \eta_{xy} \\ \eta_{xy} & \overline{R}_2 \end{pmatrix} \begin{pmatrix} \langle S_Y \rangle(\tau) \\ \langle 2I_Z S_Y \rangle(\tau) \end{pmatrix} \quad (203)$$

in which  $\overline{R}_2 = (R_2 + R_{2IS})/2$ , where  $R_2$  and  $R_{2IS}$  are the self-relaxation rates of  $\langle S_Y \rangle$  and  $\langle 2I_Z S_Y \rangle$ , respectively. Two experiments are performed in which after the  $\tau$  period, either  $\langle S_Y \rangle$  or  $\langle 2I_Z S_Y \rangle$  are selectively detected and the ratios of the intensities of these two experiments yields:

$$\frac{I_A}{I_B} = \tanh(\eta_{xy}\tau) \quad (204)$$

An experiment has also been designed to measure  $\eta_z$  by an analogous method of Fig. 73(b), which averages the relaxation rates of  $\langle S_Z \rangle$  and  $\langle 2I_Z S_Z \rangle$ . During this experiment, the cross relaxation (NOE) between  $\langle S_Z \rangle$  and  $\langle I_Z \rangle$  as well as cross-correlation between  $\langle I_Z \rangle$  and  $\langle 2I_Z S_Z \rangle$  are suppressed, retaining exclusively the cross-correlation  $\eta_z$  between  $\langle S_Z \rangle$  and  $\langle 2I_Z S_Z \rangle$ . As shown in Fig. 73(b), the proton magnetization  $\langle I_Z \rangle$  is converted via an INEPT transfer into the two-spin order  $\langle 2I_Z S_Z \rangle$  prior to the relaxation period  $\tau$ . The composite  $^{15}\text{N}$   $180^\circ$  pulse in the middle of the  $\tau$  period suppresses the cross-correlation between the  $^1\text{H}$  CSA and  $^1\text{H}$ - $^{15}\text{N}$  dipolar interactions. This reduces the  $3 \times 3$  rate equation between  $\langle S_Z \rangle$ ,  $\langle I_Z \rangle$  and  $\langle 2I_Z S_Z \rangle$  into a  $2 \times 2$  [Eq. (A11)] containing only  $\langle S_Z \rangle$  and  $\langle 2I_Z S_Z \rangle$ , with  $\eta_z$  as the rate constant between them. Further averaging in the self-relaxation rates of  $\langle S_Z \rangle$ ,  $R_1$  and  $\langle 2I_Z S_Z \rangle$ ,  $R_{1IS}$  is achieved by a series of pulses, represented by a transformation  $U$ , mid-way between each half of the  $\tau$  period. The rate equation describing the time evolution of the longitudinal one and two spin order in analogy with Eq. (203) is then given by:

$$\frac{d}{dt} \begin{pmatrix} \langle S_Z \rangle(\tau) \\ \langle 2I_Z S_Z \rangle(\tau) \end{pmatrix} = - \begin{pmatrix} \overline{R}_1 & \eta_z \\ \eta_z & \overline{R}_1 \end{pmatrix} \begin{pmatrix} \langle S_Z \rangle(\tau) \\ \langle 2I_Z S_Z \rangle(\tau) \end{pmatrix} \quad (205)$$

where  $\overline{R}_1 = (R_{1S} + R_{1IS})/2$  and  $R_{1S} = \rho_S$  and  $R_{1IS} = \rho_{IS}$  of Eq. (63). Two experiments are again carried out; experiment A monitors the decay of the two-spin order and experiment B the transfer of two-spin order to single-spin order via the cross-correlation.

The ratio of these two intensities is obtained as:

$$\frac{I_B}{I_A} = \tanh(\eta_z\tau). \quad (206)$$

The ratio of the transverse and longitudinal cross-correlations thus obtained, is given by:

$$\frac{\eta_{xy}}{\eta_z} = \frac{4J(0) + 3J(\omega_S)}{6J(\omega_S)}, \quad (207)$$

and is independent of the principal values and orientations of the CSA tensors and is sensitive only to internal and overall motions that contribute to dipolar and CSA relaxation mechanisms. Kroenke et al. measured the  $^{15}\text{N}$ - $^1\text{H}$  dipolar and  $^{15}\text{N}$  CSA cross-correlations in  $^2\text{H}$ ,  $^{15}\text{N}$  enriched RNaseH [365]. The same ratio (Eq. (207)) has been utilized by Kojima et al. [366], to obtain the ratio between the spectral densities at zero and at  $\omega_S$  as:

$$\frac{J(0)}{J(\omega_S)} = \frac{3}{4} \left( 2 \frac{\eta_{xy}}{\eta_z} - 1 \right) \quad (208)$$

They have monitored the  $^{13}\text{C}$ - $^1\text{H}$  dipolar and  $^{13}\text{C}$  CSA cross-correlation in  $^{13}\text{C}$ - $^1\text{H}$  doublets of C8-H8 and C2-H2 in a DNA decamer duplex with purine randomly  $^{13}\text{C}$  enriched to 15%. The spectral density at zero frequency  $J(0)$  is independent of chemical exchange effects. With limited internal motions, the ratio also enables an accurate evaluation of the correlation time for overall molecular tumbling as well as the anisotropic rotational diffusion tensor. Application of these techniques for investigating dynamics in biomolecules have been demonstrated [365,366].

Fushman and Cowburn [367] have also suggested a method, which combines the transverse self-relaxation rate  $R_2$  of  $^{15}\text{N}$  and the cross-correlation rate ( $\eta_{xy}$ ), between  $^{15}\text{N}$ - $^1\text{H}$  dipolar and  $^{15}\text{N}$  CSA. Extending the works of Tjandra et al. [239] and Tessari et al. [241], they observed that the spectral densities responsible for these rates have some common features, which can be further exploited. For example they note that  $R_2$  for  $^{15}\text{N}$  is given by:

$$R_2 = \frac{1}{2}(d^2 + c^2)[4J(0) + 3J(\omega_N)] + P_{\text{HF}} + R_{\text{ex}} \quad (209)$$

where  $P_{\text{HF}}$  contains the high frequency contributions

to  $R_2$  and is given by:

$$P_{\text{HF}} = \frac{1}{2}d^2[J(\omega_{\text{H}} - \omega_{\text{N}}) + 6J(\omega_{\text{H}}) + 6J(\omega_{\text{H}} + \omega_{\text{N}})] \quad (210)$$

and  $R_{\text{ex}}$  corresponds to a conformational exchange contribution if any. (Here  $\omega_{\text{N}}$  and  $\omega_{\text{H}}$  are Larmor frequencies of  $^{15}\text{N}$  and  $^1\text{H}$ , respectively). Eq. (209) can be obtained from Eq. (107), except for  $R_{\text{ex}}$ . For high-field spectrometers,  $\omega_{\text{H}}\tau_{\text{c}} \gg 1$  and  $P_{\text{HF}}$  is often negligible. Further assuming  $R_{\text{ex}}$  to be negligible,  $R_2 \approx (1/2)(d^2 + c^2)[4J(0) + 3J(\omega_{\text{N}})]$ .

Fushman and Cowburn further note that, since the cross-correlation rate ( $\eta_{xy}$ ) between  $^{15}\text{N}$ – $^1\text{H}$  dipolar and  $^{15}\text{N}$  CSA for transverse relaxation, given by Eq. (202) and  $R_2$  given above contain exactly the same combination of spectral densities, the ratio,  $(\eta_{xy}/R_2) \approx [2dc/(d^2 + c^2)]P_2(\cos \theta)$ . Since  $\eta_{xy}/R_2$  does not contain any direct dependence on spectral densities, this ratio provides a basis for a direct, model independent determination of  $^{15}\text{N}$  CSA from experimentally measured parameters, without explicit knowledge of the microdynamic parameters and without any assumption about the model of overall motion [367]. Published  $^{15}\text{N}$  relaxation data on human ubiquitin [239,360] have been analyzed using the above argument. It is found that (i) the ratio  $\eta_{xy}/R_2$  values lie within 0.7–0.8 for various residues. This variation is likely due to deviations in  $\theta$ , variations in CSA values and/or to experimental errors. The solid state NMR studies have indicated CSA of  $^{15}\text{N}$  to be  $\approx -160$  ppm and  $\theta \approx 20$ – $24^\circ$ . A statistical analysis of the above ubiquitin data indicates that CSA is  $\approx -170$  ppm and  $\theta$  lies between 10 and  $25^\circ$  [368].

### 7.6. TROSY: transverse relaxation optimized spectroscopy

The DLB (which can also be appropriately called differential line narrowing) due to CSA–dipole cross-correlations has recently been shown to lead to a significant narrowing of one of the lines of a J-split multiplet in 2D correlation experiment, which in turn leads to improved signal to noise ratio of the sharp peak and hence its detectability [369].

At high magnetic fields, the CSA relaxation of  $^1\text{H}$ ,  $^{13}\text{C}$  and  $^{15}\text{N}$  in enriched proteins, forms a significant source of relaxation along with dipole–dipole relaxation. This leads to an overall increase in the trans-

verse relaxation rate. The transverse relaxation of amide protons has been successfully reduced by large-scale deuteration of non-labile protons. In such circumstances, the DLB effect arising from CSA–dipole cross-correlation leads to further narrowing of one of the components of the  $^{15}\text{N}$ – $^1\text{H}$  fragment of the peptide bond. Theoretical calculations indicate that for proteins of size  $>25$  kDa, at proton frequencies near 1 GHz, almost complete cancellation of all transverse relaxation within a  $^{15}\text{N}$ – $^1\text{H}$  moiety can be achieved for one of the four multiplet components in a  $^{15}\text{N}$ – $^1\text{H}$  correlation experiment [369]. TROSY observes exclusively the narrow component for which the residual linewidth is entirely due to dipolar relaxation with remote protons in the protein. This protocol increases significantly the size of biomolecules that can be studied by multi-dimensional NMR. TROSY has been discussed in detail [369–371], with further improvements in  $S/N$  ratio by utilization of steady-state magnetization as well as echo–antiecho pathways [372,373]. The method has also been applied to  $^{13}\text{C}$ – $^1\text{H}$  system [374–376]. The main features of TROSY are explained in the following. Details are contained in the above references.

TROSY (Fig. 74) is basically a heteronuclear correlation experiment, in which the proton magnetization is first transferred to  $^{15}\text{N}$  (or  $^{13}\text{C}$ ) which evolves during  $t_1$  period (with differential relaxation rate of the  $^{15}\text{N}$  doublet due to CSA( $^{15}\text{N}$ )–dipole ( $^{15}\text{N}$ – $^1\text{H}$ ) cross-correlation) and transferred back to proton with detection during  $t_2$ , again with differential line broadening of the proton doublet due to CSA( $^1\text{H}$ )–dipole ( $^1\text{H}$ – $^{15}\text{N}$ ) cross-correlation. The resulting heteronuclear cross peak (Fig. 75) is a multiplet of four peaks each having different widths, in the  $\omega_1$  and  $\omega_2$  dimensions. One of the cross-peak components is narrow and the other broad in both dimensions with the remaining two peaks being broad in one and narrow in the other dimension. The ST2-PT step in Fig. 74 has been introduced to effect single-transition to single-transition polarization transfer (ST2-PT) which adds up the magnetization of various quadrants of the 2D experiment, canceling out all but the narrowest component.

The experiment starts with a  $90^\circ$  pulse on proton and transferring this magnetization to  $^{15}\text{N}$ ( $^{13}\text{C}$ ). The



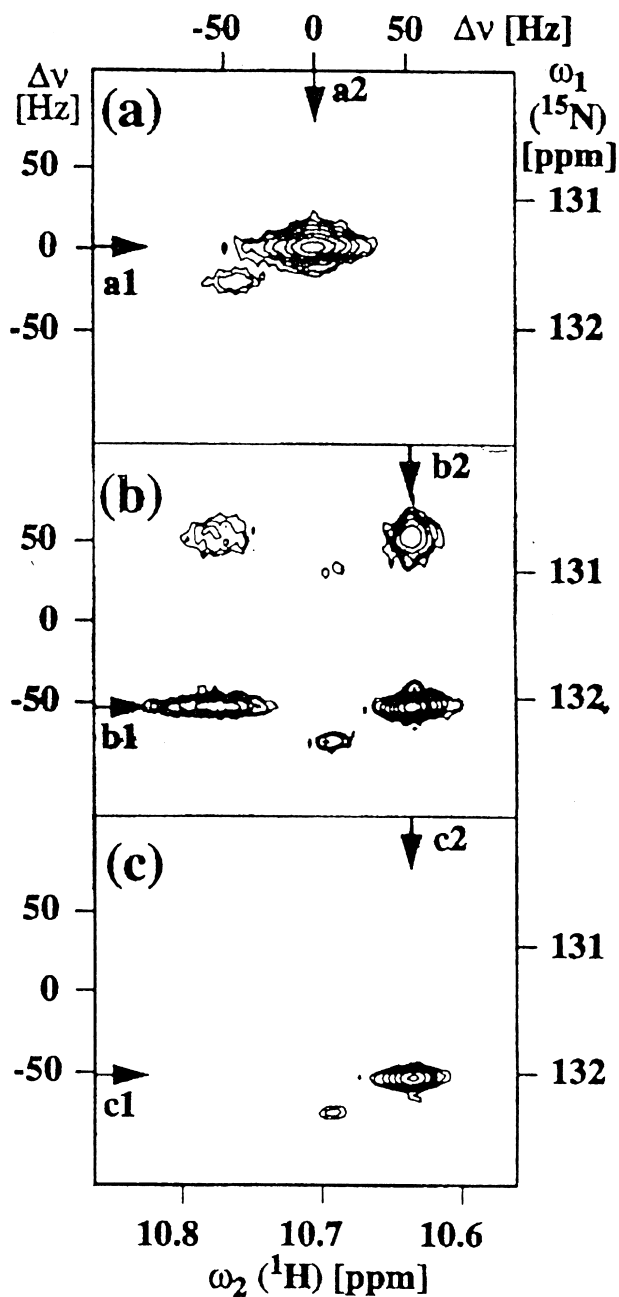


Fig. 75. Contour plots of  $^{15}\text{N}$ ,  $^1\text{H}$  correlation spectra showing the indole  $^{15}\text{N}$ - $^1\text{H}$  spin system of Trp-48 recorded in a 2 mM solution of uniformly  $^{15}\text{N}$  labeled *fushi tarazu* (ftz) homeodomain complexed with an unlabeled 14-bp DNA duplex in 90%  $\text{H}_2\text{O}$ /5%  $^2\text{H}_2\text{O}$  at 4°C, pH = 6.0, measured at the proton frequency of 750 MHz. (a) Conventional broadband decoupled [ $^{15}\text{N}$ ,  $^1\text{H}$ ] COSY spectrum. The evolution caused by  $J(^1\text{H}, ^{15}\text{N})$  scalar coupling was refocused in the  $\omega_1$  and  $\omega_2$  dimensions by a  $180^\circ$  proton pulse in the middle of the  $^{15}\text{N}$  evolution in  $t_1$  and by WALTZ composite pulse decoupling on  $^{15}\text{N}$  during data acquisition, respectively. (b) Conventional [ $^{15}\text{N}$ ,  $^1\text{H}$ ] COSY spectrum recorded without decoupling during  $t_1$  and  $t_2$ . (c) TROSY-type [ $^{15}\text{N}$ ,  $^1\text{H}$ ] correlation spectrum recorded with the pulse sequence of Fig. 74. Chemical shifts relative to DSS in ppm and shifts in Hz relative to the center of the multiplet are indicated in both dimensions. The arrows identify the locations of the cross-sections shown in Fig. 76. [Reproduced with permission from K.V. Pervushin, R. Riek, G. Wider, K. Wüthrich, Proc. Natl. Acad. Sci. USA, 94 (1998) 12366.]

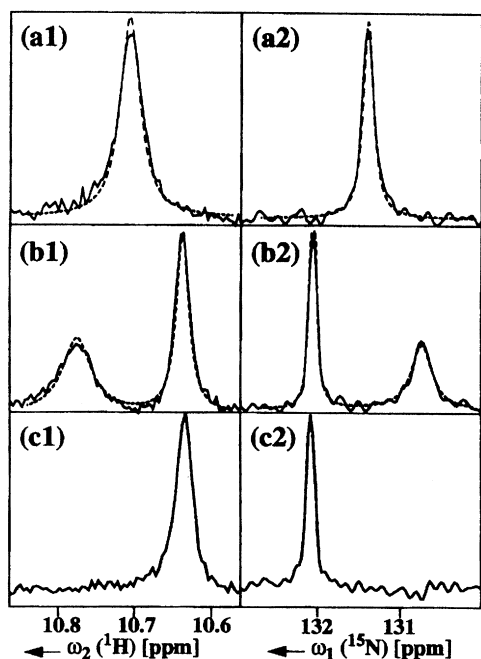


Fig. 76. Cross-sections through the spectra of Fig. 75 (solid lines). To facilitate a comparison of the linewidths in the different spectra the cross-sections were normalized to the same maximal signal amplitude. (a1), (a2) etc. refer to the arrows in Fig. 75. Simulated line shapes (dashed lines in (a) and (b)) were calculated using  $J(^1\text{H}, ^{15}\text{N}) = -105$  Hz,  $\tau_c = 20$  ns, chemical shift anisotropies of  $\Delta\sigma_{\text{H}} = -16$  ppm,  $\Delta\sigma_{\text{N}} = -160$  ppm. For  $^1\text{H}^{\text{N}}$ , the relaxation due to dipolar coupling with the other protons in the nondeuterated complex was approximated by three protons placed at a distance of 0.24 nm from  $^1\text{H}^{\text{N}}$ . [Reproduced with permission from K.V. Pervushin, R. Riek, G. Wider and K. Wüthrich, Proc. Natl. Acad. Sci. USA, 94 (1998) 12366.]

one of the components is narrower in both dimensions than the decoupled line and exclusively observed after ST2-PT step (Fig. 76c). The S/N ratio of the narrow component further increases by a factor  $\sqrt{2}$  on coaddition of echo–antiecho parts [371] and further more by 10–15% by addition of the equilibrium  $^{15}\text{N}$  magnetization [370].

The sensitivity gain of TROSY has been exploited for mapping the binding surface of chaperone FimC (a protein of 23 kDa) for the adhesin FimH (28 kDa). The conventional spectrum of the 51 kDa complex gave a few, very broad, almost undetectable signals. The  $^{15}\text{N}$ -labeled FimC and unlabeled FimH complex, gave many signals in

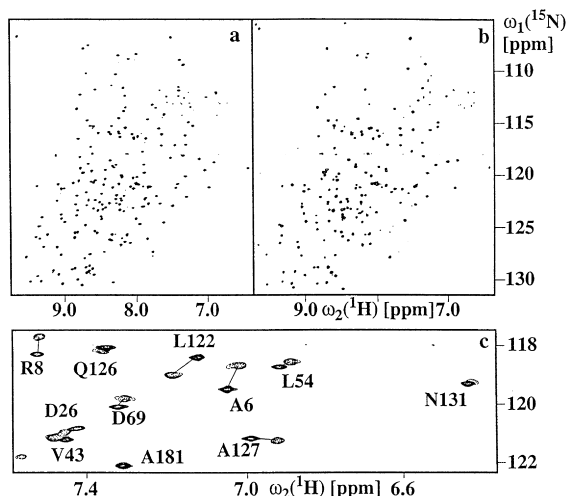


Fig. 77. (a) TROSY-type  $^{15}\text{N}$  &  $^1\text{H}$  correlation spectra (recorded on a Bruker DRX-750 MHz spectrometer) of uncomplexed  $^{15}\text{N}/^2\text{H}$  labeled FimC (left spectrum) and of  $^{15}\text{N}/^2\text{H}$  labeled FimC complexed with unlabeled FimH (right spectrum). Both samples contained 0.4 mM of  $^{15}\text{N}/^2\text{H}$ -labeled FimC, pH 5.0 in 90%  $\text{H}_2\text{O}$ , 10%  $\text{D}_2\text{O}$ . A slight excess of FimH was used in the complex to ensure that FimC was fully bound. Both spectra were measured at 38°C. The panel (c) shows an expanded view of the superposition of the spectra in (a) and (b). In (c), the cross peaks are labeled with their corresponding amino acid number and the cross peaks that have shifted in the complex by a large amount are linked to their nearest neighbor by a line. [Reproduced with permission from M. Pellecchia, P. Sebbel, U. Hermans, K. Wüthrich, R. Glockshuber, Nature, Structural Biology 6 (1999) 336.]

correlation spectra, but still all cross peaks were not present. Perdeuteration of FimC except at amide positions, dramatically improved the situation. Further improvement was achieved by using TROSY. The TROSY type  $^{15}\text{N}$ – $^1\text{H}$  correlation spectrum of  $^{15}\text{N}/^2\text{H}$  labeled FimC in free state and complexed with unlabeled FimH, yielded TROSY spectra with narrow peaks for all the  $^{15}\text{N}$  in the protein, many of which show significant chemical shift changes near the binding sites (Fig. 77) [377]. This demonstrates a methodology not achievable for complexes of this size with conventional methods. Similar improvements have also been reported for  $^{13}\text{C}$ – $^1\text{H}$  system in a  $^{13}\text{C}$  labeled 18 kDa protein cyclophilin [374,375]. Here it is shown that for the aromatic carbon the CSA( $^{13}\text{C}$ )–dipole( $^{13}\text{C}$ – $^1\text{H}$ ) cross-correlation narrows one of the

$^{13}\text{C}$  doublet component considerably. The optimum effect is observable in the  $^1\text{H}$  resonance frequency range of 600–800 MHz and leads to a sensitivity gain by a factor of 10. Several groups have reported TROSY enhancement and given further improvements/variations in the TROSY scheme [378–385].

Recently several groups have reported direct evidence of the existence of hydrogen bonds in  $^{15}\text{N}$ -labeled oligonucleotides and  $^{15}\text{N}$ – $^{13}\text{C}$  labeled proteins by NMR, utilizing the sensitivity gain and line-narrowing features of TROSY [386–391].

### 7.7. Cross-correlation under magic angle spinning

Chung and Oldfield reported the presence of CSA–dipole cross-correlation effects in the nuclear spin relaxation of polymers under magic angle sample spinning [392]. Differential relaxation was observed in proton-coupled  $^{13}\text{C}$  MAS inversion-recovery spectra for the methine C–H spin groups in poly(*cis*-isoprene). Further experiments have substantiated the presence of temporal cross-correlations between the  $^{13}\text{C}$ –H dipolar and  $^{13}\text{C}$  CSA interactions in the spin–lattice relaxation rates of olefinic and methine carbons in polymeric species [393].

## 8. Experiments that avoid cross-correlations

There have been several techniques and experimental methodologies proposed to suppress cross-correlation effects. In longitudinal relaxation, the multiplet effects can be suppressed easily in homonuclear spin systems, by the use of a non-selective  $90^\circ$  measuring pulse. In heteronuclear spins,  $90^\circ$  pulses would be needed on two or more spins to suppress the multiplet effect. The net effects can be avoided by the use of short mixing times as they are second order in time. This pertains only to NOE measurements and not to inversion-recovery  $T_1$  measurements where the use of long mixing times is unavoidable. In general, unlike the multiplet effects, the net effects persist in all the experiments and are difficult to suppress.

Boyd et al. have used the idea that avoiding the creation of multi-spin orders can suppress cross-correlation effects in  $T_1$  measurements of a spin, which can be achieved if all the other relaxation-coupled spins are selectively saturated during the relaxation recovery period [394]. This has been used in measuring  $^{15}\text{N}$

$T_1$  in  $^{15}\text{N}$ – $^1\text{H}$  systems with proton broad-band decoupling, which essentially causes saturation of proton magnetization, during the recovery period. Kay et al. have come up with pulse sequences for removal of cross-correlation effects on the measurement of heteronuclear  $T_1$  and  $T_2$  values in proteins [395]. Cross-correlation effects on  $T_1$  can be removed by applying  $^1\text{H}$   $180^\circ$  pulses during the time allowed for longitudinal relaxation at a rate at least five times faster than the decay rate of the fastest decaying multiplet component. Alternative pulse schemes are also suggested that involve  $^1\text{H}$  saturation or  $^1\text{H}$  decoupling during the time allowed for longitudinal relaxation, which is similar to the approach used by Boyd et al. [394].

The cross-correlation effects on  $T_2$  can also be removed by the use of a series of  $180^\circ$  pulses applied selectively to J-coupled spin. The rapid  $180^\circ$  pulsing interchanges the labels of the spin states of the two transitions which otherwise relax with different  $T_2$  due to cross-correlations if they are J resolved, which relax with an average rate devoid of cross-correlations. These ideas have been used to measure  $^{15}\text{N}$   $T_1$  and  $T_2$  for uniformly  $^{15}\text{N}$ -labeled SNase [390]. Broad-band decoupling was shown to be effective in removing the cross-correlation effects in  $T_2$  measurements by Palmer et al. [396]. They have shown that application of a  $180^\circ$  pulse to the protons attached to the heteronucleus synchronously with every second echo of the heteronuclear spin, efficiently eliminates the effects of cross-correlations. Composite pulse decoupling of the protons during the CPMG sequence and application of a single  $180^\circ$  pulse to the protons at the midpoint of the CPMG sequence are not very effective in removing the cross-correlation effects [396].

As it has been discussed in detail in Sections 5.2 and 5.3, selective spin lock of a particular spin, in a group of coupled spins makes the CSA–dipole cross-correlation rate zero and hence can be thought of as a way of suppressing cross-correlations. Also the experiment proposed by Levitt and Di Bari, discussed in Section 3.5.2, can also isolate relaxation pathways removing certain cross-correlations. For example, if  $180^\circ$  pulses are applied on all the relaxation-coupled spins, then the even and odd order modes have different symmetry, avoiding cross-correlations which couple them [214,215].

## 9. Conclusions

Cross-correlations affect the longitudinal relaxation including NOE via spectral densities at the Larmor frequency. They affect transverse relaxation via spectral densities at zero frequency as well. Therefore, in biomolecular studies the most significant observation of cross-correlations are the differential transverse relaxation or differential line broadening/narrowing of various single- and multiple-quantum coherences. Some of these effects of cross-correlations have been utilized for obtaining additional information on structures and dihedral angles of the biomolecules. The differential line broadening which narrows one of the components of the multiplet has been utilized for increasing the resolution and  $S/N$  ratio leading to enhancing the sizes of the biomolecules that can be studied by NMR. Recently, several applications of the enhanced resolution and sensitivity arising out of transverse cross-correlations have been demonstrated. In future, cross-correlations will therefore continue to play a dominant role in biomolecular NMR.

## Acknowledgements

We thank authors of several papers who readily sent us reprints and lists of their publications. We especially acknowledge Prof. Larry Werbelow for a complete list of publications on cross-correlations that he maintains. We also acknowledge with thanks permission to reproduce figures in this article from numerous authors. Anil Kumar acknowledges the position of “Chaire Condorset” at Ecole Normale Supérieure at Paris, France during spring of 1998 and a visit at University of Michigan, Ann Arbor, USA, during winter of 1998–99, during which periods this article continued to be compiled. One of the authors R.C.R. Grace acknowledges the financial support by Council of Scientific and Industrial Research, India. We also thank Mr. Rangeet Bhattacharyya of our laboratory, for painstakingly cross-checking with a “MATHEMATICA” programme, the analytical expressions for various  $J(\omega)$  and  $K(\omega)$  for CSA and dipolar relaxation mechanisms, including strongly coupled spins, given in this article. We thank Prof. K.V. Ramathan and Mr. G. Karthik of our group for

discussions. Use of NMR Spectrometers of Sophisticated Instruments Facility of Indian Institute of Science, Bangalore is gratefully acknowledged.

## Appendix A. Operator formalism for relaxation

The expectation values of any operator  $Q$  is given by  $\text{Tr}\{\sigma(t)Q\}$ . Using the equation of motion of the density matrix (Eq. (8)), the time evolution of the expectation value of any operator is obtained as [1,238]:

$$\frac{d\langle Q \rangle}{dt} = -\frac{1}{2} \int_{-\infty}^{+\infty} \text{Tr}\{[[Q, \mathcal{H}^{l*}(t)], \mathcal{H}^{l*}(t-\tau)](\sigma^* - \sigma_0)\} d\tau \quad (\text{A1})$$

The trace in the integral on the RHS is a difference of expectation values of the type:

$$\langle [[Q, \mathcal{H}^{l*}(0)], \mathcal{H}^{l*}(\tau)] \rangle - \langle [[Q, \mathcal{H}^{l*}(0)], \mathcal{H}^{l*}(\tau)] \rangle_{\text{eq}}$$

In order to calculate the time evolution of the expectation value of any observable, one needs to calculate the commutators of various operators with the relaxation Hamiltonians and there is no need either to make any assumption about the form of the density matrix during the evolution of the system, or to calculate explicitly the variation of its matrix elements. The evolution of any desired physical quantity is obtained by proper choice of the operator  $Q$ . When considering a spin operator,  $I_\alpha$  ( $\alpha = x, y, z$ ), we treat its projection on the subspace of  $S_z = +1/2$  and  $-1/2$  (for a two-spin system; can be easily extended to higher order systems) as:

$$I_\alpha^{(1)} = I_\alpha(\frac{1}{2} + S_z) \quad I_\alpha^{(2)} = I_\alpha(\frac{1}{2} - S_z) \quad (\text{A2})$$

It is often more convenient to calculate the expectation values of linear combination:

$$I_\alpha = I_\alpha^{(1)} + I_\alpha^{(2)} \quad 2I_\alpha S_z = I_\alpha^{(1)} - I_\alpha^{(2)} \quad (\text{A3})$$

For a two-spin system  $IS$ , considering relaxation via CSA of spins  $I$  and mutual dipolar interaction, the rate equation for the longitudinal relaxation is given by

[238]:

$$\frac{d}{dt} \begin{pmatrix} \langle I_z \rangle \\ \langle S_z \rangle \\ \langle 2I_z S_z \rangle \end{pmatrix} = - \begin{pmatrix} A_1 & E_1 & B_1 \\ E_1 & A'_1 & B'_1 \\ B_1 & B'_1 & C_1 \end{pmatrix} \cdot \begin{pmatrix} \langle I_z - 2I_0 \rangle \\ \langle S_z - 2S_0 \rangle \\ \langle 2I_z S_z \rangle \end{pmatrix} \quad (\text{A4})$$

where

$$A_1 = D\tau_c \left\{ \frac{6(1 + \alpha^2)}{1 + \omega_I^2 \tau_c^2} + \frac{2}{1 + (\omega_I - \omega_S)^2 \tau_c^2} + \frac{12}{1 + (\omega_I + \omega_S)^2 \tau_c^2} \right\}$$

$$B_1 = D\tau_c \left\{ \frac{12\alpha}{1 + \omega_I^2 \tau_c^2} \right\}$$

$$E_1 = D\tau_c \left\{ \frac{12}{1 + (\omega_I + \omega_S)^2 \tau_c^2} - \frac{2}{1 + (\omega_I - \omega_S)^2 \tau_c^2} \right\}$$

$$C_1 = D\tau_c \left\{ \frac{6(1 + \alpha^2)}{1 + \omega_I^2 \tau_c^2} + \frac{6}{1 + \omega_S^2 \tau_c^2} \right\}$$

$$A'_1 = D\tau_c \left\{ \frac{6}{1 + \omega_S^2 \tau_c^2} + \frac{2}{1 + (\omega_I - \omega_S)^2 \tau_c^2} + \frac{12}{1 + (\omega_I + \omega_S)^2 \tau_c^2} \right\} \quad (\text{A5})$$

with  $D = (1/4\pi)d^2 = (1/20)(\mu_0/4\pi)^2 \gamma_I^2 \gamma_S^2 \hbar^2 r^{-6}$  and  $\alpha = -(2/3)H(\sigma_{\parallel} - \sigma_{\perp})r^3/(\gamma_S \hbar)$ . Eq. (A4), is identical to a reduced Eq. (61) for a two-spin system, with  $A_1 = \rho_I = \rho_A$ ,  $A'_1 = \rho_S = \rho_M$ ,  $E_1 = \sigma_{IS} = \sigma_{AM}$ ,  $B_1 = \delta_{I,IS} = \delta_{A,AM}$ ,  $B'_1 = \delta_{S,IS} = \delta_{M,AM} = 0$  and  $C_1 = \rho_{IS} = \rho_{AM}$ .

Similarly for transverse relaxation, one obtains the rate equation as:

$$\frac{d}{dt} \begin{pmatrix} \langle I_+ \rangle \\ \langle 2I_+ S_z \rangle \end{pmatrix} = - \begin{pmatrix} A_2 & B_2 \\ B_2 & C_2 \end{pmatrix} \cdot \begin{pmatrix} \langle I_+ \rangle \\ \langle 2I_+ S_z \rangle \end{pmatrix} \quad (\text{A6})$$

which is formally identical to Eq. (105), with  $A_2 = (1/2)(D_1 + D_2) + C$ ,  $B_2 = (1/2)(D_1 - D_2)$  and  $C_2 = (1/2)(D_1 + D_2) - C$ . Eq. (A6) can be transformed into

expectation values of single transition operator equation as:

$$\frac{d}{dt} \begin{pmatrix} I_+^{(1)} \\ I_+^{(2)} \end{pmatrix} = - \begin{pmatrix} +(iJ/2) + \lambda + \eta & \mu \\ \mu & -(iJ/2) + \lambda - \eta \end{pmatrix} \begin{pmatrix} I_+^{(1)} \\ I_+^{(2)} \end{pmatrix} \quad (\text{A7})$$

This equation is equivalent to Eq. (103), with  $D_1 = \lambda + \eta$ ,  $D_2 = \lambda - \eta$  and  $C = \mu$ . Here it is noticed that both  $\lambda$  and  $\mu$  contain only auto-correlation spectral densities while  $\eta$  gives the cross-correlation spectral densities.

Kroenke et al. have recently rewritten the expressions for various constants in the above formalism without defining  $\alpha$  as the ratio between CSA and dipolar magnitudes [365]. The cross-correlation in longitudinal and transverse relaxation have been unified into a single notation as  $\eta_z$  and  $\eta_{xy}$ . The equation of motion for transverse relaxation is given by:

$$\frac{d}{dt} \begin{pmatrix} \langle S_y \rangle(\tau) \\ \langle 2I_z S_y \rangle(\tau) \end{pmatrix} = - \begin{pmatrix} \overline{R}_2 & \eta_{xy} \\ \eta_{xy} & \overline{R}_2 \end{pmatrix} \begin{pmatrix} \langle S_y \rangle(\tau) \\ \langle 2I_z S_y \rangle(\tau) \end{pmatrix} \quad (\text{A8})$$

where  $\overline{R}_2 = (R_2 + R_{2IS})/2$ , and for longitudinal relaxation is given by:

$$\frac{d}{dt} \begin{pmatrix} \langle S_z \rangle(t) \\ \langle 2I_z S_z \rangle(t) \end{pmatrix} = \begin{pmatrix} R_1 & \eta_z \\ \eta_z & R_{1IS} \end{pmatrix} \begin{pmatrix} \langle S_z \rangle(t) \\ \langle 2I_z S_z \rangle(t) \end{pmatrix} \quad (\text{A9})$$

with the  $I$  spin evolution decoupled. The above equation has been written assuming that, the contribution from equilibrium  $I$  and  $S$  magnetization have been removed by subtracting pairs of experiments in which, the sign of  $I_0$  and  $S_0$  are altered, that the small effect of  $I$  spin dynamics is removed by inverting all  $S$  spin operators at time  $(\tau/2)$  (only the ungerade space dynamics is included in the above). Furthermore, it is assumed that one is dealing with a two-spin system, since all the other spins (protons) have been removed by deuteration. In Eqs. (A8) and (A9), the cross-correlation spectral densities are given

by:

$$\eta_z = -4cdP_2(\cos \theta)J(\omega_S) \quad (A10)$$

$$\eta_{xy} = -\frac{2}{3}cdP_2(\cos \theta)[4J(0) + 3J(\omega_S)]$$

where  $c = (\gamma_S B_0 \Delta \sigma_S) / \sqrt{30}$ ,  $d = (\sqrt{3} \mu_0 \hbar \gamma_I \gamma_S) / (4\pi r_{IS}^3 \sqrt{10})$ ,  $\theta$  is the angle between the principal axis of the CSA tensor and the dipolar vector and  $cdP_2(\cos \theta)J(\omega_S) = J_{S,IS}(\omega_S)$ . The auto-correlation spectral densities are given by:

$$R_1 = \rho_S = (d^2/4)[3J(\omega_S) + J(\omega_I - \omega_S) + 6J(\omega_I + \omega_S)] + c^2 J(\omega_S)$$

$$R_2 = \frac{1}{2}(D_1 + D_2) = (d^2/8)[4J(0) + 3J(\omega_S) + J(\omega_I - \omega_S) + 6J(\omega_I) + 6J(\omega_I + \omega_S)] + (c^2/6)[4J(0) + 3J(\omega_N)] + R_{ex}$$

$$R_{1IS} = \sigma_{IS} = (d^2/4)[3J(\omega_S) + 3J(\omega_I)] + c^2 J(\omega_S) + R_{II}$$

$$R_{2IS} = C = (d^2/8)[4J(0) + 3J(\omega_S) + J(\omega_I - \omega_S) + 6J(\omega_I + \omega_S)] + (c^2/6)[4J(0) + 3J(\omega_S)] + R_{ex} + R_{II}, \quad (A11)$$

where  $R_{ex}$  represents the additive effect of chemical exchange line broadening and  $R_{II}$  is the longitudinal relaxation rate constant resulting from dipolar interactions between the amide  $^1H^N(I)$  spin and other remote protons that are near in space.

Experiments have been designed to monitor the time evolution of  $\langle S_{x,y} \rangle$ ,  $\langle 2S_{x,y}I_z \rangle$ ,  $\langle S_z \rangle$  and  $\langle 2I_z S_z \rangle$  operators directly, rather than the conventional observables, such as  $I_\alpha^{(1)}$  and  $I_\alpha^{(2)}$ . The selective observation of  $I_\alpha^{(1)}$  and  $I_\alpha^{(2)}$  requires well-resolved multiplets. Rapid interconversion of  $I_\alpha^{(1)}$  and  $I_\alpha^{(2)}$  by appropriately placed  $\pi$  pulses allows the monitoring of  $\langle I_\alpha \rangle$  and  $\langle 2I_\alpha S_z \rangle$  operators.

Goldman in the first part of the paper [238] assumes that the principal axis of the axially symmetric CSA tensor is parallel to the internuclear dipolar vector. He

then introduces an angle between the two, showing that auto-correlation terms involving CSA do not depend on the angle and only the cross terms between the CSA and dipolar relaxation are to be multiplied by a factor  $(3 \cos^2 \theta - 1)/2$ , yielding the spectral density as outlined by Eq. (A8). In the next part of the paper, Goldman considers the case of non-axial CSA tensors such that the principal values are all different, with the following Hamiltonian:

$$\mathcal{H}_{CS} = \gamma_I [\sigma_{x'} H_{x'} I_{x'} + \sigma_{y'} H_{y'} I_{y'} + \sigma_{z'} H_{z'} I_{z'}] \quad (A12)$$

where  $Ox'y'z'$  represents the molecule fixed principal-axes frame of the CSA tensor, with  $z'$  being the principal axis. The laboratory frame is represented by  $OXYZ$  with  $\theta'$  being the angle between  $OZ$  and  $Oz'$  and  $\phi'$  being the angle between  $OX$  and the projection of  $Oz'$  on the plane  $OXY$ . The isotropic part of  $\mathcal{H}_{CS}$  is given by:

$$\mathcal{H}_{CSI} = \frac{1}{3} \gamma_I (\sigma_{x'} + \sigma_{y'} + \sigma_{z'}) H \cdot I \quad (A13)$$

However, it is only the anisotropic part which contributes to relaxation and can be expressed as the sum of two axially symmetric anisotropic chemical shift tensors as:

$$\mathcal{H}_{CSA} = \mathcal{H}_{CSA}^{(1)} + \mathcal{H}_{CSA}^{(2)} \quad (A14)$$

with

$$\mathcal{H}_{CSA}^{(1)} = \frac{1}{3} \gamma_I (\sigma_{x'} - \sigma_{z'}) [2H_{x'} I_{x'} - H_{y'} I_{y'} - H_{z'} I_{z'}]$$

$$\mathcal{H}_{CSA}^{(2)} = \frac{1}{3} \gamma_I (\sigma_{y'} - \sigma_{z'}) [2H_{y'} I_{y'} - H_{x'} I_{x'} - H_{z'} I_{z'}] \quad (A15)$$

There are cross terms between  $\mathcal{H}_{DD}$  and each of the  $\mathcal{H}_{CSA}^{(1)}$  and  $\mathcal{H}_{CSA}^{(2)}$ . The cross terms between these two CSA tensors (the angle between them being  $\pi/2$ ) affects both the transitions of the  $I$  spin equally, since these terms do not depend on  $S_z$ . By analogy with the expression for  $\alpha$ , Goldman defines the cross-correlation in this case as:

$$\alpha_1 = -(2/3)H(\sigma_{x'} - \sigma_{z'})r^3/(\gamma_S \hbar) \quad (A16)$$

$$\alpha_2 = -(2/3)H(\sigma_{y'} - \sigma_{z'})r^3/(\gamma_S \hbar)$$

In the auto-correlation expression given by  $A_1$  and  $C_1$

in Eq. (A5),  $\alpha^2$  is then replaced by

$$(\alpha_1^2 + \alpha_2^2 - \alpha_1\alpha_2) = (4H^2r^6/9\gamma_S^2\hbar^3)[\sigma_{x'}^2 + \sigma_{y'}^2 + \sigma_{z'}^2 - \sigma_{x'}\sigma_{y'} - \sigma_{y'}\sigma_{z'} - \sigma_{z'}\sigma_{x'}],$$

and in the cross-correlation term  $B_1$  (Eq. (A5)),  $\alpha$  is replaced by

$$\frac{1}{2}[\alpha_1(3\cos^2\theta_{x'z} - 1) + \alpha_2(3\cos^2\theta_{y'z} - 1)].$$

## References

- [1] A. Abragam, Principles of Nuclear Magnetic Resonance, Clarendon, Oxford, 1961.
- [2] H.M. McConnell, J. Chem. Phys. 25 (1957) 709.
- [3] H. Shimizu, J. Chem. Phys. 40 (1964) 3357.
- [4] P.B. Ayscough, Electron Spin Resonance in Chemistry, Methuen, London, 1967.
- [5] N.M. Atherton, Electron Spin Resonance, Theory and Applications, Wiley, New York, 1973.
- [6] J. McConnell, The Theory of Nuclear Magnetic Relaxation in Liquids, Cambridge University Press, London, 1987.
- [7] J.H. Freed, G.K. Fraenkel, J. Chem. Phys. 39 (1963) 326.
- [8] R.R. Ernst, J. Chem. Phys. 45 (1966) 3845.
- [9] A. Kumar, B.D.N. Rao, Mol. Phys. 15 (1968) 377.
- [10] A. Kumar, N.R. Krishna, B.D.N. Rao, Mol. Phys. 18 (1970) 11.
- [11] A. Kumar, S.L. Gordon, J. Chem. Phys. 54 (1971) 3207.
- [12] B.D.N. Rao, in: J.S. Waugh (Ed.), Advances in Magnetic Resonance, vol. 4, Academic Press, New York, 1970, p. 271.
- [13] H. Schneider, Ann. Phys. 13 (1964) 313.
- [14] H. Schneider, Ann. Phys. 16 (1965) 135.
- [15] J.S. Blicharski, H. Schneider, Ann. Phys. 22 (1969) 306.
- [16] H. Schneider, J.S. Blicharski, Ann. Phys. 23 (1969) 139.
- [17] J.S. Blicharski, Phys. Lett. A 24 (1967) 608.
- [18] J.S. Blicharski, Acta Phys. Polon. 34 (1969) 211.
- [19] J.S. Blicharski, Acta Phys. Polon. 38 (1970) 19.
- [20] J.S. Blicharski, W. Nosel, Acta Phys. Polon. A 38 (1970) 25.
- [21] P.S. Hubbard, Phys. Rev. 180 (1969) 319.
- [22] N.C. Pyper, Mol. Phys. 21 (1971) 1.
- [23] N.C. Pyper, Mol. Phys. 22 (1972) 433.
- [24] R.L. Vold, R.R. Vold, D. Canet, J. Chem. Phys. 66 (1977) 1202.
- [25] R.E. Stark, R.L. Vold, R.R. Vold, J. Magn. Reson. 33 (1979) 421.
- [26] D. Canet, R.R. Vold, R.L. Vold, J. Chem. Phys. 64 (1976) 900.
- [27] A. Kratchwill, R.L. Vold, R.R. Vold, J. Chem. Phys. 71 (1979) 1319.
- [28] A. Kratchwill, R.L. Vold, J. Magn. Reson. 40 (1980) 197.
- [29] R. Poupko, R.L. Vold, R.R. Vold, J. Phys. Chem. 84 (1980) 3444.
- [30] J. Courtieu, N.T. Lai, C.L. Mayne, D.M. Grant, J. Chem. Phys. 76 (1982) 257.
- [31] E.P. Black, J.M. Bernassau, C.L. Mayne, D.M. Grant, J. Chem. Phys. 76 (1982) 265.
- [32] M. Brown, C.L. Mayne, D.M. Grant, T.C. Chou, E.L. Allred, J. Phys. Chem. 88 (1984) 2708.
- [33] M. Brown, D.M. Grant, W.J. Horton, C.L. Mayne, G.T. Evans, J. Am. Chem. Soc. 107 (1985) 6698.
- [34] M.F. Baud, P.S. Hubbard, Phys. Rev. 170 (1970) 384.
- [35] S.A. Albert, J.A. Ripmeester, J. Chem. Phys. 57 (1972) 356.
- [36] R.L. Hilt, P.S. Hubbard, Phys. Rev. 134 (1964) A392.
- [37] M. Mehring, H. Raber, J. Chem. Phys. 59 (1973) 1116.
- [38] S. Schaublin, A. Höhner, R.R. Ernst, J. Magn. Reson. 13 (1974) 196.
- [39] V.A. Daragan, Doklady Akad. Nauk SSSR 213 (1973) 657.
- [40] V.A. Daragan, T.N. Khazanovich, A.U. Etepanyants, Chem. Phys. Lett. 26 (1974) 89.
- [41] V.A. Daragan, T.N. Khazanovich, Zhur. Struct. Khim. 19 (1978) 49.
- [42] J. Keeler, F.S. Ferrando, J. Magn. Reson. 75 (1987) 96.
- [43] L.E. Kay, J.H. Prestegard, J. Am. Chem. Soc. 109 (1987) 3829.
- [44] A.G. Palmer, P.E. Wright, M. Rance, Chem. Phys. Lett. 185 (1991) 41.
- [45] C. Dalvit, G. Bodenhausen, Chem. Phys. Lett. 161 (1989) 554.
- [46] N. Muller, G. Bodenhausen, J. Chem. Phys. 98 (1993) 6062.
- [47] A. Kumar, R.R. Ernst, K. Wuthrich, Biochem. Biophys. Res. Commun. 95 (1980) 1.
- [48] K. Wuthrich, NMR of Proteins and Nucleic Acids, Wiley, New York, 1986.
- [49] R.R. Ernst, G. Bodenhausen, A. Wokaun, Principles of Nuclear Magnetic Resonance in One and Two Dimensions, Oxford Science Publication, London, 1991.
- [50] T.L. James, Curr. Opin. Struct. Biol. 1 (1991) 1042.
- [51] V.A. Daragan, K.H. Mayo, J. Magn. Reson. B 110 (1996) 164.
- [52] M. Hricovini, G. Torri, Chem. Papers 48 (1994) 211.
- [53] Y.W. Kim, A. Labouriace, C.M. Taylor, W.L. Earl, L.G. Werbelow, J. Phys. Chem. 98 (1994) 4919.
- [54] A. Kalk, H.J.C. Berendsen, J. Magn. Reson. 24 (1976) 343.
- [55] T. Bremi, M. Ernst, R.R. Ernst, J. Phys. Chem. 98 (1994) 9322.
- [56] V.A. Daragan, M.A. Kloczewiak, K.H. Mayo, Biochemistry 32 (1993) 10580.
- [57] V.A. Daragan, M.A. Kloczewiak, K.H. Mayo, Biochemistry 32 (1993) 11488.
- [58] L.G. Werbelow, D.M. Grant, Adv. Magn. Reson. 9 (1977) 189.
- [59] R.L. Vold, R.R. Vold, Prog. NMR Spectrosc. 12 (1978) 79.
- [60] D. Canet, Prog. NMR Spectrosc. 21 (1989) 237.
- [61] T.E. Bull, Prog. NMR Spectrosc. 24 (1992) 377.
- [62] L.G. Werbelow, in: R. Tycko (Ed.), Nuclear Magnetic Resonance Probes of Molecular Dynamics, Kluwer Academic, Dordrecht, 1994, p. 223.
- [63] R.N. Bracewell, The Fourier Transform and its Applications, McGraw-Hill, New York, 1986.
- [64] L.G. Werbelow, in: D.M. Grant, R. Harris (Eds.), Encyclopaedia of NMR, Wiley, New York, 1996, p. 1776.

- [65] A.G. Redfield, *Adv. Magn. Reson.* 1 (1966) 1.
- [66] A. Kumar, B.D.N. Rao, *J. Magn. Reson.* 8 (1972) 1.
- [67] J. McConnell, *Physica A* 127 (1994) 152.
- [68] S.A. Smith, W.E. Palke, J.T. Gerig, *Conc. Magn. Reson.* 4 (1992) 107.
- [69] S.A. Smith, W.E. Palke, J.T. Gerig, *Conc. Magn. Reson.* 4 (1992) 181.
- [70] M. Mehring, *Principles of High Resolution NMR in Solids*, Springer, Berlin, 1983.
- [71] F. Bloch, *Phys. Rev.* 70 (1946) 460.
- [72] P.K. Madhu, A. Kumar, *J. Magn. Reson.* A114 (1995) 201.
- [73] P.K. Madhu, A. Kumar, *Conc. Magn. Reson.* 9 (1997) 1.
- [74] C.P. Slichter, *Principles of Magnetic Resonance*, Harper and Row, New York, 1963.
- [75] V.V. Krishnan, Theoretical and experimental investigations of nuclear Overhauser effect in nuclear magnetic resonance, PhD thesis, Indian Institute of Science, Bangalore, 1991.
- [76] V.V. Krishnan, A. Kumar, *J. Magn. Reson.* 92 (1991) 293.
- [77] V.V. Krishnan, A. Kumar, *Conc. Magn. Reson.* 4 (1992) 245.
- [78] C. Dalvit, G. Bodenhausen, *Adv. Magn. Reson.* 14 (1990) 1.
- [79] I. Solomon, *Phys. Rev.* 99 (1955) 559.
- [80] M. Mortimer, E.A. Moore, M.A.K. Williams, *J. Chem. Soc. Faraday Trans.* 88 (1992) 2393.
- [81] V.A. Daragan, E.E. Ilina, *Izv. Akad. Nauk SSSR, Ser. Khim.* 6 (1988) 1277.
- [82] V.A. Daragan, E.E. Ilina, *Izv. Akad. Nauk SSSR, Ser. Khim.* 6 (1988) 1281.
- [83] L.G. Werbelow, *J. Magn. Reson.* 71 (1987) 151.
- [84] E. Königsberger, H. Sterk, *J. Chem. Phys.* 83 (1985) 2723.
- [85] J. Brondeau, D. Canet, C. Millot, H. Nery, L. Werbelow, *J. Chem. Phys.* 82 (1985) 2212.
- [86] M.T. Chenon, J.M. Bernassau, C. Couprie, *Mol. Phys.* 54 (1985) 277.
- [87] H. Oschkinat, D. Limat, L. Emsley, G. Bodenhausen, *J. Magn. Reson.* 81 (1989) 13.
- [88] R.C.R. Grace, A. Kumar, *J. Magn. Reson.* 99 (1992) 81.
- [89] V.A. Daragan, K.H. Mayo, *Chem. Phys. Lett.* 206 (1993) 393.
- [90] H. Sterk, E. Königsberger, *J. Phys. Chem.* 90 (1986) 916.
- [91] L.G. Werbelow, D. Ikenberry, G. Pouzard, *J. Magn. Reson.* 51 (1983) 409.
- [92] T.E. Bull, *J. Magn. Reson.* 72 (1987) 397.
- [93] P.K. Madhu, R.C.R. Grace, A. Kumar, *Bull. Magn. Reson.* 16 (1994) 115.
- [94] P.K. Madhu, A. Kumar, *Conc. Magn. Reson.* 8 (1996) 139.
- [95] P.K. Madhu, A. Kumar, *J. Magn. Reson.* A 127 (1997) 168.
- [96] P.S. Hubbard, *Phys. Rev.* 111 (1958) 1746.
- [97] P.S. Hubbard, *Phys. Rev.* 128 (1962) 650.
- [98] P.S. Hubbard, *Rev. Mod. Phys.* 33 (1961) 249.
- [99] W. Mandema, N.T. Trappeniers, *Physica* 76 (1974) 73.
- [100] J.S. Blicharski, W. Nosel, H. Schneider, *Ann. Phys.* 27 (1971) 17.
- [101] L.G. Werbelow, A.G. Marshall, *Mol. Phys.* 28 (1974) 113.
- [102] H. Nery, D. Canet, W.M.M.J. Bovee, J. Vriend, *Mol. Phys.* 42 (1981) 683.
- [103] N.K. Andreev, M.R. Zaripov, M.M. Bil'danov, *Sov. Phys. Sol. St.* 18 (1976) 511.
- [104] L.G. Werbelow, D.M. Grant, *J. Magn. Reson.* 29 (1978) 603.
- [105] P.S. Hubbard, *Phys. Rev.* 109 (1958) 1153.
- [106] P.S. Hubbard, *J. Chem. Phys.* 51 (1969) 1647.
- [107] P.S. Hubbard, *J. Chem. Phys.* 52 (1970) 563.
- [108] G.W. Kattawaar, M. Eisner, *Phys. Rev.* 126 (1962) 1054.
- [109] S. Emid, R.A. Wind, *Chem. Phys. Lett.* 27 (1962) 312.
- [110] J.S. Blicharski, *Can. J. Phys.* 55 (1977) 31.
- [111] R.A. Wind, S. Emid, *Phys. Rev. Lett.* 33 (1974) 1422.
- [112] K. van Putte, *J. Magn. Reson.* 5 (1971) 367.
- [113] S. Albert, H.S. Gutowsky, J.A. Ripmeester, *J. Chem. Phys.* 56 (1972) 1332.
- [114] S. Albert, H.S. Gutowsky, J.A. Ripmeester, *J. Chem. Phys.* 56 (1972) 3672.
- [115] S. Albert, J.A. Ripmeester, *J. Chem. Phys.* 57 (1972) 2641.
- [116] S. Albert, J.A. Ripmeester, *J. Chem. Phys.* 58 (1973) 541.
- [117] L.J. Burnett, B.H. Muller, *Chem. Phys. Lett.* 18 (1973) 553.
- [118] A. Kumar, C.S. Johnson, *J. Chem. Phys.* 60 (1974) 137.
- [119] M.T. Chenon, J.M. Bernassau, D.M. Grant, C.L. Mayne, *J. Phys. Chem.* 86 (1982) 2733.
- [120] C.L. Mayne, D.W. Alderman, D.M. Grant, *J. Chem. Phys.* 63 (1975) 2514.
- [121] W.M.M.J. Bovee, *Mol. Phys.* 29 (1975) 1673.
- [122] M.M. Fuson, A.M. Belu, *J. Magn. Reson.* A 107 (1994) 1.
- [123] L.G. Werbelow, *J. Chem. Phys.* 77 (1982) 5849.
- [124] M.M. Fuson, J.H. Prestegard, *J. Chem. Phys.* 76 (1982) 1539.
- [125] M.M. Fuson, J.H. Prestegard, *J. Magn. Reson.* 41 (1980) 179.
- [126] M.M. Fuson, J.H. Prestegard, *Biochemistry* 22 (1983) 1311.
- [127] M.M. Fuson, J.H. Prestegard, *J. Am. Chem. Soc.* 105 (1983) 168.
- [128] L.Y. Zhu, M.D. Kemple, S.B. Landy, P. Buckley, *J. Magn. Reson. B* 109 (1995) 19.
- [129] M.M. Fuson, J.B. Miller, *Macromolecules* 26 (1993) 3218.
- [130] N.K. Gaisin, I.R. Manyrov, K.M. Enikeev, *Mol. Phys.* 80 (1993) 1049.
- [131] M.M. Fuson, D.M. Grant, *Macromolecules* 21 (1988) 944.
- [132] M.M. Fuson, D.J. Anderson, F. Liu, D.M. Grant, *Macromolecules* 24 (1991) 2594.
- [133] M. Geringer, H. Sterk, *J. Magn. Reson.* 85 (1989) 470.
- [134] Z. Zheng, C.L. Mayne, D.M. Grant, *J. Magn. Reson. A* 103 (1993) 268.
- [135] A.D. Bain, R.M. Lynden-Bell, *Mol. Phys.* 30 (1965) 325.
- [136] V.A. Daragan, I.V. Zlokazova, N.K. Gaisin, Kh.Z. Khusainov, *Theo. Exp. Chem.* 17 (1981) 458.
- [137] J. Schrieffer, L.H. Zuiiderweg, J.C. Leyte, *Mol. Phys.* 34 (1977) 635.
- [138] L.G. Werbelow, D.M. Grant, *J. Chem. Phys.* 63 (1975) 544.
- [139] L.G. Werbelow, D.M. Grant, *J. Chem. Phys.* 63 (1975) 4742.
- [140] D. Yang, C. Ye, *Chem. Phys. Lett.* 183 (1991) 309.
- [141] F. Liu, W.J. Horton, C.L. Mayne, T.-X. Xiang, D.M. Grant, *J. Am. Chem. Soc.* 114 (1992) 5281.
- [142] M. Poschl, G. Althoff, S. Killie, E. Wenning, H.G. Hertz, *Ber. Bunsenges. Phys. Chem.* 95 (1991) 1084.
- [143] B. Blicharska, *Acta Phys. Polon.* A70 (1986) 127.
- [144] B. Blicharska, *Acta Phys. Polon.* A 147 (1988) 601.
- [145] E. Haslinger, H. Kalchhauser, W. Robien, *J. Mol. Liq.* 28 (1984) 223.

- [146] Y.L. Pascal, O. Convert, Y. Ahomadegbe, *J. Chim. Phys. (Paris)* 78 (1981) 771.
- [147] L.E. Kay, T.A. Holak, J.H. Prestegard, *J. Magn. Reson.* 76 (1988) 30.
- [148] E. Haslinger, W. Robien, *J. Am. Chem. Soc.* 102 (1980) 1237.
- [149] B.I. Geller, V.A. Daragan, I.V. Zlokazova, *Russ. J. Phys. Chem.* 54 (1980) 1726.
- [150] V.A. Daragan, I.V. Zlokazova, V.F. Edneral, *Theo. Exp. Chem.* 16 (1980) 543.
- [151] L.G. Werbelow, *J. Magn. Reson.* 34 (1979) 439.
- [152] D. Canet, H. Nery, J. Brondeau, *J. Chem. Phys.* 70 (1979) 2098.
- [153] J.F. Rodrigues de Miranda, C.W. Hilbers, *J. Magn. Reson.* 19 (1975) 11.
- [154] G.B. Matson, *J. Chem. Phys.* 65 (1976) 4147.
- [155] D. Pumpernik, A. Azman, *Adv. Mol. Relax. Inter. Processes* 11 (1977) 243.
- [156] L.G. Werbelow, D.M. Grant, *Can. J. Chem.* 55 (1977) 1558.
- [157] K. van Putte, G.J.N. Egmond, *J. Magn. Reson.* 4 (1971) 236.
- [158] K. van Putte, *J. Magn. Reson.* 5 (1971) 307.
- [159] W. Buchner, B. Emmerich, *J. Magn. Reson.* 4 (1971) 90.
- [160] W. Buchner, *J. Magn. Reson.* 11 (1973) 46.
- [161] W. Buchner, *J. Magn. Reson.* 12 (1973) 79.
- [162] W. Buchner, *J. Magn. Reson.* 12 (1973) 82.
- [163] W. Buchner, *Z. Naturforsch A* 26 (1971) 775.
- [164] W. Buchner, *J. Magn. Reson.* 17 (1975) 229.
- [165] L.G. Werbelow, A.G. Marshall, *J. Magn. Reson.* 11 (1973) 299.
- [166] J. Brown, O.W. Howarth, P. Moore, A.D. Bain, *J. Magn. Reson.* 28 (1977) 317.
- [167] M.D. Zeidler, *Ber. Bunsenges. Phys. Chem.* 72 (1968) 481.
- [168] J.F.R. Miranda, C.W. Hilbers, *J. Magn. Reson.* 19 (1975) 11.
- [169] V.A. Daragan, *Doklady Akad. Nauk SSSR* 232 (1977) 114.
- [170] J.W. Harrell, *J. Magn. Reson.* 15 (1974) 157.
- [171] L.G. Werbelow, *J. Magn. Reson.* 51 (1983) 323.
- [172] L.G. Werbelow, *J. Magn. Reson.* 71 (1987) 151.
- [173] R. Konrat, H. Sterk, J. Kalcher, *J. Chem. Soc. Faraday Trans.* 86 (1990) 265.
- [174] T.S. Lee, L.P. Hwang, *J. Magn. Reson.* 89 (1990) 51.
- [175] L.E. Kay, D.A. Torchia, *J. Magn. Reson.* 95 (1992) 536.
- [176] R. Konrat, H. Sterk, *J. Phys. Chem.* 94 (1990) 1291.
- [177] G.B. Matson, *J. Chem. Phys.* 67 (1977) 5152.
- [178] K. Dorai, A. Kumar, unpublished results.
- [179] K. Dorai, Investigations of coupled spins in NMR: selective excitation, cross-correlations and quantum computing, PhD thesis, Indian Institute of Science, Bangalore, 1999.
- [180] A. Thevand, G. Pouzard, L.G. Werbelow, *J. Phys. Chem.* 85 (1981) 29.
- [181] W.T. Huntress, *Adv. Magn. Reson.* 4 (1970) 1.
- [182] A. Dölle, T. Bluhm, *Prog. NMR Spectrosc.* 21 (1989) 175.
- [183] M.R. Bendall, D.T. Pegg, *J. Magn. Reson.* 53 (1983) 40.
- [184] L.E. Kay, T.E. Bull, L.K. Nicholson, C. Griesinger, H. Schwalbe, A. Bax, D.A. Torchia, *J. Magn. Reson.* 100 (1992) 538.
- [185] H. Nery, D. Canet, *J. Magn. Reson.* 42 (1981) 370.
- [186] H. Nery, D. Canet, F. Toma, S. Femandjian, *J. Am. Chem. Soc.* 105 (1983) 1482.
- [187] P.E. Fagerness, D.M. Grant, K.F. Kuhlmann, C.L. Mayne, R.B. Parry, *J. Chem. Phys.* 63 (1975) 2524.
- [188] D.M. Grant, C.L. Mayne, F. Liu, T.-X. Xiang, *Chem. Rev.* 91 (1991) 1591.
- [189] E.L. Mackor, C. MacLean, *J. Chem. Phys.* 44 (1966) 64.
- [190] C.L. Mayne, D.M. Grant, D.W. Aldermann, *J. Chem. Phys.* 65 (1976) 1684.
- [191] M. Guéron, J.L. Leroy, R.H. Griffey, *J. Am. Chem. Soc.* 105 (1983) 7262.
- [192] C. Dalvit, *J. Magn. Reson.* 95 (1991) 410.
- [193] K. Elbayed, D. Canet, *Mol. Phys.* 68 (1989) 1033.
- [194] G. Kontaxis, N. Müller, H. Sterk, *J. Magn. Reson.* 92 (1991) 332.
- [195] G. Batta, J. Gervay, *J. Am. Chem. Soc.* 117 (1995) 368.
- [196] J.W. Peng, G. Wagner, *J. Magn. Reson.* 98 (1992) 308.
- [197] R.C.R. Grace, A. Kumar, *J. Magn. Reson.* A115 (1995) 87.
- [198] C.-L. Tsai, W.S. Price, Y.-C. Chang, B.-C. Perng, L.-P. Hwang, *J. Phys. Chem.* 95 (1991) 7546.
- [199] T.C. Farrar, I.C. Locker, *J. Chem. Phys.* 87 (1987) 3281.
- [200] L. Mäler, J. Kowalewski, *Chem. Phys. Lett.* 190 (1992) 241.
- [201] L. Mäler, J. Kowalewski, *Chem. Phys. Lett.* 190 (1992) 595.
- [202] L. Mäler, L. Di Bari, J. Kowalewski, *J. Phys. Chem.* 98 (1994) 6244.
- [203] V.A. Daragan, K.H. Mayo, *J. Am. Chem. Soc.* 114 (1992) 4326.
- [204] L.P. Haiducu, Cross-correlation effects in multi-spin relaxation of nucleotides—Advisor: B.D.N. Rao, MSc Project, Indiana University—Purdue University at Indianapolis, USA, 1996.
- [205] Gy. Batta, K.E. Kover, J. Kowalewski, *J. Magn. Reson.* 136 (1999) 37.
- [206] C. Dalvit, G. Bodenhausen, *J. Am. Chem. Soc.* 110 (1988) 7924.
- [207] J.M. Böhlen, S. Wimperis, G. Bodenhausen, *J. Magn. Reson.* 77 (1988) 589.
- [208] R.C.R. Grace, A. Kumar, *Bull. Magn. Reson.* 14 (1992) 42.
- [209] L. Di Bari, J. Kowalewski, G. Bodenhausen, *J. Chem. Phys.* 93 (1990) 7698.
- [210] R. Brüschweiler, C. Griesinger, R.R. Ernst, *J. Am. Chem. Soc.* 111 (1989) 8034.
- [211] I. Burghardt, R. Konrat, G. Bodenhausen, *Mol. Phys.* 75 (1992) 467.
- [212] B. Boulat, R. Konrat, I. Burghardt, G. Bodenhausen, *J. Am. Chem. Soc.* 114 (1992) 5412.
- [213] G. Jaccard, S. Wimperis, G. Bodenhausen, *Chem. Phys. Lett.* 138 (1987) 601.
- [214] M.H. Levitt, L. Di Bari, *Phys. Rev. Lett.* 69 (1992) 3124.
- [215] M.H. Levitt, L. Di Bari, *Bull. Magn. Reson.* 16 (1994) 94.
- [216] J. Jeener, *Adv. Magn. Reson.* 10 (1982) 1.
- [217] E.L. Mackor, C. MacLean, *J. Chem. Phys.* 42 (1965) 4254.
- [218] C. MacLean, E.L. Mackor, *J. Chem. Phys.* 44 (1966) 2708.
- [219] E.L. Mackor, C. MacLean, *Prog. NMR Spectrosc.* 3 (1967) 129.
- [220] P.M. Runnels, *Phys. Rev.* 132 (1963) 27.
- [221] J.M. Anderson, *Mol. Phys.* 8 (1964) 505.

- [222] S. Wimperis, G. Bodenhausen, *Chem. Phys. Lett.* 140 (1987) 41.
- [223] S. Wimperis, G. Bodenhausen, *Mol. Phys.* 66 (1989) 897.
- [224] S.G. Withers, N.B. Matsen, B.D. Sykes, *J. Mag. Reson.* 61 (1985) 545.
- [225] J. Boyd, U. Hommel, V.V. Krishnan, *Chem. Phys. Lett.* 187 (1991) 317.
- [226] F.A.L. Anet, *J. Am. Chem. Soc.* 108 (1986) 7102.
- [227] R. Konrat, H. Sterk, *Chem. Phys. Lett.* 203 (1993) 75.
- [228] R.R. Vold, R.L. Vold, *J. Chem. Phys.* 64 (1976) 320.
- [229] J.H. Prestegard, D.M. Grant, *J. Am. Chem. Soc.* 100 (1978) 4664.
- [230] L.E. Kay, T.E. Bull, *J. Magn. Reson.* 99 (1992) 615.
- [231] L.G. Werbelow, A.G. Marshall, *Chem. Phys. Lett.* 22 (1973) 568.
- [232] P. Kumar, A. Kumar, *J. Magn. Reson. A* 115 (1995) 155.
- [233] P. Kumar, A. Kumar, *J. Magn. Reson. A* 119 (1996) 29.
- [234] P. Kumar, Cross-correlation studies in relaxation of coupled spins in NMR, PhD thesis, Indian Institute of Science, Bangalore, 1996.
- [235] A. Wokaun, R.R. Ernst, *Mol. Phys.* 36 (1978) 317.
- [236] L.G. Werbelow, D.M. Grant, *J. Magn. Reson.* 20 (1975) 554.
- [237] N. Müller, G. Bodenhausen, R.R. Ernst, *J. Magn. Reson.* 75 (1987) 297.
- [238] M. Goldman, *J. Magn. Reson.* 60 (1984) 437.
- [239] N. Tjandra, A. Szabo, Ad Bax, *J. Am. Chem. Soc.* 118 (1996) 6986.
- [240] N. Tjandra, Ad Bax, *J. Am. Chem. Soc.* 119 (1997) 8076.
- [241] M. Tessari, F.A.A. Mudler, R. Boelens, G.W. Vuister, *J. Magn. Reson.* 127 (1997) 128.
- [242] N. Tjandra, Ad Bax, *J. Am. Chem. Soc.* 119 (1997) 9576.
- [243] M.W.F. Fischer, L. Zeng, Y. Pang, W. Hu, A. Majumdar, E.R.P. Zuiderweg, *J. Am. Chem. Soc.* 119 (1997) 12629.
- [244] L. Zeng, M.W.F. Fischer, E.R.P. Zuiderweg, *J. Biomol. NMR* 7 (1996) 157.
- [245] V.A. Daragan, K.H. Mayo, *J. Magn. Reson. B* 107 (1995) 274.
- [246] J.A. Pople, W.G. Schneider, H.J. Bernstein, *High Resolution Nuclear Magnetic Resonance Spectroscopy*, McGraw-Hill, New York, 1959.
- [247] B.W. Goodwin, R. Wallace, R.K. Harris, *J. Magn. Reson.* 22 (1976) 491.
- [248] J.D. Cutnell, J.A. Glasel, *J. Am. Chem. Soc.* 98 (1976) 7542.
- [249] J.D. Cutnell, W. Venable, *J. Chem. Phys.* 59 (1974) 258.
- [250] L.J. Burnett, B.H. Muller, *Chem. Phys. Lett.* 18 (1973) 553.
- [251] P. Meakin, J. Jesson, *J. Magn. Reson.* 19 (1975) 37.
- [252] C.J. Hertzell, P.C. Stein, T.J. Lynch, L.G. Werbelow, W.L. Earl, *J. Am. Chem. Soc.* 111 (1989) 5114.
- [253] R.L. Vold, H.S. Gutowsky, *J. Chem. Phys.* 47 (1967) 4782.
- [254] L.G. Werbelow, J. Kowalewski, *J. Chem. Phys.* 107 (1997) 2775.
- [255] L.G. Werbelow, J. Kowalewski, *J. Magn. Reson.* 128 (1997) 144.
- [256] T.C. Farrar, R.A. Quintero-Arcaya, *Chem. Phys. Lett.* 122 (1982) 41.
- [257] T.C. Farrar, R.A. Quintero-Arcaya, *J. Phys. Chem.* 91 (1987) 3224.
- [258] T.C. Farrar, B.R. Adams, G.C. Grey, R.A. Quintero-Arcaya, Q. Zuo, *J. Am. Chem. Soc.* 108 (1986) 8190.
- [259] T.C. Farrar, M.J. Jablonsky, J.L. Schwartz, *J. Phys. Chem.* 98 (1994) 4780.
- [260] L.-P. Hwang, P.-L. Wang, T.C. Wong, *J. Phys. Chem.* 92 (1988) 4753.
- [261] N. Müller, G. Bodenhausen, K. Wuthrich, R.R. Ernst, *J. Magn. Reson.* 65 (1985) 531.
- [262] M. Rance, P.E. Wright, *Chem. Phys. Lett.* 124 (1986) 572.
- [263] T.C. Wong, P.-L. Wang, D.-M. Duh, L.P. Hwang, *J. Phys. Chem.* 93 (1989) 1295.
- [264] N. Müller, *Chem. Phys. Lett.* 131 (1986) 218.
- [265] N. Müller, *Monatshfte fur Chemie* 120 (1989) 801.
- [266] N. Müller, *J. Magn. Reson.* 81 (1989) 520.
- [267] M. Pellicchia, Y. Pang, L. Wang, A.V. Kurochkin, A. Kumar, E.R.P. Zuiderweg, *J. Am. Chem. Soc.* 121 (1999) 9165.
- [268] T.J. Norwood, M.L. Tillett, L.Y. Lian, *Chem. Phys. Lett.* 300 (1999) 429.
- [269] B. Brutscher, N.R. Skrynnikov, T. Bremi, R. Bruschweiler, R.R. Ernst, *J. Magn. Reson.* 130 (1998) 346.
- [270] D. Yang, R. Konrat, L.E. Kay, *J. Am. Chem. Soc.* 119 (1997) 11938.
- [271] Q. Teng, M. Iqbal, T.A. Cross, *J. Am. Chem. Soc.* 114 (1992) 5312.
- [272] D. Yang, K.H. Gardner, L.E. Kay, *J. Biomol. NMR* 11 (1998) 213.
- [273] B. Reif, M. Hennig, C. Griesinger, *Science* 276 (1997) 1230.
- [274] D. Yang, L.E. Kay, *J. Magn. Reson. B* 110 (1996) 213.
- [275] D. Yang, L.E. Kay, *J. Am. Chem. Soc.* 120 (1998) 9880.
- [276] P. Pelupessy, E. Chiarparin, R. Ghose, G. Bodenhausen, *J. Biomol. NMR* 13 (1999) 375.
- [277] G. Kontaxis, H. Sterk, J. Kalcher, *J. Chem. Phys.* 95 (1991) 7854.
- [278] D. Muhandiram, T. Yamazaki, B.D. Sykes, L.E. Kay, *J. Am. Chem. Soc.* 117 (1995) 11536.
- [279] L.C. TerBeek, E.E. Burnell, *Phys. Rev. B* 50 (1994) 9245.
- [280] M. Ishiwata, *J. Phys. Soc. Jpn* 60 (1991) 1379.
- [281] M. Ishiwata, Y. Ishii, *J. Phys. Soc. Jpn* 60 (1991) 1743.
- [282] R.P. Lubianez, A.A. Jones, *J. Magn. Reson.* 38 (1980) 331.
- [283] R.E. London, D.M. LeMaster, L.G. Werbelow, *J. Am. Chem. Soc.* 116 (1994) 8400.
- [284] R.L. Vold, R.R. Vold, R. Poupko, G. Bodenhausen, *J. Magn. Reson.* 38 (1980) 141.
- [285] E.J. Pedersen, R.L. Vold, R.R. Vold, *Mol. Phys.* 41 (1980) 811.
- [286] J. Voigt, J.P. Jacobsen, *J. Chem. Phys.* 78 (1983) 1693.
- [287] D. Petit, J.P. Korb, A. Delville, J. Grandjean, P. Laszlo, *J. Magn. Reson.* 96 (1992) 252.
- [288] L.G. Werbelow, *J. Magn. Reson.* 67 (1986) 66.
- [289] H. Gutowsky, R.L. Vold, *J. Chem. Phys.* 47 (1967) 4782.
- [290] L.G. Werbelow, A. Allouche, G. Pouzard, *J. Chem. Soc. Faraday Trans.* 83 (1987) 871.
- [291] L.G. Werbelow, A. Allouche, G. Pouzard, *J. Phys. Chem.* 88 (1984) 4692.
- [292] P. Granger, K. Elbayed, J. Raya, P. Kempgens, J. Rose, *J. Magn. Reson. A* 117 (1995) 179.

- [293] K. Elbayed, P. Kempgens, J. Rose, P. Granger, J. Rose, *J. Magn. Reson.* 130 (1998) 209.
- [294] L.G. Werbelow, G.A. Morris, P. Kumar, J. Kowalewski, *J. Magn. Reson.* 140 (1999) 1.
- [295] T.E. Bull, *J. Magn. Reson.* 80 (1988) 470.
- [296] T.E. Bull, *J. Magn. Reson.* 93 (1991) 596.
- [297] R. Brüschweiler, R.R. Ernst, *J. Magn. Reson.* 53 (1983) 521.
- [298] Ad Bax, D.G. Davis, *J. Magn. Reson.* 65 (1985) 355.
- [299] D.G. Davis, Ad Bax, *J. Am. Chem. Soc.* 107 (1985) 2820.
- [300] A.A. Bothner-By, R.L. Stephens, J.M. Lee, C.D. Warren, R.W. Jeanloz, *J. Am. Chem. Soc.* 106 (1984) 811.
- [301] Ad Bax, D.G. Davis, *J. Magn. Reson.* 63 (1985) 207.
- [302] H.C. Torrey, *Phys. Rev.* 76 (1949) 1059.
- [303] L. Emsley, G. Bodenhausen, *J. Magn. Reson.* 82 (1989) 211.
- [304] R. Brüschweiler, R.R. Ernst, *J. Chem. Phys.* 96 (1992) 1758.
- [305] L. Poppe, H. van Halbeek, *Magn. Reson. Chem.* 31 (1993) 665.
- [306] V. Varma, N.D. Kurur, G. Bodenhausen, *J. Magn. Reson. A* 118 (1996) 64.
- [307] N. Tjandra, S. Grzesiek, A. Bax, *J. Am. Chem. Soc.* 118 (1996) 6264.
- [308] L.G. Werbelow, *J. Chem. Phys.* 70 (1979) 5381.
- [309] L.G. Werbelow, A. Thevand, G. Pouzard, *J. Chem. Soc. Faraday Trans. 2* 75 (1979) 971.
- [310] J.L. Bjorkstam, *J. Mol. Struct.* 111 (1983) 135.
- [311] N. Murali, B.D.N. Rao, *J. Magn. Reson. A* 118 (1996) 202.
- [312] C.E.M. Fouques, L.G. Werbelow, *Can. J. Chem.* 57 (1979) 2329.
- [313] L.G. Werbelow, R.E. London, *Conc. Magn. Reson.* 8 (1996) 325.
- [314] R. Bruschiweiler, *Chem. Phys. Lett.* 257 (1996) 119.
- [315] S. Grzesiek, Ad Bax, *J. Am. Chem. Soc.* 116 (1994) 10196.
- [316] S. Grzesiek, J. Anglister, H. Ren, Ad Bax, *J. Am. Chem. Soc.* 115 (1993) 4369.
- [317] R. Bruschiweiler, *J. Chem. Phys.* 105 (1996) 6164.
- [318] R.H. Tromp, J. de Bleijser, J.C. Leyte, *Chem. Phys. Lett.* 175 (1990) 568.
- [319] W. Price, N.-H. Ge, L.-P. Hwang, *J. Magn. Reson.* 98 (1992) 134.
- [320] D. Brinkmann, M. Mali, J. Roos, R. Messner, H. Birli, *Phys. Rev. B* 26 (1982) 4810.
- [321] D.T. Amm, S.L. Segel, *Solid State Ionics* 8 (1983) 155.
- [322] M.W. Germann, J.M. Aramini, H.J. Vogel, *J. Am. Chem. Soc.* 116 (1994) 6971.
- [323] J.M. Aramini, H.J. Vogel, *J. Am. Chem. Soc.* 115 (1993) 245.
- [324] J.M. Aramini, M.W. Germann, H.J. Vogel, *J. Am. Chem. Soc.* 115 (1993) 9750.
- [325] J.M. Aramini, H.J. Vogel, *J. Am. Chem. Soc.* 116 (1994) 1988.
- [326] J.M. Aramini, D.D. McIntyre, H.J. Vogel, *J. Am. Chem. Soc.* 116 (1994) 11506.
- [327] L.G. Werbelow, A.G. Marshall, *J. Magn. Reson.* 43 (1981) 443.
- [328] A. Briguet, J.C. Duplan, J. Delmau, *J. Magn. Reson.* 42 (1981) 141.
- [329] V. Mlynarik, *J. Magn. Reson.* 79 (1988) 322.
- [330] S. Szymanski, G. Binsch, *J. Magn. Reson.* 87 (1990) 166.
- [331] L.G. Werbelow, G. Pouzard, *J. Phys. Chem.* 85 (1981) 3887.
- [332] L.G. Werbelow, R.E. London, *J. Chem. Phys.* 102 (1995) 5181.
- [333] D.M. Kushlan, D.M. LeMaster, *J. Biomol. NMR* 3 (1993) 701.
- [334] D.M. Kushlan, D.M. LeMaster, *J. Am. Chem. Soc.* 115 (1993) 11026.
- [335] G. Wagner, *Prog. NMR. Spectrosc.* 22 (1990) 101.
- [336] S.W. Fesik, E.R.P. Zuiderweg, *Quat. Rev. Biophys.* 23 (1990) 97.
- [337] A.G. Marshall, T. Cottrell, L.G. Werbelow, *J. Am. Chem. Soc.* 104 (1982) 7665.
- [338] H. Monoi, H. Uedaira, *J. Magn. Reson.* 38 (1980) 119.
- [339] U. Eliav, H. Shinar, G. Navon, *J. Magn. Reson.* 94 (1991) 439.
- [340] U. Eliav, G. Navon, *J. Chem. Phys.* 95 (1991) 7114.
- [341] S.A. Gabel, L.A. Luck, L.G. Werbelow, R.E. London, *J. Magn. Reson.* 128 (1997) 101.
- [342] J.S. de Ropp, G.N. La Mar, *J. Am. Chem. Soc.* 113 (1991) 4348.
- [343] L. Banci, I. Bertini, P. Turano, M.V. Oliver, *Eur. J. Biochem.* 204 (1992) 107.
- [344] J. Qin, F. Delaglio, G.N. La Mar, A. Bax, *J. Magn. Reson. B* 102 (1993) 332.
- [345] I. Bertini, F. Capozzi, S. Ciurli, C. Luchinat, L. Messori, M. Piccioli, *J. Am. Chem. Soc.* 114 (1992) 3332.
- [346] L. Banci, I. Bertini, E. Pease, M. Tien, P. Turano, *Biochemistry* 31 (1992) 10009.
- [347] I. Bertini, C. Luchinat, D. Tarchi, *Chem. Phys. Lett.* 203 (1993) 445.
- [348] I. Bertini, C. Luchinat, A. Rosato, *Chem. Phys. Lett.* 250 (1996) 495.
- [349] L. Maler, F.A.A. Mulder, J. Kowalewski, *J. Magn. Reson. A* 117 (1995) 220.
- [350] L.G. Werbelow, A. Thevand, *J. Magn. Reson. A* 101 (1993) 317.
- [351] T. Ohmura, E. Harada, T. Fujiwara, G. Kawai, K. Watanabe, H. Akutsu, *J. Magn. Reson.* 131 (1998) 367.
- [352] R. Ghose, J.H. Prestegard, *J. Magn. Reson.* 128 (1997) 138.
- [353] J.R. Tolman, J.H. Prestegard, *J. Magn. Reson. B* 106 (1995) 97.
- [354] H. Desvasix, M. Gochin, *Mol. Phys.* 96 (1999) 1317.
- [355] J.A. Reimer, R.W. Vaughan, *J. Chem. Phys.* 41 (1980) 483.
- [356] R. Gerald II, T. Bernhard, U. Haebleren, J. Rendell, S. Opella, *J. Am. Chem. Soc.* 115 (1993) 777.
- [357] C.H. Wu, A. Ramamoorthy, L.M. Gierasch, S. Opella, *J. Am. Chem. Soc.* 117 (1995) 6148.
- [358] C. Dalvit, *J. Magn. Reson.* 97 (1992) 645.
- [359] G. Lipari, A. Szabo, *J. Am. Chem. Soc.* 104 (1982) 4546.
- [360] N. Tjandra, Ad Bax, *J. Am. Chem. Soc.* 117 (1997) 12562.
- [361] A. Chaudhry, J. Pereira, T.J. Norwood, *J. Magn. Reson. A* 111 (1994) 215.
- [362] T.J. Norwood, J. Pereira, *J. Magn. Reson. A* 112 (1995) 160.
- [363] T.J. Norwood, J. Pereira, A. Chaudhry, *J. Magn. Reson. A* 119 (1996) 180.
- [364] M. Ernst, R.R. Ernst, *J. Magn. Reson. A* 110 (1994) 202.

- [365] C.D. Kroenke, J.P. Loria, L.K. Lee, M. Rance, A.G. Palmer III, *J. Am. Chem. Soc.* 120 (1998) 7905.
- [366] C. Kojima, A. Ono, M. Kainosho, T.L. James, *J. Magn. Reson.* 136 (1999) 169.
- [367] D. Fushman, D. Cowburn, *J. Am. Chem. Soc.* 120 (1998) 7109.
- [368] G.S. Harbison, L.W. Jelinski, R.E. Stark, D.A. Torchia, J. Herzfeld, R.G. Griffin, *J. Magn. Reson.* 60 (1984) 79.
- [369] K.V. Pervushin, R. Riek, G. Wider, K. Wuthrich, *Proc. Natl Acad. Sci. USA* 94 (1997) 12366.
- [370] K.V. Pervushin, G. Wider, K. Wuthrich, *J. Biomol. NMR* 12 (1998) 345.
- [371] K.V. Pervushin, R. Riek, G. Wider, K. Wuthrich, *J. Am. Chem. Soc.* 120 (1998) 6394.
- [372] M. Czisch, R. Boelens, *J. Magn. Reson.* 134 (1998) 158.
- [373] J. Weigelt, *J. Am. Chem. Soc.* 120 (1998) 10778.
- [374] M. Salzmann, K.V. Pervushin, R. Reik, G. Wider, H. Senn, K. Wuthrich, *Proc. Natl Acad. Sci. USA* 95 (1998) 13585.
- [375] M. Salzmann, K.V. Pervushin, R. Reik, G. Wider, H. Senn, K. Wuthrich, *Proc. Natl Acad. Sci. USA* 95 (1998) 14147.
- [376] M. Salzmann, K.V. Pervushin, G. Wider, H. Senn, K. Wuthrich, *J. Biomol. NMR* 14 (1999) 85.
- [377] M. Pellecchia, P. Sebbel, U. Hermanns, K. Wuthrich, R. Glockshuber, *Nature Struct. Biol.* 6 (1999) 336.
- [378] G. Zhu, X. Kong, X. Yan, K. Sze, *Ang. Chem.* 37 (1998) 2859.
- [379] M. Rance, J.P. Loria, A.G. Palmer III, *J. Magn. Reson.* 136 (1999) 92.
- [380] D. Fushman, D. Cowburn, *J. Biomol. NMR* 13 (1999) 139.
- [381] A. Meissner, O.W. Sorensen, *J. Magn. Reson.* 139 (1999) 439.
- [382] A. Meissner, O.W. Sorensen, *J. Magn. Reson.* 139 (1999) 447.
- [383] R. Riek, G. Wider, K. Pervushin, K. Wuthrich, *Proc. Natl Acad. Sci. USA* 96 (1999) 4918.
- [384] F. Cordier, A.J. Dingley, S. Grzesiek, *J. Biomol. NMR* 13 (1999) 175.
- [385] P. Andersson, A. Annala, G. Otting, *J. Magn. Reson.* 133 (1998) 364.
- [386] A.J. Dingley, S. Grzesiek, *J. Am. Chem. Soc.* 120 (1998) 8293.
- [387] K. Pervushin, A. Ono, C. Fernandez, T. Szyperski, M. Kainosho, K. Wuthrich, *Proc. Natl Acad. Sci. USA* 95 (1998) 14147.
- [388] G. Cornilescu, J.S. Hu, Ad Bax, *J. Am. Chem. Soc.* 121 (1999) 2949.
- [389] G. Cornilescu, B.E. Ramirez, M.K. Frank, G.M. Clore, A.M. Gronenborn, Ad Bax, *J. Am. Chem. Soc.* 121 (1999) 6275.
- [390] Y.X. Wang, J. Jacob, F. Cordier, P. Wingfield, S.J. Stahl, S. Lee-Huang, D. Torchia, S. Grzesiek, Ad Bax, *J. Biomol. NMR* 14 (1999) 181.
- [391] S. Borman, *Chem Engng News* 10 (1999) 36.
- [392] J. Chung, E. Oldfield, A. Thevand, L. Werbelow, *J. Magn. Reson.* 100 (1992) 69.
- [393] E. Oldfield, J. Chung, H. Le, T. Bowers, J. Patterson, *Macromolecules* 25 (1992) 3027.
- [394] J. Boyd, U. Hommel, I.D. Campbell, *Chem. Phys. Lett.* 175 (1990) 477.
- [395] L.E. Kay, L.K. Nicholson, F. Delaglio, A. Bax, D.A. Torchia, *J. Magn. Reson.* 97 (1992) 359.
- [396] A.G. Palmer III, N.J. Skeleton, W.J. Chazin, P.E. Wright, M. Rance, *Mol. Phys.* 75 (1992) 699.